University of Southampton

Faculty of Medicine

Clinical and Experimental Sciences

Magnetic Resonance Imaging-based structural markers of altered fluid dynamics in the Pediatric Brain

by

Nivedita Agarwal

Doctor of medicine, Consultant Neuroradiologist

ORCID ID 0000-0002-1387-9566

Doctor of Philosophy

March 2026

University of Southampton

Abstract

Faculty of Medicine

Clinical and Experimental Sciences

Thesis for the degree of Doctor of Philosophy

Magnetic Resonance Imaging-based structural markers of altered fluid dynamics in the Pediatric Brain

by

Nivedita Agarwal

Neurofluids encompass a variety of fluids in the central nervous system, including cerebrospinal fluid (CSF), interstitial fluid (ISF), arterial and venous blood. The dynamic exchange of these fluids in the brain parenchyma is essential for delivering nutrients, maintaining homeostasis, and removing metabolic waste. Two primary pathways responsible for waste clearance in the brain are the glymphatic pathway and the intramural periarterial drainage pathway, both of which utilize the perivascular spaces (PVS) surrounding arteries and veins to facilitate the exchange of CSF and ISF, coordinating with blood flow dynamics.

Recent discoveries have identified lymphatic vessels in the dural meningeal layer and associated parasagittal tissue (PSD), revealing additional CSF drainage routes and highlighting novel sites for neuroimmunological surveillance. Impairment of CSF-ISF drainage pathways can result in the accumulation of toxic waste in the brain, potentially leading to cell death, neuroinflammation, and neurodegeneration in adults. Although these pathways have been widely researched in animal models and adult humans, the early development of their anatomical structures and pathological significance in infants and young children is poorly understood.

PVS and PSD are emerging as potential structural MRI biomarkers for altered CSF and ISF drainage in neurodegenerative and neuroinflammatory disorders in adults but their significance in the developing pediatric brain remains unexplored. The developing pediatric brain is very different from the adult brain. The anatomical structures such as the meninges, neurons and the glial cells together with fluids such as CSF and ISF develop in different phases in a perfectly orchestrated manner. This supports critical processes such as neurotransmitter signaling, myelination, and neuronal migration. Genetic or environmental toxins can hinder this process and likely affect the development of drainage pathways.

Building upon this context, I set out to investigate these biomarkers in a pediatric cohort with autism spectrum disorder (ASD). ASD is a complex condition influenced by a combination of genetic and epigenetic factors. Neuroimaging studies reveal that children with ASD often have enlarged CSF filled subarachnoid spaces, likely due to altered drainage pathways but a thorough investigation of PVS and PSD has yet to be done.

In this study, I present findings from my recently completed research, which has largely been published, where I quantified and analyzed MRI metrics related to PVS and PSD in relation to the severity of ASD symptoms using deep learning methods.

Table of Contents

Table of Tables

Table of Figures

List of accompanying materials

Dataset 1: https://doi.org/10.5258/SOTON/PG/D071

Dataset 2: https://doi.org/10.6084/m9.figshare.24582369

Research Thesis: Declaration of Authorship

Print name: Nivedita Agarwal

Title of thesis: Magnetic Resonance Imaging-based structural markers of altered fluid dynamics in the Pediatric Brain

I declare that this thesis and the work presented in it are my own and has been generated by me as the result of my own original research.

I confirm that:

1. All of this work was done while in candidature for a research degree at this University;
2. No part of this thesis has previously been submitted for a degree or any other qualification at this University or any other institution;
3. Where I have consulted the published work of others, this is always clearly attributed;
4. Where I have quoted from the work of others, the source is always given. With the exception of such quotations, this thesis is entirely my own work;
5. I have acknowledged all main sources of help;
6. Where the thesis is based on work done by myself jointly with others, I have made clear exactly what was done by others and what I have contributed myself;
7. Parts of this work have been published as full paper in peer-reviewed journal and are presented as chapters

Signature 03/Sept/2025

Acknowledgements

I would like to express my heartfelt gratitude to those who supported me throughout the journey of writing this thesis.

First and foremost, I would like to thank my supervisor, Prof Roxana Octavia Carare, for her invaluable guidance, encouragement, and expertise. Her insightful feedback and unwavering support were instrumental in shaping my research and helping me stay focused.

I am grateful to my fellow biomedical engineers, medical colleagues and friends, especially Denis Peruzzo, Tommaso Ciceri, Letizia Losa, Giulia Frigerio, Gloria Rizzato and Elisa Mani, for their expertise in developing deep learning models necessary for the building of this thesis and to pursue the goal of this project Chapters 4, 5 and 6 contain works developed in close collaboration with biomedical engineers. Together we worked on the segmentation of PVS and PSD and trained neural networks for optimal segmentation. Our discussions and exchanges of ideas made this experience not only productive but also enjoyable.

I would also like to extend my appreciation to the internal reviewers, for their constructive criticism and valuable suggestions that greatly improved the quality of my work. I would like to thank Ms. Sandrine Willamine Morawek, for being very helpful in guiding me as I worked remotely from Italy. I thank the iSolutions department, in particular Jonathan Lightfoot who took great care in helping me format the thesis.

A special thank you goes to my Institution, Scientific Institute IRCCS Eugenio Medea for providing with the necessary equipment and financial support needed to pursue the project. To this regard I am grateful to the Director of the Scientific Board of the Institute, Dr. Maria Teresa Bassi and to her entire staff.

Lastly, I wish to acknowledge my family and my husband, Silvio Baroldi, for their unconditional love and encouragement. Their belief in me fueled my determination to succeed, and I would not have come this far without them.

Thank you all for being an integral part of this journey.

Definitions and Abbreviations

APP.....amyloid precursor protein

AQP4 .....aquaporin 4

ASD .....Autism Spectrum Disorder

BBB.....blood brain barrier

BM .....basement membrane

ChP.....choroid plexus

CSF.....cerebrospinal fluid

eaCSF .....extra-axial CSF

ECM.....extracellular matrix

ECS.....extracellular space

GM .....gray matter

IPAD.....intramural periarterial drainage pathway

ISF .....Interstitial fluid

MRI .....magnetic resonance imaging

PGBM.....pial glial basement membrane

PSD.....parasagittal dura

PVS.....perivascular space

SAS.....subarachnoid space

SSS.....superior sagittal sinus

WM .....white matter

Chapter 1 Introduction

1.1 Objective of the thesis

The anatomy, physiology and the dynamics of neurofluids is now of increasing importance to understand some of the most devastating neurological disorders in human adults such as dementia and neurovascular diseases. The last decade has significantly advanced our approach in diagnosing and developing novel treatment strategies in diseases such as Alzheimer's disease, cerebral amyloid angiopathy and cerebral small vessel disease.

"Neurofluids" refers to all fluid compartments within the brain, including cerebrospinal fluid (CSF), interstitial fluid (ISF), and both arterial and venous blood (1,2). These compartments are in constant contact with one another, facilitating the exchange of fluids, ions, molecules, gases, and nutrients. The synchronous movement of these fluids, governed by cardiac and respiratory activity is crucial to maintain a homeostatic environment, required for optimal neuronal and glial functions. The last decade has directed our attention on the role of ISF in the brain development and funciton (3). ISF fills the extracellular space (ECS) made up of extracellular matrix (ECM) to allow for the movement of nutrients and neurotransmitters while facilitating removal of metabolic waste products. The precise anatomical pathways are still poorly understood, and attempts are ongoing in the field of pre-clinical and human research to better elucidate them.

There is a vacuum of knowledge regarding the development of neurofluids related to anatomical structures and their nature during embryonic, fetal, neonatal and early childhood periods. Such information will become crucial for advancing our knowledge of normal brain development, and comprehension of the etiologies of various pediatric neurological disorders. The role of neurofluids, in particular that of CSF and ISF appear significant in neurodevelopment, particularly during synaptic pruning, volume transmission of neurotransmitters and myelination—processes essential for neuronal circuitry formation and cognitive development (4–7). Such knowledge may also facilitate the development of targeted therapies in the pediatric brain. Extensive research using magnetic resonance imaging (MRI) has explored indirect structural markers such as perivascular spaces (PVS) and the parasagittal dura (PSD) in adults, particularly in relation to neuroinflammation and neurodegeneration. However, there is limited understanding of what these structures signify in neonates, infants, and in pediatric neurological conditions. Since PVS and PSD are thought to reflect altered neurofluid and solute drainage in

adults, this project aims to investigate the developmental biology of the anatomical structures involved in these drainage pathways during early brain development.

1.2 Presentation of the thesis

In this introductory chapter, I will synthesize the existing literature on the developmental timeline of key anatomical structures related to neurofluids. This work aims to serve as a foundational reference for future research in this domain and to establish a critical framework for interpreting subsequent findings. I also provide an overview of Autism Spectrum Disorder (ASD), whose etiology remains largely elusive, believed to involve a complex interplay of neurodevelopmental and neuroinflammatory factors. The two most established structural biomarkers in MRI for assessing the severity of neuroinflammatory and neurodegenerative diseases in adults are the PVS and the PSD. ASD was selected as a potential model to investigate these biomarkers in a pediatric neurological condition, particularly due to the well-known neuroradiological feature of an enlarged subarachnoid space (SAS) over the cerebral convexity frequently observed in individuals with ASD. The reasons for this increased space remain unclear, with one hypothesis suggesting that it may be linked to alterations in CSF drainage.

Chapter 2 is a published review on our current understanding of the cerebral vasculature in the human adult brain. Since its publications, this review has been cited more than 100 times.

In Chapter 3, I present a published review that I wrote on the role of MRI to study neurofluids in the developing brain and discuss several neurological disorders that might be related to abnormal flow dynamics.

Chapters 4 and 5 are two original research published papers that provide evidence of MR based biomarkers of altered fluid dynamics in ASD.

Chapter 6 presents a manuscript intended for submission, detailing an in-house developed methodology for segmenting PSD in the pediatric brain using automated deep learning-based neural networks.

Chapter 7 discusses the key findings from the published studies and outlines potential directions for future research aimed at advancing our understanding and exploring possible applications in pediatric neurological disorders.

Here below is a summary of the literature regarding the development of the different brain structures that are involved in fluid dynamics such as the development of ventricles, choroid plexi, the SAS, the cerebrovasculature, the meninges and the meningeal lymphatics, during the

embryonic, fetal and early human life. This forms the foundation of all original research articles presented in the other chapters.

1.3 Developmental embryology of Neurofluids

1.3.1 The formation of the ventricular system

The central nervous system, comprising the brain and spinal cord, originates from the embryonic neural plate, also known as the neuroectoderm. This plate folds to create the neural tube, which typically closes around four weeks after fertilization. As brain development progresses, the central canal of the neural tube expands to form the ventricles—fluid-filled cavities that produce and circulate CSF. The neural tube differentiates into three primary brain vesicles: the prosencephalon, mesencephalon, and rhombencephalon. The prosencephalon further divides into the telencephalon (which develops into the cerebral hemispheres) and the diencephalon (encompassing the thalamus, basal ganglia, hypothalamus, and epithalamus). The mesencephalon remains undivided, while the rhombencephalon splits into the metencephalon (which gives rise to the pons and cerebellum) and the myelencephalon (which forms the medulla oblongata). As the brain matures, the ventricles expand and adapt to accommodate the growth of surrounding brain structures.

Each of the two lateral ventricles arises from the telencephalon and connects to the third ventricle via the foramen of Monro. The third ventricle, a small cavity located between the thalami, is linked to the fourth ventricle by the cerebral aqueduct, which runs along the dorsal side of the mesencephalon. The fourth ventricle, forming the posterior wall of the pons, contains three openings: two lateral apertures known as the foramina of Luschka and a median aperture called the foramen of Magendie. The foramina of Luschka connect the ventricular system to the cerebral subarachnoid space (SAS), while the foramen of Magendie links the ventricular system to the central ependymal canal and the spinal SAS.

The neuroepithelium lining the neural canal consists of a single layer of interconnected cells held together by tight junctions and adherence molecules. This arrangement creates a barrier between the interior and exterior of the neural tube. The apical surface of the neuroepithelium faces the ventricular cavity, while the basal surface is aligned with the neural tissue. The shaping of the brain ventricles occurs through stereotypical bends and constrictions, processes that necessitate genetically regulated midline separation, as well as the involvement of the cytoskeleton and extracellular matrix for structural support.

1.3.2 Production of the embryonic and fetal CSF

Before the closure of the neural tube, its cavity is filled with amniotic fluid, which later becomes the precursor to CSF after the tube closes. The closure of the anterior and posterior neuropores prevents any communication between the amniotic fluid and the embryonic CSF (eCSF) within the neural tube. The neuroepithelial cells that come into contact with this embryonic CSF then undergo proliferation and differentiation, forming what is known as the embryonic CSF-brain barrier (4). This transitory barrier, formed by tight junctions, establishes a division between the brain and the developing ventricular cavity, limiting the entry of all molecules except for very small, lipid-insoluble ones (8,9). This interface gradually disappears and ultimately evolves into the ependymal wall in adults. Since the SAS and ventricles are yet to develop, eCSF is entirely produced by neuroepithelial cells and remains within the primary brain vescicles as opposed to fetal CSF.

Once the neural tube is closed, the secretion of eCSF begins via the neuroepithelium, which is crucial for establishing the appropriate intraluminal pressure needed to inflate the ventricular cavity. Research on chick embryos indicates that the Na^+/K^+-ATPase ion pump plays a significant role in CSF production. Additionally, the secretion of proteoglycans into the embryonic CSF by neuroepithelial cells is important for fluid accumulation and transport within the ventricles (10,11). The apical surface of these cells is rich in proteoglycans, chondroitin sulfate, and hyaluronic acid, which help regulate the osmolality of the CSF and intracranial pressure (10,11).

The increase in intraluminal pressure results in the rapid inflation of the ventricles at a pace significantly faster than brain growth (12). Around four weeks into human embryonic development, an occlusion develops between the brain ventricles and the spinal canal, causing a sudden shift in the pressure gradient that promotes further enlargement of the ventricles (13). The transition from eCSF to fully developed CSF is primarily indicated by the appearance of the choroid plexus, which assumes responsibility for CSF production in the fetus, coinciding with the opening of the rhombencephalic roof. At this stage, the tela choroidea appears, a structure that is genetically determined and also facilitates the development of the future SAS (14). The foramen of Magendie emerges around four months, while the foramina of Luschka develop at six months (15), suggesting that communication between the ventricles and the SAS occurs rather late in embryonic development (4).

1.3.3 Choroid plexus development

The choroid plexuses (ChP) are highly vascularized structures attached to the ependymal walls of the ventricles. The tela choroidea begins to form around the 7th week of human embryonic development and gradually matures by birth (16). The ChP appear in a specific order: first in the fourth ventricle, followed by the lateral ventricles, and then the third ventricle. This development occurs in four stages. In the second stage, around the 9th week of development, microvilli begin to form on the apical surface of the ChP, which faces the ventricular cavity. By the third stage, around the 17th week, well-defined vascular walls and large blood vessels can be observed (17). The development of the ChP signifies the onset of fetal CSF formation. In adults, the ChP consists of a monolayer of cuboidal epithelial cells. Adjacent epithelial cells are connected by tight junctions, which prevent the paracellular passage of molecules from the bloodstream into the ventricles. These tight junctions also contribute to the establishment of apico-basal polarity of membrane proteins (18). This barrier is referred to as the blood-CSF barrier (BCSFB). In addition to forming a barrier that regulates the movement of molecules and fluids across the BCSFB, stromal cells in the ChP also produce trophic factors and contribute to immune functions to support optimal brain health during postnatal development and in adult life (19–21)(19,20).

1.3.4 Composition of embryonic and fetal CSF

Embryonic CSF contains unique markers of neuronal development including markers that signal neural stem cells and regulate neurogenesis. eCSF is a protein-rich fluid that changes composition during development and between the different chambers of the ventricular system(22–24). eCSF contains more than 200 different proteins that are fundamental in cellular signaling, growth factors and regulation of osmotic pressure. The complex protein composition of eCSF includes the presence of extracellular matrix proteins, transport and carrier proteins, enzymes and proteases. The fluids also promote cell survival, proliferation and neurogenesis. The major growth factors in the eCSF are transforming growth factor (TGF), insulin growth factor (IGF) and fibroblast growth factor (FGF). Bone morphogenic proteins (BMP), a part of the TGF family, are involved in the developing brain and promote cell growth, cell proliferation and inhibit neuronal death. They regulate neurogenic properties of neural precursor cells during brain corticogenesis. BMPs are also important for the specification of CF epithelium, an inhibition of which can result in the absence of ChP (25).

Fetal CSF is primarily produced by ChP and is less rich in protein with respect to eCSF. It has a regulated set of growth factors and signalling molecules.

1.3.5 Functions of the embryonic and fetal CSF

One of the well-established functions of CSF in the adult brain is to serve as a protective buffer, effectively cushioning the brain from mechanical impacts, which is particularly important in infants. CSF provides buoyancy, reducing the brain's weight and assisting in the prevention of potential damage caused by gravitational forces. In addition to these protective functions, CSF has several other crucial roles that evolve over time to meet the varying needs of the developing and adult brain.

The eCSF contains proliferating pluripotent neuroepithelial cells, which are considered neural stem cells. This fluid bathes the neuroepithelial cells in signaling molecules and growth factors that stimulate neurogenesis, neuronal differentiation, and synapse formation (4). These signaling factors also help regulate pressure within the brain's ventricles. Increased pressure within the ventricles appears to be necessary for stimulating neuroepithelial mitosis. Changes in CSF dynamics and its composition significantly influence brain development and plasticity, including the proliferation of neural progenitors, which affects processes such as learning and memory. Overall, CSF is essential not only for its protective functions but also for metabolic and developmental processes that are crucial during the early stages of brain growth and maturation (26).

Fetal CSF continues to be produced via the developing ChP facilitating the transport of essential nutrients, electrolytes, and metabolites to and from neuronal cells, which is critical for supporting the development and functioning of neural tissue and maintaining a homeostatic environment. Disruption in the absorption or production of fetal CSF leads to fetal hydrocephalus, a well-known medical condition (27)

1.3.6 CSF egress pathways in the developing brain

CSF drainage pathways via the arachnoid granulations (AG) or villi (AV) do not appear until around 14-24 wk of gestational age (15). Rudimental AG appear at around embryonic 26 week in the human and are evident by week 35. However, they may not be functional. Meningeal lymphatics in the mice appear just before birth and continue to develop post-natal suggesting that alternative drainage routes exist and may be more functional in neonates (28).

The mechanisms for CSF absorption during the perinatal period in humans is largely unknown. In addition to AG, recent research identifies several potential routes for CSF clearance in humans, including perineural, paravascular, and meningeal lymphatics (29–32). However, when these pathways develop and become fully functional is yet to be understood. It is known that AG in humans are not fully formed until 18 months of age (33). In other mammals, lymphatic

vessels start contributing to CSF clearance during perinatal brain development. In mice, lymphatic structures begin to develop at birth and mature post-natal (28). Clearly, the existing evidence indicates that the identified CSF clearance routes in adults may not fully explain CSF outflow during early developmental phase. Gaining insight into these early CSF clearance mechanisms may be crucial for tackling neurodevelopmental disorders associated with CSF dysregulation and could also have relevance for fluid disorders in adults.

Papaiconomou et al, used constant pressure-perfusion system in 2- to 6-day-old lambs and observed that the recovery patterns of a radioactive protein CSF tracer in various lymph nodes and tissues indicated that CSF transport occurred through multiple lymphatic pathways (29). An especially important route was transport through the cribriform plate into extracranial lymphatics located in the nasal submucosa. Suppression of cribriform plate substantially impaired CSF drainage was observed suggesting that the lymphatics were essential in neonatal CSF transport when AGs are still underdeveloped (29).

In later life, CSF homeostasis is maintained by collaborative efforts from multiple putative players in the brain, including the ChP, the dural lymphatics, leptomeningeal vasculature and intracranial pressure (34). An imbalance in the production and absorption of CSF leads to pediatric neurological disorders and life-threatening implications in the developing child (35,36).

1.3.7 Arachnoid granulations

Arachnoid granulations (AG) are formed from connective tissue derived from the leptomeninx. These granulations begin to appear as depressions around the 26th week of fetal development. By the 35th week, AG become visible, and by the 39th week, AGs can be observed. They continue to mature and achieve functionality roughly 18 months after birth. The number, location, and size of AGs can vary with age (15). More recent studies have assessed the number, size, and distribution of AGs across a lifespan from birth to 80 years (37). The largest concentration of AGs is found in the superior sagittal sinus. In infants aged 0 to 2 years, the reported average number of AGs is 0.1 ± 0.3, while this number increases to 1.2 ± 2.5 by age 10. Notably, 85% of neonates and 2-year-olds show no observable AGs. Since AGs are hypertrophied AV (29), it is important to note that the presence of AV, which are often difficult to visualize via MRI, cannot be ruled out. At age 10, the majority of AGs measure below 4 mm, whereas older individuals may have AGs measuring up to 15 mm. The same authors note that an increase in the number or size of AGs in later life does not necessarily indicate enhanced functionality. They suggest that such increases may instead reflect chronic biophysical interactions between CSF pressure and surrounding vascular and bony structures, likening these outpouchings to intestinal diverticula (Fig 3-1).

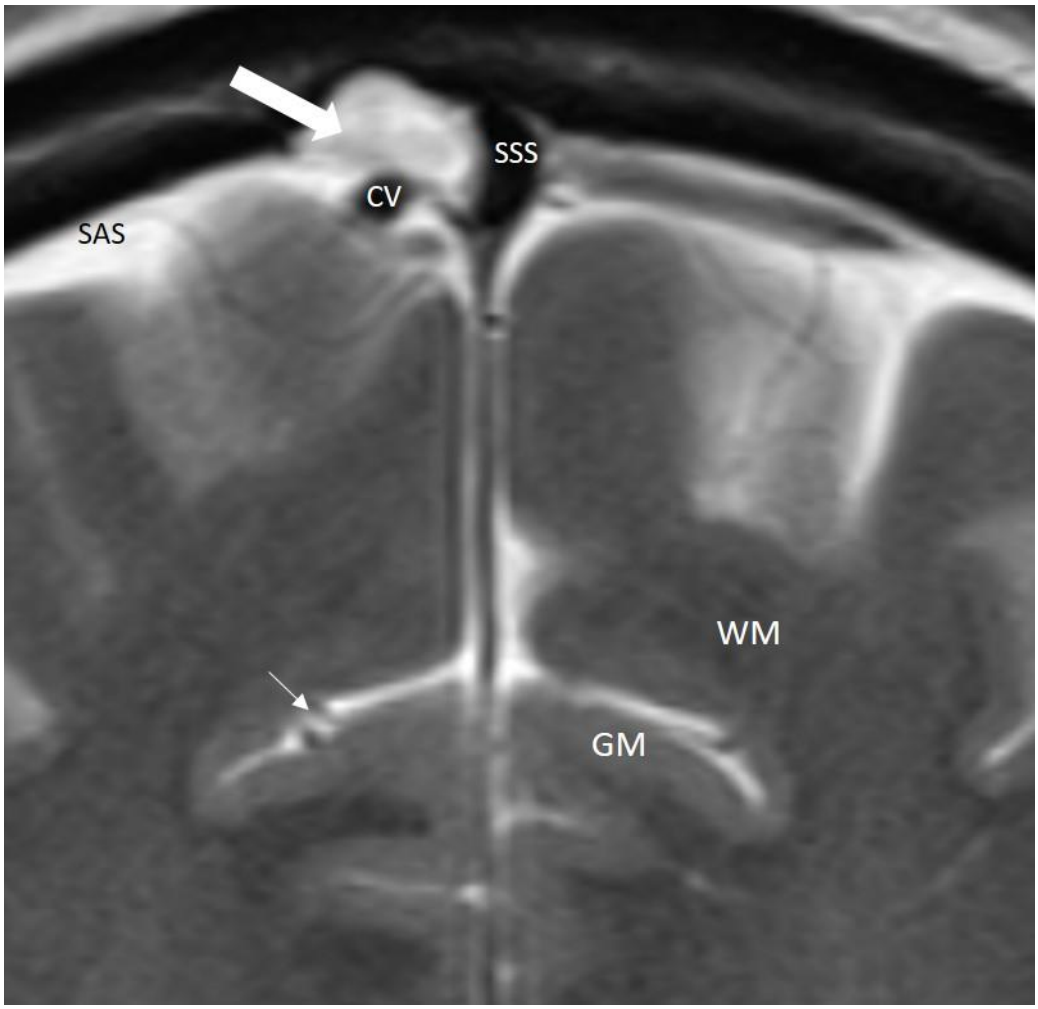

Figure 1-1 T2 coronal shows a large arachnoid granulation (white solid arrow) abutting inside the superior sagittal sinus. Small white arrow shows penetrating cortical arteries. CV= cortical vein; SSS= superior sagittal sinus; SAS=subarachnoid space; GM= gray matter and WM= white matter.

1.3.8 Meningeal layers

The term "meninges" is derived from the Greek word “meninx,” which means membrane. There are three membranes, or meninges, that encase the adult brain parenchyma. The outermost layer, known as the dura mater (from Latin meaning "tough mother"), is also referred to as the pachymeninx. It consists of two layers: an outer endosteal layer that tightly adheres to the bony skull, including sutures and foramina at the base of the skull, and a thinner inner meningeal layer (the dura mater proper) (38). The outer layer is thicker and rich in blood vessels, particularly veins. These two layers are generally fused together, with the exception of areas that contain dural venous sinuses. The second layer of the meninges is the avascular arachnoid mater, which gets its name from "arachne", meaning spider. It comprises two layers: the arachnoid barrier cell layer, which is in direct contact with the inner dural layer and is separated by a virtual space known as the subdural space, and the arachnoid border cell layer (39,40). This membrane is composed of collagen and elastic fibers and has two layers (39). Between these two layers lies the SAS, which is filled with CSF. The external layer of the arachnoid forms arachnoid granulations that project into the dural venous sinuses. A thick basement membrane lies underneath the inner portion of the outer arachnoid layer. The inner layer is also called the reticular layer (41) It is arranged more loosely with collagen fibers and fibroblasts. A reticular mesh of trabeculae traverses the outer layer to reach the inner layer of the arachnoid mater. It is between the two layers that the subarachnoid space lies. The SAS contains a complex network of connective tissue comprised of collagenous trabeculae, and all major intracranial blood vessels traverse this space.

The innermost meninx is the pia mater, a delicate single cell layer that tightly adheres to the surface of the brain, as well as to the glia limitans. Blood vessels in the SAS branch out and penetrate the brain parenchyma, accompanied by their perivascular connective tissue and perivascular space (PVS). The coverings around the external walls of these penetrating arteries are extensions of the pia mater (39). This pial basement membrane contains an ECM made up of laminins, collagen IV, heparan sulfate, and proteoglycans (42). Pial cells are joined by tight junctions thereby making this layer impermeable to CSF. Pia mater contains lymphocytes and mast cells.

1.3.8.1 Development of meninges

As the neural tube closes around 5 weeks of gestation in human embryos, mesenchymal cells spread and surround the neural tube, starting from the hindbrain and advancing toward the forebrain. This structure, known as the primitive meninx or *meninx primitiva*, serves as the precursor to the skull, meninges, and scalp (38). It is noteworthy, that the embryonic origin of the

brain meninges is still debated and is likely that both neural crest cells and the mesoderm contribute to their development (38). The primary meninx also houses a vascular plexus. It then divides into two layers: an outer dense layer and an inner reticular layer, which is considered the meningeal mesenchyme. By the sixth week of gestation, this mesenchyme progressively differentiates into multiple layers. The outer layer forms the dermis, while the middle layer gives rise to the calvarium. Just beneath the calvarial layer, primordial mesenchymal cells separate to form the pachymeninx (dura mater) and the leptomeningeal layer (which will become the arachnoid and pia mater), with the dural limiting layer marking their boundary. The leptomeningeal layer undergoes cavitation at around 44 days, developing into the SAS, which forms interconnected trabeculae and cavities that eventually fill with CSF (43). Meanwhile, the dura mater becomes progressively vascularized and develops lymphatic vessels in early postnatal life (28).

1.3.8.2 Role of meninges in the developing brain

The brain meninges are most commonly thought to serve supportive and protective functions. Recent work has established the fundamental role of meningeal cells as regulators for brain development (44). Meninges form a complex microenvironment that secrete several soluble trophic and components of the ECMs (laminins, heparin sulfate proteoglycans, collagen IV and fibronectin), to assist in the survival and development of the cortex (45). The meningeal cells regulate the migration and positioning of neurons by secreting molecules such as chemoattractants CXCL12. CXCL12 promotes the movement of Cajal-Retzius cells along the cortical surface (46). Molecules such as BMP4, BMP7 and TGFβ1 secreted by the meninges repel cells and regulates migration of cortical neurons. Other important molecules playing critical functional roles secreted by meningeal cells include fibroblast growth factors (47), insulin-like growth factor II (48) and retinoic acid (49). The meninges regulate generation of neurons (44). Meninges are important in the proper development of the corpus callosum. BMP7 produced by the meninges inhibits growth of the callosal axons (50). The meninges regulate the development of the blood vessels of the brain (51). Injury to meninges is followed by an increase in the proliferation rate, increase in expression of progenitor markers and migration (52).

The pial glial basement membrane (PGBM) plays an important structural role and also controls neuronal migration and their positioning. A special population of radial glial cells sends out processes centrifugally from the ventricular zone to the surface of the brain for radial migration of the neurons providing thus a structural scaffold for the correct positioning and migration of neurons (53). The endfeet reach and attach to the pial basement membrane which regulates the migration of the neurons.

Defects in the meninges can therefore have a profound effect on the brain development and has been linked to neurodevelopmental disorders. Cobblestone lissencephaly is one such malformation in which defects in the pial basement membrane results in poor development of the brain surface.

1.3.9 Parasagittal dura

Between the two layers of the dura mater, along the external walls of the superior sagittal sinus, lies a variable amount of tissue known as the parasagittal dura (PSD). This structure is easily identifiable in all conventional MRI T1 and T2 weighted sequences (Fig. 3-2, 3-3). Recently, it has been recognized not only for its significant role in neuroinflammation but also as a potential drainage site for CSF from the subarachnoid space. Intrasinus AGs are extensions of the arachnoid mater that fuse with the dura mater and project into the dural venous sinuses. Weed described arachnoid villi or AGs as “voluminous, delicate, and lace-like sleeves.” Non-sinus AGs can be found within the stromal PSD, in the diploë, as well as in the epidural or subdural spaces (54).

In the early 1900s, Weed also observed the presence of lymphatic channels in the dura mater, which drain towards the cervical lymph nodes (55). The anatomical characteristics of the PSD were first detailed by Fox et al. in 1996 (33). Their dissection of the superior wall, or roof, of the SSS revealed several septae, with AGs measuring 1-2 mm observed along the SSS. These were found to be small, unilobed spherical pouches in term infants, while they appeared multilobular in adults. AGs were also identified at the junction of the cortical bridging veins and the SSS, but were noted to be absent in infants and fetal specimens.

Running parallel to the SSS are tributary veins that converge at their termination into lacunar sacs or lacunae lateralis (LL) resident within the PSD. Numerous granulations have been observed within these venous lacunae in adults (33)Coronal histological sections of the SSS in infants indicated that the PSD is approximately 1-2 mm thick, whereas in adults, it measures about 5 mm thick. Multiple channels within the PSD coalesce to form lacunae in its middle third, resembling conventional venous LL. These channels are absent in preterm infants but appear in those born at or after 37 weeks of gestation, with their numbers increasing with age. These intradural channels run superficial to the cortical bridging veins within the PSD and are particularly abundant around AGs. They likely conduct CSF, as no thrombus has ever been observed within them during postmortem examinations(56).

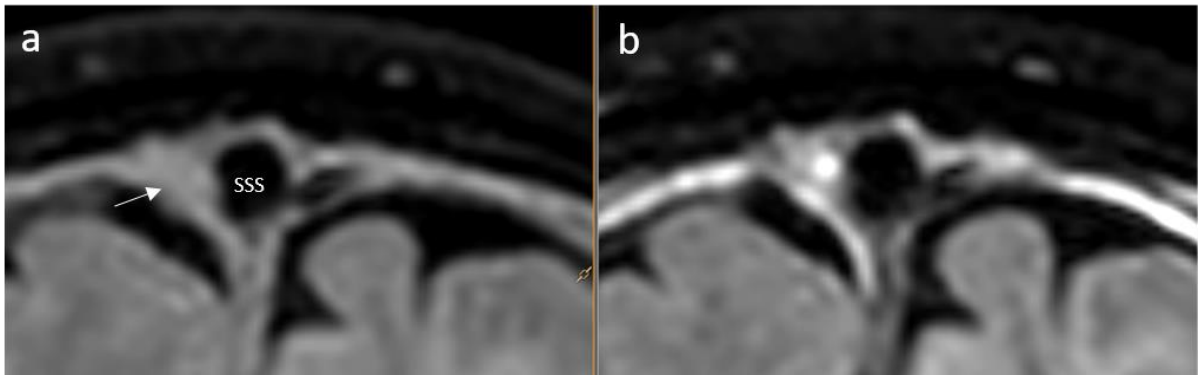

Figure 1-2 The appearance of PSD (white arrow) on a T2-FLAIR coronal image in a 16 yr old M with post-operative medulloblastoma a) before and b) after intravenous gadolinium. SSS= superior sagittal sinus

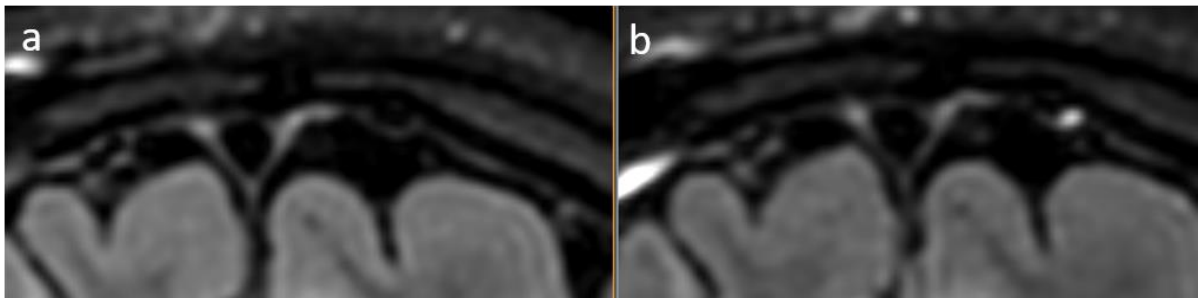

Figure 1-3 The appearance of PSD on a T2-FLAIR coronal image in a 14 yr old F with mild traumatic brain injury a) before and b) after intravenous gadolinium.

1.3.10 Meningeal lymphatic vessels and clearance of ISF

Lymphatic fluid in the body originates from the extracellular fluid that enters specific lymphatic vessels that lie within body organs except inside the central nervous system (57). Lymphatic vessels lie alongside venules and veins and have a well-defined parietal structure. Lymph fluid generally contain an ultrafiltrate of plasma proteins and metabolic waste that is a combination of the interstitial fluid that contains products of tissue metabolism and catabolism, apoptotic cells, cellular debris, and circulating immune cells (58). The fluid reaches pivotal lymph nodes where endogenous and exogenous pathogens are presented to immune cells. Maintaining optimal lymph role is critical for optimal macromolecule uptake from interstitial fluid, removal of cellular debris and immune cell-trafficking. This build and maintain immunologic tolerance, immunity to a variety of pathogens and reduce inflammation (59).

While the first description of lymphatic vessels in the brain was described by Paolo Mascagni in 1784, it has only recently been accepted that traditional lymphatic vessels exist within the dura mater in animals and human adults (60–65).

The development of body lymphatic vessels in mice initiates at day 9.5 which is equivalent to 27 days in humans (66) with the coalescence of venous endothelial cells. Subsequent processes characterized by sprouting, lymphangiogenesis, further develop lymphatic vasculature. Meningeal lymphatic vessels however appear just before birth and continue to mature postnatal. These vessels are seen around the foramina of the skull base alongside blood vessels and nerves. Meningeal lymphatic vessels grow alongside the jugular veins and enter via the jugular foramen towards the sigmoid sinus, the SSS and extends onwards to the anterior portion of the sinus. Development of these vessels progresses after birth induced by lymph flow (32).

1.3.11 Development of the brain vasculature

Primordial islands of angioblasts appear within the leptomeningeal plexus of endothelium-lined sinusoidal channels at about 24 days of gestation within the meninx primitiva (67). These islands progressively become canalized. These channels arise at the skull base and grow towards the cerebral convexity in four phases: first, endothelial cells of the leptomeningeal plexus make contact with the external basal lamina of the cortex overlying the marginal glial. The cells align with the marginal glia and their basal lamina becomes continuous with the cortical basal ganglia. Such contact points determine future perforating sites for developing filopodia; second, the filopodia derived from the leading endothelium penetrates into the cortex together with the basal membranes of the vascular and the cortex to a certain depth (68). The leading cells and the endfeet disintegrate leading to filopodia devoid of basal lamina to freely penetrate the neural tissue; third, continuous advancement of endothelial cells leads to the formation of anastomosis to form a subependymal matrix which provides blood to the germinal matrix. In the latter half of the gestation, as the brain continues to expand in surface area and the distance between the ventricular wall and the pia mater grows, the newer tissue is supplied by increasing number of shorter penetrating vessels to meet the growing demands of the developing cortex (69); fourth, proliferation and progressive canalization occurs and creates a new capillary in situ. At the point of entry, glial elements surround the cortical capillary wall and a distinct space is identified between the vessels wall and the cerebral cortex. Collagen fibers and protoplasmic prolongations of leptomeningeal cells fill this shallow space which represents the embryonic origin of the Virchow-Robin or PVS.

By mid-gestation, the leptomeningeal arteries gradually develop the tunica media which is robust and well-defined in the vessels at the base with respect to the ones lying over the convexity. Leptomeningeal vessels lie within the subarachnoid space between the pia mater and the barrier layer of the arachnoid. Smaller branches from these arteries penetrate the pia mater. A distinction is made between the striatal and extrastriatal arteries because of their different

origins and branching patterns. Striatal arteries arise from the inner arterial circle, circle of Willis and supply blood to the thalamus and basal ganglia whereas the extrastriatal arteries are branches of the leptomeningeal arteries over the convexity that supply blood to the telencephalon. Striatal arteries are ventriculofugal arteries whereas the extrastriatal vessels are centripetal (67,70).

Striatal vessels are clearly discernible by 24 weeks of gestation. The development of the tunica media is centripetal in continuity with that of the leptomeningeal vessels. The tunica media of the striatal arteries starts to develop earlier in gestation. Extrastriatal arterial trunks arise from leptomeningeal arteries and penetrate perpendicularly or at right angles, the surface of the pia mater. Some reach the ventricular surface and others divide into smaller capillaries. Branching patterns of the striatal vessels are distinct from the extrastriatal vessels. The tunica media of the extrastriatal arteries does not develop until the final weeks of gestation. Muscular development occurs from the periphery towards to the center.

1.3.12 Perivascular spaces

PVS were first noted by the father of French gerontology, Maxime Durant-Fardel in 1843 (71)He specifically described PVS as *"the cavities that lodged dilated blood vessels having returned to their normal size after death"* and so distinguished them from cerebral lacunes which are a result of a pathologic insult to the brain parenchyma. In 1851, Rudolph Virchow, the father of modern pathology was the first to provide a detailed description of spaces surrounding the outer and middle lamina of arterial blood vessels (72). These findings were later confirmed by a French physician Charles-Philippe Robin in 1859 describing detailed information revealed under a microscope (73)(73).

Before the development of MRI, the anatomy of PVS was studied using histological specimens viewed under electron microscopy. In 1923, Weed proposed that fluid could freely communicate between the subarachnoid space and the PVS surrounding penetrating arterioles (55). However, subsequent tracer studies, in which radiolabeled tracers were injected into the rat brain parenchyma, detected the tracers within the PVS but not in the bulk CSF (74). This finding suggested that interstitial fluid ISF does not drain into CSF spaces but instead follows PVS pathways along cerebral vessels. Electron microscopy provides evidence that a single-layer of pial cells adheres to the outer wall of the subarachnoid arteriole (75). A thin layer of collagenous connective tissue separates the pia layer from the underlying layers of smooth muscle cells in the arterial wall. Veins in the subarachnoid space are also covered by a thin layer of pia mater which is separated from the endothelium by collagenous connective tissue. PVS are spaces whose

outer walls are made up of glia limitans and the PGBM whereas the inner wall is made up of adventitial wall of the penetrating arteries and their relative basement membranes(75).

From an MRI perspective, PVS appear as CSF filled either linear or dot like structures within the white matter (WM) and the basal ganglia of the brain (Fig. 3-3). The morphology depends on the slice orientation with respect to the main length of the PVS. PVS are usually very small and under 3mm in diameter. The presence of PVS must be considered normal in a healthy subject, however when large and relatively numerous with neurological conditions, PVS tend to represent an indirect marker of neurodegeneration and neuroinflammation (Appendix A).

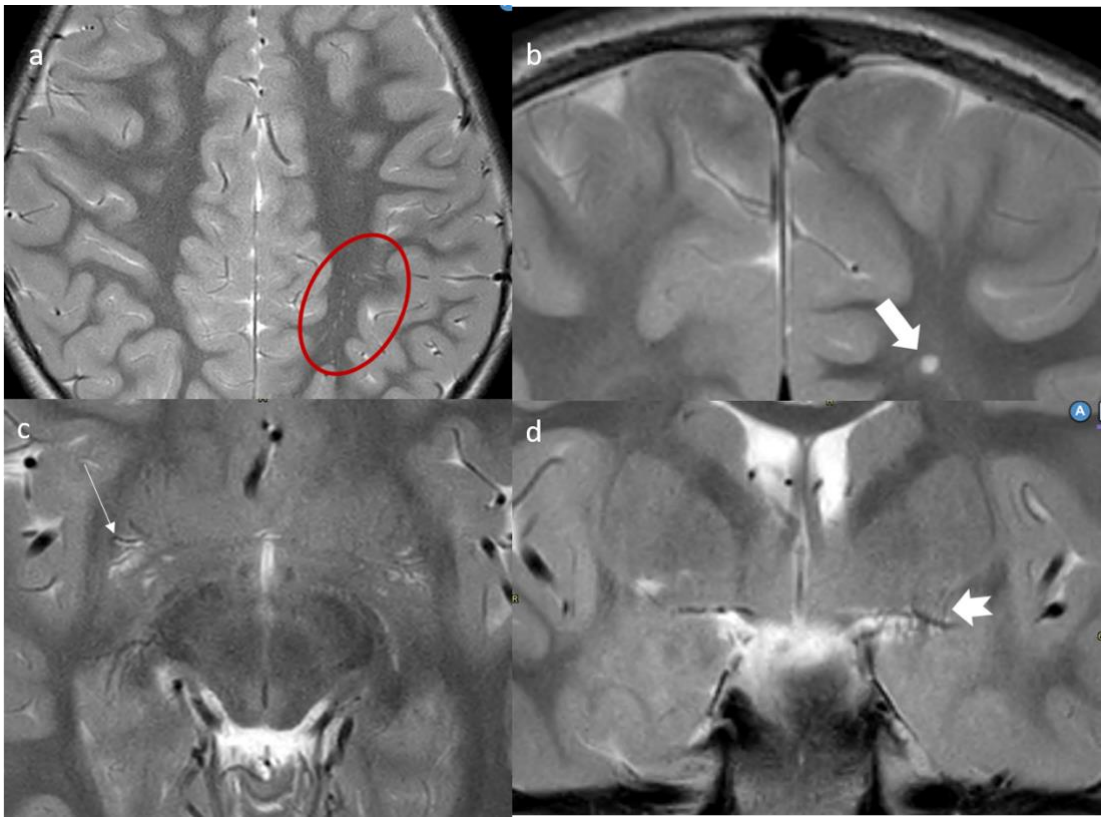

Figure 1-4 Images of perivascular spaces on T2 weighted images in the centrum semiovale (a and b) and in the basal ganglia (c and d).a) axial image showing a bunch of linear and round structures (within the red oval figure) in the white matter with a signal intensity similar to cerebrospinal fluid and b) coronal image showing an enlarged rounded appearance of a PVS (white thick arrow). c) axial image showing a sleeve of CSF filled space around lenticulostriate penetrating arteries (black linear structures) and d) coronal image shows lenticulate striate branching out of the middle cerebral artery (thick arrow) surrounding by almost virtual CSF space or PVS.

1.3.13 Extracellular matrix

In clinical practice, intracranial fluids have traditionally been considered to reside solely within the brain vasculature and CSF compartments, with limited attention to ISF. However, ISF represents the largest fluid compartment within the brain tissue**.** It occupies approximately 15-20% of the adult brain parenchyma, which in a 1400mL adult human brain is approximately 280mL of ISF (76). This percentage is higher in neonates and drops to adult levels with continuous processes of neurogenesis, gliogenesis and myelinogenesis over the first few years of life. ISF and CSF are not entirely separate; they intermingle at the tissue level, contributing to fluid and solute exchange across compartments. ISF serves as a vital medium for the exchange of solutes, gases, and metabolic waste (77). The ISF volume changes with age, brain region, hydration status, and in various disease states such as ischemia and traumatic brain injury (77,78). With aging, the ECS and ISF volumes increase as neurons and glia degenerate. The ISF circulates through the ECS, which lies between neurons and glial cells and is structured by the ECM. The ECM provides an architectural framework for the ECS and is essential for maintaining brain homeostasis (79).

The ECM is composed of several valuable proteins, including glycosaminoglycans (such as hyaluronic acid**),** chondroitin sulfate proteoglycans**,** link proteins**,** tenascins**,** laminins**,** fibronectin**,** collagens**,** and matrix metalloproteinases (79,80)**.** These proteins constitute the structural backbone of the ECS, providing stability, regulating synaptic plasticity, and modulating cellular adhesion. The ECM also plays a key role in remodeling the ECS after injury and supporting blood vessels. The ISF within this matrix facilitates the diffusion of essential molecules, including neuropeptides**,** neurotransmitters, and nutrients**,** while also enabling the removal of metabolic waste and toxic byproducts from the brain parenchyma (81). The ECM is a complex and dynamic network of molecules that fills the space between neurons and glial cells in the CNS. In the adult brain, the ECM is compact, stable, and rigid to support mature neural circuits and maintain tissue integrity. It is restrictive to change, has a stable level of hyaluronic acid, and presents prominent perineuronal nets around adult synapses (82). Perineuronal nets are specialized structures rich in chondroitin sulfate proteoglycans that envelop the soma and proximal dendrites of specific neurons. They play a key role in regulating neural plasticity, particularly during the critical period of development, when synaptic connectivity is at its peak (83).

1.3.14 Extracellular matrix in the developing brain

The ECM in the developing brain differs from that in the adult brain but serves foundational roles similar to those of the adult ECM in supporting and guiding neural cells. The difference in its composition, organization, and functional properties reflect the changing needs of the brain from a highly plastic, developing organ to a more stable, mature system (84,85). The developmental ECM is more dynamic and permissive for growth and remodeling. It has a higher quantity of hyaluronic acid and is looser in structure. The several components of the ECM in the developing brain facilitate cell migration, axonal growth, synaptogenesis and promotes neurogenesis. During neurulation, or early neural tube development, the neural plate and mesoderm are tightly connected and guided by laminin and fibronectin (86). During the later phase of neural development, ECM proteins regulate the neocortical size, radial glial migration and cortical folding. It has been shown that disruptions in the development of ECM proteins will lead to neurodevelopmental disorders such as ASD (87,88). Proteoglycans in the developing brain are less abundant with respect to adult brain. They are however critical in the processes of neurogenesis, gliogenesis and neuronal migration and are present in sites of rapidly developing areas (84). The percentage of water in the brain parenchyma differs between neonates and adults. At birth, term infants typically have around 88% brain water by wet weight, which declines to ≈ 85% by 6 months of age (89) (90) (91). Across major brain regions, water content remains in the mid-80% range in infants—slightly higher in cortical areas vs. cerebellum. The rapid decrease in water content occur in the first two years postnatally which is also the period of rapid growth spurt (92). This significant difference reflects the developmental stage of the brain and the higher plasticity and metabolic activity in neonates. With development into adulthood, the proportion of water in the brain decreases as the brain matures and undergoes changes in cellular composition and myelination. Myelination is a process that occurs once the both neuronal and glial cell populations have developed and this occurs during the later phase of gestation and continues post-natally. Myelin is mainly composed of cholesterol and other lipids which are hydrophobic. From an MRI perspective, changes in water content in the white matter and the gray matter tissue can be observed by ADC maps and T1, T2 weighted images. Rapid changes in signal intensity are observed in both white matter and the gray matter as myelination continues to occur and the brain tissue appears more compact.

1.4 Glymphatic system in the developing brain

Using an in vivo two photon microscopy technique, Iliff et al., demonstrated that fluorescent dextran tracers injected into the cisterna magna rapidly moved along paravascular spaces surrounding arteries, penetrating deep into the brain parenchyma within 30 minutes in live mice (93). Smaller tracers (e.g. 3 kD dextran) diffused into the interstitium, while larger tracers (e.g. 2000 kD dextran) remained confined to perivascular corridors, indicating size-dependent distribution barriers. After exchange in parenchyma, through aquaporin-4 (AQP4) water channels—normally located on the perivascular endfeet of astrocytes— interstitial solutes travel toward paravenous spaces, eventually exiting into CSF compartments or systemic circulation via AGs and meningeal lymphatics (64). They also demonstrated that in mice lacking AQP4, the clearance of tracers from the interstitial space was significantly impaired. This finding highlighted the crucial role of astrocytes in brain solute clearance and led to the naming of this pathway as the *glymphatic system*. The glymphatic system has been extensively examined in a variety of adult neurological disorders and it is widely accepted to play an essential role in the development of neurodegenerative diseases such as Alzheimer's disease.

Serial MRI examinations conducted after the intrathecal administration of gadolinium-based contrast agents have significantly advanced our understanding of the glymphatic system in vivo within the adult human brain (94). Following injection of gadolinium into the lumbar thecal sac, the contrast agent in CSF, is observed to reach the cranial SAS within several hours, subsequently entering the brain parenchyma. This observation confirmed the movement of CSF and solutes through an extravascular pathway into the parenchyma, perhaps via PVS (95). The same group also showed that patients with normal pressure hydrocephalus retained gadolinium in the brain parenchyma for a longer time with respect to healthy adults, indicating that the glymphatic system is compromised under pathological conditions (96). Additionally, the intrathecal gadolinium introduced into the cranial SAS is also detected in the PSD, where meningeal lymphatics have been identified, suggesting the CSF along with solutes enters PSD (97). The role of PSD has evolved in the recent years and is likely to serve as a neuroimmune hub for immunesurvellaince in addition to facilitating CSF drainage from the SAS (98,99).

The glymphatic system in the developing brain is an emerging area of research with significant implications for understanding brain maturation**,** waste clearance**,** and early neurological health**.** While the glymphatic system is well studied in adults, especially in the context of aging and neurodegeneration, its function during development is less understood but increasingly recognized as important. The glymphatic clearance depends on polarized AQP4 expression in astrocytes, which emerges gradually during late gestation and postnatal life, particularly over the first few weeks to months (100). AQP4 channels are first detectable at around

14 weeks gestational age in the archicortex, and appears in the neocortex ~6–7 weeks later. By term in human babies, AQP4 channels are detectable in perivascular astrocyte endfeet, at the ventricular wall, pial surface, and around developing capillaries (101). In humans, AQP4 expression begins as early as 13 weeks of gestation in the hippocampal archicortex and expands to the neocortex by around 25 weeks (102). This spatial pattern aligns with the anatomical establishment of glymphatic structures, suggesting that the scaffold for glymphatic flow is present before birth. However, functional glymphatic activity—dependent on the polarized localization of AQP4 to astrocyte end-feet—appears to mature later, particularly after birth, as shown in rodent models (103). In mice, AQP4 becomes polarized by postnatal day 3 and continues to increase in expression and organization through early life, coinciding with improved glymphatic flow (104). Disruptions to AQP4 development, such as neonatal stress, can impair this system long-term, reducing brain waste clearance efficiency into adulthood (105). These findings indicate that the neonatal period is critical for establishing glymphatic competence and that AQP4 is a crucial molecular gatekeeper of this system's maturation (106).

During the first two years of life, the mechanisms of brain water and solute clearance—including CSF and ISF drainage pathways—are not yet fully mature (107). While adult brains utilize multiple well-established routes (e.g., arachnoid villi, perineural routes, meningeal lymphatics, and the glymphatic system), these pathways develop postnatally and undergo significant remodeling during infancy. Arachnoid granulations are rudimentary at birth and become prominent only later in life (37,108). The meningeal lymphatics appear to be functionally immature at birth, maturing over the first postnatal year in rodents and likely later in humans (28). Therefore, given that brain water content decreases significantly (~88% to ~78%) during the first two years, yet the mature drainage systems are not fully operational, how water efflux is achieved remains incompletely understood.

It is suggested that alternative pathways for CSF drainage such as perineural pathways may be more active in the child (107). The most prominent route for CSF efflux from the SAS in neonates and early infancy appears to along cranial nerves, especially the olfactory nerves (via the cribriform plate) and optic and vestibulocochlear nerves. These pathways drain into nasal lymphatics, deep cervical lymph nodes, and extracranial tissues. Animal and limited human studies show high reliance on these routes in the absence of mature arachnoid villi (109,110).

1.5 Intramural periarterial drainage pathway in the developing brain

The IPAD refers to the movement of interstitial fluid and solutes (including potentially toxic substances like amyloid-beta) along the BM of arteries in the brain (74). ISF containing waste products drains along the BM of capillaries and arteries. This drainage moves in the opposite direction to blood flow - *from the brain parenchyma outward,* through the walls of cerebral arteries. The solutes are transported through the smooth muscle BMs of these arteries and eventually reach the cervical lymph nodes**,** outside the brain (111). The pumping action of the vascular smooth vessels, also called vasomotion, is the primary driving force for ISF and solute removal along IPAD (112–114). IPAD is one of the primary mechanisms by which amyloid-β **—**a protein implicated in Alzheimer's disease—is cleared from the brain. It is also implicated in the removal of amyloid beta in cerebral amyloid angiopathy (115–117).

Very little research has directly investigated IPAD during early development or neonatal stages specially in the human species. IPAD depends on well-formed BMs, vascular smooth muscle cell maturity, vasomotion and neurovascular coupling—features that are still under development in utero and postnatally**.** Therefore, while the anatomical components of IPAD start forming in early development, its efficiency maybe less in neonates and infants until vascular maturation, gliogenesis and neurovascular regulation are complete. But this remains to be empirically demonstrated.

The BM is a specialized ECM that plays a critical role in vascular integrity**,** BBB formation**,** and neurovascular unit function (118). Vascular BM maturation in the developing human brain refers to the structural and molecular changes that occur in the BM of cerebral blood vessels during brain development. The major ECM proteins that constitute the BM are collagen IV, laminin, nidogen and perlecan which are synthesized by pericytes, endothelial cells and astrocytes (119). In rats, astrocytes continue to proliferate reaching final adult numbers rapidly by the first few postnatal weeks (120). Studies show BM elements such as laminin and agrin are well expressed at birth, but astrocyte-endothelial interactions and BM refinement continue through the first 2–3 postnatal weeks in rodents, corresponding to early infancy in humans (121,122). In the developing mouse, vascular BMs in the brain mature structurally and functionally starting prenatally and continuing postnatally (123). Both pericytes and astrocyte development are key in the formation of BMs (124). The growth of cerebral vasculature continues to occur post-natally and parallels the development of nerve tissue (125) (126). Knockout mice models have revealed the importance of these proteins in the development of BM and the BBB (127). BM density and thickness increase progressively during infancy, driven by secretion from endothelial cells, pericytes, and eventually astrocytes. Specific mutations in genes that code for

collagen IV, laminins, nidogen and perlecan can lead to various degree of consequences such as vascular defects, BBB disruption, intracerebral hemorrhage and embryonic death (127).

In premature babies the vascular BM is thinner, less well-organised and often incomplete. The major BM components, laminin, collagen IV, perlecan are expressed at lower levels compared to full term neonates. The astrocytes are lesser in number and the BBB is immature (8). Since gliogenesis, neurogenesis, vascular development, synaptogenesis all occur in a well-orchestrated manner in utero and postnatal, newborns and infants are particularly vulnerable due to immature BBB, poor vascular smooth muscle contractility and ischemia (125,128). In addition, immature hemodynamics, lower arterial pulsatility will also affect IPAD in the young developing brain. Although empirical, there is strong reason to believe that the efficiency of IPAD and glymphatic system is poor in early stages of human life. Understanding this pathway in the developing brain may provide further insights into neurodevelopmental disorders and potential early-life risk factors in neurological disorders.

1.6 Autism spectrum disorder as a model of altered CSF circulation

1.6.1 Overview

Autism spectrum disorder (ASD) is a complex neurodevelopmental disorder characterized by restricted and repetitive stereotypical behaviors, verbal and non-verbal communication deficits and lack of social skills according to the Diagnostic and Statistic Manual V (DSM-V) (129) (Appendix B). It was first coined in 1911 by a German psychiatrist Eugen Bleuler who described autism as a subject's "inner life" which is not accessible to observers (130). Developmental disruption may occur in critical phases causing shifts, extension or disruption of such periods leading to difficulty in sensory processing, social bonding and language acquisition. Both inherited genetics and environmental factors, such as those associated with prenatal maternal environment, interact in a complex manner and contribute to ASD (131). Maternal factors such as obesity, infection during pregnancy, diabetes mellitus, use of antibiotics are some of the factors implicated that can hinder development during critical phases of fetal life specially in genetically susceptible individuals (132). Exposure to pollutants and pesticides may also Potential pathways of disruption are dysregulation of the immune system, oxidative stress and gut-microbiome interactions (133,134).

1.6.2 Neurodevelopmental hypothesis

The neurodevelopmental hypothesis views ASD as a disorder of brain development, where early disruptions in neurogenesis, synaptogenesis, and circuit formation lead to the behavioral

symptoms of autism. It integrates genetic, molecular, and systems-level evidence to explain how early differences in the brain can result in the diverse and complex features of ASD (135). Children with ASD may show increased brain volume reflecting excessive proliferation of neurons, abnormal perfusion and delayed pruning. Abnormal genes such as SHANK3, NRXN1, NLGN3/4 are involved in synaptic structure and signaling**,** pointing to altered excitatory/inhibitory balance in the brain (136). Functional and structural MRI studies have suggested abnormal connectivity and brain growth volume anomalies identifying patterns that may explain the intense focus on details and difficulty integrating social or contextual information (137,138). In addition, environmental risk factors may interact with genetic susceptibility during brain development leading to the formation of aberrant neuronal and glial connections.

1.6.3 Neuroimmunological hypothesis

The neuroimmunological hypothesis suggests that immune system disturbances—particularly during critical periods of brain development—can disrupt neural circuits and lead to the behavioral and cognitive features of ASD (139). This perspective does not negate genetic or other environmental contributions but highlights the immune system as a key mediator between genetic susceptibility and environmental exposures (140). Several levels of immunological anomalies, both cellular and humoral immunity, have been described in ASD. Elevated levels of pro-inflammatory cytokines (like IL-6**,** TNF-α, and IL-1β) have been found in the blood, cerebrospinal fluid, and postmortem brains of individuals with ASD (141–143). These cytokines can influence neurodevelopment, synaptic pruning, and brain connectivity (144,145). Maternal autoimmune response to fetal antigens may cause microglial activation affecting synaptic function and connectivity (146). Environmental pollutants such as pesticides also play a role in neurodevelopmental disorders (147). Other exogenous factors that affect neuronal development are related to maternal risk factors such as obesity, autoimmune disorder, diabetes, and infections (146). The underlying pathways of these risk factors remain uncertain, with varying levels of evidence implicating immune dysregulation, mitochondrial dysfunction, oxidative stress, gut microbiome alterations, and hormonal disruptions.

Genes involved in immune function (e.g., major compatibility complex**,** complement system**,** cytokine genes) may increase susceptibility to ASD in the presence of environmental triggers (148). Both genetic susceptibility and a cascade of neuroinflammatory response to external stress triggers appear to result in early onset of behavioral abnormalties. Many of these processes may start at the fetal stage and during the entire gestational period.

Several neuroradiological abnormalities have been identified in children with ASD. However, most qualitative findings are non-specific and inconclusive for diagnostic purposes.

Reported abnormalities include aspecific signal changes in white matter, enlarged PVS, anomalies in the corpus callosum, increased volume of SAS, cerebellar abnormalities, and associated Chiari malformations, along with alterations in cranial volume when compared to healthy controls (149). While these changes are indicative of underlying pathologic processes, it remains uncertain whether they serve as markers of neurodevelopmental processes or are linked to ongoing neuroinflammatory activity (150).

A more consistent MRI finding is that children with ASD have an increase in CSF volume and in particular the extra-axial CSF (ea-CSF) is larger in ASD than in typically developing children (151). This has also been suggested as a possible marker in infants who are at a high risk of developing ASD in the first two years of life (152). Garic et al., also recently provided evidence that ea-CSF is directly related to the presence of enlarged PVS in neonates and infants (153).

With our current understanding of CSF dynamics and its relationship to ISF, PVS, and meningeal lymphatics, ASD presents a valuable model for investigating altered CSF circulation. The current work is focused on quantifying PVS and PSD and examining their correlation with CSF volume and disease severity.

Chapter 2 Paper 1: Cerebral Vessels: An Overview of Anatomy, Physiology, and Role in the Drainage of Fluids and Solutes.

This chapter is the Accepted Manuscript of the published version that appears in its final form in Frontiers in Neurology. The full reference is: Agarwal N and Carare RO (2021) Cerebral Vessels: An Overview of Anatomy, Physiology, and Role in the Drainage of Fluids and Solutes Front. Neurol. 11:611485. The text, spelling, and references for this paper are original as in the published article, while the formatting has been slightly modified to improve readability. To access the final edited and published work see DOI: 10.3389/fneur.2020.611485" (111)

Chapter 2

Abstract

The cerebral vasculature is made up highly specialized structures that assure constant brain perfusion necessary to meet the very high demand for oxygen and glucose by neurons and glial cells. A dense, redundant network of arteries is spread over the entire pial surface from which penetrating arteries dive into the cortex to reach the neuro vascular units. Besides providing blood to the brain parenchyma, cerebral arteries are key in the drainage of interstitial fluid (ISF) and solutes such as amyloid-beta. This occurs along the basement membranes that surround vascular smooth muscle cells, towards leptomeningeal arteries and deep cervical lymph nodes. The dense microvasculature is made up of fine capillaries. Capillary walls contain pericytes that have contractile properties and are lined by a highly specialized blood brain barrier that regulate the entry of solutes and ions and maintain the integrity of the composition of ISF. They are also important for the production of ISF. Capillaries drain into venules that course centrifugally towards the cortex to reach cortical veins and empty into dural venous sinuses. The walls of the venous sinuses are also home to meningeal lymphatic vessels that support drainage of cerebrospinal fluid (CSF), although such pathways are still poorly understood. Damage to macro and microvasculature will compromise cerebral perfusion, hamper the highly synchronized movement of neurofluids, affect drainage of waste products leading to neuronal and glial degeneration. This review will present vascular anatomy, their role in fluid dynamics and a summary on how their dysfunction can lead to neurodegeneration.

Chapter 2

Introduction

Damage to cerebral vasculature and reduction in cerebral perfusion initiates a cascade of events that rapidly leads to disturbed cellular homeostasis and death of neurons and glial cells (154). Cerebral arterial network of vessels is unique in its anatomy and its flow dynamics is inextricably intertwined with those of other fluids such as venous blood, cerebrospinal fluid (CSF) and the interstitial fluid (ISF) (155,156). Emerging evidence regarding the role of cerebral vasculature in the drainage of solutes and fluids, adds to the complexity of the overall interaction with neurofluids.

The arteries of the brain have a dual function: to supply oxygenated blood to neurons and glia and to drain ISF. Neurons and glial cells are constantly "at work", even during rest, and this very high demand for oxygen and glucose requires a steady supply of oxygenated blood. Histological and tracer studies reveal the intricate relationship of cortical arteries with meningeal sheaths and the constitution of perivascular compartment and spaces, that provide a pathway for inflow and outflow of ISF (69,74,75). Cerebral capillaries are considered important sites of CSF and ISF production and absorption. Capillaries drain into venules that are hierarchically organized and run centrifugally towards the cortex. All venous drainage occurs through dural venous sinuses that drain towards the neck veins. The walls of dural venous sinuses are also home to meningeal lymphatic vessels (65,157), with a role in the drainage of CSF. In this review, a brief overview of the current evidence for the anatomy and function of vessels in the brain will be provided, followed by a summary of mechanisms of interaction of what we term "neurofluids": blood, CSF and ISF (155). A disruption of such mechanisms will trigger a series of pathological events such as microvascular injury, failure of ISF drainage, local deposition of amyloid-beta as cerebral amyloid angiopathy (CAA), focal ischemia and demyelination.

The arterial and capillary systems

The brain parenchyma is supplied by two internal carotid arteries (ICA) and two vertebral arteries (VA). The ICA enters the skull-base through the carotid canal, located in the petrous portion of the temporal lobe. It pierces through the dura mater at the level of the cavernous sinus and bifurcates within the subarachnoid space (SAS) into middle cerebral arteries and anterior cerebral arteries. The ICA carries approximately 80% of the total blood to the brain. The vertebral arteries enter the vertebral foramina at the level of C6, they exit out of C1 foramina, loop around the posterior arch of the atlas as they enter the foramen magna and lies on the ventral surface of the brain stem to form the basilar artery (BA). The BA terminates into two posterior cerebral

arteries. The anterior (ICA and its branches) and the posterior circulation (VA and its branches) arteries come together at the base of the skull to form the circle of Willis that lies in the cisternal space (158).

A rich, anastomotic network of leptomeningeal arteries spreads over the pial surface from which numerous branches (arterioles) sprout out and pierce the glia limitans to dive into the cortex at approximately right angles to it. From a structural point of view, both pial arteries and penetrating arterioles lack an external elastic lamina but leptomeningeal arteries retain an internal elastic lamina (159) The gray matter (GM) has a larger number of arterioles with respect to those in the white matter (WM) with a ratio of 8:1, which is proportionate to the elevated energy demand of the more cellular GM (160,161). Penetrating arterioles are completely encased by a sheet of pia mater which reflects off the cortical surface separating them from the surrounding SAS and from the brain parenchyma (75) (Fig. 2-1). However, around the perivascular compartment of the arterioles in the WM, there are two such sheaths, creating a potential space for the accumulation of edematous fluid (162). At capillary level, direct observations under the electron microscope in a variety of species reveal that the basement membrane of the pial sheath and the basement membranes of the astrocytes (glia limitans) fuse together to create a perivascular compartment, or periarterial space, filled with extracellular matrix which is not continuous with the SAS (75,163) and referred to as the "perivascular space" (PVS) (Fig.1). Indeed, PVS, or more appropriately the periarterial spaces, are not visible within the cortical GM even under pathological conditions whereas they are seen in the WM both in histological specimens and on neuroimaging (162,164). Changes in the walls of capillaries and arterioles associated with ageing, hypertension or diabetes mellitus lead to small vessel disease (SVD) and vascular dementia (165,166).

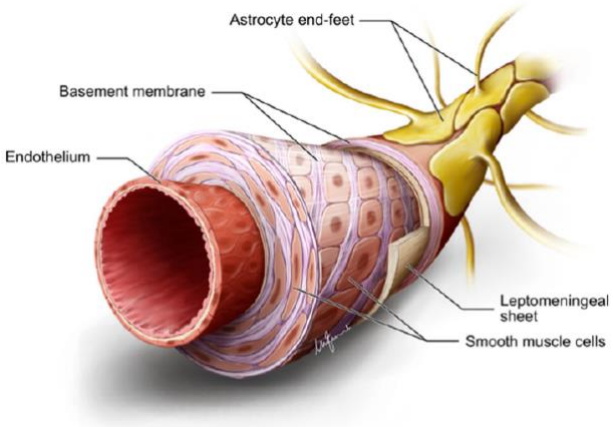

Figure 2-1 Diagrammatic summary of the structure of an arteriole in the grey matter.The endothelium hosts the blood brain barrier. There are several layers of smooth

muscle cells separated by basement membranes. The adventitial leptomeningeal sheath has its own basement membrane that fuses with the basement membrane of astrocyte end feet, to form a perivascular compartment, or perivascular space. Diagram drawn by Marco Fanuli.

Pial surface arterial network are richly innervated by sympathetic nerves from the superior cervical ganglion, sphenopalatine, otic and trigeminal ganglia that release several neurotransmitters and neuromodulators such as vasoactive intestinal peptide, nitric oxide synthase, acetylcholine, norepinephrine and substance P (167). This innervation also termed "extrinsic" innervation ends in the pre-capillary segment and more precisely where the PVS terminates. The extrinsic innervation is primarily responsible for a prompt myogenic response to temporary pressure differences. According to Poiseuille's law, a change in radius directly affects resistance to flow to the fourth power, thereby modulating blood flow instantly and efficaciously (168). Intraparenchymal arterioles are innervated by nerves arising from the nuclei of basal forebrain such as the locus coeruleus, nucleus basalis of Meynert and raphe nuclei in the brain stem that release norepinephrine, acetylcholine and 5-hydroxythyrosine as well as other neuropeptides either directly to the walls of capillaries or indirectly via local interneurons and astrocytes (167,169). Such nerve endings are likely to control intrinsic spontaneous contractile activity of VSMC in the tunica media, also termed "vasomotion". Vasomotor oscillations form the basis of ultra-slow 0.1Hz wave activity in the microvasculature independent of neuronal activity (170,171).

A dense capillary anastomotic network characterizes the GM and varies with its depth (172). About 50-60% of total blood volume is within the capillaries (172). Capillary walls are made up of a single layer of endothelial cells, pericytes and a basal lamina made up of collagen type IV, heparan sulphate proteoglycans, laminin, fibronectin, and other extracellular matrix proteins, in various proportions and with different isoforms depending on the type of vessel (173–175)(173,174). The endothelial cells are bound together by tight junction proteins such as claudins and occludins, creating a highly regulated blood brain barrier (BBB) that restricts transcellular flux of ions and hydrophilic solutes shielding the internal parenchymal milieu from even the slightest fluctuations in the osmolarity of surrounding tissues and blood plasma (176,177). The endothelium contains a spectrum of receptors essential for the entry and efflux of peptides, such as low density lipoprotein related protein-1 (LRP-1) or ATP-binding cassette transporters which are essential for the efflux of soluble amyloid-beta from the brain

parenchyma (178). The abluminal surface of the capillaries is continuous with astrocytic end-feet (or glia limitans), containing aquaporin-4 (AQP4) water channels.

The venous system

The parenchymal microvasculature drains deoxygenated blood centrifugally from the ventricular ependymal surface towards the cortical pial surface, via medullary venules and veins that are arranged hierarchically and centrifugally from the ventricular ependymal wall towards the cortex (179). Large cortical bridging veins, such as the vein of Labbè and the Trolard vein, empty into the superficial dural venous sinuses (180). The SSS subdivides into right and left transverse sinus and continues directly via sigmoid sinuses into the internal jugular veins, extracranial neck vessels and the intra- and extra-spinal venous plexi, conveying deoxygenated blood to the right atrium (181–183). Deep internal veins form the inferior sagittal sinus, the vein of Galen and the straight sinus to drain into the SSS posteriorly. Anteriorly venous drainage occurs through the cavernous sinus, sphenopetrosal sinuses and sigmoid sinuses. Several anatomical variations exist, and veins can vary in number, size, symmetry across hemispheres and also in their extracranial venous drainage patterns, adding to the complexity of the cerebral venous system (184). It is important to note that dural venous sinuses are valveless making cephalad, retrograde flow possible in cases of obstruction to downward flow (185).

Surrounding each parenchymal arteriole are eight venules (69). Venules typically have a larger lumen area and a thinner vessel wall with respect to arterioles (186). Exiting venules in the cortex are surrounded by an incomplete layer of pia mater (75). Paravenous spaces communicate with the SAS directly. The first reports of the presence of lymphatic vessels in the dura mater were reported in 1787, while histologic evidence of their existence was provided much later (187). More recently lymphatic channels were described lining the dural venous sinuses that appear to be additional routes for the drainage of fluids and cells towards the deep cervical lymph nodes (65,157). Lymphatic channels are also found in the cribriform plate that drain fluids, cells and solutes via nasal lymphatics towards the superficial cervical lymph nodes (188).

The production and drainage of cerebrospinal fluid and interstitial fluid

Our classic understanding of CSF fluid production and absorption is being challenged as new evidence suggests that CSF production also occurs at other sites such as the capillary endothelial surface, as formulated by the Bulat-Klarica-Orešković hypothesis (189). Almost 80% of CSF is secreted by fenestrated capillaries in the choroid plexi at a rate of approximately 0.3-

0.4ml/min for a total production of 430-580ml daily. CSF secretion across the blood-CSF barrier, depends on hydrostatic and osmolarity gradients that exist between the plasma and the intraventricular CSF fluids. CSF is made up of 99% water, some ions and negligible quantities of proteins and glucose. Arachnoid granulations found in the dural venous sinuses are traditionally recognized to play a prime role in CSF reabsorption. However, the contemporary presence of the meninx *primitiva* and the lack of arachnoid granulations in the fetus suggests that there must be alternative routes for its absorption (188,190).

There are multiple sources of ISF production such as filtration across the capillaries via the development of hydrostatic and osmotic pressures across the endothelium, secretion through choroid plexi and cellular metabolism (108,191). ISF fills the extracellular or interstitial space (ECS). This space contains extracellular matrix (ECM) which is made up of glycosaminoglycans, glycoproteins (e.g. laminins, collagen, chondroitin, fibronectin) and proteoglycans (e.g. hyaluronic acid, heparan sulfate). Such an environment determines a negatively charged ambient necessary for cellular communication, volume transmission, immunosurveillance and a binding capacity for solutes to be transported around brain areas. ECS occupies around 15-20% of the total brain volume and this volume can change in physiologic and pathologic conditions such as sleep, under anesthesia and stroke (192–195). ISF is also the primary fluid medium for waste removal, however the presence of BBB notably restricts movement of proteins across the capillaries, which suggested that there must be alternative pathways. Bulk flow of ISF through the brain parenchyma was proposed as a route to flush out waste products and fluids towards the ventricular ependymal walls (196). In the past decade, multiple waste clearance pathways have been characterized in the brain: the glymphatic pathway, intramural periarterial drainage pathway (IPAD), flow along cranial nerves and meningeal lymphatics along the dural venous sinuses (74,93,190), still extensively debated (197,198). The glymphatic system proposes that CSF from the SAS, recycles along the para-arterial spaces and enters the brain tissue via astrocytic AQP-4 water channels. CSF intermingles with ISF which flows towards paravenous spaces via bulk flow thus flushing out fluids and solutes from the brain (3,199). However, diffusion rather than bulk flow may be the likely principal mechanism for flow with an unclear role for AQP-4 channels (191,200–203). Also, the mechanism of unidirectional CSF flow along intraparenchymal para-arterial spaces remains debatable as arterial pulsations alone do not determine such flow (204). Furthermore, the glymphatic hypothesis does not explain why in CAA, the deposition of proteins occurs in the tunica media of arterioles and arteries, spreading to occupy the whole of the arterial wall and rarely involves veins (117,205,206).

On the other hand, tracer injection studies in animal brains have unequivocally demonstrated that one important route for ISF and solute removal is the intramural periarterial drainage pathway (IPAD). For decades, perivascular compartments have been considered to play a fundamental role in removal of waste products (187,207,208). According to this mechanism, fluids and waste products flow within the basement membranes of arterioles and arteries in the opposite direction to arterial blood flow within their lumen and is primarily driven by vasomotion (112,114,209,210). The ultra-slow frequency oscillation (< 0.1Hz) appear to be critical to clearance of solutes. Electrophysiologically observed slow wave oscillations characteristic of sleep are intricately associated with large CSF flow oscillations suggestive of vasomotion driven clearance of CSF and thereby of solutes and supportive of IPAD pathways of clearance (211).

Neurofluid physiology:

To understand the interaction between the several space-competing compartments within the cranium, we must remind ourselves of the Monro-Kellie hypothesis which remains a cardinal principle in the understanding of fluid movements (212). This hypothesis maintains that since the brain contents are enclosed in a non-expandable bony skull, the total brain volume must remain constant at all times to avoid dangerous increase in ICP (213). However, the recent discoveries of meningeal lymphatics and the understanding of mechanisms for brain waste clearance mechanisms, it has become necessary to revisit the original Monro-Kellie doctrine (214). With every systole, an increase in arterial pressure pumps approximately 700ml of oxygenated blood causing inflation of arteries, arterioles and the microvascular bed (215). This expansion of vessels will squeeze ISF and CSF from the interstitium and promote flow. The creation of a pressure gradient between the cranial SAS and the spinal SAS, will cause displacement of CSF towards the spinal SAS and facilitate venous outflow towards the extracranial neck vessels (156,216). During diastole, as the elastic vessels relax, CSF flows back with little net forward displacement. Such pulsatile forces will also create variable magnitude of brain tissue deformation, generating additional forces affecting blood flow, production and absorption of ISF and CSF. The intrinsic viscoelasticity of the brain, or brain compliance, is the capacity of brain tissue to deform in conditions of intracranial pressure changes. Such mechanical and viscoelastic properties vary in different brain regions and depends on cellular morphology, capillary distribution, the compactness of white matter axons, their orientation and ECM composition (217). These properties are different both at a macroscale (WM is stiffer than GM) and at a microscale (cortical GM is stiffer than hippocampal GM; WM in the corpus callosum

is stiffer than WM in the corona radiata) (217). WM is three times stiffer than GM accounting for differential response to compression load (218). Physiologic rheological properties of the brain can be measured in-vivo by magnetic resonance elastography (MRE) (219,220). Thus, in one MRE study, the compression of internal jugular veins in the neck was shown to increase CSF pulsatility in the brain but also to increase stiffness within the brain parenchyma in accordance with the Monro-Kellie doctrine (220).

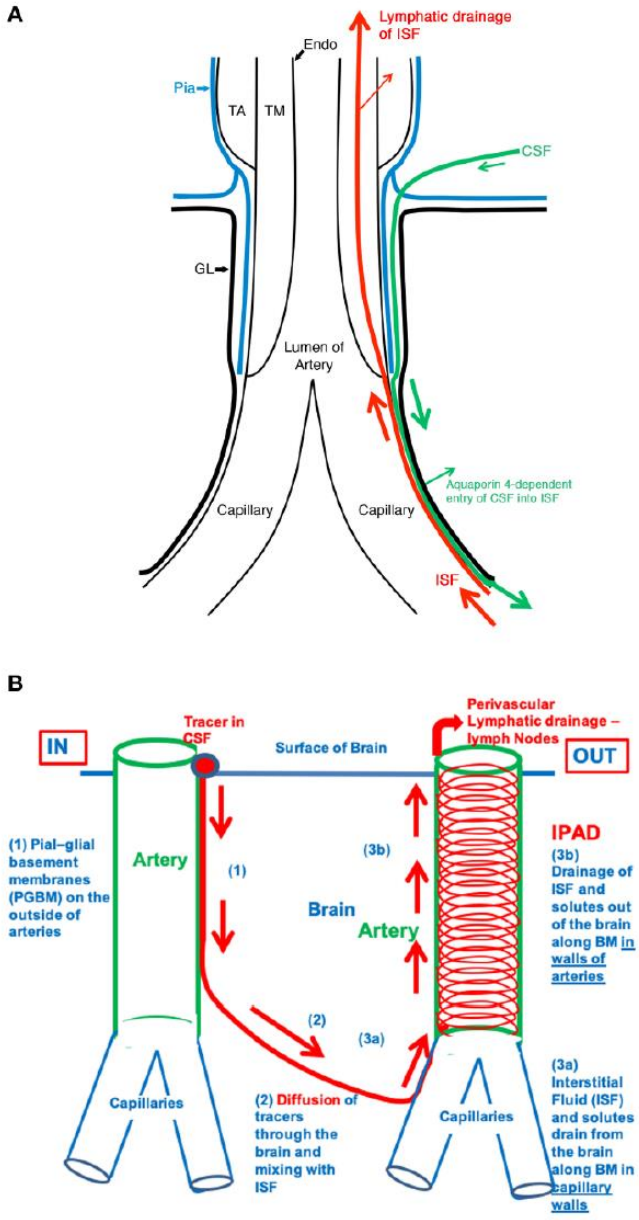

Figure 2-2 Schematic representation of the IPAD and convective influx/glymphatic systems of the brain. An artery enters the brain from the subarachnoid space and an arteriole divides into capillaries. At the top of the figure, the artery is lined by endothelium (Endo), and coated by the tunica media (TM) composed of smooth muscle cells and by the outermost tunica

adventitia (TA) composed of connective tissue. As it enters the brain, the artery loses the tunica adventitia but is still coated by a layer of pia-arachnoid (Pia) that intervenes between the artery and the glia limitans (GL) of the brain. As the arteriole divides into capillaries, the tunica media and the layer of pia mater are lost. Thus, at the level of the capillary, the glia limitans is in direct contact with the wall of the capillary. On the right-hand side of the diagram, the red arrows indicate the intramural perivascular lymphatic drainage pathway by which interstitial fluid (ISF) and solutes pass out of the brain along basement membranes in the walls of capillaries and along basement membranes surrounding smooth muscle cells in the tunica media of arterioles and arteries. Tracers in the CSF enter the brain along the pial-glial basement membrane between the pia mater and the glia limitans (indicated by a green arrow) and enter the brain parenchyma and interstitial fluid by an aquaporin 4-dependent mechanism, which is the glymphatic pathway. Reproduced with permission from Morris AWJ etal Acta Neuropathologica 2016, 131(5) 725-736.

Cerebrovascular damage and neurodegeneration

Our attention is drawn to the intricate coupling of arterial, venous, CSF and brain parenchymal dynamics, damage to anyone of them can initiate a cascade of events affecting clearance of waste products in the brain and leading thereby to neurodegeneration. Reduced cerebral perfusion is considered a potential link between vascular risk factors and the development of SVD, vascular dementia and Alzheimer's disease (AD) (221). Most important risk factors are advancing age and hypertension, both of which will hamper cerebral blood flow by directly damaging arterial walls and the microvasculature. Patients with SVD and AD often present with increased arterial stiffness, altered BBB permeability, VSMC loss, multiple fenestrations in the IEL, remodeled arterial wall basement membranes, pericyte degeneration, increased intercapillary distance, reduced capillary density, increased arteriolar tortuosity and swelling of astrocyte end-feet, ultimately reducing the capacity for optimal exchange of substances across the capillary endothelium (222–225). The inefficient transfer of pulsatile energy from the arterial bed towards the capillaries and the venous walls will disrupt hydrostatic forces. Arterial vasomotion will also be affected in several ways: direct arterial wall damage, deposition of amyloid-beta and loss of cholinergic innervation of VSMCs. The geometry of ECS changes with age and disease as free water within the parenchyma increases and toxic solutes such as amyloid-beta deposit within the extracellular space (226). In this scenario, the glymphatic/convective influx as well as IPAD will be hampered.

As the density of capillaries is lower in the white matter than in grey matter and capillary basement membranes are the entry portals for IPAD by which ISF and solutes drain from brain tissue the shortage of capillaries in the white matter may be a factor in a reduced capacity for IPAD in the white matter (227). Obstruction of CSF drainage from the cerebral ventricles results in dilatation of the ventricular system and the accumulation of fluid in the periventricular white matter in the acute stages of hydrocephalus with the slowly progressive destruction of white matter fibres and gliosis, suggesting that the capacity for IPAD is lower in the white matter compared to the grey matter (228).

Damage to veins, venules and capillaries can also characterize other subtypes of SVD such as perivenous collagenosis (229). This is characterized by concentric thickening of venular walls and pathological deposition of collagen resulting in leukoaraiosis or white matter hyperintensities (WMH) on MRI. Occlusion of venules and veins causes hypoperfusion and ischemia but also affect drainage of CSF via meningeal lymphatics (230).

There are several, albeit non-specific, MRI biomarkers such as dilated PVS, WMH, cerebral microbleeds and superficial siderosis that characterize SVD, AD and CAA that are an expression of impaired clearance of proteins and fluids, focal ischemia, deposition of amyloid-beta within the walls of capillaries and neurodegeneration (227,231–234). Neural tissue can become stiffer via several processes such as Wallerian degeneration, axonal atrophy, loss of oligodendroglial cells, microglial activation, neuroinflammation and microvascular damage, resulting in a range of microstructural changes from increased tissue water content to progressive gliosis and loss of volume.

There is substantial evidence that fluid movements in the brain are related such that damage to one compartment can lead to several events leading to neuro-glial vascular compromise (Fig 2-2). In particular, the morphological damage to macro/microvasculature or their dysfunction will most likely compromise the movement of fluids, with impact on the perfusion of the brain and the drainage of CSF, ISF, altering the homeostasis of the brain, which in turn leads to neuronal cell loss and dementia.

Funding: The authors thank the Stroke Association of UK for financial support.

Chapter 3 Paper 2: MR Imaging of Neurofluids in the Developing Brain

This chapter is the Accepted Manuscript of the published version that appears in its final form in Neuroimaging Clinics of North America. The full reference is: Agarwal N, Klein Willemijn, Tuura Ruth O'Gorman. Neuroimaging Clin N Am. 2025 May;35(2):287-302. The original content of the article has not been changed but the formatting has been slightly tweaked for easier readability. To access the final edited and published work see DOI 10.1016/j.nic.2024.12.005" (235). It brings together the current state-of-the-art on magnetic resonance imaging of neurofluids in the pediatric brain.

This work was built on the current understanding of the anatomy of neurofluids in human embryological, fetal and post-natal developmental phases.

Chapter 3

Introduction

Neurofluids, including cerebrospinal fluid (CSF) and interstitial fluid (ISF), play key roles in brain development, maintaining local homeostasis, and clearing metabolic waste (3). The glymphatic system, a recently discovered network, clears metabolic waste from the central nervous system (CNS) by utilizing the perivascular spaces (PVS) around arteries and veins for the exchange of CSF and ISF, facilitating the removal of neurotoxic substances (236). Ongoing research has established the important role of neurofluids in the developing brain, particularly in the clearance of waste products, volume transmission of neurotransmitters and myelination—processes essential for neuronal circuitry formation and cognitive optimization (4,5,7). Advances in pediatric neuroimaging, especially MRI-based quantitative assessments, are increasingly enabling the detection of both normal and pathological changes in neurofluid dynamics. This progress aims to facilitate a more precise understanding of the etiology of neurodevelopmental disorders (6). An improved understanding of this system has the potential to create novel therapeutic strategies to optimize brain health from prenatal stages through adolescence. This review aims to consolidate current knowledge on neurofluids in the developing brain and magnetic resonance imaging techniques employed in common pediatric neurological conditions.

Brain parenchyma and the interstitial space

During the embryonic and fetal periods, the brain undergoes rapid neural development, characterized by processes such as synaptogenesis, programmed cell death, dendritic proliferation, and the growth of glial cells. Throughout the first few years of life, the volumes of white matter (WM), gray matter (GM), and the ventricles change at varying rates, with the brain reaching about 90% of its adult size by age five (237). These changes in intracranial volume (ICV), WM, GM, and ventricular volume are crucial markers of normal brain development. In addition, a normal growth trajectory of the skull and the timely closure of the fontanelles is also important for understanding fluid dynamics during the first two years of life (7). Abnormalities in brain and skull growth can lead to fluid accumulation within the brain parenchyma or in the subarachnoid and cisternal spaces, compromising brain function.

The interstitial space (ISS), which contains ISF, is predominantly composed of extracellular matrix (ECM) secreted by surrounding cell membranes. This space is dynamic, involving continuous ECM secretion and degradation to support synaptic plasticity and local homeostasis (76). The ECM, consisting of components such as proteoglycans, collagen, elastin, and

glycoproteins like laminin, reelin, and fibronectin, varies between neonates and adults, reflecting the evolving ISS. ECM components play a critical role in proteolytic processes and in maintaining the viscoelasticity of the ISS, which is key for healthy brain development. As the brain develops, the ISS increases in volume and decreases in structural tortuosity, facilitating faster, low-resistance fluid flow and the transport of large molecules necessary for growth (76,238). The ECM also contributes to neural development and synaptic plasticity (80,239).

Cerebrospinal Fluid Circulation in the Developing Brain

Neurulation is completed around the fourth week of gestation, marked by the closure of the anterior and posterior neuropores. The hollow center of the neural tube then develops into the future ventricular system (12). During the first trimester, CSF is primarily secreted by the neuroepithelium lining the neural tube cavity, filling the entire structure with primitive CSF (26). The rapid increase in the intraluminal pressure causes significant expansion of the neural tube, with ventricular volume outpacing that of the brain (240). Ventricles are formed several weeks before the formation of the choroid plexi, indicating that primitive CSF is derived from sources that are different from the blood-CSF barrier at the level of the choroid plexi. The protein content of fetal CSF is considerably higher than that observed postnatally (240). In the embryonic and fetal periods, CSF plays a crucial role in transporting growth factors and nutrients, even before the formation of blood vessels. Normal values for ventricular width in fetuses, as well as premature and term infants, have been established through ultrasonography (US) and MRI.

The subarachnoid space (SAS) develops independently of the ventricular system, and the fluid it contains is not directly related to the development of the choroid plexi (188). This fluid is likely formed from the meninges, which are derived from the mesoderm (188). During the embryonic and early fetal phases, there is no communication between the fluid in the SAS and the ventricular system, as the outlets of the fourth ventricles are initially covered by a membrane (240). Measuring the thickness of the SAS is considered valuable for assessing brain development in the fetus, with standardized normal values available through MRI and US (241–243).

CSF absorption occurs due to pressure differences at the level of the arachnoid villi (244). Several other CSF drainage pathways are now established, such as through the cribriform plate, skull base neural foramina and meningeal lymphatics in the parasagittal dura. Since arachnoid granulations in the SAS mature around 18 months of age, it is likely that CSF reabsorption primarily occurs through alternative pathways such as paraneural sheaths around the cranial

nerves as they exit the basal brain, and through the cribriform plate towards the nasopharyngeal lymphatic plexus (33).

Meningeal Lymphatic System

The development of the meninges is intricately linked to the formation of brain tissues (245,246). The outermost meninx, the dura mater, lines the inner surface of the skull and is composed of dense connective tissue with two layers(43). These layers are fused except around the venous sinuses. The inner layer of the dura is loosely attached to the avascular arachnoid via trabeculae that extend to the arachnoid membrane. The pia mater, a single-celled connective tissue layer, drapes the surface of the brain and is continuous with the perivascular connective tissue surrounding the penetrating vessels. The meninges in the developing brain perform several vital functions, including the production of growth factors essential for cell survival, regulation of neuronal migration and proliferation, neurogenesis, and the development of blood vessels(247). The pial basement membrane plays a structural role, providing stability to glial processes and aiding in the migration of neuronal cells. Glymphatic activity in children is likely to differ from that in adults, as all vessel walls undergo degenerative changes with age. With increasing age the contractile force of the lymphatic vascular wall decreases, causing large diameter dysfunctional lymphatic channels (248).

Recent animal and human MRI studies have identified lymphatic channels in primates and humans (63,65,249,250). These channels are located along the walls of the dura mater, and evidence suggests that such channels are actively involved in neuroinflammatory and neurodegenerative processes (251). Meningeal lymphatic channels are directly connected to the deep cervical lymph nodes, as recently demonstrated in both contrast enhanced and unenhanced MRI studies (97,252–254). Additionally, a human autopsy study has illustrated connections between the meningeal lymphatics and the deep cervical lymph nodes(255). The development of meningeal lymphatics in humans is not fully understood; however, studies in mice have shown that all spinal and brain meningeal lymphatics develop postnatally (43,244). Peripheral lymphatic vessels drive the formation of meningeal lymphatic vessels, which enter the cranium through the skull base foramina and proceed dorsally along the superficial venous system (28). In mice, mechanical forces from lymphatic flow were reported to be needed for the postnatal formation of healthy meningeal lymphatic vessels (32).

Magnetic resonance imaging techniques

MRI has significantly enhanced our understanding of central nervous system development from the fetal period to adulthood. Within the first six months of life, changes in T1 and T2 relaxation times reveal progressive myelination of white matter structures, with the pattern of myelination closely resembling that of an adult brain by 12 months of age (256). The gradual increase in T1 signal is primarily due to the reduction in brain water content and the accumulation of myelin precursors and macromolecules (Fig. 4-1). Beyond these basic signal changes, which allow for the monitoring of temporal alterations in fluid signals in the developing brain, several advanced MRI techniques have emerged and these techniques provide deeper insights into the anatomy and physiology of fluid dynamics within the brain.

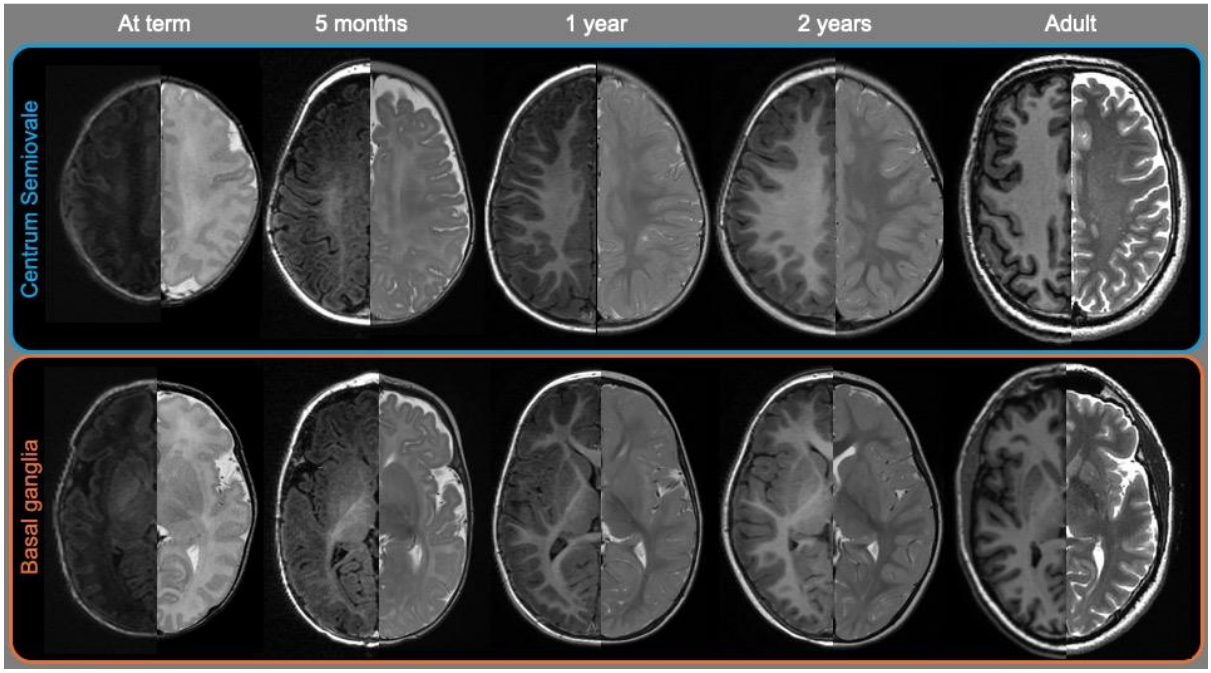

Figure 3-1 T1w and T2w images showing MRI signal of normal development over the first 2 years of life. Axial T1 (left) and T2-weighted images (right) acquired from healthy children at term, 5 months, 1 year, and 2 years, showing the changes in T1 and T2 relaxation times arising from changes in water content and myelination. Corresponding images from an adult are shown for comparison.

Imaging CSF flow: Phase contrast MRI

Phase contrast MRI (PC-MRI) methods can be used to quantify bulk neurofluid flow at a range of scales and flow rates. Typically, 2-dimensional (2D) PC-MRI methods are used, although recently 4D flow (time-resolved 3D methods) have also been applied to the brain in children as well as in adults (257,258). By appropriate choice of the velocity encoding (venc) factor, PC-MRI can be used to quantify neurofluid flow at a range of flow rates from that of CSF to that of arterial and venous blood. Recent attempts have also been made to quantify creeping flow within the dural lymphatics using PC-MRI with ultralow venc (e.g. 0.24 mm/s) 40, although the ultralow venc protocols depend on specialist, high performance gradients which are not yet widely available.

Building on earlier work examining fluid motion with echo planar imaging (259), recent developments in real-time phase contrast methods have enabled the acquisition of time-resolved data with high temporal resolution (260,261), permitting the separation of cardiac and respiratory effects on CSF flow. A series of studies using real-time PC-MRI have revealed inspiration-induced filling of the lateral ventricles in healthy adults, associated with upward (inferior to superior) motion of the CSF within the aqueduct during deep breathing (262,263), counterbalancing the increased venous flow during inspiration resulting from decreased thoracic pressure. Recent studies have also applied real-time PC-MRI in children as well as adults, reporting age- and sex-related changes in CSF flow (264). Echo planar imaging methods without velocity encoding have also demonstrated pulsatile motion of CSF in the 4th ventricle, synchronized to the blood volume changes seen in the, either during sleep (211), or with stimulation (265). In this manner, the CSF and arterial inflow to the brain balance the venous outflow, fulfilling the requirements of the Monro-Kellie doctrine (Figure 4-2).

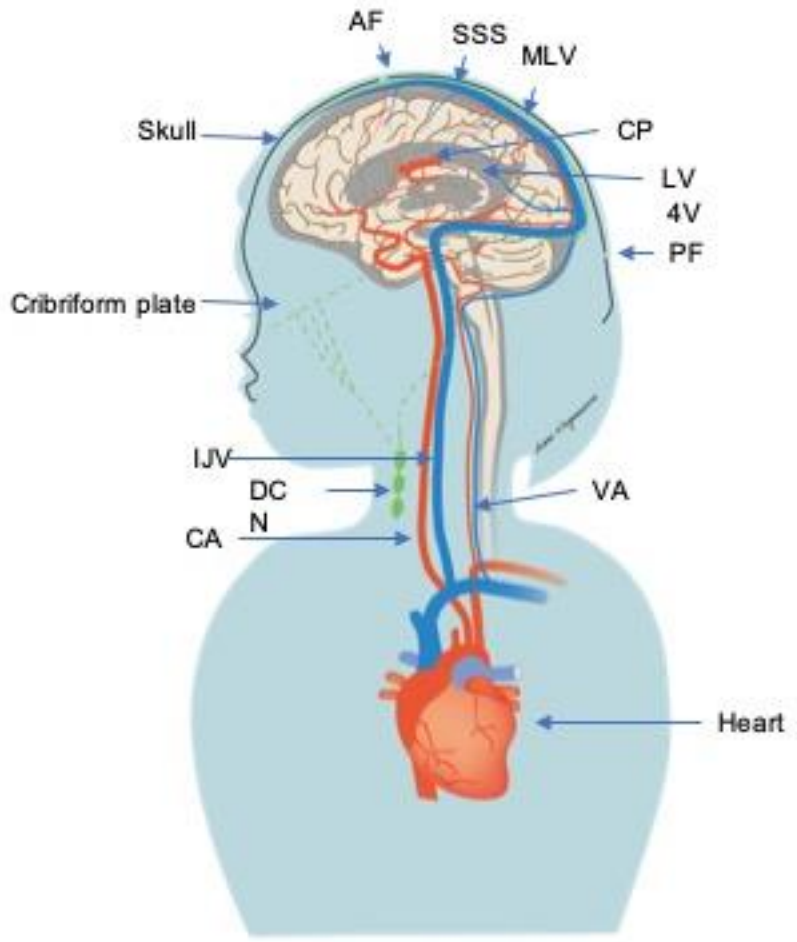

Figure 3-2 Depiction of the neurofluid system including arterial (red) and venous (blue) blood and cerebrospinal fluid (CSF) (gray). After closure of the skull fontanelles (black), the fixed volume within the cranium and the incompressibility of brain tissue give rise to the Monro-Kellie hypothesis, that the total brain and neurofluid volume must remain constant, in or- der to maintain constant intracranial pressure. A change in volume of one neurofluid is therefore compensated by a change in volume of another neurofluid. As a result, after closure of the fontanelles, CSF inflow into the brain depends on the difference between arterial inflow and venous outflow. In infants, due to the open fontanelles and suture lines, the skull is not yet rigid, so the total intracranial volume can vary. CSF flow also depends on cardiac pulsations, as well as on spinal and intracranial pressure. In addition, respiration exerts a significant effect on CSF flow, since inspiration causes a reduction in thoracic pressure, increasing the venous return and enabling increased inflow of arterial blood and CSF. CSF pro- duction primarily occurs in the choroid plexi within the lateral ventricles, while CSF absorption occurs via pressure differences generated

at the level of the arachnoid villi/arachnoid granulations. Since these arachnoid granulations mature at around 18 months of age, the reabsorption of CSF in infants is likely to occur via alternative pathways (green dotted lines) such as along the cranial nerves and through the cribriform plate toward the nasopharyngeal lymphatic plexus, and subsequently to the cervical lymph nodes (green). 4V, fourth ventricle; AF, anterior fontanelle; CA, carotid arteries; CP, choroid plexus; DCN, deep cervical lymph nodes; IJV, internal jugular veins; LV, lateral ventricle; MLV, meningeal lymphatic vessels; PF, posterior fontanelle; SSS, superior sagittal sinus; VA, vertebral arteries. (Picture credit Aimi Nagasawa.)

Imaging of intraparenchymal fluid transport: gadolinium based MRI

In adults, fluid transport between the CSF and tissue compartments has been demonstrated with serial T1-weighted imaging after intrathecal injection of a contrast agent, showing enhancement around the middle cerebral arteries, basal cisterns, and Sylvian fissure, proceeding along the vessels and into the brain from the subarachnoid space (94,96,266). Similarly, fluid transport between the blood and CSF compartments has been demonstrated using serial, heavily T2-weighted FLAIR imaging following intravenous injection of a contrast agent, showing delayed enhancement of the perivascular spaces and CSF (267,268). These contrast-enhanced methods represent the current gold standard for imaging clearance in vivo in human (269), as well as for the assessment of blood brain barrier permeability (270). However, with the exception of specific patient groups in whom contrast is needed for other reasons (271), contrast-based methods are not appropriate for studying glymphatic function in children due to the invasive nature of such studies.

Imaging water motion and its directionality: Diffusion MRI

Unlike contrast-based methods, diffusion-based methods are fully noninvasive and suitable for use in pediatrics, healthy volunteers, and other groups for whom a contrast injection is not indicated. Analogous to the velocity encoding gradients used in PC-MRI, the diffusion gradients in diffusion MRI can be used to sensitize the images to the motion of water on a range of spatial scales, ranging from intra- and extra-cellular water diffusion to microvascular perfusion. One metric which has already been widely applied to pediatric groups is the Diffusion Tensor Imaging-analysis along the perivascular space (DTI-ALPS) index (272). The DTI-ALPS index is calculated from the ratio of the diffusivity parallel to the PVS at the level of the corona radiata, lateral to ventricles, relative to the perpendicular (radial) diffusivities in the projection and association

tracts, and has revealed changes in children with autism spectrum disorder 58, spastic cerebral palsy (273), epilepsy (274–276), acute lymphoblastic leukemia (277), multiple sclerosis with cognitive impairment (278), hydrocephalus (279), and attention-deficit hyperactivity disorder (280). While the physiological meaning of this index has recently been re-appraised (281), in light of the variability in perpendicular diffusivities potentially arising from non-glymphatic effects, the DTI-ALPS index has the advantage of being noninvasive, readily calculable using the high b-values typically applied in diffusion tensor MRI, and sensitive to changes in clearance observed following an intrathecal injection of Gadolinium (282). However, since the DTI-ALPS index is calculated at a single spatial location, it is not sensitive to changes in clearance elsewhere in the brain.

In contrast to the high b-value diffusion imaging used to assess molecular diffusion, low b-value diffusion imaging can be used to assess the pseudo-diffusion signal from microvascular perfusion or circulatory flow. Combining diffusion gradients over a range of low to high b-values, as in the intravoxel incoherent motion (IVIM) method (283), the diffusion signal can be modeled to estimate both perfusion and diffusion components. Two components, corresponding to microvascular perfusion and molecular diffusion, are typically modeled in the IVIM signal, but recent work suggests that a third, intermediate component can be detected within brain regions where perivascular spaces are visible 70. The origin of this signal has not yet been validated, but this intermediate IVIM signal is thought to be related to perivascular edema, or an increased fraction of ISF (284). The IVIM method has been widely used in children 58 and in fetal and placental MRI (285,286) as a non-contrast perfusion imaging method, but to our knowledge the spectral IVIM analysis and the intermediate IVIM signal have not yet been assessed in pediatric brain MRI.

Imaging of perfusion and blood brain barrier permeability - Arterial Spin Labeling

Arterial spin labeling (ASL) is a non-contrast method for measuring perfusion using blood water as an endogenous contrast agent (287). Images are sensitized to perfusion through the application of a labeling pulse, typically an inversion pulse, which inverts the spins in blood in the feeding vessels. During a post-labeling delay, the spins flow into the brain and exchange across the blood brain barrier, reducing the magnetization by an amount proportional to the perfusion. Perfusion can be quantified after collecting two sets of images, one after prior labeling of the spins and one as a control image with no spin labeling (288). The ASL technique can be modified to sensitize the images to blood brain barrier permeability, using multiple delay times and/and kinetic modeling to estimate the exchange times between the blood, tissue, and CSF

compartments (289). Diffusion and ASL methods can also be applied in combination, either within the same acquisition as in the diffusion-weighted ASL method (290), or in separate acquisitions, where ASL can help to clarify the perfusion contribution to the IVIM signal.

To date, the ASL method has been widely used to measure perfusion in pediatrics and is part of the standard clinical evaluation for a number of indications (291,292). In healthy children, perfusion has been shown to increase rapidly after birth, reaching a peak in middle childhood (293,294) and then decrease throughout later childhood and adolescence, but during puberty the change in perfusion is non-linear and varies between males and females and across brain regions (295) (Fig. 4-3).

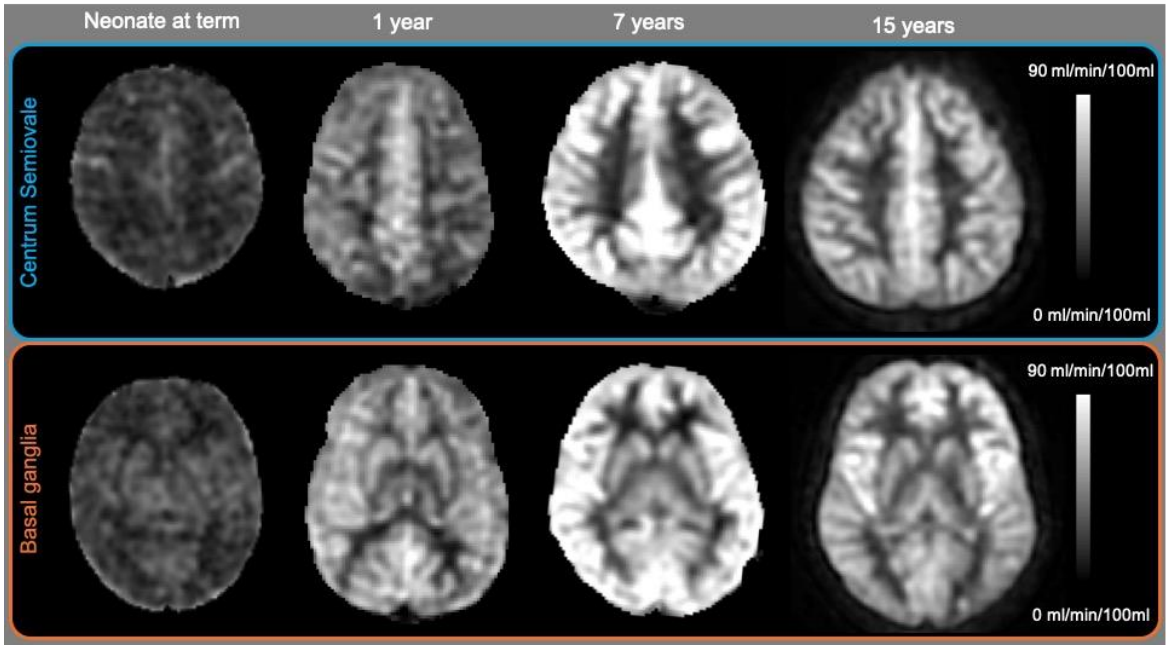

Figure 3-3 Normal arterial spin labeling (ASL)-based perfusion signa from neonate to adolescence. Axial perfusion maps at the level of the centrum semiovale (top) and basal ganglia (bottom), acquired from healthy children ranging in age from the neonatal period to adolescence. All images are scaled to the same range of perfusion values in order to facilitate the comparison of absolute perfusion values across age. The perfusion increases rapidly after birth and appears to peak in middle childhood and then decreases in late childhood and adolescence.

Imaging of perivascular spaces: indirect marker of altered clearance

PVS, also known as Virchow-Robin spaces, are spaces within the basement membranes of the pia mater surrounding perforating arteries in the white matter of the centrum semiovale (296).

PVS can also be identified as invaginations of the leptomeninges surrounding the penetrating arterioles in the basal ganglia. An increased number of dilated PVS (dPVS) in adults is considered an indirect marker of altered clearance of ISF and waste products. dPVS can be seen prenatally (Fig. 4-4) and in the newborn and in the pediatric age group without any relationship with cognitive deficits or indication of pathology, making it difficult to attribute any clinical significance (297,298) (Fig. 4-5).

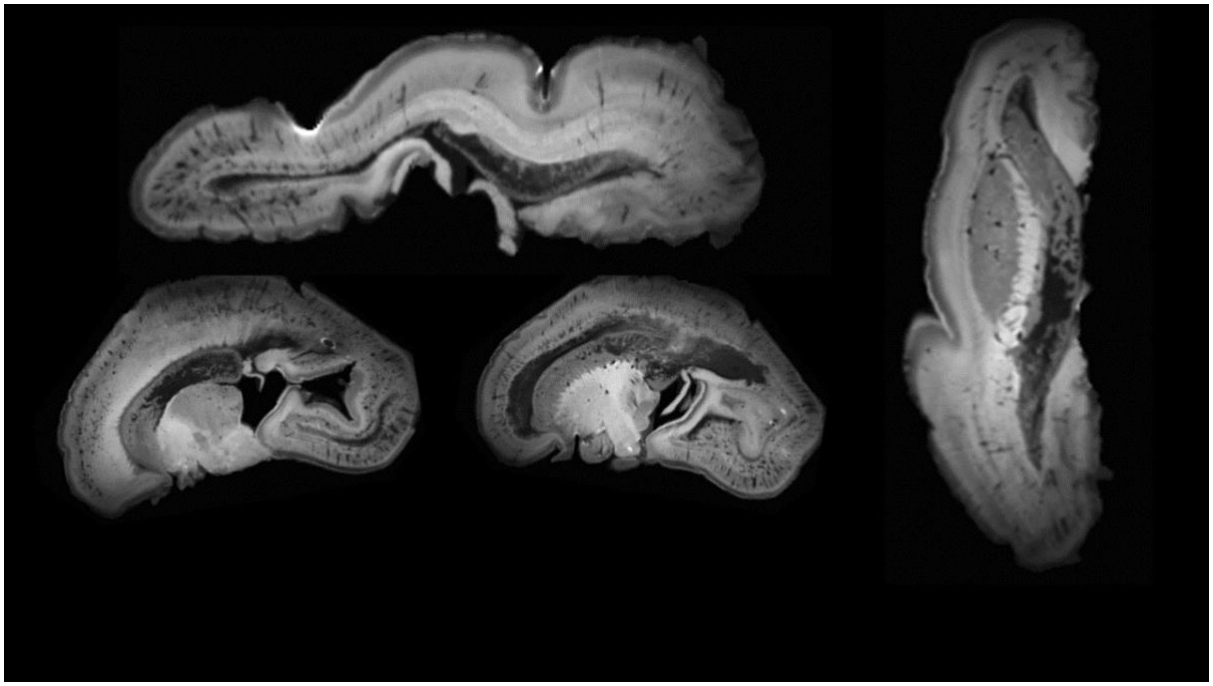

Figure 3-4 Average isotropic diffusion-weighted image from a postmortem brain sample from a 20-week-old fetus, scanned at 9.4 T over 85 hours, depicting perivascular spaces during gestation.(Acknowledgments: Andras Jakab, Center for MR Research, University Children's Hospital, Zu¨ rich, Christoph Ruegger, Neonatology, University Hospital of Zurich, Dominic Gascho, Institute of Forensic Medicine, University of Zurich, Mark Augath, Preclinical Im aging Center, ETH Zurich.)

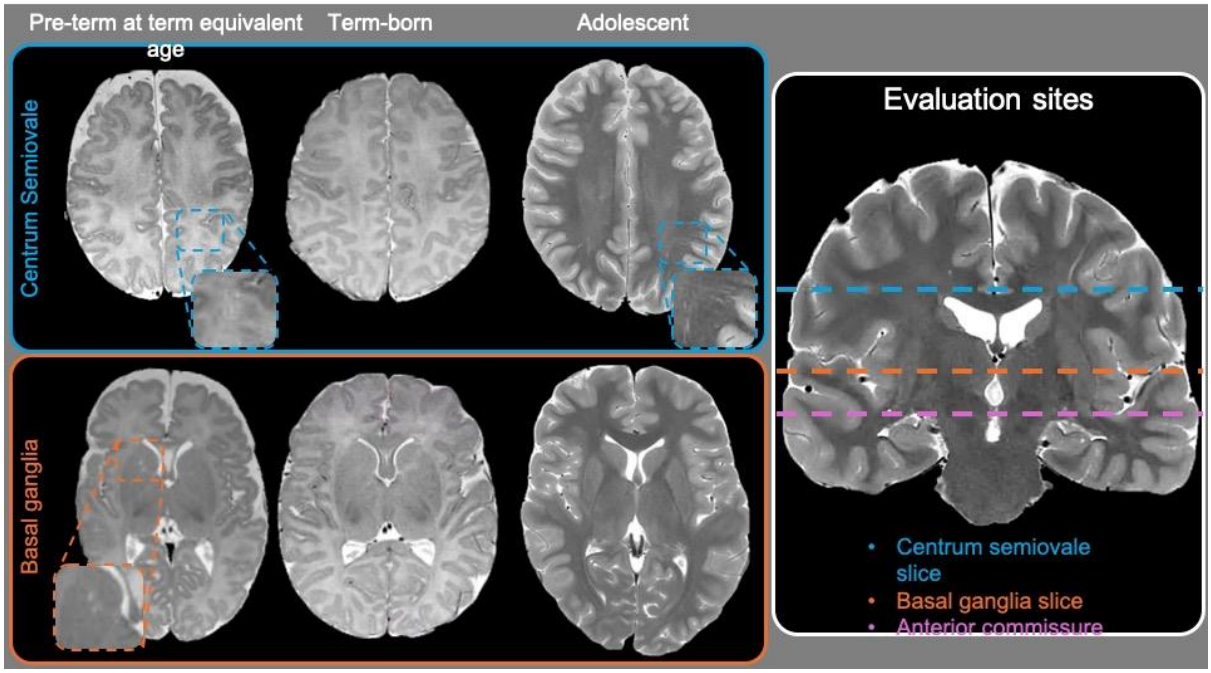

Figure 3-5 Axial T2-weighted images acquired at the level of the centrum semiovale (top) and basal ganglia (bottom) from a preterm-born neonate scanned at term-equivalent age and a term-born control infant. Corresponding images from an adolescent are depicted for comparison, together with an illustration of the slices used for evaluation of the perivascular spaces.

PVS are defined as areas of hyperintense signal on conventional T2-weighted image and hypointense signals on T1-weighted image, but their visibility is field strength (299,300) and protocol-dependent (301). The number or size of PVS can be assessed visually using standardized scoring systems, typically applied to axial T2-weighted images through the basal ganglia and centrum semiovale (164,302,303). PVS counts can also be calculated using Frangi filters, thresholding, machine learning or deep learning algorithms to detect and segment the PVS automatically throughout the brain or within predefined region masks (303,304).

PVS counts are higher in healthy males in comparison to females (298,304). In healthy adolescents, PVS counts were not associated with age or pubertal status in one study (298), although a recent longitudinal study reported a slight increase in PVS volume from age 12-22 years, and with basal metabolic index (305,306). These studies provide initial evidence for maturational changes in PVS through infancy, childhood, and adolescence, but further studies examining PVS across a wide age range in healthy and pathological groups are needed to characterize the typical and atypical developmental profiles of PVS (297). A large body of literature suggests that enlarged PVS are a common denominator in multiple neurological disorders. These have been reported in epilepsy (307,308), autism (153) ADHD (280), headache

(308,309), developmental delay (309), pediatric multiple sclerosis (310) and PTEN Hamartoma Tumor Syndrome (PHTS) (311). Enlarged PVS seem to be related to disrupted sleep (153).

Preterm Birth

In the preterm neonates that are hospitalized, it is a normal finding to see widening of the subarachnoidal spaces as well as widening of the Virchow Robin spaces in the basal ganglia (called lenticulostriatal vasculopathy, which seems a misnomer) (312) (Fig. 4-6). Yet it is unknown whether this is a disruption of the normal neurofluid flow. Infection and inflammation are known risk factors for preterm birth (313) and inflammatory processes may affect perivascular structures (314,315). In addition, preterm neonates show incomplete autoregulation and vascularization (316,317), and meningeal lymphatic vessels and astrocytes are not fully formed until the postnatal period (32,318).

A number of alterations in neurofluid markers have been reported in preterms, including significantly increased cerebral perfusion in comparison to that seen in term-born controls (316,319–321) thought to be due to rapid increase in perfusion after birth (293,321,322), arising from the additional stimulation ex utero. A recent study also reported fewer basal ganglia PVS in preterm-born neonates in comparison to term-born controls, as well as a decrease in basal ganglia PVS with postmenstrual age (PMA) (323). Preterm neonates have also been reported to show lower ALPS indices and an increase in DTI-ALPS with PMA (324).

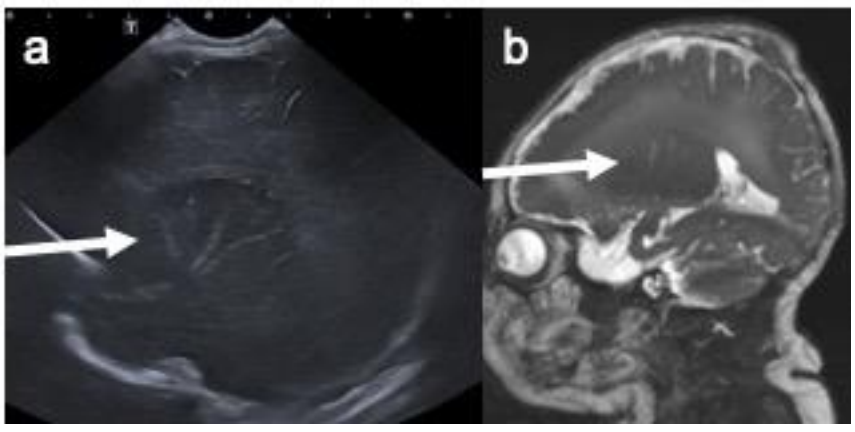

Figure 3-6 Lenticulostriatal vasculopathy in a term neonate, hospitalized for a perinatal asphyxia. Ultrasound in the sagittal oblique direction, demonstrating the typical lenticulostriatal vasculopathy as echogenic lines. (B) Re- constructed heavily weighted T2 sagittal image shows high signal of the lenticulostriate arteries in the same neonate.

In recent years, new imaging techniques for visualizing lymphatic vessels in the body have been developed, most notably intranodal MR lymphangiography. This method involves injecting a contrast agent into the lymph nodes in the groin, which enhances the visualization of central lymphatic vessels in the retroperitoneum and posterior mediastinum (325). This advancement has provided significant new insights into the complex lymphatic anomalies in the body. Given that these anomalies are typically congenital and often associated with syndromal or genetic abnormalities (326), it is plausible that there is a correlation between lymphatic anomalies and glymphatic abnormalities. This connection is particularly evident in patients with Noonan syndrome, who frequently exhibit abnormal lymphatic anatomy and functionality, as well as neurological and developmental challenges (327) (fig 4-7).

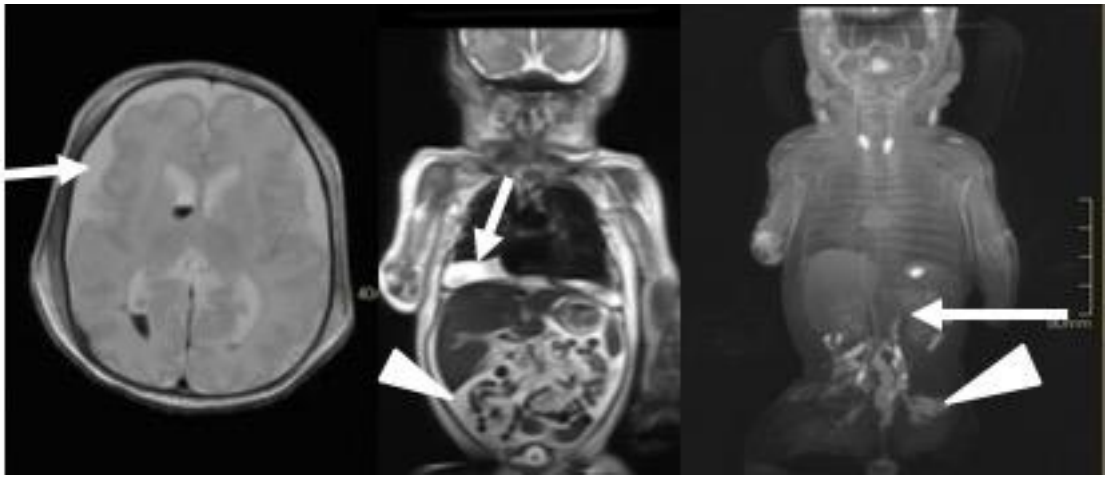

Figure 3-7 Neonate born at 33 weeks with fetal hydrops and a RASopathy (Noonan (-like) syndrome). (A) Transversal T2-weighted MR image of the brain, demonstrating the wide subarachnoidal space (arrow). (B) Coronal T2- weighted MR image demonstrating the pleural fluid (arrow), ascites (arrowhead), and subcutaneous edema. (C) MR lymphangiography, coronal T1-weighted image after intranodal contrast injection, demonstrating the stop in the central lymphatic flow (arrow) and the retrograde lymphatic contrast dermal backflow (arrowhead). These images are typical for Central Conducting Lymphatic Anomaly that may occur in several syndromic diseases that also have developmental abnormalities, typically in Noonan (-like) syndrome.

Congenital heart disease

Congenital heart defects (CHD), particularly the Fontan circulation in univentricular CHD, are likely to impact the body's lymphatic flow. It remains unclear whether lymphatic vessels are primarily affected or if the changes are secondary to abnormal venous pressure, or a

combination of both mechanisms. Previous studies have identified a correlation between increased central venous pressure and enlarged cerebrospinal fluid (CSF) volumes (6), which have also been associated with impaired neurodevelopment. Children with CHD have demonstrated altered CSF flow pulsatility (328), and adults with CHD seem to have an increased risk of early dementia, particularly in cases of severe heart defects such as univentricular heart disease (329) . Despite these findings, there is still limited knowledge about changes in lymphatic and glymphatic flow in CHD.

Epilepsy

Histological studies in children with intractable focal epilepsies have revealed an association between enlarged perivascular spaces, white matter angiopathy and disrupted blood brain barrier permeability (330). Enlarged perivascular spaces in children with intractable focal epilepsies have been associated with white matter angiopathy and disrupted BBB permeability (330), as well as with the seizure duration and the interval between the last seizure and MRI (307)(Fig. 4-8).

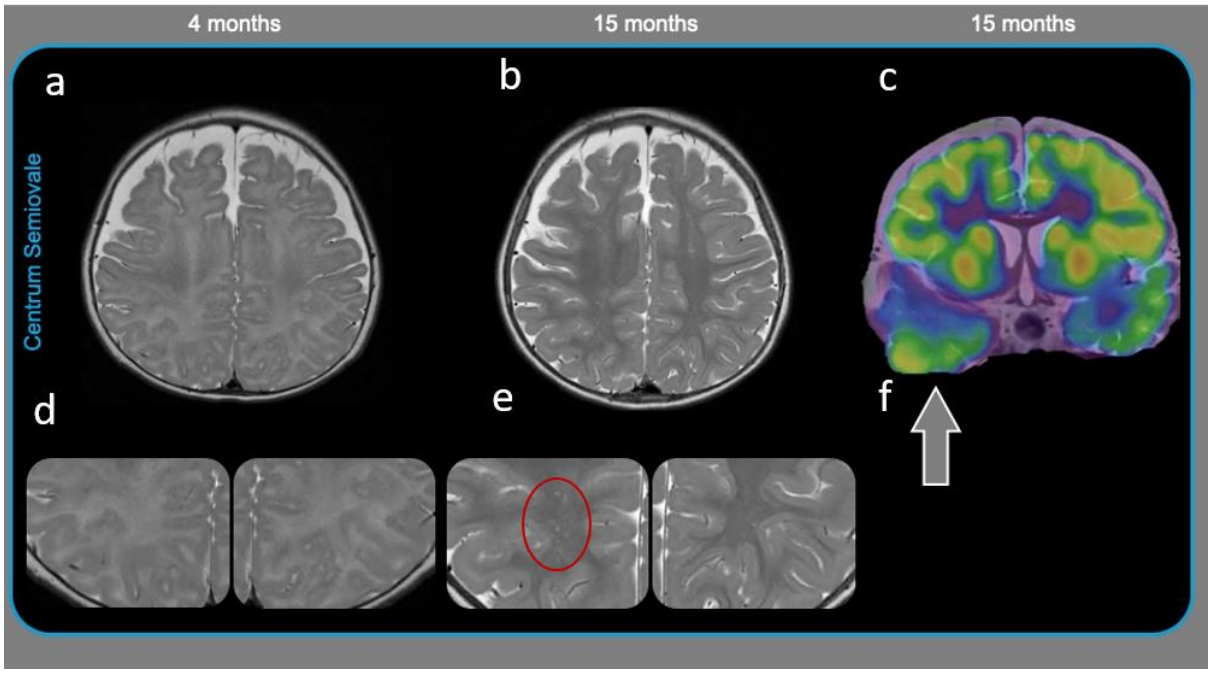

Figure 3-8 Axial T2-weighted images acquired at the level of the centrum semiovale in a girl who presented with epileptic spasms due to focal lesional epilepsy at 4 months of age.and at 15 months of age (B). PET (C) demonstrates a hypometabolic area in the right temporal lobe (arrow), which, after surgical resection, was histologically diagnosed as a type II a focal cortical dysplasia. perivascular spaces (PVS) count varied at different time points (D and E) and seemed

slightly higher in the hemisphere ipsilateral to the epileptogenic lesion (red oval circle in figure part E).

Other neurological disorders

Enlarged subarachnoid spaces in some infants combined with rapidly growing head circumference without ventricular enlargement is defined as benign hydrocephalus. While a specific etiology has not been identified, it could be an expression of immature arachnoid granulations. In the context of neurofluids, it is interesting to note that certain systemic conditions, such as thrombosis of the superior vena cava, children may develop extraventricular hydrocephalus (331,332). Increased central intracranial pressure is directly linked to central venous pressure whereby an increase in the latter will obstruct intracranial venous outflow via the internal jugular veins, affecting CSF absorption via arachnoid villi. Venous obstruction may be due to idiopathic intracranial hypertension and requires investigation especially in infants and toddlers who have retinal hemorrhages (Fig. 4-9). Such diagnosis may be delayed due to reopening of the fontanelles. Immature arachnoid villi in the newborn may also result in abnormal accumulation of CSF in the SAS (333).

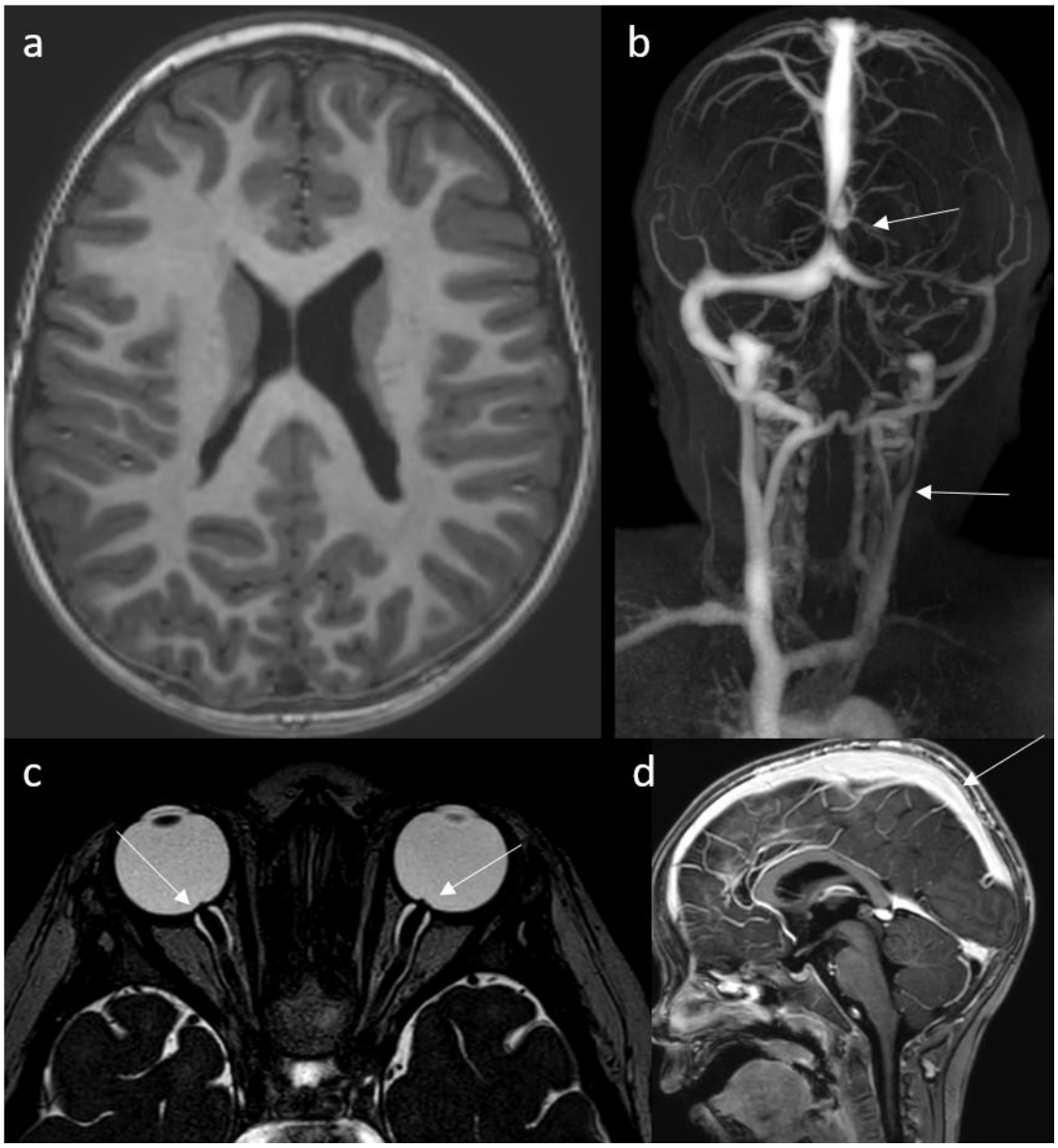

Figure 3-9 Incidental findings of intracranial hypertension in a 26-month-old patient with autism spectrum disorder undergoing a routine MR imaging. (A) axial T1-weighted image shows abnormal morphology and size of the lateral ventricles; (B) contrast-enhanced MR imaging venography shows focal stenosis of the superior sagittal sinus and severe stenosis of the left transverse sinus, sigmoid sinus, and the left internal jugular veins; (C) protrusion of bilateral optic discs (white arrows) and (D) contrast-enhanced MR image shows engorged veins (white arrow), depression of the sinus rectus, and initial crowding of the foramen magnum. Opening pressure at lumbar puncture was 40 mm Hg (normal 15– 17 mm Hg).

There is a high incidence of enlarged CSF spaces is seen in children at high risk of developing autism spectrum disorder (ASD) and those with a confirmed diagnosis of ASD (152,334,335) (Fig. 4-10). Increased CSF volume is linked to poor sleep quality in children with ASD (153). Since glymphatic drainage is facilitated during sleep, it is highly likely that patients with ASD are also affected with poor waste clearance (336,337). Recent studies have also shown a higher incidence of enlarged perivascular spaces in children with ASD (153,338). One study showed that the volume of parasagittal dura, a tissue that harbors meningeal lymphatics, is related to neurodevelopmental delay (339).

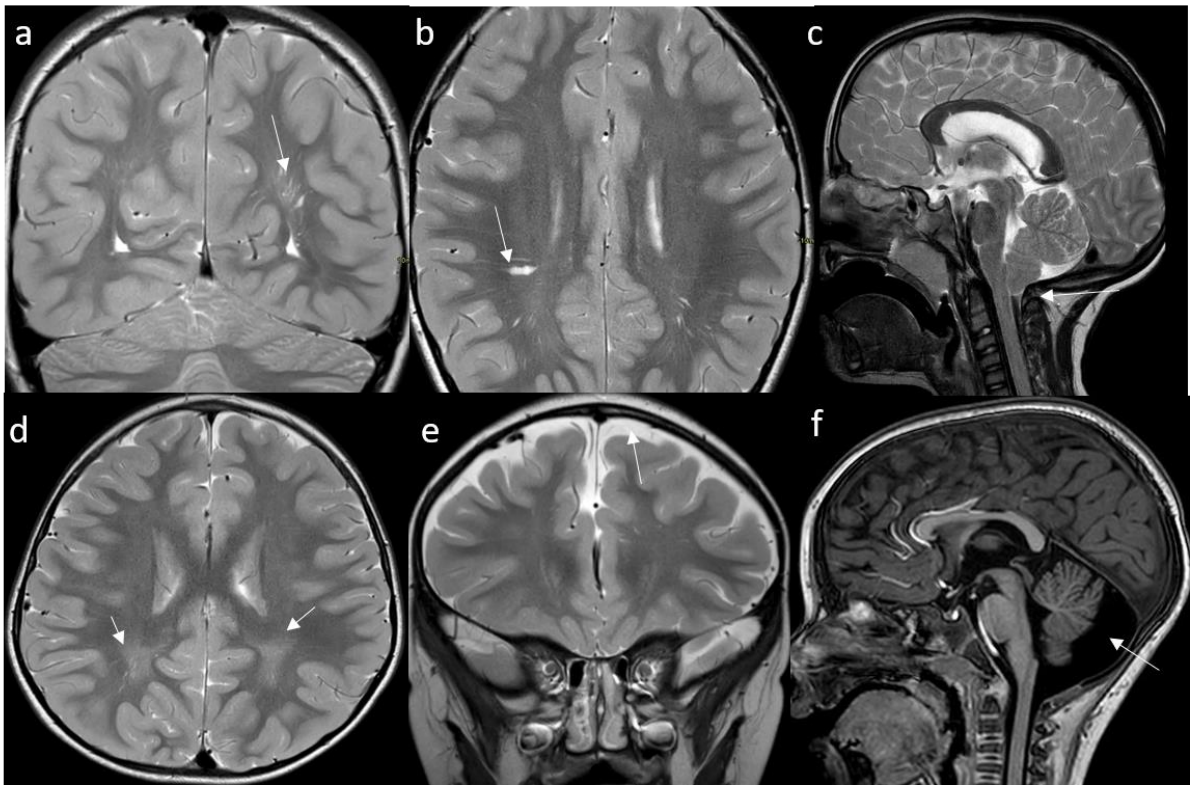

Figure 3-10 Common aspecific incidental neuroimaging findings in children with Autism spectrum disorders (ASD).(A) Coronal and (B) axial T2-weighted image showing prominent PVS in the peritrigonal parietal region (white arrows) in a 28-month-old female; (C) a 34-month-old male with ASD shows tonsillar herniation in a T2- weighted sagittal image (white arrow); (D) aspecific white matter abnormalities in bilateral peritrigonal regions (white arrows) are seen in a 32-month-old male with ASD on axial T2-weighted image; (E) prominent frontal sub- arachnoid spaces (white arrow) are visible in a 46-month-old male with ASD on coronal T2-weighted image; (F) mega cisterna magna (white arrow) is seen in a 27-month-old female with ASD on a T1-weighted axial image.There is recent evidence that children with craniosynostosis may suffer with anatomical and functional dysfunction of the meningeal lymphatic vessels (340) and

specific treatments are being pursued to improve cognitive functions in craniosynostosis (6). Studies using animal models have demonstrated that meningeal lymphatic impairment leads to altered brain perfusion and increased ICP, which can drive neurocognitive dysfunction (6). These findings highlight the interaction between the skull and meninges, offering new avenues for treatment. For instance, understanding how the mechanoceptor Piezo-1 regulates lymphatic flow has prompted investigations into Piezo-1 agonists, such as Yoda1, as potential treatments for cognitive dysfunction in patients with craniosynostosis.(340,341).

Conclusion/Summary

Over the past decades the concept of neurofluids has provided a new dimension to our understanding of brain development, anatomy, brain function and the possible role of disrupted fluid transport in neurological disorders. MRI is an important tool in our assessment of neurofluid flow and development, providing important insight into the connections and transport of fluids between different compartments within the brain.

Acknowledgements

The authors gratefully acknowledge the assistance of Andras Jakab, Antonio Gennari and Aimi Nagasawa for help in preparing figures for inclusion in the manuscript.

Declaration of AI and AI-assisted technologies in the writing process: During the preparation of this work the authors used GenAI. The authors reviewed and edited the content as needed and takes full responsibility for the content of the publication. This declaration does not apply to the use of basic tools for checking grammar, spelling, references, etc. If there is nothing to disclose, there is no need to add a statement.

Chapter 4 Paper 3: Perivascular Space Burden in Children with Autism Spectrum Disorder Correlates with Neurodevelopmental severity

This chapter is the Accepted Manuscript of the published version that appears in its final form in Frontiers in Neurology. The full reference is: Frigerio G et al. Journal of Magnetic Resonance Imaging, 29 June, 2025. The original content of the article has not been changed but the formatting has been slightly tweaked for easier readability.To access the final edited and published work see DOI: 10.1002/jmri.70023" (342).

Abstract

Background: Cerebral perivascular spaces (PVS) are involved in cerebrospinal fluid (CSF) circulation and clearance of metabolic waste in adult humans. A high number of PVS has been reported in autism spectrum disorder (ASD) but its relationship with CSF and disease severity is unclear.

Purpose: To quantify PVS in children with ASD through MRI.

Study Type: Retrospective.

Population: 66 children with ASD (mean age: 4.7 ± 1.5 years; males/females: 59/7).

Field Strength/Sequence: 3T, 3D T1-weighted GRE and 3D T2-weighted turbo spin echo sequences.

Assessment: PVS were segmented using a weakly supervised perivascular spaces algorithm. PVS count (WM-PVS_{tot}) and normalized volume(WM-PVS_{voln}), were analyzed in the entire white matter. Six regions: frontal, parietal, limbic, occipital, temporal, and deep WM (WM-PVS_{sr}).) WM, GM, CSF and extra-axial CSF (eaCSF) volumes were also calculated. Autism Diagnostic Observation Schedule, Wechsler Intelligence Scale and Griffiths Mental Developmental scales were used to assess clinical severity and developmental quotient (DQ).

Statistical Tests: Kendall correlation analysis (continuous variables) and Friedman (categorical variables) tests were used to compare medians of PVS variables across different WM regions. Post-hoc pairwise comparisons with Wilcoxon tests were used to evaluate distributions of PVS in WM regions. Generalized linear models were employed to assess DQ, clinical severity, age, and eaCSF volume in relation to PVS variables. A p-value <0.05 indicated statistical significance.

Results: severe DQ (β=0.0089), mild form of autism (β=-0.0174), and larger eaCSF (β=0.0082) volume was significantly associated with greater WM-PVS_{tot} count. WM-$PVS_{voln}$was predominantly affected by normalized eaCSF volume ($eaCSF_{voln}$) (β=0.0242; adjusted for WM volumes). The percentage of WM-PVS_{sr} was higher in the frontal areas (32%) and was lowest in the temporal regions (11%).

Data Conclusion: PVS count and volume in ASD are associated with $eaCSF_{voln}$. PVS count is related to clinical severity and DQ. PVS count was higher in frontal regions and lower in temporal regions.

Keywords: Perivascular Spaces, Autism Spectrum Disorder, Pediatric, CSF drainage, Neurodevelopment, Deep learning

Introduction

There is a growing body of evidence suggesting that an increased number of perivascular spaces (PVS) identified by MRI may represent a marker for altered drainage of CSF and therefore clearance of waste products in the adult brain (343). Specifically, PVS are present within the basement membranes of the penetrating arterial walls (75). They are natural conduits for the entry of cerebrospinal fluid (CSF) and exit of interstitial fluid (ISF) and metabolic waste (344). Regarding their structure, PVS are linear or ovoid in shape and typically show a signal intensity similar to that of CSF - hyperintense on T2-weighted (T2w) images, and hypointense on T1-weighted (T1w) and fluid-attenuated inversion recovery (FLAIR) (344) images. The burden of PVS can be determined using a visual rating (VR) scale (grade 0: none; grade 1: 1-10; grade 2: 11-20; grade 3: 21-40; grade 4: >40) (302). This scale is used to quantify the number of PVS (perivascular spaces) observed in an axial plane that cuts through the basal ganglia (BG), or in a plane through the white matter (WM) in the centrum semiovale(164). However, for a more precise and detailed evaluation of the presence of PVS in the entire WM, application of VR scale is not feasible. Although the VR scale is considered the reference standard assessment scale and has demonstrated good reliability and repeatability, this qualitative method is relatively insensitive and limited by floor and ceiling effects.

Automatic and semi-automatic techniques have been developed that can improve the segmentation of PVS, considering morphological features, signal intensity, and deep learning approaches. These techniques aim to enhance accuracy, improve reproducibility and efficiency of PVS quantification, thus providing more reliable biomarkers for both clinical and research applications (345,346). In this context, an increased number of PVS quantified by both the VR scale and automatic methods is strongly correlated with advancing age, vascular risk factors, as well as neurodegenerative disorders like Alzheimer's disease (297,347). Previous studies in the pediatric population suggest that their numbers increase in neurodevelopmental disorders (308,309). However, their significance in the developing brain remains unclear (323). Additionally, there is a lack of studies quantifying PVS in the pediatric brain using deep neural network-based semi-automatic or automatic tools, particularly in disorders like autism spectrum disorder (ASD).

ASD is a complex neurodevelopmental disorder affecting communication, behavior, and social interaction (348) . In this context, MRI-based markers in children at the age of 4 to 10 years with ASD are often times unspecific, but a larger volume of subarachnoid spaces, presence of multiple PVS, and brain overgrowth are considered salient features and can be frequently observed (150,349). These findings likely support the notion that enlarged perivascular spaces reflect an alteration in cerebrospinal fluid circulation within the developing brain. Previous work has shown neuroanatomical differences in individuals with ASD, including enlarged PVS

(153,338,350,351), elevated levels of amyloid beta (352), and an increased volume of extra-axial CSF (eaCSF) (353). However, there is a lack of quantification of PVS in the whole brain in children with ASD using deep learning algorithms. One study quantified PVS using a Frangi filter-based deep learning algorithm on two-dimensional (2D) MRI data acquired at 1.5-T in children with ASD (338), while two other study relied on visual assessments of PVS (350,351). Given that PVS are associated with neurodegenerative and neurodevelopmental processes (309,354), clinical assessment (such as developmental delay or severity of disease) of PVS in children with ASD could enhance our understanding by stratifying children based on PVS count to support treatment strategies

Against this background, we aimed to quantify PVS using a deep learning-based automatic approach, with the goal of correlating the results with brain morphological volumes and clinical severity in children with ASD. Additionally, we sought toto analyze the spatial distribution of PVS in white matter (WM-PVS_{tot}) to explore spatial patterns of PVS.

Materials and Methods

This retrospective study was approved by the local Institutional Review Board of our institute. Due to the retrospective nature of the study, a waiver was obtained to permit the reuse of existing data.

Participant Characteristics

Data were collected as part of a single-center study involving children with a diagnosis of ASD, who had undergone clinical MRI as part of their diagnostic work-up between July 2021 and September 2023. Demographic and clinical characteristics of the study participants are shown in Table 6-1 (Table 6-5 S1 in Supplementary Materials for sex-based stratification).

Table 4-1 Patient Demographics and Clinical Characteristics

Patient Demographics and Clinical Characteristics	n = 66
Age (years) (mean ± std)	4.67 ± 1.46
IQ-class* (number)	Normal (n = 21) Mild (n = 21) Moderate (n = 10) Severe (n = 14)
CSS** (number)	4 (n = 5) 5 (n = 7) 6 (n = 16) 7 (n = 14) 8 (n = 7) 9 (n = 10) 10 (n = 7)

*IQ-class: Developmental delay class ; ** CSS: Clinical Severity Score (metric to assess the severity of autistic symptoms)

The initial dataset consisted of 149 subjects. The inclusion criteria were: age range between 2 and 8 years at time of MRI and an established diagnosis of ASD. The exclusion criteria were: 1) age less than 2 or greater than 8 years (n = 21), 2) lack of availability of MRI sequences of interest (n = 13), 3) insufficient MRI quality (n = 20), 4) incomplete clinical information (n = 29), and 5) history of traumatic brain injury, other neurodevelopmental comorbid disorders, macroscopic brain malformations, or severe prematurity (<28 weeks). Age cut-offs were determined using the age of the child with a diagnosis of ASD at the time of MRI acquisition. Breathing-related artifacts and radiofrequency-induced inhomogeneity artifacts were the primary factors contributing to poor MRI quality in certain images that the Human Connectome Project (HCP) pipeline could not process (355). Sedated children maintained spontaneous breathing. No sequence was repeated if deemed diagnostically adequate to prioritize patient comfort. The eligible population for this study comprised 66 children (mean: 4.7 ± 1.5 years, age range: 2.2-7.9yrs); males/females: 59/7).

The diagnosis of ASD was determined by a multidisciplinary team according to the Diagnostic and Statistical Manual of Mental Disorders criteria (356). This diagnosis was supported by tests administered to both parents and children. Specifically, the Autism Diagnostic Interview-Revised (ADI-R) (357)was provided to the parents, while the Autism Diagnostic Observation Schedule-second edition (ADOS-2) was conducted with the child (358). The Calibrated Severity Score (CSS) was employed as a metric for assessing the severity of autistic symptoms (358) . The scale ranges from 1 to 10, classifying severity into three categories: 1–3 for non-spectrum, 4–5 for autism spectrum disorder, and 6–10 for autism (359,360). The developmental quotient (DQ) was assessed using Wechsler Intelligence Scale for Children (WISC-IV) or the Wechsler Preschool and Primary Scale of Intelligence-III (WPPSI-III), based on the child's age and cognitive-linguistic abilities (360). Griffiths Mental Development Scales-extended revised version (GMDS-ER) was used for children unable to complete these tests due to lack of cooperation, age, or language difficulties (361). The scores obtained are grouped into five classes: normal (>70), mild (50–70), moderate (35–49), severe (20–34), and extreme (<20). None in our cohort was in the extreme subclass, leaving us with four DQ subclasses

MRI Protocol

All MRI scans were acquired on a 3 Tesla scanner (Achieva dStream; Philips Healthcare, Best, The Netherlands) equipped with a 32-channel head coil. All patients underwent three-dimensional (3D)-T1 GRE and 3D-T2w turbo spin echo sequences covering the brain. The 3D-T1w sequences were acquired with one out of two available setups. In 29 subjects, 3D-T1w image parameters were as follows: repetition time (TR) = 8.3 ms; echo time (TE) = 3.9 ms; echo train length (ETL) = 256; flip angle = 8°; 1x1x1 mm^3 voxel size. In 37 subjects, 3D-T1w image parameters were as follows: TR = 8.01 ms; TE = 3.7 ms; ETL = 228; flip angle = 5 °; 1x1x1 mm^3 voxel size. The 3D-T2w image parameters were as follows: TR = 2.5; TE = 195.5 ms; ETL = 117; flip angle = 90; 1 average; 1x1x1 mm^3 voxel size. All patients underwent MRI under sedation using a continuous intravenous infusion of weight-adjusted dosage of propofol (Fresenius Kabi Austria GmbH/Graz/Austria; 2.5-4mg/kg).

Image Processing

All 3D-T1w and 3D-T2w images were pre-processed with the HCP (https://github.com/Washington-University/HCPpipelines, v4.7.0) minimal preprocessing pipeline (Figure 6-1) (355). This pipeline includes several steps: correction of MR gradient non-linearity distortions, co-registration of T1w and T2w images, and alignment to Montreal Neurological Institute space to ensure anatomical consistency. Futhermore, the pipeline performs the tissue segmentation and parcellation through FreeSurfer pipeline version 6

(http://surfer.nmr.mgh.harvard.edu/).to improve the contrast between PVS and the surrounding WM.(346,355).

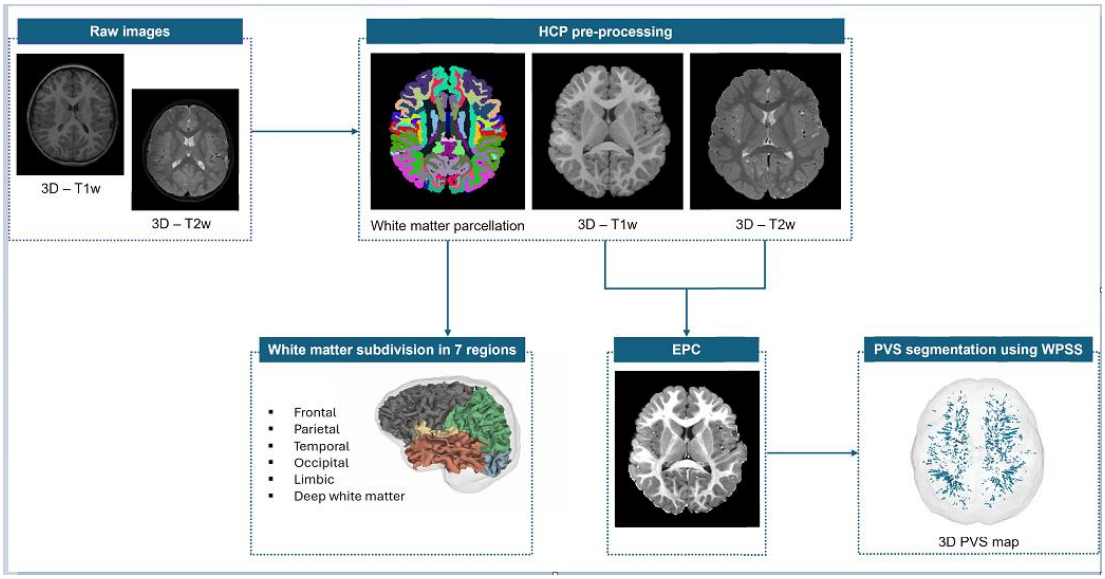

Figure 4-1 Overview of the adopted workflow. Workflow used for analyzing 3D- T1w and 3D- T2w DICOM files. Initially, the images underwent preprocessing via the HCP preprocessing pipeline. Then, WM parcellation was utilized to generate a mask of WM regions of interest. Additionally, pre- processed T1w and T2w images were used to generate Enhanced Perivascular space Contrast (EPC) images, which served as input for the WPSS algorithm for PVS segmentation.

Segmentation masks for intracranial volume (ICV), WM, and cortical gray matter (cGM) were obtained from the HCP outputs. Six WM subregions were then defined by merging with the FreeSurfer WM parcellation version 6 (http://surfer.nmr.mgh.harvard.edu/) using the WM lobes subdivision described in a previous study: temporal, frontal, occipital, limbic, parietal, and deep WM (Figure 6-2).

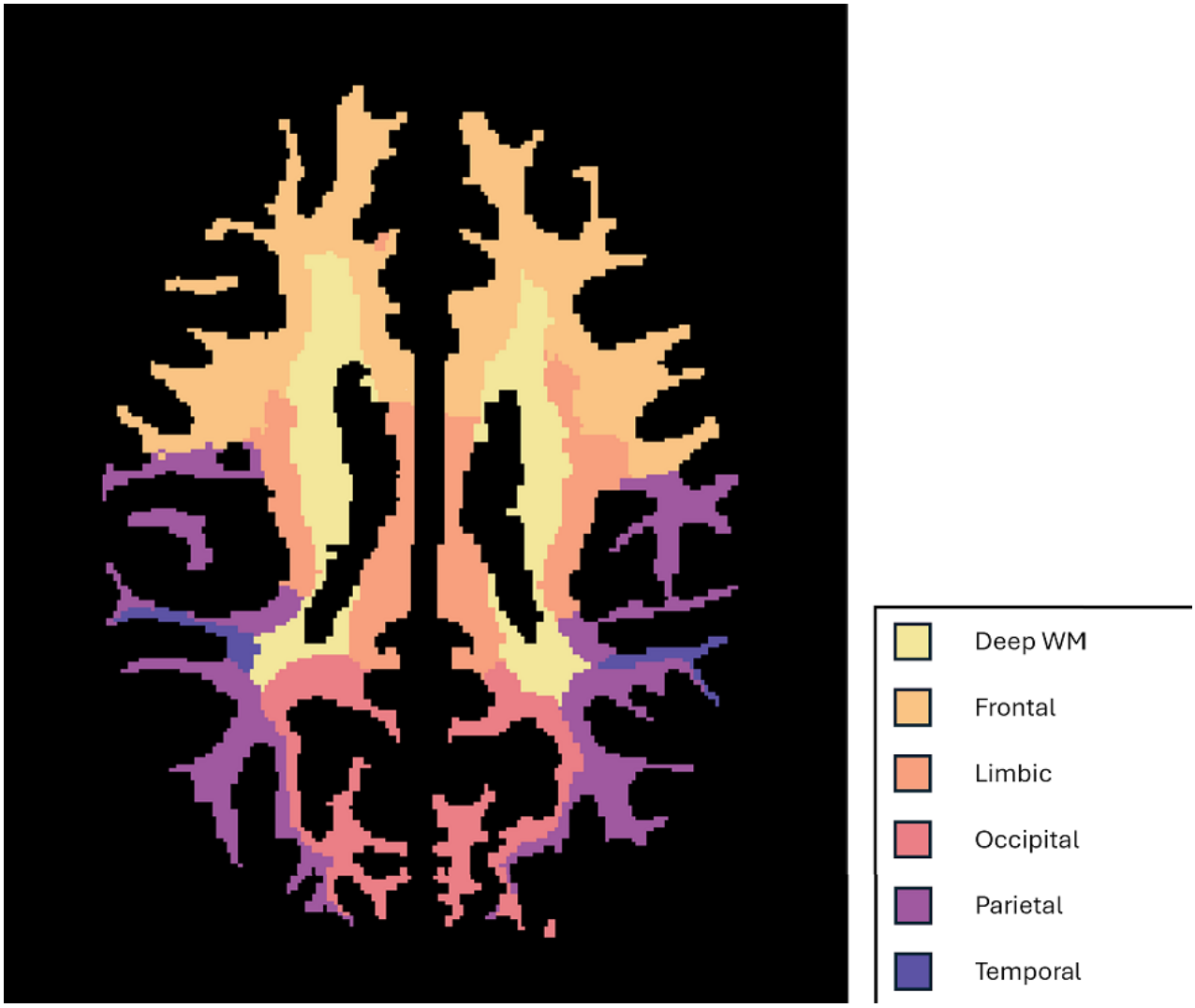

Figure 4-2 T1w image and WM regions of interest. T1w image (left); WM parcellation masks were merged to create six WM regions of interest (right). These include deep WM, frontal, limbic, occipital, parietal, and temporal lobes.

Since the CSF masks from HCP processing covered only a portion of the entire CSF space, additional masks were generated by segmenting 3D-T1w images. An in-house pipeline was applied to 3D-T1w images, involving the following steps: (1) brain extraction combining different tools:Brain extraction tool (BET), robust learning-based brain extraction system (ROBEX), advanced normalized tools(ANTs) (362–364); (2) correction of bias field intensity artifacts using the N4BC algorithm (365); (3) rigid registration to MNI space using ANTs; and (4) brain tissue segmentation (CSF, WM, cGM, BG, brain stem, cerebellum) with Atropos (algorithm distributed with ANTs), utilizing the Pediatric Template of Brain Perfusion (PTBP) priors (366). The CSF mask was then reviewed and manually corrected by one reader (NA, 14 years of experience) to remove any voxels outside the skull (Dice Similarity score = 0.9981, Volume Similarity = 0.9963). Then, eaCSF was subsequently derived from the CSF mask by manually removing the ventricles and

regions below the anterior commissure – posterior commissure line (https://www.itksnap.org/pmwiki/pmwiki.php, version 3.6).

PVS Segmentation

Regarding PVS segmentations, an automated approach was chosen using (*Weakly supervised perivascular spaces segmentation with salient guidance of Frangi filter)* (WPSS) with salient guidance of the Frangi filter algorithm as developed by Lan et al (346). WPSS integrates the Frangi filter method with a U-Net architecture enhanced by conditional random field theory, resulting in an end-to-end segmentation tool with hyperparameters optimized during training. In this study, we employed the WPSS model as trained by Lan et al. This tool effectively identifies vessels and tubular structures while excluding cysts and other white matter lesions, such as germinal matrix hemorrhages. The EPC images (i.e., multi-contrast images generated by combining pre-processed T1w and T2w images to enhance the contrast between PVS and surrounding WM) were used as input to the WPSS algorithm for PVS segmentation. However, WPSS might incorrectly classify ventricular horns as PVS, resulting in an overestimation of PVS variables. To address this, a neuroradiologist (NA; 14 years of experience) reviewed the segmentations, and manually removed all erroneously identified PVS (e.g., along the occipital ventricular horns). Furthermore, since the tool struggles to accurately detect very large PVS (Figure 6-8 S4 in the supplementary materials), these missed PVS were also manually segmented by the same neuroradiologist and included in the analysis. Manual segmentation was performed using ITK-SNAP (https://www.itksnap.org/pmwiki/pmwiki.php, version 3.6).

The WM-PVS_{tot} variables were quantified both for the total WM and for each subregion (temporal, frontal, occipital, limbic, parietal, and deep WM). The volume fraction (VF) of PVS was calculated as the ratio of the PVS volume within a region to the total volume of that region. Subregional (WM-PVS_{sr}) count was normalized by the total PVS count and expressed as a percentage. If a PVS was found in two different adjacent subregions, it was decided to include them in both regions to calculate the WM-PVS_{sr} count. Since PVS are located in WM, their volume was normalized for total WM volume (WM-$PVSvol_n$). eaCSF volume was also normalized for total WM volume ($eaCSF_{voln}$). Interhemispheric comparisons were also performed.

Statistical Analysis

All statistical tests were conducted using R software (version 4.3.1; https://www.r-project.org/). The GLM statistics were conducted using Python (version 3.8.10; https://www.python.org/), To address the difference in parameter settings during the acquisition of 3D-T1w images and any impact on the extracted features, harmonization was considered prior to analysis. With the aim to remove unwanted scanner effects while preserving associations,

NeuroCombat (Python version 3.8.10) was employed (367). Age, sex, and all clinical variables (DQ and CSS) were considered as covariates.

Descriptive statistics for the WM-PVS_{sr} count and number obtained from MRI scans of the study population were initially computed, with a data distribution check using the Shapiro test. The Friedmann test was then employed to compare the medians of PVS variables across different WM subregions described above. For significant results, post-hoc pairwise comparisons were conducted using the Wilcoxon test.

To investigate the potential impact of disease severity, age, and brain derived volumes (WM, GM, CSF and eaCSF) on the extracted PVS variables, we performed a generalized linear model (GLM) analysis. We set the PVS features (either volume or count) as dependent variables, whereas other imaging-derived measures (eaCSF volume), demographic (age), and clinical data (DQ and CSS) were set as independent variables. Sex was excluded due to the highly unbalanced dataset (male/female: 59/7). A backward selection approach was chosen to improve model interpretability while accounting for possible interactions among the pool of potential predictors. The most parsimonious model explaining the PVS variables was determined using the Akaike Information Criterion (AIC) (368). A p-value <0.05 was considered statistically significant (2-sided) for all statistical analyses.

Furthermore, a post-hoc GLM analysis was conducted on the subgroup (N=21) of patients with normal DQ scores to specifically investigate the effect of ASD. In this model, eaCSF volume, DQ, CSS, and age were included as independent variables, with PVS count as the dependent variable.

Results

Patient characteristics

The final study cohort included 66 patients (male/females: 59/7) with a diagnosis of ASD. Average brain morphological volumes are reported in Table 6-2. (Figure 6-5 S1 in Supplementary Materials).

Table 4-2 Volume of Brain structures of interest

Brain structure	**Volume [cm^3]** (mean ± std)
Intracranial volume (ICV)	1327.8 ± 119.6
White Matter (WM)	339.7 ± 41.8
Cortical Gray Matter (cGM)	606.9 ± 57.4
Cerebrospinal Fluid (CSF)	149.9 ± 26.3
Extra-axial CSF (ea-CSF)	79.7 ± 15.8
Perivascular Spaces (PVS)	4.3 ± 1.2

Descriptive Statistics for PVS

Distribution of PVS variables in both total WM and WM subregions is shown in Table 6-3 and the Shapiro test indicates that they do not follow a normal distribution. The Friedman test revealed A significant region effect in WM-PVS_{sr} count across the six subregions of interest was observed. Post-hoc analysis indicated that WM-PVS_{sr} count was significantly higher in the frontal region and significantly lower in the temporal region compared to all other subregions (Figure 6-3). No significant differences between the left and right hemispheres were found (Figure 6-6 S2 in the supplementary materials).

Table 4-3 PVS distribution in both total WM and WM subregions

	PVS count	**PVS VF**** [%]
Total WM*	995.4 ± 365.5	1.3 ± 0.4
Deep WM	21.0 ± 4.3 %	2.2 ± 0.7
Frontal	29.4 ± 4.2 %	2.0 ± 0.9
Limbic	14.8 ± 2.5 %	1.5 ± 0.5
Occipital	15.5 ± 3.1 %	1.4 ± 0.6
Parietal	19.7 ± 3.0 %	2.1 ± 0.8
Temporal	10.3 ± 2.3 %	1.5 ± 0.7

*WM: white matter

**VF: volume fraction (PVS volume in a region divided by the region volume)

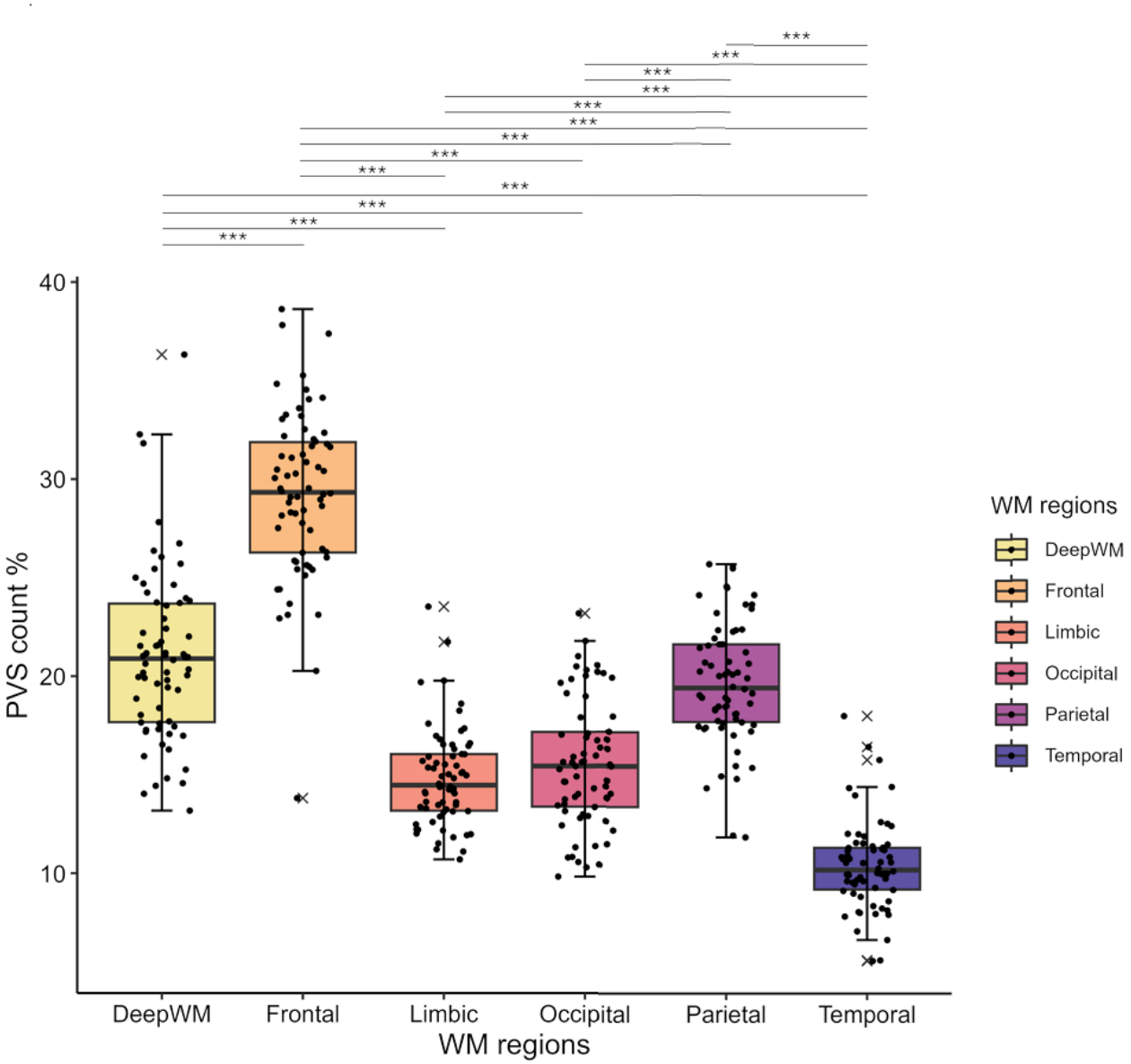

Figure 4-3 PVS count distribution in WM regions. The percentage of PVS is significantly higher in the frontal region and lower in the temporal region. X: Outliers; ***: Significant difference with $p < 0.0001$ (Bonferroni corrected). WM: white matter, PVS: perivascular spaces.

A significant regional effect was observed for PVS VF. Specifically, PVS VF as a percentage was significantly lower in the temporal region with respect to all subregions. It was also significantly higher in deep WM with respect to all subregions except for parietal WM (Figure 6-4). As with WM-PVS_{sr} count, no significant differences were found between the left and right hemispheres for PVS VF (Figure 6-7 S3 in the supplementary material).

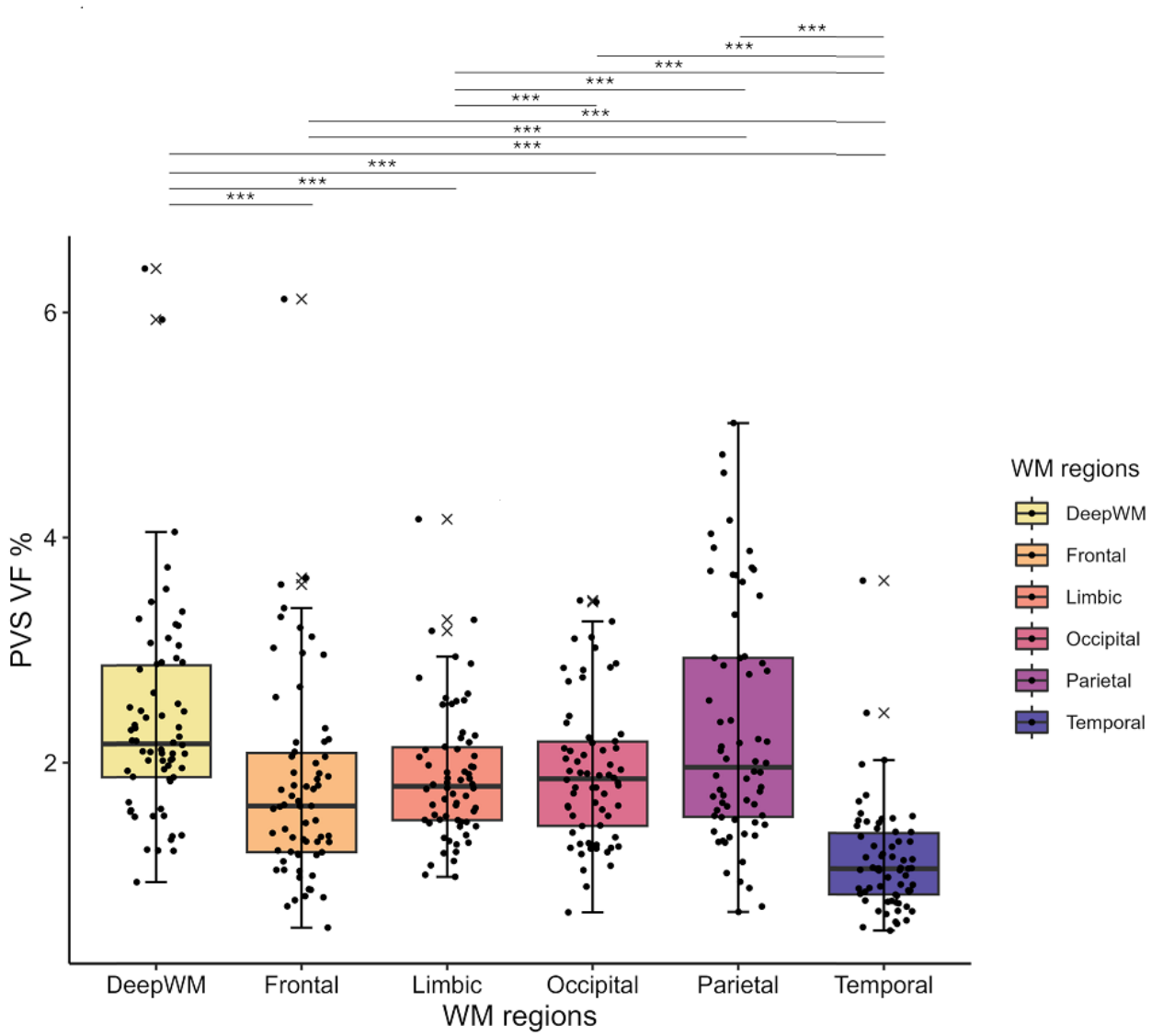

Figure 4-4 PVS VF in WM regions.The percentage of PVS VF is higher in the deep WM region (showing no statistically significant difference with respect to the parietal region) and lower in the temporal region. p- values are Bonferroni corrected. X: Outliers; ***: Significant difference with $p < 0.0001$. WM: white matter, PVS: perivascular spaces, VF: volume fraction.*Generalized Linear Models*

For PVS count, the backward model selection procedure was identified as the best GLM model, including DQ, CSS, and eaCSF as independent variables (F-stat = 54; Table 6-4). Considering the identified model, the GLM indicated that DQ (β = 0.0089) and eaCSF (β = 0.0082) were significantly and positively associated with an increased PVS count, while CSS (β = -0.0174) had a negative effect. These findings indicated that DQ, eaCSF, and CSS explained 0.07%, 14.50%, and 0.76% of the variance in PVS counts, respectively. The model demonstrated a pseudo-R^2 of 0.16, indicating that 16% of the variability in predictions can be explained by the included variables.

Table 4-4 Characteristics of the best GLM explaining WM-PVS count

WM-PVS count	Coefficient	Std error	z-statistic	p-value
Intercept	6.2919	0.026	243.602	< 0.000001
IQ*	0.0087	0.004	2.347	1.89e-2
CSS**	-0.0155	0.002	-6.864	<0.000001
ea-CSF***	0.0088	0.000	37.220	<0.000001

*IQ: Developmental delay

** CSS: Clinical Severity Score (metric to assess the severity of autistic symptoms)

*** ea-CSF: extra-axial cerebrospinal fluid

The average WM-PVS_{tot} volume was 5.5 ± 1.2 cm^3 (median: 5.2 cm^3, min = 3.6 cm^3, max = 9.0 cm^3). The optimal GLM model identified WM-PVS_{voln} as a function of $eaCSF_{voln}$ (F-stat = 6.3). Model parameters are summarized in Table 5. Specifically, GLM indicated a direct association between $eaCSF_{voln}$ and WM-PVS_{voln} (β = 0.0242). A one-unit increase in $eaCSF_{voln}$ corresponded to -1.12% regarding increases in WM-PVS_{voln}.

Post-hoc analysis in the subgroup of patients with normal DQ scores showed a significant negative correlation between the PVS count and CSS (Table 6-5 S2 in Supplementary Material).

Discussion

In this study, we applied WPSS, a recently developed automatic PVS segmentation tool, together with visual inspection and manual correction steps (346), to segment PVS in children that were diagnosed with ASD, with the aim of characterizing the PVS burden in WM. Our results indicated that WM-PVS_{tot} count is significantly associated with DQ, clinical severity, and eaCSF volume, whereas WM-PVS_{voln} was significantly associated with $eaCSF_{voln}$. We also observed that while frontal WM had the highest percentage of PVS, the VF of PVS in this region was not elevated with respect to other WM regions. The lowest percentages of both WM-PVS_{sr} count and VF were observed in the temporal regions.

The GLM analysis indicated that PVS count and volume were associated with an increased volume of eaCSF in our cohort. The concept of eaCSF was first introduced by Shen et al.and refers to the volume of the subarachnoid space above the Sylvian fissures (353). This excludes the CSF in the ventricles and basal cisterns. Previous work showed that eaCSF volume was elevated in children (6-24 months old) at high familial risk of ASD, who later developed ASD compared to infants with high familial risk but who did not develop ASD (353,369). Furthermore, previous work found that children with ASD in the age range of 2 to 4 years also had higher eaCSF with respect to neurotypical children (370). The authors suggested that increased eaCSF volume may serve as an early biomarker for abnormal brain development in infancy (370). However, another study found no significant differences in eaCSF between neurotypical and ASD individuals aged 3 to 42 years (371). The first three years are crucial for brain development, influencing various aspects such as WM growth, cortical thickness, closure of cranial sutures, formation of meningeal lymphatics, and the maturation of arachnoid granulations (235,372,373) . The discrepancies in literature regarding eaCSF volume may be explained by the different patient populations examined (e.g., in terms of age) (369–371) . Furthermore, PVS are closely linked to waste and CSF drainage pathways in the brain, such as the glymphatic system and the intramural periarterial drainage pathways, and are considered MR biomarker of several neurodegenerative and neuroinflammatory diseases in the adult human brain. An elevated number of PVS has been shown to be directly linked to CSF flow dynamics (374). Our results are in accordance with literature that shows a direct correlation of PVS numbers with an increased volume of eaCSF in infants with high familial risk of ASD and toddlers with a diagnosis of ASD. The authors suggested that malabsorption of CSF could lead to an increase in the number and volume of PVS, especially noticeable once the cranial sutures are closed (153). Several other developmental processes could also account for our findings. These include the maturation of arachnoid granulations during the first few years of life, and the physiologic development of meningeal lymphatics in the parasagittal dura, possibly leading to impaired CSF drainage in ASD and stagnation of fluid within the PVS.

Two prior studies have evaluated PVS in children with ASD (153,338). Garic et al. conducted visual assessments to determine the presence of PVS in infants at high familial risk for ASD, while Sotgiu et al. employed a combination of filtering and intensity-based segmentation tools on 2D images from a 1.5T scanner in children with ASD within the age range of 2 to 7 years. The study by Garic et al. found a significantly higher prevalence of PVS in infants at high risk for developing ASD and who later developed ASD compared to infants who had a high risk of developing ASD but did not develop ASD and to infants with low likelihood to develop ASD (353). In contrast, Sotgiu et al. found no significant differences in PVS count between children with ASD and neurotypical children, but they observed a significantly higher PVS count in children with ASD younger than 4 years compared to those above 4 years (338). The discrepancies between the two studies may stem from differences in patient cohort, methodology and the different age groups examined (153,338). One study focused on infants at high or low familial risk for ASD, whereas the study by Sotgiu et al. examined children with a confirmed ASD diagnosis (338,353). The age differences between participants in these previous studies are particularly important, as the brain undergoes rapid development in the first few years of life. For instance, WM growth during this period could alter PVS visualization. Additionally, myelination maturation may impact tissue contrast on MRI, influencing both visual and automated detection of PVS.

Furthermore, PVS are observed in healthy neonates and typically developing children (298,323,375) . Kim et al. used VR scores to assess PVS in neonates, showing grade 1 PVS in BG and grade 0 in WM, with preterm neonates exhibiting higher PVS volumes in the BG. Additionally, two studies have characterized PVS in healthy individuals over the age of 8 years using semi-automatic algorithms, both reporting an age-related change in PVS count among those aged 8 to 30 years. Piantino et al. also demonstrated a high count of PVS in healthy adolescents aged 12 to 21 years old (298). However, the clinical relevance of these findings in the developing brain is not yet well understood. The question of whether the presence of PVS in the developing brain results from a compromised clearance pathway, an underlying genetic process, or neuroinflammation requires further investigation. In the developing brain and in children with autism, interpretation of such markers will require an in-depth understanding and correlations with the development trajectories of the choroid plexus, arachnoid granulations, myelination stages, meningeal growth, parasagittal dura, and neurodevelopmental molecular mechanisms (373,376,377).

Only the PVS count in children with ASD was found to be associated with the DQ and inversely related to the severity of the disease (as assessed by CSS). In this regard, PVS counts are inheritable and may have a genetic basis. Additionally, a recent genome-wide association study has demonstrated a correlation between an increased number of PVS and genes associated with neurodevelopment (378). This may explain the association between more severe neurodevelopmental delay and higher PVS counts in ASD.

The negative correlation between PVS count and clinical severity is difficult to explain by the known effects of age, with an earlier diagnosis of ASD often associated with more severe disease (338). Additionally, evidence suggests that disease severity is affected by various factors, including neural maldevelopment and altered brain growth trajectories, which should be considered in future research (379,380) .

Our study revealed a non-uniform spatial distribution of WM-PVS_{tot} in children with ASD. We found significantly higher WM-PVS_{sr} counts in the frontal regions of both hemispheres, while the temporal lobe exhibited significantly lower counts. Specifically, PVS VF in the temporal lobe was significantly lower, given the low PVS count in this region. However, contrary to what we would expect, PVS VF was significantly higher in the deep WM but not in the frontal lobes. Two potential explanations could clarify this. First, although the percentage of WM-PVS_{sr} count in the frontal region was high, the single spaces may be small, resulting in no significant increase in VF. Second, it is possible that there were few PVS but each large enough to increase the total PVS VF, such as in the temporal lobe.

We evaluated the distribution of PVS in six regions of the brain. We found a high number of PVS in the frontal and parietal regions, whereas the lowest numbers were found in the temporal lobes. Lynch et al. reported a high number of PVS in the frontal regions and lower counts in the temporal regions in children above the age of 8 years (297). They found higher PVS VF in the cingulate and frontal regions and lower VF was shown in the temporal, inferior frontal, and lateral occipital regions (297). Piantino et al. reported similar findings in healthy adolescents (14-18 years) whereby the highest numbers of PVS were in the frontal and the parietal lobes, while the lowest numbers were found in the temporal and occipital lobes (298). In this regard, PVS are spaces related to penetrating vessels that are likely arterioles (111). The frontal, parietal, deep WM, temporal, and the limbic regions are supplied largely by the middle cerebral artery and the anterior cerebral artery, whereas the occipital region is supplied by the posterior cerebral artery (381) . The higher burden of PVS in the arterial territories belonging to the middle and the anterior cerebral artery in healthy subjects appears intriguing and could be associated with specific hemodynamic parameters, arterial wall composition, and arterial pulsatility. Furthermore, disruption in the blood-brain barrier permeability that has been implicated in ASD could contribute to enlargement of PVS. However, more insights are necessary to explain our current findings in the context of ASD and neurodevelopmental disorders. Any correlation with specific cognitive domains will necessitate a more specific WM parcellation, which was beyond the scope of this work.

As the demand for detailed quantification of PVS increases, automatic segmentation tools are becoming essential for capturing PVS that are not visible to the human eye, thereby facilitating

a deeper understanding and analysis of these structures. Different methods have been developed, depending on factors such as available computational resources, MRI field strengths, and distinct MRI sequences. In this study, the WPSS tool was applied, which employs a weakly supervised approach integrating convolutional neural networks (CNNs) with filter-based segmentation methods (346). This tool was specifically developed to analyze multi-contrast images, enhancing the differentiation between PVS and adjacent WM, and it was evaluated on HCP data spanning ages 8 to 90 years. Specifically, WPSS requires 3D-T2w sequences, which are not usually part of clinical MRI sequence protocols. As such, 2D sequences acquired in the three different planes can be reconstructed to obtain 3D-T2w images, but this development was out of the scope of the present study.

Limitations

The major limitation is the lack of a control group, which restricts the ability to draw definitive conclusions regarding the differences in PVS characterization between children with ASD and typically developing children. By comparing PVS variables between children with ASD and a control group, we could better isolate the specific effects of the condition. However, there is a relative vacuum of MRI data in the literature, and public data repositories lack 3D-T2w images that were necessary to apply WPSS in children under 5 years of age. In addition, gathering MRI data in children under 5 years of age even without sedation requires specific research setups (382). Successful implementation of MRI during deep sleep in young children is possible, however this requires the creation of a specific ambiance and modification of the MRI protocol to allow for a shorter duration of the scan. Such scanning poses ethical and practical challenges on our studies. Additionally, all children with ASD in our study were sedated. While we do not expect structural changes in PVS during a brief 30-min MRI scan under sedation, there is no existing data on the effects of sedation or deep sleep on PVS counts and volumes, which adds to the complexity of the study. While obtaining MRI data from this vulnerable population is challenging, it is crucial that such populations are not excluded from clinical research.

We also recognize the limitation of the small sample size. The limited number of participants for each sub-category of autism severity and DQ may impact the statistical power and generalizability of our findings. Therefore, further studies with larger and independent groups are necessary, and future research should focus on longitudinal studies to investigate the developmental trajectory of PVS in children with ASD. Concerning sex, our cohort exhibited a strong bias towards male children, reflecting the fact that ASD is a male-dominant neurodevelopmental disorder. While our study did not detect any sex-related effects, we cannot rule out their presence, as the imbalance in sex may have masked such findings. Our cohort included only two subjects born preterm (at 34 and at 36 weeks of gestation). However, after

performing outlier detection, neither the PVS volume nor the PVS count showed any outliers for these two subjects. Furthermore, in this retrospective study, gene-specific data was not collected. The role of genes in determining PVS numbers therefore cannot be excluded. Additionally, it is important to recognize that both the VR scale and automatic segmentation tools can only offer an estimate of the actual number of PVS. For studies to be comparable and provide meaningful clinically relevant findings , current PVS segmentation tools must be validated against the reference standard (i.e., VR scale) to provide a more robust evaluation of segmentation accuracy and reliability. WPSS was used for the first time in a pediatric cohort without any specific fine-tuning o re-training steps. WPSS cannot reliably segment very large PVS or accurately distinguish linear shaped ventricular horns most prominent in the frontal and the occipital regions. All automatically segmented masks were therefore also manually refined by an experienced neuroradiologist and results obtained were not different from those derived from WPSS alone.

Conclusion

In this study, we used a multi-contrast, deep learning-based segmentation tool with manual correction for PVS analysis to investigate relationships between PVS variables and CSF volume in children with ASD in the age group of 2 to 8 years, and explored the spatial distribution of PVS in WM. The number and volume of PVS in WM in children with ASD may be associated with the volume of eaCSF and the severity of developmental delay.

Supplementary Material

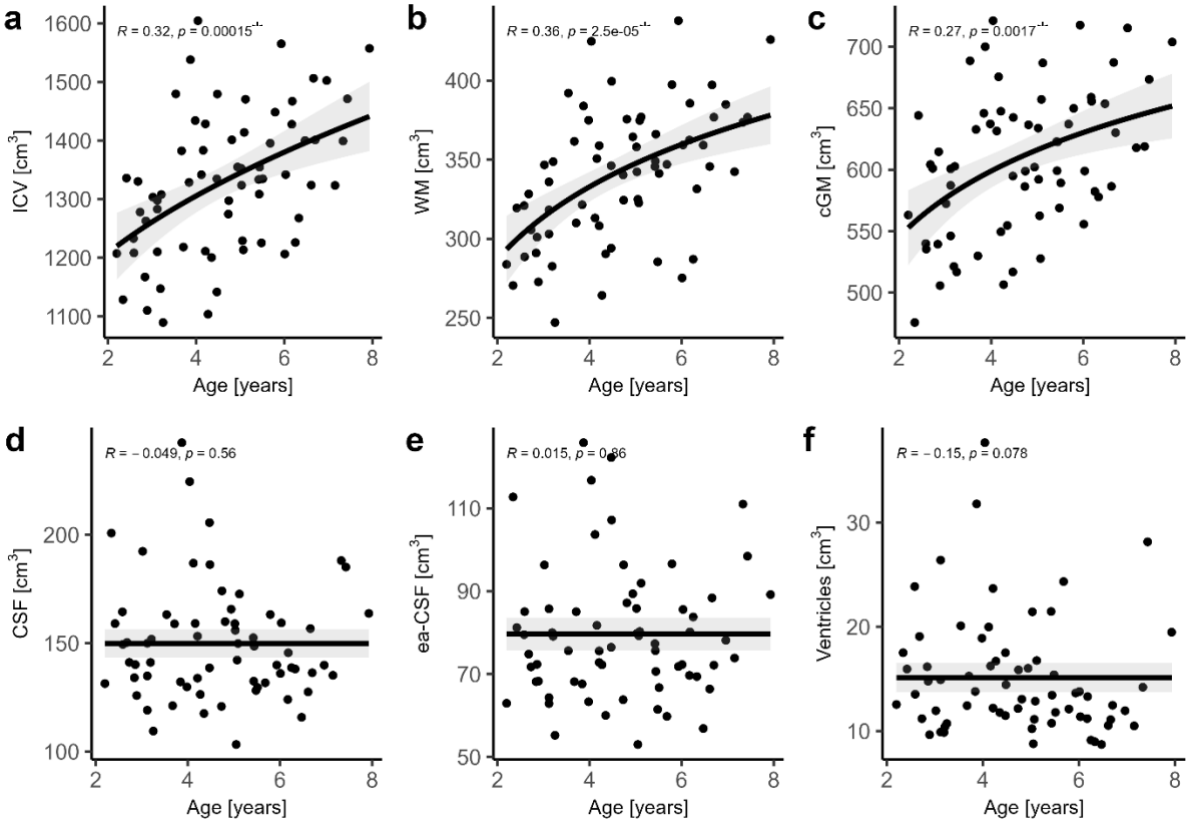

Figure 4-5 S1 Age-related trends of brain morphological variables. **a**) intracranial volume (ICV), **b**) white matter (WM), **c**) cortical gray matter (cGM), **d**) cerebrospinal fluid (CSF), **e**) extra-axial cerebrospinal fluid (ea-CSF), and **f**) ventricles. The best fitting models for each variable are reported as trend lines with 95th confidence interval: exponential for ICV, logarithmic for WM and cGM and constant for CSF, ea-CSF and ventricles. Correlations are quantified using Kendall correlation coefficient (R) and p-value (p). A significant increase in ICV, WM and cGM with age was observed, consistent with existing literature on healthy children.

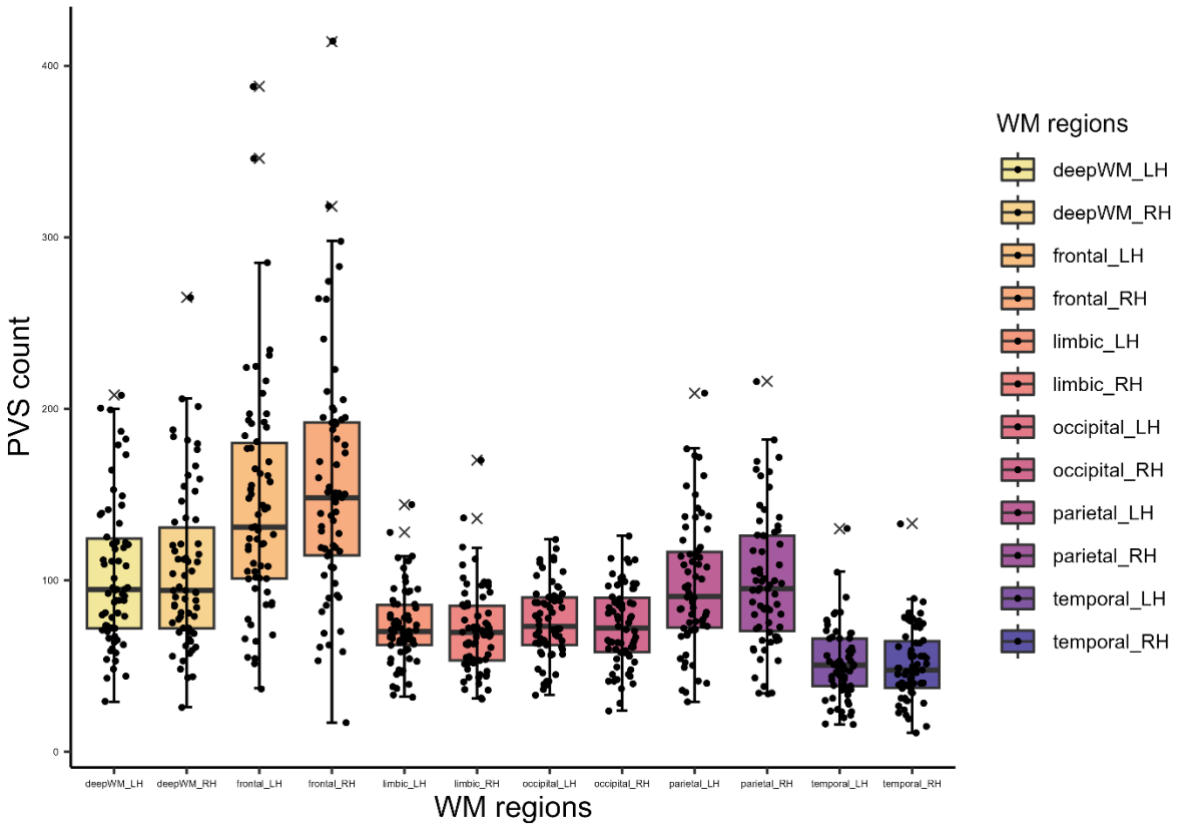

Figure 4-6 S2 PVS count distribution in left and right hemispheres (WM-PVSsr). No significant differences between the two hemispheres were observed ($p>0.05$).

x: outliers

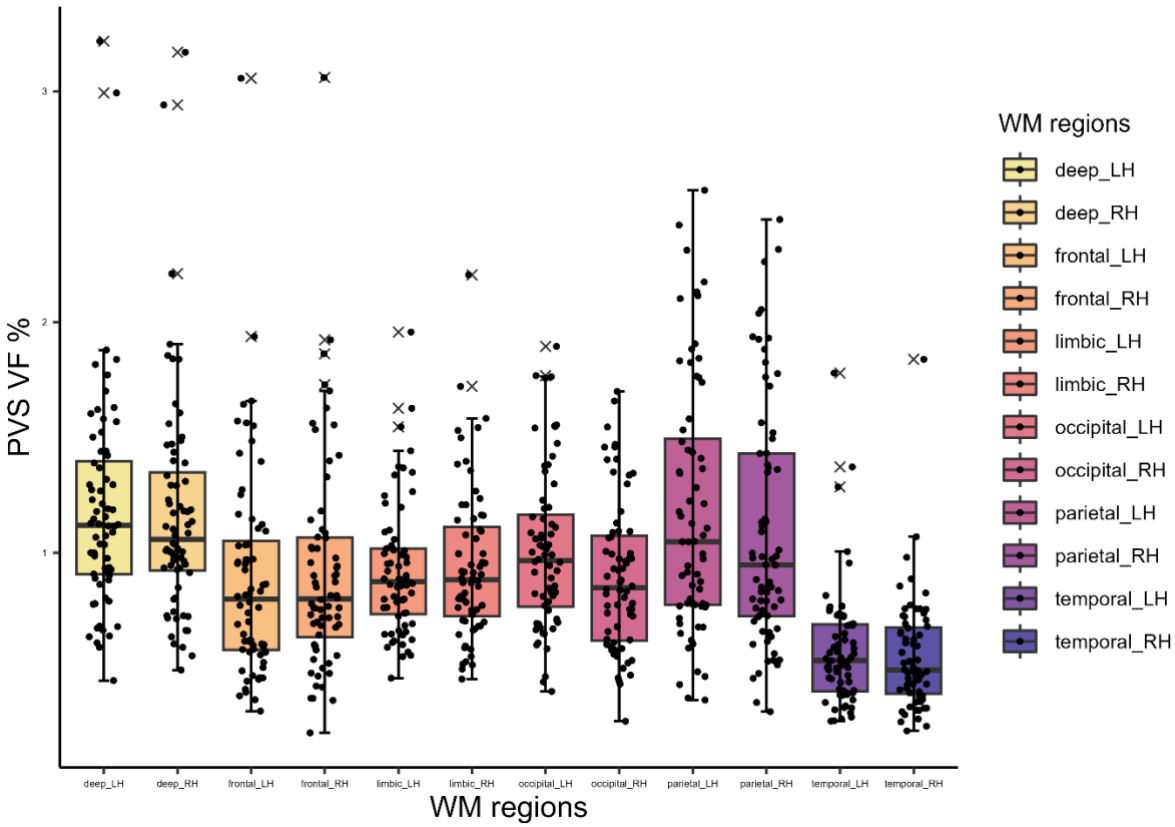

Figure 4-7 S3 Distribution of PVS VF in the left and right hemispheres. No significant differences between the two hemispheres were observed ($p>0.05$).

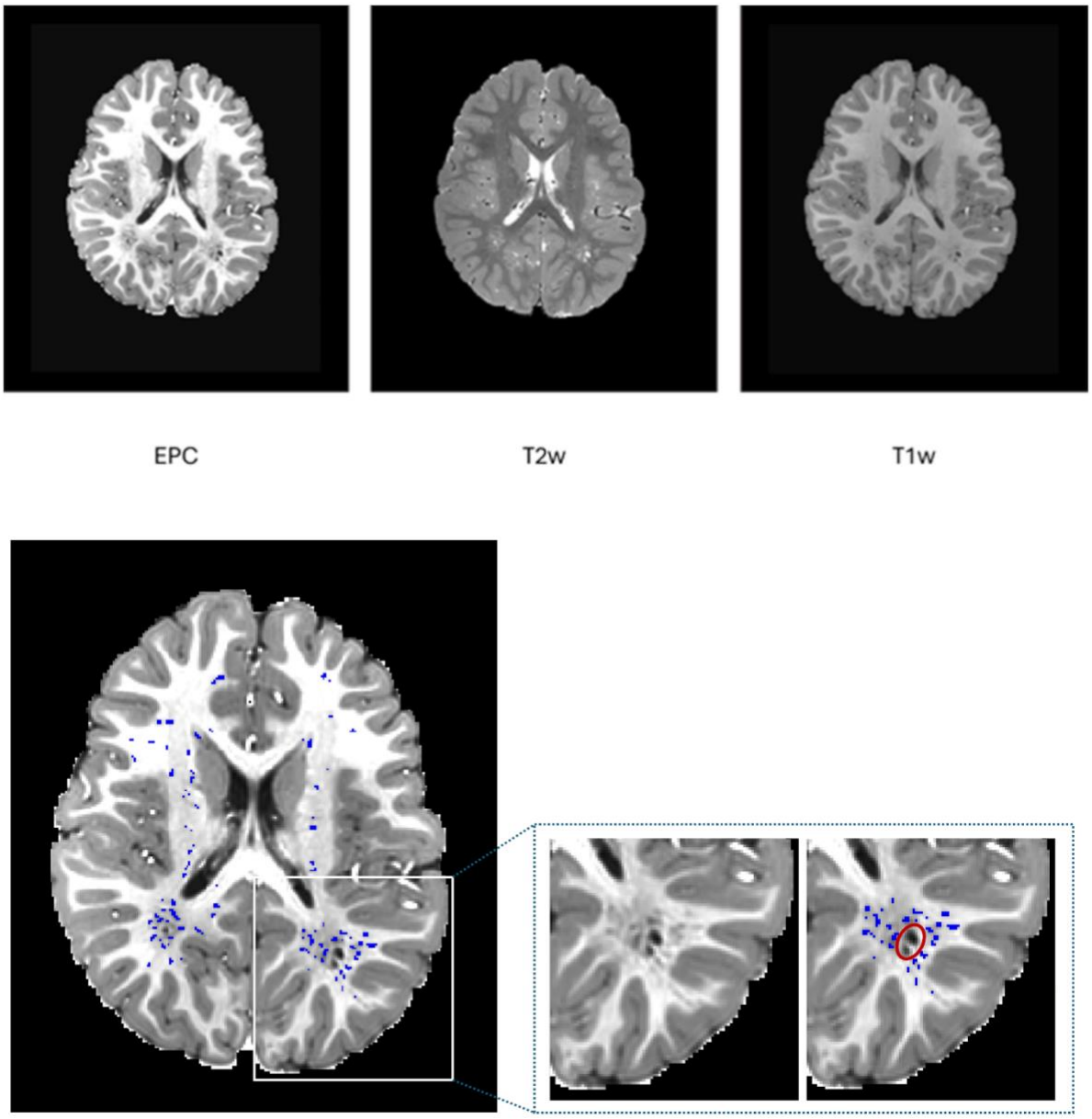

Figure 4-8 S4 Limitation of the applied algorithm. First row (left to right): example of EPC, T2w and T1w images from a random subject. Second row (left to right): very large PVS were not segmented in the studied population. Given this limitation, we chose to manually segment enlarged PVS.

Table 4-5 S1 Patient Demographics and Clinical Characteristics, stratified by sex

Patient Demographics and Clinical Characteristics	Males (n = 59)	Females (n = 7)
Age (years) (mean ± std)	4.73 ± 1.45	4.14 ± 1.47
DQ-class* (number)	Normal (n = 20)	Normal (n = 1)
	Mild (n = 17)	Mild (n = 4)
	Moderate (n = 10)	Moderate (n = 0)
	Severe (n = 12)	Severe (n = 2)
CSS** (number)	4 (n = 5)	4 (n = 0)
	5 (n = 6)	5 (n = 1)
	6 (n = 15)	6 (n = 1)
	7 (n = 12)	7 (n = 2)
	8 (n = 6)	8 (n = 1)
	9 (n = 8)	9 (n = 2)
	10 (n = 7)	10 (n = 0)

GLM considering only patients with a normal DQ

Subject: N = 21, M/F = 20/1

The model remains significant ($p < 0.000001$), with a negative beta coefficient for CSS. The model parameters are reported in Table S2.

Model: PVS count ~ const + CSS + ea-CSF

Table 4-6 S2 Characteristics of GLM model

Model Observations: 21

Degrees of freedom for residuals: 19

Degrees of freedom for model: 2

PVS count	Coefficient	Std error	z-statistic	p-value
Intercept	7.64	0.049	147.134	0.000
CSS*	-0.0675	-0.005	-11.226	<0.000001
eaCSF**	-0.0001	0.000	1.693	<0.5

* CSS: Clinical Severity Score (metric to assess the severity of autistic symptoms)

** eaCSF: extra-axial cerebrospinal fluid

Chapter 5 Paper 4: Parasagittal dural volume correlates with cerebrospinal fluid volume and developmental delay in children with autism spectrum disorder.

This chapter is the Accepted Manuscript of the published version that appears in its final form in Communications Medicine. The full reference is: Nivedita Agarwal, Giulia Frigerio, Gloria Rizzato, Tommaso Ciceri, Elisa Mani, Fabiola Lanteri, Massimo Molteni, Roxana O. Carare, Letizia Losa, Denis Peruzzo; Communications Medicine 2024: 1-9 The original content of the article has not been changed but the formatting has been slightly tweaked for easier readability. To access the final edited and published work see 10.1038/s43856-024-00622-8" (377)

Abstract

Background The parasagittal dura, a tissue that lines the walls of the superior sagittal sinus, acts as an active site for immune-surveillance, promotes the reabsorption of cerebrospinal fluid, and facilitates the removal of metabolic waste products from the brain. Cerebrospinal fluid is important for the distribution of growth factors that signal immature neurons to proliferate and migrate. Autism spectrum disorder is characterized by altered cerebrospinal fluid dynamics.

Methods In this retrospective study, we investigated potential correlations between parasagittal dura volume, brain structure volumes, and clinical severity scales in young children with autism spectrum disorder. We employed a semi-supervised two step pipeline to extract parasagittal dura volume from 3D-T2 Fluid Attenuated Inversion Recovery sequences, based on U-Net followed by manual refinement of the extracted parasagittal dura masks.

Results Here we show that the parasagittal dura volume does not change with age but is significantly correlated with cerebrospinal fluid (p-value=0.002), extra-axial cerebrospinal fluid volume (p-value=0.0003) and severity of developmental delay (p-value=0.024).

Conclusions These findings suggest that autism spectrum disorder children with severe developmental delay may have a maldeveloped parasagittal dura that potentially perturbs cerebrospinal fluid dynamics.

Plain language summary

Cerebrospinal fluid (CSF) is produced in the brain. It is a medium of transport for neural growth factors and waste products. CSF is drained out of the brain through multiple pathways, one of them being the recently identified parasagittal dura (PSD) which also plays a role in the immune system within the brain. We estimated the PSD volume in children with autism spectrum disorder (ASD) and found the volume was associated with the amount of CSF in the brain. We also found that the PSD volume is smaller in children who have severe forms of developmental delay. Our findings suggest problems in the development of the PSD could have in impact on brain development and waste removal in children with ASD. More research in this area could enable a better understanding of the underlying causes of ASD.

Introduction

The parasagittal dura (PSD) is a parasinus tissue located along the exterior walls of the superior sagittal sinus(97). The PSD hosts meningeal lymphatic channels, stromal elements, immune cells, and arachnoid granulations (63,65,249,383). Recent experimental studies demonstrate that this dura-arachnoid tissue serves multiple roles: acts as a conduit for the flow of cerebrospinal fluid (CSF) towards meningeal lymphatics (MLs), facilitates elimination of metabolic waste from the brain and plays a pivotal role in brain immune-surveillance (2,190,250,384,385). PSD contains diverse immune cell subsets actively monitoring for cerebral antigens that find their way into peripheral lymph nodes (251,386).

There are few studies that have employed magnetic resonance imaging (MRI) to quantify the volume of PSD in adults (98,387,388). PSD volumes increase during lifespan which is likely a compensatory response to age-related impairment of the lymphatic drainage and MLs (387–389). In patients with Alzheimer's disease, PSD volume was directly correlated with greater load of amyloid beta deposition in the brain parenchyma, suggesting that a hypertrophic PSD reflects altered dynamics in neurofluids and poor waste clearance (390).

Autism Spectrum Disorder (ASD) is a complex neurodevelopmental disorder characterized by heterogeneous manifestations of symptoms. These include stereotypical behaviors, social and communication skill deficits (391). Epidemiologic studies suggest that the prevalence of ASD is increasing worldwide estimated at 27.6 per 1,000 children (392). The increase in prevalence is likely a combination of enhanced diagnostic criteria but also the presence of more recently discovered epigenetic and multiple environmental factors. The etiology of ASD remains largely elusive with both genetic and environmental factors being variably involved in the expression of ASD phenotype (391,393,394).

Some evidence suggests that CSF dynamics are disrupted in ASD, potentially due to an imbalance between CSF production and absorption(151,353). Furthermore, several studies have suggested that immunological dysregulation in children with ASD initiates a subtle neuroinflammatory process that hinders typical development of the central nervous system(140,395).

MRI is a non-invasive tool to study the anatomy, biochemistry and function of the brain. While diagnosis of ASD is based mostly on clinical scales, an MRI is usually requested to rule out structural or organic etiologies of cognitive dysfunction(149). To date, no studies have evaluated PSD in the developing brain. Our objective was to delineate PSD within our in-patient ASD cohort and explore potential correlations between PSD volume, brain tissue volumes, and clinical

severity scales in ASD by utilizing a semi-automatic segmentation pipeline including a convolutional neural network and manual refinement. Our results suggest that PSD volume does not change with age but is significantly correlated with CSF, extra-axial cerebrospinal fluid volume and severity of developmental delay in patients with ASD.

Ethical approval: This retrospective study was approved by the IRCCS Eugenio Medea Institutional Review Board (Protocol No. 1022) and written informed consent was obtained from all legal representatives (parents or legal guardians) of the children.

Study participants: Children clinically diagnosed with ASD were selected for this study. The diagnosis was conducted by a multidisciplinary team at the Child Psychopathology Unit of the Scientific Insitute IRCSS E. Medea (Bosisio Parini, Italy), according to DSM-5 criteria (American Psychiatric Association, 2013. Diagnostic and statistical manual of mental disorders. Fifth edition. Washington, DC: American Psychiatric Association) and regardless of the presence of global developmental delay or intellectual disability. The diagnostic instruments employed included the Autism Diagnostic Interview – Revised (ADI-R)(357) administered to parents and the Autism Diagnostic Observation Schedule - second edition (ADOS-2)(358) conducted with the child. The Calibrated Severity Score (CSS) was employed as a metric for assessing the severity of autistic symptoms(359,360). The scale ranges from 1 to 10, classifying severity into three categories: 1-3 for non-spectrum, 4-5 for autism spectrum disorder, and 6-10 for autism. IQ was assessed using either the Wechsler Intelligence Scale for Children (WISC-IV)(396)or the Wechsler Preschool and Primary Scale of Intelligence - III (WPPSI-III)(396) selecting the test based on the child's age and cognitive-linguistic abilities. For children unable to complete these tests due to lack of cooperation, age, or absence/difficulty with language we conducted a psychomotor development assessment using the Griffiths Mental Development Scales (cGMDS-ER)(361). IQ score were further grouped in four classes: normal (>70), mild (50-70), moderate (35-49) and severe (20-34). This classification was preferred over the use of a continuous variable because we believe that global functioning is a variable that correlates better with neuroradiological data than small numerical variations within the functioning class. As part of the clinical diagnostic process, all children underwent brain MRI examinations, as well as etiologic instrumental investigations, such as electroencephalograms and genetic tests, between January 2022 and March 2023. The initial clinical sample consisted of a total of 67 patients with a diagnosis of ASD. The following criteria led to the exclusion of patients from the study: (1) age less than 2 or greater than 8 years and; (2) reduced MRI quality. As a result, this retrospective study included a total of 56 children.

MRI acquisition protocol: All our participants were sedated with continuous intravenous infusion of propofol. MRI data were acquired on a 3T scanner (Achieva dStream; Philips Medical Systems)

with a 32-channel head coil at the Diagnostic Imaging and Neuroradiology Unit of the Institute. The MRI protocol included two anatomical sequences: a) 3D-T1 weighted (3D-T1w): sagittal scanning plane; repetition time (TR) = 8,3 ms; echo time (TE) = 3,9 ms; echo train length (ETL) = 256; flip angle = 8°; 1 average; 1x1x1 mm^3 voxel size. Acquisition time: 5 min and 38 s; b) 3D T2-Fluid Attenuated Inversion Recovery (3D-FLAIR): sagittal scanning plane; TR = 4800 ms; TE = 298 ms; inversion time = 1650 ms; ETL = 167; flip angle = 90°; 2 averages; 1x1x1 mm^3 voxel size. Acquisition time: 6 min.

MRI volumetric assessment: 3D-T1w images were processed using an ad-hoc pipeline developed in-house which briefly consists in the following steps: (1) brain extraction from the

acquired images combining multiple tools [BET, ROBEX, ANTS](362,364,366) , (2) bias field intensity artifacts correction using the N4BC algorithm(365), (3) rigid registration to MNI space(363), and (4) segmentation of the main brain structures with Atropos using the PTBP (Pediatric Template of Brain Perfusion) priors(366). From the processed 3D-T1w images the following volumes were derived for each child: ICV, CSF, WM and cGM. The ea-CSF was derived from the CSF mask by manually removing the ventricles and the component below the anterior commissure – posterior commissure line (AC-PC line) (Fig. 7-1) (353) .

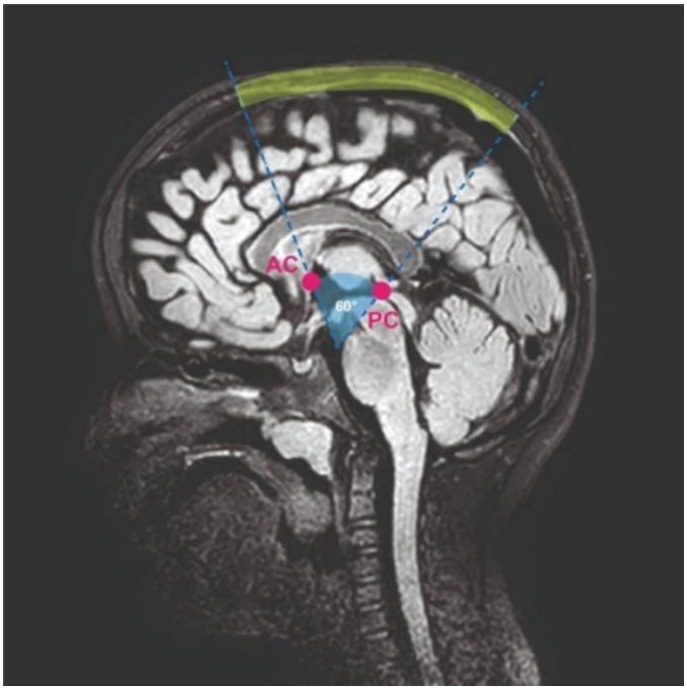

Figure 5-1 PSD segmentation criteria on 3D-T2 Fluid Attenuation Inversion Recovery sequence.AC anterior commissure and PC posterior commissure. The segmented PSD is colored yellow.

PSD segmentation and volumetric assessment:

PSD segmentation was obtained from 3D-FLAIR images as they provide a larger contrast between the PSD and the CSF than the 3D-T1w images. Acquired images were processed using the N4 algorithm to remove any bias field intensity artifact. In this context, convolutional neural networks (CNNs), particularly the U-Net architecture and its variants, have become the state-of-the-art approach to perform an automatic and user independent segmentation(397,398) . Thus, we developed an in house 2D U-Net backbone-based architecture with an intent to facilitate the segmentation process(399). Notably, the network was trained on an independent dataset including 10 healthy adults (32.6±12.5 years) whose images were manually segmented by an expert neuroradiologist. Each participant dataset comprised of at least 150 images for a total training set of 2250 coronal images. Validation was performed on 418 coronal images from 2 healthy adults and the test set comprised of 1941 coronal images derived from 10 ASD children. This U-Net was then applied on our cohort of 56 children with ASD. All the resulting segmentations were manually refined by the neuroradiologist to correct for erroneous segmentations. The performance metrics between the U-Net based automatic segmentation results and the manually corrected segmentations are presented in supplementary figures 7-8 S1 and 7-9 S2. The U-Net architecture was employed given the constrained training dataset, as implemented in previous PSD segmentation studies(398).

The anterior and the posterior segments of PSD in the very young developing brain are either absent or very difficult to disentangle from the surrounding brain structures. Furthermore, PSD aspect in the anterior and posterior segments is very different from the central one due to the relative inclination of the coronal plane with the PSD skeleton direction. As a consequence, we decided to restrict the PSD segmentation to its central components to enhance reproducibility. More precisely, we delineated a region of interest for the PSD segmentation by tracing an arc on the cranial circumference, subtended by a 60° angle passing through the anterior commissure-posterior commissure (AC-PC) landmarks (Fig. 7-1). Finally, the volume of the central component of the PSD was derived from the segmentation and used as a proxy of the whole PSD volume.

Statistics: This study involved the presence of both continuous (e.g. brain structure volumes, age) and categorical variables (e.g. IQ classes, ADOS). Normal distribution of variables was verified with the Shapiro-Wilk test and compared using the student's t-test for independent samples. Correlations were determined by Kendall correlation tests. ANOVA test was used for assessing differences between groups in categorical variables. Data were analyzed using statistical analysis with R setting the significant threshold for the p-value to 0.05 or p-value of 0.01 in case of Bonferroni correction. In the analysis comparing PSD volume with five distinct

cerebral volumes (ICV, WM, cGM, CSF, and ea-CSF), the Bonferroni correction was utilized to tackle the issue of multiple comparisons in statistical testing. This correction involved setting the p-value threshold at 0.01 (calculated as 0.05 divided by the number of comparisons), ensuring a more stringent criterion for determining statistical significance in each individual comparison.

Results

Study participants: The study included 56 patients with confirmed ASD diagnosis that met the inclusion criteria defined in the Materials and Methods section. The characteristics of the study participants are provided in Table7- 1.

Table 5-1 Demographic and clinical characteristics of patients

	Male (N=48)	Female (N=8)
Age (years) Mean ± SD	4.5 ± 1.5	3.9 ± 1.5
ADOS-2 CSS*	Number of patients	Number of patients
• ASD • Autism • N/A**	12 35 1	1 7 0
IQ class***	Number of patients	Number of patients
• Normal • Mild • Moderate • Severe • N/A**	12 11 9 15 1	0 3 0 2 3

*Autism Diagnostic Observatory Schedule – Clinical Severity Score (ADOS-CSS); **N/A = not available; ***Intelligent Quotient class.

Brain volumetrics and age: The average volumes of intracranial volume (ICV), cortical gray matter (cGM), white matter (WM), CSF, extra-axial CSF (ea-CSF) and PSD are reported in Table 7-2. A significant age-related increase in ICV (R = 0.28, p-value = 0.00027), WM (R = 0.34, p-value = 0.0002) and cGM (R=0.18, p-value = 0.049) was observed. In contrast, no significant correlations were found with, CSF, ea-CSF and PSD with age, as depicted in Fig. 7-2.

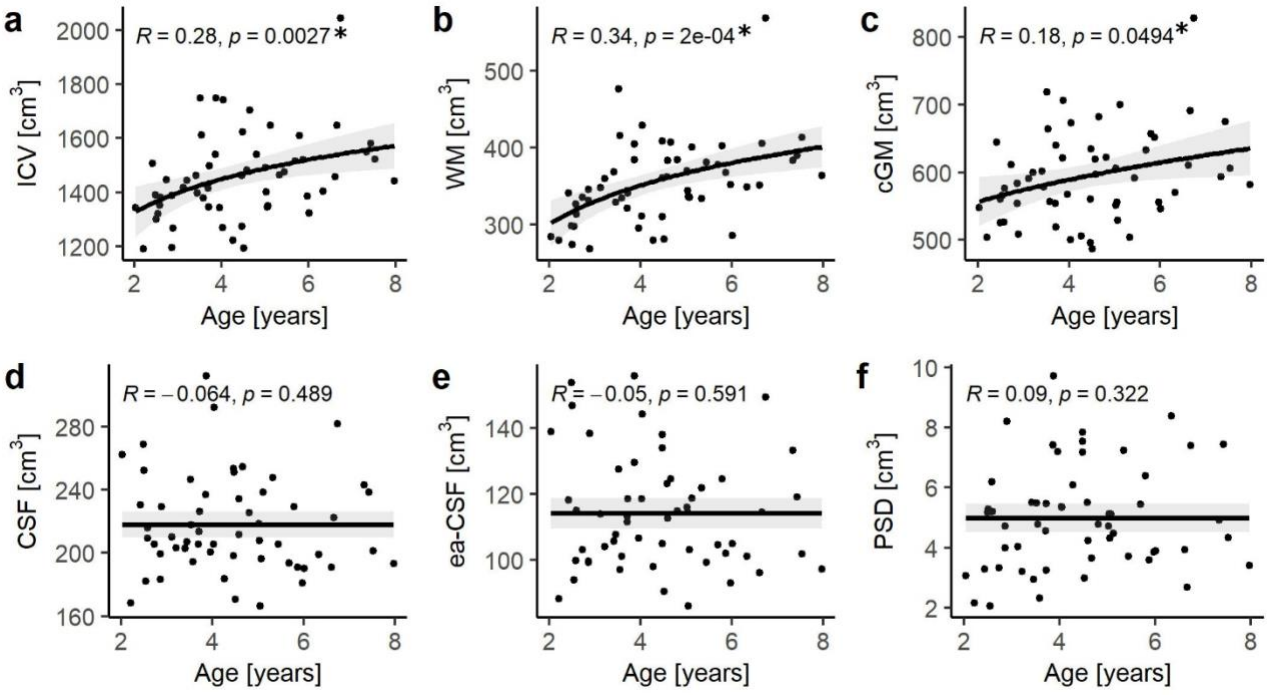

Figure 5-2 Correlation ofage and volume of different brain structures. a intracranial volume (ICV), b white matter (WM), c cortical gray matter (cGM), d cerebrospinal fluid (CSF), e extra-axial cerebrospinal fluid (ea-CSF), and fparasagittal dura (PSD). The best model fits (logarithmic fit for ICV and WM; square fit for cGM and constant fit for all other brain structures) are reported as trend line (continuous line) with 95th confidence intervals. Volume/age relationships were quantified in terms of Kendall correlation coefficient (R) and p-value (p). Significant age-related correla- tions were observed with ICV and WM. After correcting for multiple comparisons no significant correlation was found between age and cGM. Number of patients (N) = 56.

Table 5-2 Mean volumes of all brain structures

Brain Structure	Volumes [cm^3] (Mean ± SD)	
	Males	Females
Cortical Gray Matter (cGM)	599 ± 57	563 ± 112
White Matter (WM)	358 ± 41	329 ± 101
Cerebrospinal Fluid (CSF)	219 ± 29	208 ± 43
Extra-axial Cerebrospinal Fluid (ea-CSF)	114 ± 15	114 ± 27
Intracranial Volume (ICV)	1471 ± 129	1373 ± 282
Parasagittal Dura (PSD)	5 ± 1.7	5 ± 2

PSD and brain volumes: An example of PSD segmentation is represented in Fig. 7-3. The average PSD volume was 5 ± 2 cm^3. Significant correlations were identified between PSD volume and ea-CSF volume (R=0.33; p-value=0.0003), CSF volume (R=0.29; p-value=0.002) (Fig. 7-4). No correlations were identified between PSD volume and ICV, WM, or cGM (Table 7-3).

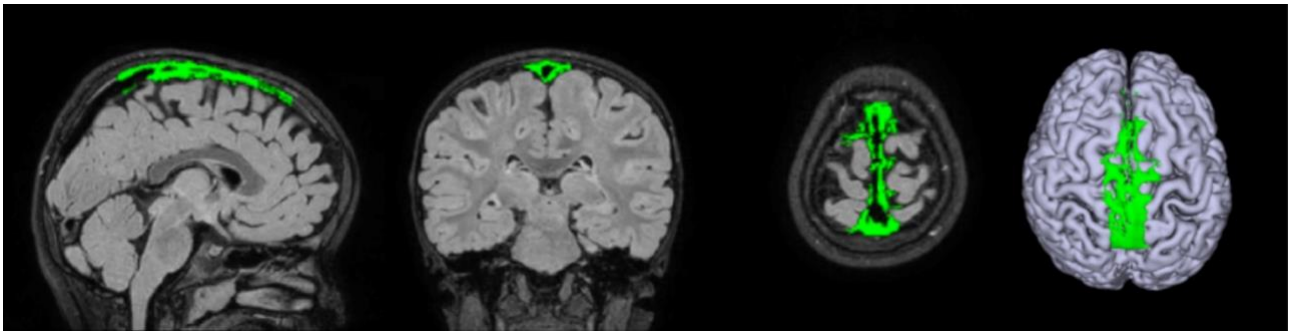

Figure 5-3 Example of segmented PSD. The binary mask ofthe segmented PSD structure is highlighted in green in the three orthonormal planes and superimposed to the FLAIR sequence used in the segmentation. A 3D render of the cGM and the PSD structure is reported in the right panel.

Table 5-3 PSD volume and its correlation with brain morphological variables

Brain Structure	Correlation coefficient with PSD volume	P-value
Intracranial Volume (ICV)	0.119	0.193
White Matter (WM)	0.126	0.170
Cortical Gray Matter (cGM)	0.009	0.921
Cerebrospinal Fluid (CSF)	0.287	0.002*
Extra-axial Cerebrospinal Fluid (ea-CSF)	0.330	0.0003*
*: p-value < 0.01 (after Bonferroni correction for multiple comparisons)		

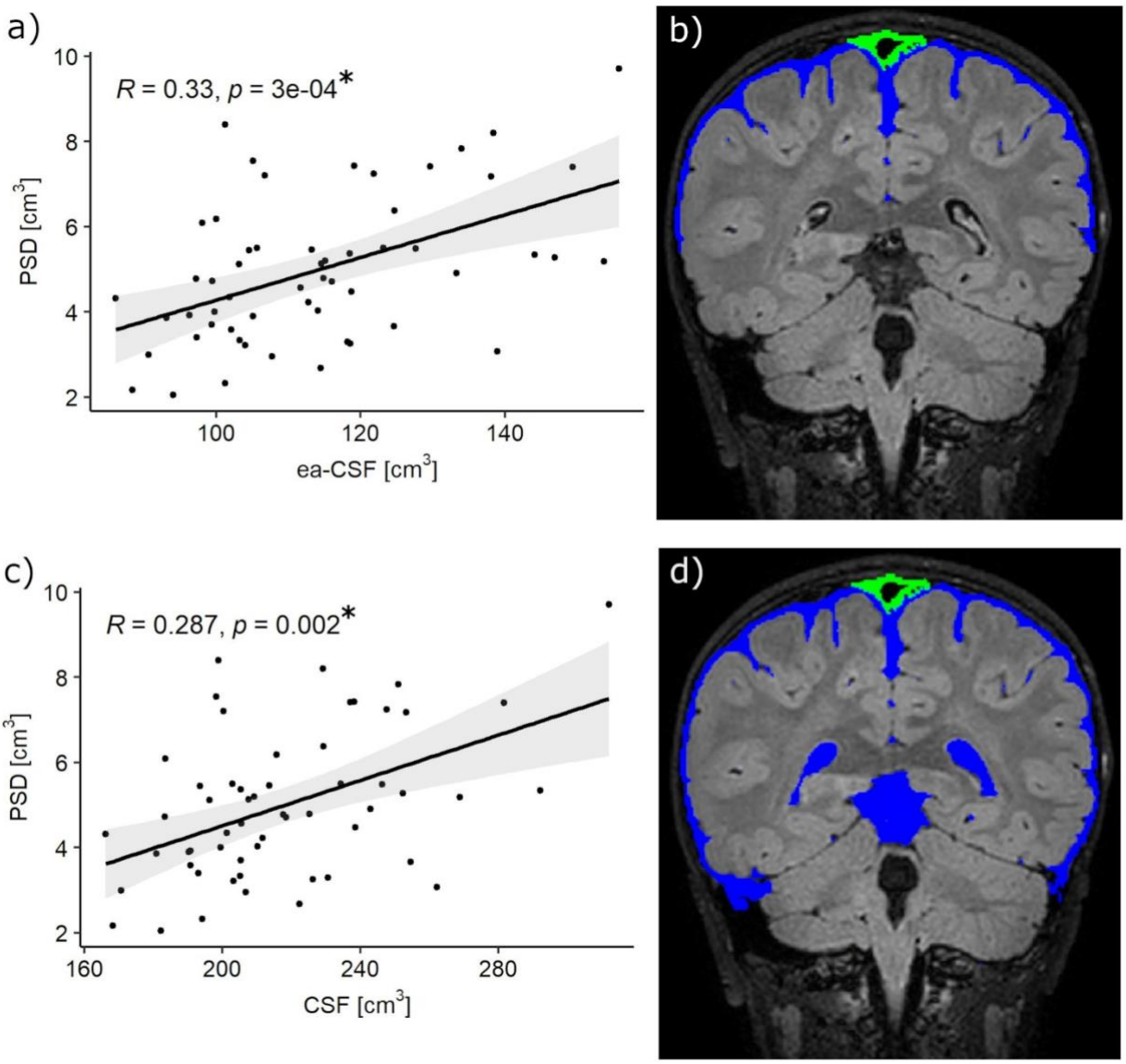

Figure 5-4 Correlation between PSD volume, extra- axial CSF (ea-CSF) and CSF. a) Asignificant positive correlation was observed between PSD volume and ea-CSF; b) schematic representation ofea-CSF (blue) and segmented PSD (green); c) significant positive correlation between PSD and CSF; d) schematic representation of CSF (blue) and segmented PSD (green). Correlations were calculated using the Kendall correlation coefficient. Number of patients (N) = 56.

PSD volume and clinical scores: PSD volume displayed an overall significant inverse relationship with IQ class (p-value = 0.0242, F-value = 3.071; one-way ANOVA) (Fig. 7-5), but not with ADOS-2 CSS scale (p-value = 0.126, F-value = 2.157; one-way ANOVA). Subsequent post-hoc analyses showed only significant difference in the PSD volume between patients with normal and with severe IQ deficit scores (p-value=0.022; one-tailed t-test). No other brain structure volume was correlated with clinical severity.

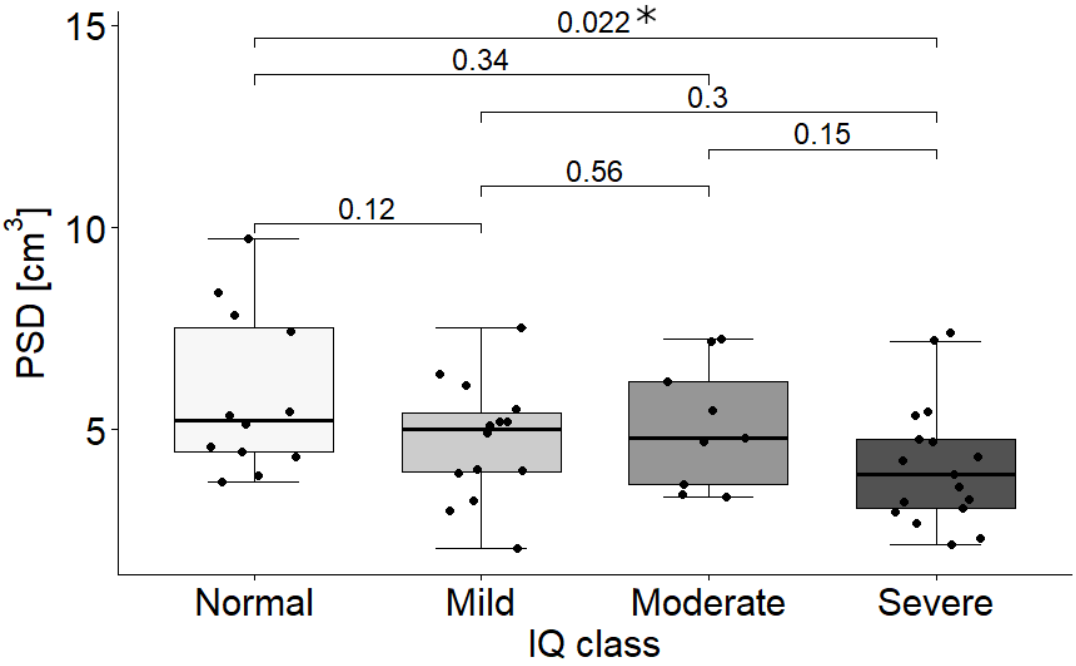

Figure 5-5 PSD volume distribution in patients with different IQ classes (normal, mild, moderate, and severe). The subsequent statistical comparisons (t-test) highlight a significant difference in PSD volume between patients with normal (N= 12) and severe (N= 17) IQ class (p-value = 0.022). Box limits indicate the range of the central 50% of the data, with a central line indicating the median value, and data points outside the upper and lower bounds are considered outliers.

PSD and ea-CSFvolume correlation in developmental delay: In children with severe developmental delay the PSD volume is smaller compared to those with normal IQ, despite having the same volume of ea-CSF. In other words, the correlation between PSD volume and ea-CSF fails to reach statistical significance in children with severe developmental delay (R = 0.103; p-value = 0.6), whereas in children with normal IQ this correlation appears to be statistically significant (R = 0.515; p-value = 0.02) (Fig. 7-6).

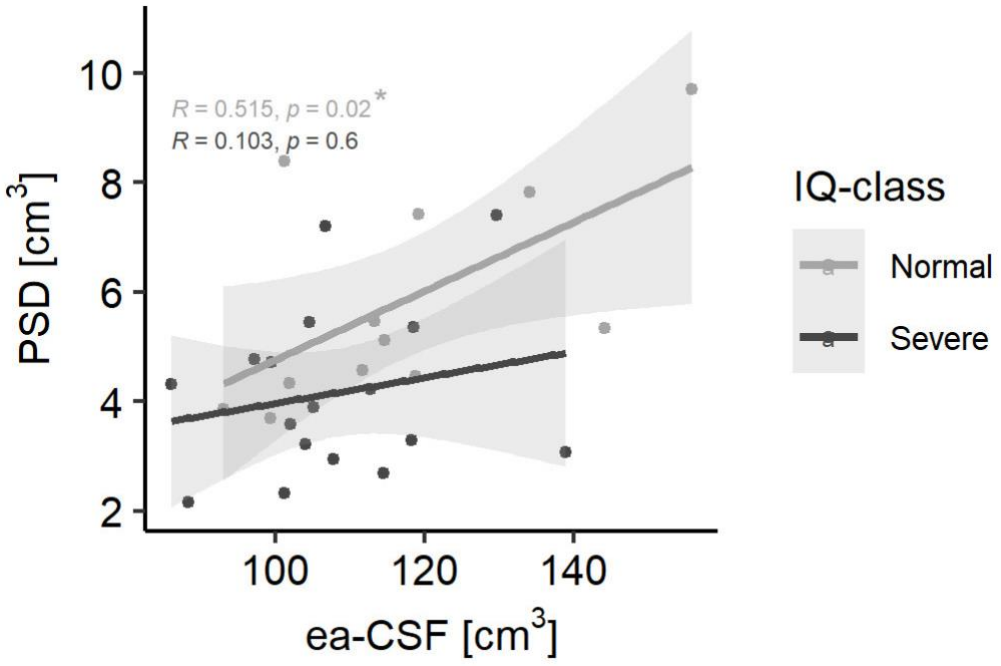

Figure 5-6 Correlation between PSD volume and ea-CSF. Children without developmental delay (N= 12) present a strong positive correlation between PSD and ea- CSF whereas in children with severe developmental delay (N= 17) this correlation does not reach statistical significance. Correlations were calculated using the Kendall correlation coefficient

Discussion

The role of PSD as a CSF draining pathway is unexplored in both healthy developing children and ASD. We found a robust positive correlation between PSD volume, CSF and ea-CSF volume and an inverse relationship between PSD volume and the severity of developmental delay, or IQ, in our cohort of ASD children. Severe developmental delay may be a consequence of an underdeveloped PSD which is inefficient in draining CSF, contributing thereby to the accumulation of toxic substances and promoting subtle neuroinflammatory process often associated with ASD(140,143,335). These findings hold importance in light of the growing understanding of the role that PSD plays in promoting the drainage of CSF from the brain, in the removal of waste materials and in facilitating immune-survellaince(97,140,400).

The ea-CSF has been described as the CSF space that envelops the cerebral dorsal subarachnoid space which contains CSF that is in direct proximity with the cerebral meninges and PSD(353). It excludes the ventricular space and the lower or ventral portion of the subarachnoid space. Increased ea-CSF volume is a well-documented potential MRI biomarker in children with ASD and those at high risk of developing ASD(151,353,369). Our findings add to the substantial body of literature that indicate altered CSF dynamics in this population(151,335).

In the traditional model, arachnoid granulations (AGs) are recognized as the primary sites of CSF absorption(55). A recent study described five different types of AGs in the adult brain possessing different capacities for CSF transfer into MLs(401). AGs typically reach maturity by the age of 18 months, but their numbers change over the lifespan(37,244). In some individuals, AGs are completely absent without changes in CSF homeostasis, suggesting that there are alternative routes to CSF absorption, the PSD being one of them(37,402).

Age-related developmental trajectories for WM and cGM are well-documented in typically developing children with cGM showing an inverted U-shape growth trajectory compared to the WM that continues to increase till early adulthood(403,404). In our cohort, WM, cGM and ICV volumes increased with age. This closely mirrors the developmental trajectories reported in a large longitudinal study on children with ASD and normally developing children(405). Structural organization of the brain tissue and the maturation process of CSF production and absorption pathways in the developing brain are thought to affect CSF volume trajectories with age(406). Recent works suggest that beyond the age of 4 years, no change in ea-CSF is observed in children with ASD(407,408). Our work also confirms that the volume of ea-CSF does not change with age.

The development of meninges in the postnatal period reveals that MLs, including the meninges and the calvarium, continue to develop postnatally(188,373). Although a few studies have explored PSD volume in healthy adults and individuals with neurodegenerative conditions, the PSD volume in both typically developing children and those with ASD has yet to be explored in the literature. Melin et al. (2023) reported a PSD volume of 4.19 ± 2.07 cm^3 in a heterogenous group comprising healthy adults and individuals with CSF disorders, whereas Song et al. reported an average PSD volume of 11.85 ± 2.16 cm^3 among adults diagnosed with Alzheimer's disease (98,390). Therefore, although direct evidence is lacking, the growth trajectory of the PSD in the developing brain is expected to follow the growth of the meninges, the dural venous system and the calvarium in early childhood(409). The volume of PSD did not correlate with the volumes of WM, cGM, or ICV but it strongly correlated with the volumes of CSF and ea-CSF. Although we report findings on children, they align with existing literature that have utilized similar deep learning-based algorithms to derive PSD volumes in adult humans over the age of 20 years(387–389). These results further emphasize the crucial role of PSD in the exchange of CSF from the dorsal subarachnoid space.

In our study, PSD volume did not correlate with cGM or WM volumes(387,388). Again, this finding is in line with literature on adults in which PSD volume was not correlated to age-related brain atrophy rather only with CSF volume, underscoring the important link between CSF and PSD(389). In a separate study involving patients with Alzheimer's disease, PSD volumes were significantly correlated with an increasing burden of amyloid beta deposition with no significant

correlation observed with overall brain atrophy(390). Furthermore, while studies in human adults reveal a significant positive association between PSD volume and age, in our study no age-related effect on PSD volume was observed notwithstanding changes in aforementioned brain volumes over age. Further studies are required to fully comprehend the normal development of PSD in the developing brain. In addition, there is little understanding of the relationship between PSD volume and its CSF draining capacity in very young children and needs further investigation.

Another noteworthy finding in our study is the inverse relationship between PSD volumes and IQ scores among children with ASD. This observation implies that children with severe developmental delay also have a smaller PSD compared to children with normal IQ. The recent discoveries of the role of PSD and the MLs may shed some light on CSF dynamics that are altered in ASD(65,97,250,400). The hypotrophic PSD in ASD chidren with severe developmental delay may harbour hypoplastic MLs, initiating a chain of events that hampers CSF drainage, leads to accumulation of cerebral toxins, and triggers neuroinflammatory processes affecting brain development(410). Although an inverse relationship was found between PSD volume and the degree of developmental delay, it is noteworthy that CSF volume remains constant across various IQ levels (Fig.7-7). No correlations were found with ADOS-2 CSS scale.

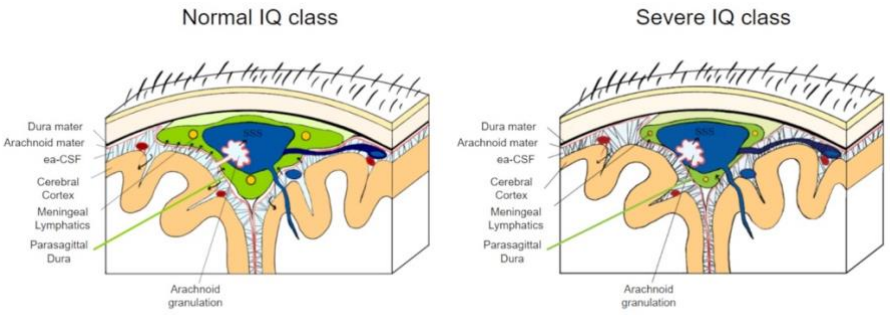

Figure 5-7 Schematic representation of the parasagittal dura (PSD) in the coronal section in children with normal and severe IQ class. In the left panel, a normal- appearing PSD is represented whereas in the right panel, an underdeveloped PSD is noted. Note that in both figures the volume of CSF remains constant. Black arrows represent the direction of movement of CSF. SSS: superior sagittal sinus.It is well-known that PSD is not the only pathway for CSF efflux. Since the ea-CSF volume remained constant in children with normal and severe developmental delay, it is likely that CSF drains more effectively through other CSF-draining pathways. Previous investigations have underscored the primary involvement of the PSD in neuroimmune functions, positing its role in CSF drainage as secondary. It is important to note that our study cohort predominantly consists of children with moderate to severe ASD, which limits our ability to establish meaningful correlations with milder forms of the condition. On the contrary, our discoveries unveil a Pandora's box, suggesting that the investigation of MLs in ASD could potentially unlock neuroinflammatory process and altered CSF homeostasis in ASD.

Meningeal cells play crucial roles in guiding the development of ventricular radial glial cells, ensuring proper neuronal development, and are heavily involved in neuro-immune functions(411). While the specific origin of PSD is unknown, it is likely that this tissue contains meningeal cells and meningeal stroma, as it lies within the two layers of the dura mater. Meningeal neural progenitors migrate through multiple pathways within the brain parenchyma, contributing to cortical development, guiding neuronal connectivity, and forming membranes that delineate perivascular spaces around penetrating arterioles(412,413). Findings from 16p11.2 mouse models of ASD clearly identify that endothelium is dysfunctional and affects stability of blood vessels. This contributes to behavioural changes specific to ASD. Proper angiogenesis is also fundamental for optimal neurogenesis(414). Anomalies in meningeal tissue development during early stages of life, potentially influenced by genetic or epigenetic factors, may also contribute to established neuronal dysconnectivity in ASD. Our study suggests that PSD is underdeveloped in children with ASD who suffer more severe developmental delay. While additional investigations are necessary, it is proposed that a poorly developed PSD could potentially impact developmental processes, promote neuroinflammation leading to dysregulation of neuronogenesis and angiogenesis.

In addition to PSD volumes, dilated perivascular spaces (DPVS) are considered indirect markers of obstructed drainage of fluids(227,233,344,415). Only one study has examined DPVS in young children with ASD which reports a non-significant increase in the prevalence of DPVS in kids with severe form of ASD(338). Our observations add to the literature whereby some form of obstruction to the movement of neurofluids may be present in ASD(2).

Our choice for employing 3D-FLAIR to segment PSD was based on previous initial work employing 3D-FLAIR for imaging MLs and quantifying the volume of PSD(63,97,98,252). 3D-FLAIR is commonly used in the standard MRI protocol and is readily accessible. Neither contrast-enhanced T2-weighted black blood sequence nor sub millimetric 3D-T2 weighted sequences that have been used in other studies to segment PSD were available in this retrospective study(387,388).

Our research paves the way for exploring newer avenues in the assessment of children with ASD, with the aim of identifying MRI markers suggestive of altered fluid dynamics and identify treatment strategies. To achieve this, there are several critical steps to consider. Firstly, it is essential to establish quantitative measurements of PSD volumes in the developing brain. Secondly, the correlation between PSD volumes and serum-based markers of proinflammation should be investigated to gain deeper insights into the neuroinflammatory mechanisms involved. Thirdly, research into potential genetic alterations in children with ASD that could contribute to the underdevelopment of PSD and MLs warrants examination.

The primary constraint in our study is the lack of a reference group of typically developing children within our specified age range. There are no publicly available datasets in healthy young children that have 3D-FLAIR images that was employed for our deep learning algorithm for PSD segmentation, following established methods outlined in the work of Melin et al. (98). Large datasets on children younger than 5 years is even more scarce. Our institution's primary focus is on the diagnosis and treatment of very young children with moderate to severe neurodevelopmental disorders, which positions us favorably in acquiring MRI in young children with ASD. However, this specialized focus limits our ability to readily assemble a comparable group of healthy children. Nonetheless, this study provides greater insight and hope in our understanding of this devastating condition on the rise world-wide. Another limitation pertains to our sample size. We employed strict recruiting criteria to eliminate confounding factors. This still resulted in a sample size sufficient to detect significant associations between PSD volume, CSF, ea-CSF volume and IQ class in ASD. A third limitation concerns the PSD segmentation pipeline. The scientific community lacks consensus on the methods, procedures, and even the types of images to be used for PSD segmentation. To address this, we utilized a cutting-edge segmentation method to generate the PSD mask from our images and incorporated a manual correction step to rectify any remaining errors. Furthermore, we confined the PSD segmentation to its central component to enhance the reproducibility of the process. Nevertheless, it is important to acknowledge that each of these choices may have an impact on the ultimate results. Lastly, we are aware that sedation can affect the dynamics of neurofluids. Animal research studies indicate that glymphatic clearance in the interstitial space increases during natural sleep and sedation with ketamine(416). In another study, rats sedated with propofol exhibited an expansion of the extracellular space with improved interstitial fluid (ISF) drainage compared to other anesthetics like isoflurane(417). While preclinical research suggests that sedation positively influences ISF drainage, human studies are lacking. It remains uncertain whether a 30-minute sedation period in our study would result in significant changes in the PSD volume. This would be subject to further investigation. Even if we hypothesize an increased rate of CSF efflux into PSD during sedation, we would not expect our results to change because all our patients were under the same experimental condition during MR acquisition. Eide and Ringstad demonstrated that the rate of molecular clearance via PSD is not affected by sleep but there are no studies that determine changes in PSD volume with sleep or sedation in humans or in animals(418). Successful implementation of MRI during deep sleep in young children would be ideal, however this necessitates the creation of a specific ambiance and modification of the MRI protocol to allow for a shorter duration of the scan (419). Such scanning poses practical challenges in our research studies, which remain currently difficult to navigate.

Conclusions

This study suggests that an underdeveloped PSD may contribute to the severity of developmental delay in children with a diagnosis of ASD. Furthermore, PSD volume correlated only with total CSF and ea-CSF volume which validates its role in CSF drainage and strongly supports the emerging and ongoing revelation of CSF exchange between the subarachnoid space and the PSD.

Author contributions:

Project administration: N.A, L.L.; software - implementation of the computer code and supporting algorithms: L.L., G.R., T.C.; patient recruitment: F.L., E.M; formal analysis and visualization: G.F., T.C., L.L., D.P., G.R.; Administration and writing of the original draft N.A.; writing – editing: G.F., L.L., T.C., D.P., G.R.; Supervision: R.C., M.M., D.P. All authors approved the final manuscript.

Acknowledgements: This study was supported by Italian Ministry of Health (Ricerca Corrente 2024) and 5x1000 funds for biomedical research. The APC is funded by Bibliosan.

Competing interests The authors declare no competing interests

Data availability statement: All source data relative to images are available from the corresponding author on reasonable request. All source data to produce graphs in figures 2,4,5 and 6 are available at https://doi.org/10.6084/m9.figshare.24582369.v4 (420)

Code availability statement: codes and software versions used are available at https://doi.org/10.6084/m9.figshare.24582369.v4 (420)

Reporting summary: Further information on research design is available in the Nature Research Reporting Summary linked to this article.

Supplementary Materials

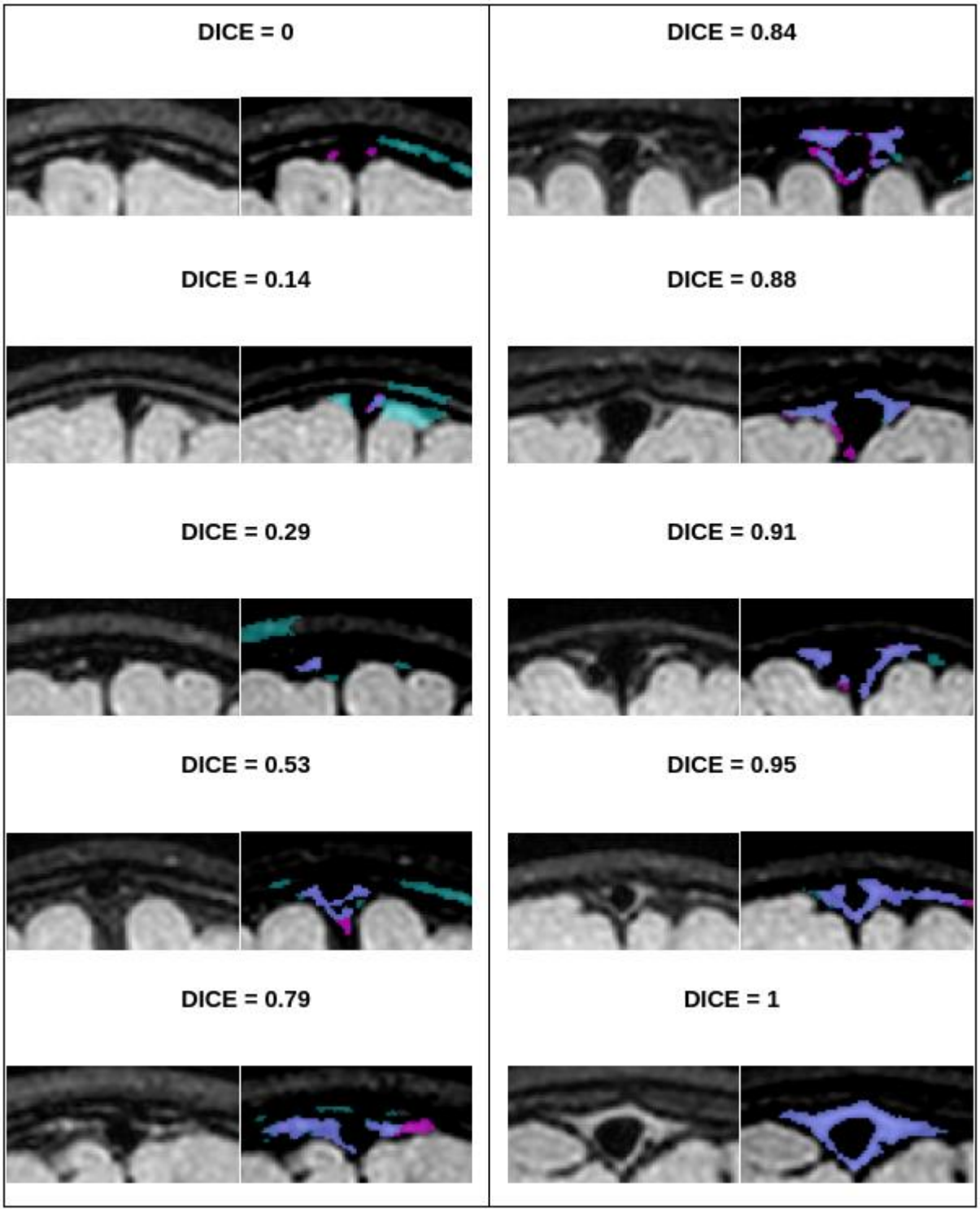

Figure 5-8 S1 Automatic segmentation masks of PSD overlapped with manually corrected masks from ten randomly selected images from the entire cohort. Each example shows cropped FLAIR images on the left side, while on the right side, FLAIR images are displayed overlapped with both manual and automatic segmentations. Additionally, the DICE-score corresponding to each example is presented.

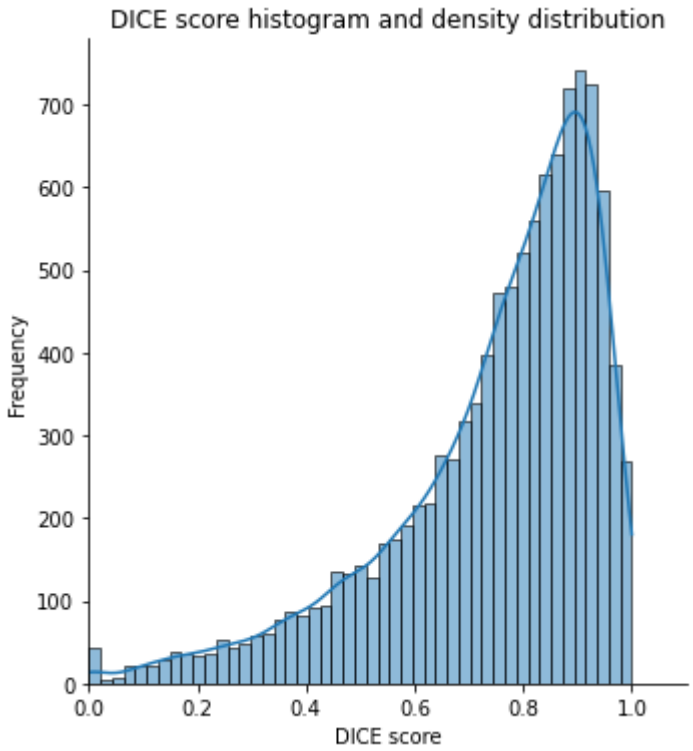

Figure 5-9 S2 Histogram and density distribution of DICE-scores, comparing the manually corrected segmentation of PSD as the ground truth with automatic segmentation of PSD across 56 children with ASD.

Chapter 6 Paper 5: 3D U-NET for automatic segmentation of PSD in children (intention to submit)

This chapter is based on work being prepared for submission to a journal. It delineates methods developed to segment the parasagittal dura of children with ASD.

Abstract

Background: The parasagittal dura (PSD) is considered to be a site of brain immune-surveillance and one of the pathways for drainage of cerebrospinal fluid. PSD is readily visible on magnetic resonance (MR) imaging and its volume changes have been associated with brain neurodegenerative processes. Different semi-automatic and automatic methods have been developed and validated for segmenting the PSD in adult cohorts. However, none of these methods are available for segmenting this structure in the developing brain.

Purpose: In this work, an automatic tool for the segmentation of PSD using 3D-T2 Fluid Attenuated Inversion Recovery (3D T2-FLAIR) MR images in the developing brain is proposed.

Study type: Retrospective.

Population: 65 children clinically diagnosed with autism spectrum disorder (M/F: 57/8; mean = 4.57 ± 1.62 years).

Field Strength/Sequence: 3.0 T 3D-T2 Fluid Attenuated Inversion Recovery and 3D T2-weighted sequences.

Assessment: PSD segmentation from 3D T2-FLAIR sequence by the developed 3D U-Net based algorithm. Manual segmentations, performed by a neuroradiologist, are considered as ground truth.

Results: The model achieved a Dice Score Coefficient of 0.85, a volumetric similarity of 0.97 and a Hausdorff distance of 22.1.

Data conclusion: This algorithm represents the first publicly available tool for automatic segmentation of PSD in young children with a diagnosis of autism spectrum disorder based on standard clinical 3D T2-FLAIR sequence.

Keywords: deep learning; single-class image segmentation; parasagittal dura; paediatrics; autism spectrum disorder; magnetic resonance imaging.

Introduction

Parasagittal dura (PSD) is a mesenchymal stromal tissue which lies within the two layers of the dura mater (1). This tissue is generally visible around the superior sagittal sinus and is frequently seen on clinical magnetic resonance (MR) imaging acquisitions (2). Little was known about the function of PSD until the recent discovery of the meningeal lymphatic network. Several studies have described the presence of meningeal immune cells within the PSD (2–5) suggesting that this structure is involved in functions such as neuro-immunosurveillance, and in supporting central nervous system homeostasis (6–8). In addition, emerging evidence suggests that PSD plays a role in the drainage of cerebrospinal fluid (CSF) acting as a sink for metabolic waste (9–11).

The evaluation of PSD has recently been proposed through the usage of semi-automatic and automatic segmentation tools applied on MR images, allowing the quantification of its volume in human adults (12–15). It has been shown that the volume of PSD increases linearly with age in healthy adults (12, 16). In a study combining positron emission tomography and MR imaging involving a cohort of patients aged between 55 and 80 years, PSD volume was found to be related to the degree of severity of Alzheimer's disease (14). Specifically, subjects with a higher deposition of amyloid-beta appear to have a larger PSD (14). The authors suggest that a larger PSD may indicate a compensatory response to age-related lymphatic drainage impairment and reflect altered neurofluid dynamics and possible presence of neuroinflammation (14, 16). Recently, quantification of PSD has been proposed in a paediatric population. A positive correlation between the volumes of PSD and CSF and a negative correlation between the volume of PSD and the severity of developmental delay were found in a population of children aged from 2 to 8 years clinically diagnosed with autism spectrum disorder (ASD) (17). The results suggest that PSD volume is linked to CSF volume corroborating its role in CSF dynamics (17). The negative correlation, however, is a novel finding and it is suggested that PSD might also play a role in neurodevelopmental processes.

Given the importance of PSD and its potential clinical impact in furthering our understanding of neurodegenerative, neuroimmunological and neurodevelopmental disorders, accurate segmentation of PSD is necessary to determine its volume and to conduct subsequent analyses. Therefore, the development of tools that facilitate its segmentation and volume quantification appear of cardinal importance. Deep learning architectures have become widely used for image segmentation in the medical field due to their capability to learn and identify detailed features within images (18, 19). U-Net architecture has proved to be successful for this kind of task and, in addition, good segmentation performance can be achieved by considering a limited amount of data and the use of data augmentation (20). Different semi-automatic and

automatic methods have been proposed to address the segmentation of PSD in a cohort of adults. Hett and colleagues (12) introduced a semi-supervised pipeline combining a fully connected neural network (FCNN) with voxel clustering based on a Gaussian mixture model to classify voxels as either PSD or sagittal sinus using 3D T2-weighted (3D-T2w) MR images. Similarly, Song et al. (14) utilized a semi-supervised algorithm that integrates a FCNN for segmenting PSD from 3D-T2w MR images. Melin and collaborators (15) developed a semi-automatic pipeline, employing 3D-T2 Fluid Attenuated Inversion Recovery images (3D T2-FLAIR) as input to a 2D U-Net for PSD segmentation, followed by manual refinement. In the study performed by Hett et al. (13), a 3D FCNN was trained on individuals aged 11 to 83 years to automatically segment PSD from 3D-T2w MR images and was then applied to a cohort of subjects ranging from 5 to 100 years. The authors found challenging to accurately determine PSD volume in children aged 5 to 10 years, with a tendency to overestimate PSD volume in this age group. In a recent work, a semi-automatic 2D U-Net-based tool to extract PSD from 3D T2-FLAIR in a population of children clinically diagnosed with ASD (age range: 2-8 years) was successfully applied (17). However, as in all previously mentioned semi-automatic segmentation tools, this approach required manual post-processing to correct errors in the generated PSD masks. This step is time-consuming and introduces both inter- and intra-rater variability (20), thus reducing the reproducibility of the studies. In summary, there is not a consolidated and validated method to automatically segment the PSD, especially in the context of the developing brain.

To address this gap, we develop and validate an automatic 3D U-Net-based algorithm to segment PSD in young children with ASD. We employed the 3D T2-FLAIR sequence, as it is commonly used in clinical practice and included in standard diagnostic protocols. Our ultimate goal was to provide both clinicians and researchers with a freely accessible tool for the automatic segmentation of PSD in children.

Materials and Methods

Ethical approval

The local Institutional Review Board of our institute approved this retrospective study. Legal representatives of all subjects gave their written informed consent prior to participating in this study.

Study Participants

All participants with an age range of 2-10 years old, clinically diagnosed with ASD and who were scanned for diagnostic purposes between July 2021 and September 2023 at our institute, were included in this study. Exclusion criteria were i) age under two or over ten years old; ii) MR image

of poor quality and iii) MR image positive for other pathologies or malformations. The resulting cohort comprised 65 children with ASD in age from 2 to 10 years (M/F: 57/8; mean = 4.57 ± 1.62 years).

MR imaging acquisition protocol

All participants underwent a standardized imaging protocol at 3T scanner (Achieva dStream; Philips Medical Systems) with a 32-channel head coil at the Diagnostic Imaging and Neuroradiology Unit of the Institute. Sedation was necessary in all patients and was administered via a continuous intravenous infusion of propofol, with the dosage adjusted according to body weight. Standard MR imaging acquisition protocol includes a 3D T2-FLAIR sequence which was used to develop the automatic segmentation tool and a 3D-T2w sequence which was used to compare the segmentations obtained through the developed algorithm with those proposed by Hett and colleagues (13). 3D T2-FLAIR was acquired in a sagittal plane (Time of Repetition (TR) = 4800 ms; Time of Echo (TE) = 298 ms; inversion time = 1650 ms; echo train length (ETL) = 167; flip angle = 90°; 2 averages; 0.5x0.5x0.5 mm^3 voxel size; 339x480x480 image dimensions; acquisition time: 6 min). The 3D-T2w sequence was acquired with a TR = 2.5; TE = 195.5 ms; ETL = 117; flip angle = 90; 1 average; 1x1x1 mm^3 voxel size.

PSD segmentation

PSD was manually segmented by an expert neuroradiologist on the 3D T2-FLAIR images. These images were preprocessed using a N4 bias field correction algorithm to correct for intensity artifacts caused by the bias field (21). No registration was applied to the preprocessed images for two reasons: first, all 3D T2-FLAIR images were acquired with similar orientations, and second, to preserve the tissue-contrast ratio, no resampling operations associated with spatial transformations were performed. In the developing brain the prefrontal and the occipital regions of PSD are highly variable in size and volume, thus to improve reproducibility, the segmentation of PSD was restricted to its central components (17). Specifically, the anterior commissure-posterior commissure (AC-PC) landmarks were manually identified for each subject. Subsequently, the region of interest for PSD segmentation was identified by tracing an arc along the cranial circumference, subtended by a 60° angle passing through the AC-PC landmarks. Manual segmentation of PSD was performed in a 2D framework by a neuroradiologist. The rater had the possibility to navigate through different slices, but the drawing was always done in the coronal view. This manual approach may introduce slight inconsistencies between consecutive slices. To address this, we applied a Gaussian spatial filter with a sigma of 0.6, followed by a binarization with a threshold set to 0.4 to the manual PSD masks (22). This process resulted in an approximate average 2% increase in PSD volume compared to the raw manually segmented

mask. We considered this increase as being of minor importance from a quantitative point of view, but rather contributes to a more physiologically accurate 3D representation of the PSD. The filtered masks were then used as the ground truth to train the model. Figure 8-1 provides an example of the raw PSD manual segmentation and the resulting one after filtering and thresholding steps for two subjects.

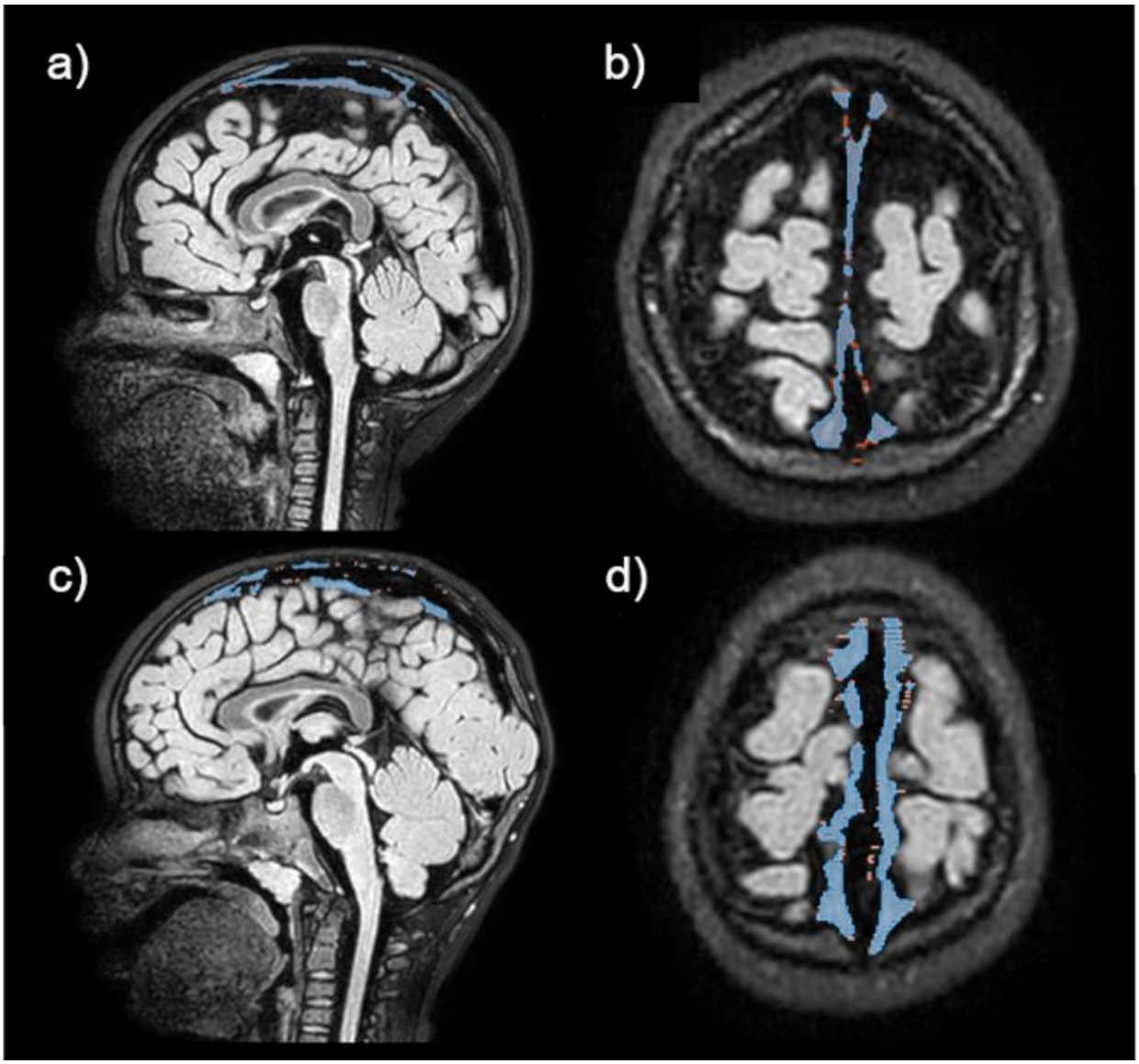

Figure 6-1 Examples of raw PSD manual segmentation (red) and filtered PSD segmentation (light blue) for two different subjects. a), c) sagittal plane views; b), d) axial plane views

Network architecture and training strategy

A 3D U-Net-based architecture to segment PSD structure was implemented in MONAI (version 1.3.0) (23), a freely available PyTorch-based framework for deep learning in healthcare imaging. The U-Net architecture is composed of two parts: a contracting path, also called encoder, which compresses the input into a latent-space representation to extract feature maps, and an expansive path, also called decoder, where the spatial resolution of the feature maps is

increased and the number of features decreases (24). Skip connections are an essential part of U-Net: they combine semantic information (of a low-resolution layer) with local information (of a high-resolution layer) allowing a better learning of the spatial information. The 3D U-Net was configured as a single input channel, five layers starting with 16 filters for the first layer and doubling the number of filters in each subsequent layer. A two-strided convolutions residual unit was set to downsample and upsample data in the encoder and decoder paths, respectively, with a 3x3x3 kernel size followed by batch normalization and parametric rectified linear unit activation blocks. All 3D T2-FLAIR images were resampled to a voxel size of 0.5x0.5x0.5 mm^3, with pixel intensities scaled to a range between zero and one.

The dataset was randomly divided into training data, validation data, and testing data on the basis of approximately 75% (N=49), 10% (N=6), and 15% (N=10) of the entire dataset. The 3D U-Net based model was trained with training data, whereas the validation set was used to determine the optimal model for PSD volume segmentation. This model was then applied to the test set to evaluate the algorithm's performance on a new dataset.

The training was performed in python version 3.10.12 on a GeForce GTX 1080Ti 11.0GB graphics processing unit (NVIDIA). To address the limited amount of memory given by the hardware, we identified the AC landmark on the sagittal 3D T2-FLAIR plane and subsequently cropped below the horizontal line passing through the AC. In other words, the tissue beneath the horizontal line was discarded but no part of the PSD was affected (Figure 8-2).

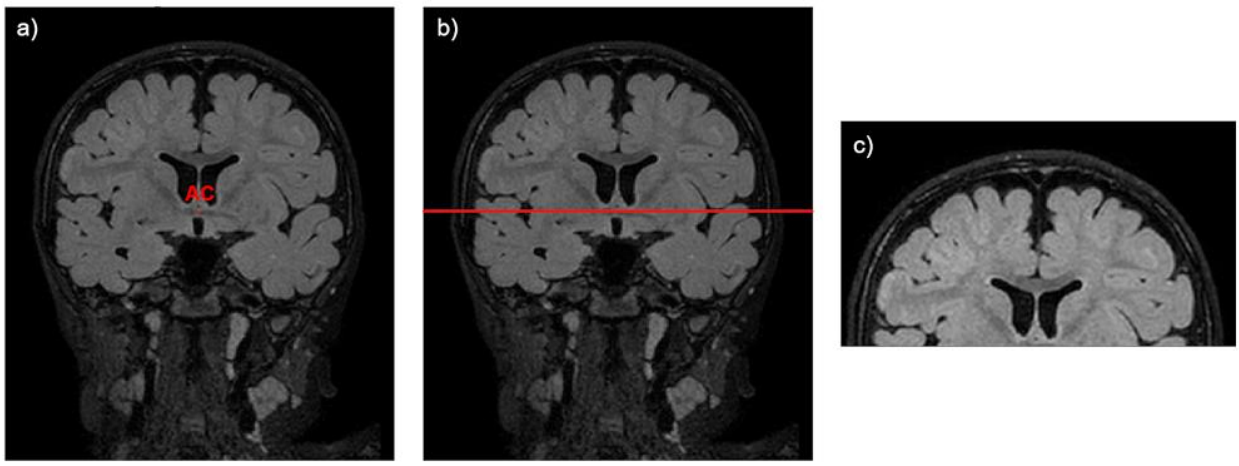

Figure 6-2 Example of cropping below AC point. a) AC landmark (red point) identified on 3D T2-FLAIR on coronal view, b) horizontal line (red line) passing though AC landmark, c) cropped image provided as input to the PSD segmentation algorithmData augmentation was performed on training data to address the limited number of samples and to mitigate overfitting (19). Randomized transformations were taken into account, more specifically concerning spatial transformation we applied

random drop out where random regions were replaced by zero values, random flipping along all three axes, random rotation around the y-axis, and random de-zooming/zooming. Four 3D patches of 96x96x96 voxels for each patient were obtained by the transformation *RandCropByPosNegLabel* implemented in MONAI and were given as input to the net. Training was conducted with optimization on the training set and early stopping on the basis of performance against the validation set. Optimization was performed with Adam optimizer with a learning rate of 10^{-4} and a batch size of two. Dice Loss was employed as a loss objective during model training. The best model was saved on the basis of improving performance on the validation set, based on DICE score. The overall time required for training was about 8 hours. Figure 8-3 summarizes the followed workflow.

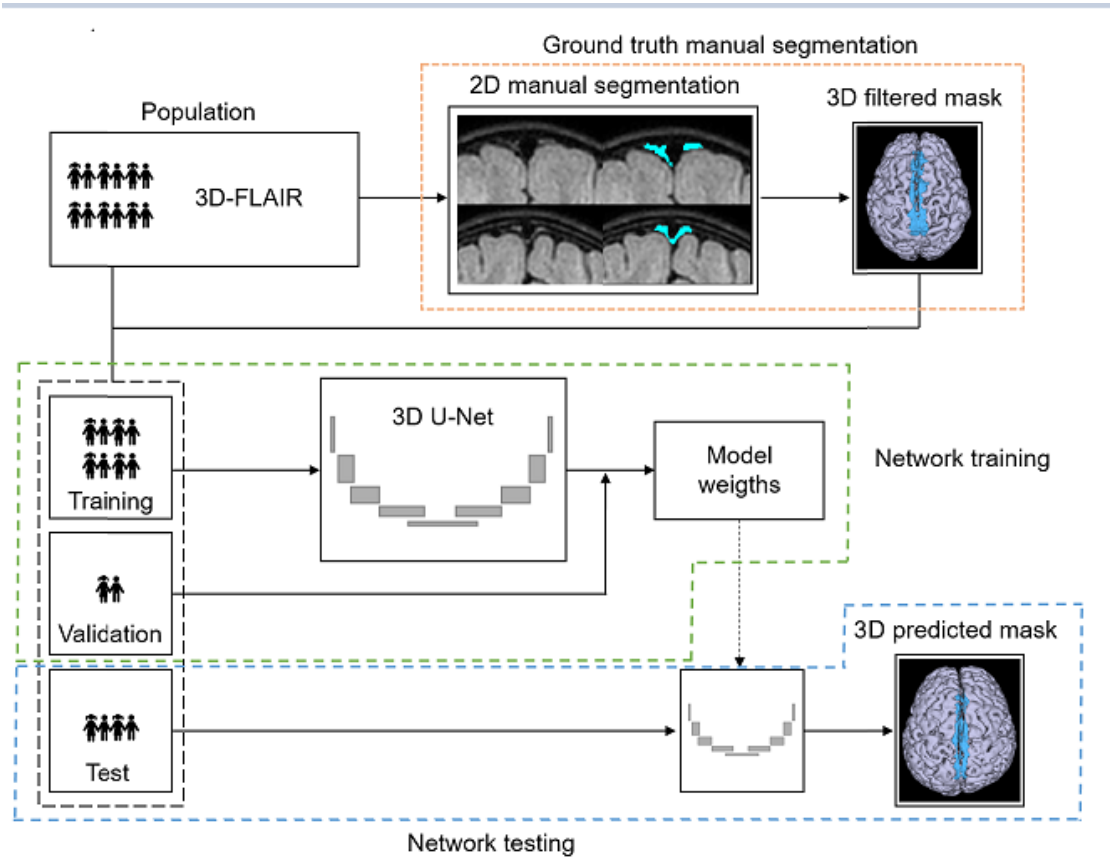

Figure 6-3 Workflow for 3D PSD segmentation. The pipeline comprises three main steps: ground truth manual segmentation, network training and testing. Three metrics were assessed to evaluate the segmentation performance of the model: i) DICE score coefficient, measuring the voxel similarity between the ground truth mask and the model output mask; ii) volumetric similarity coefficient, which considers the volume of the segmentation to indicate similarity and iii) Hausdorff distance defined as the maximum distance between any point in the ground truth mask and its nearest point in the model output mask, and vice-versa to evaluate contour distance.

$$DICE\ score\ coefficient = \frac{2\ x\ n\ true\ positive\ voxels}{2\ x\ n\ true\ positive\ voxels\ +\ n\ false\ negative\ voxels\ +\ n\ false\ positive\ voxels}$$

$$Volumetric\ similarity\ coefficient = 1 - \frac{|n\ false\ negative\ voxels\ -\ n\ false\ positive\ voxels|}{2\ x\ n\ true\ positive\ voxels\ +\ n\ false\ positive\ voxels\ +\ n\ false\ negative\ voxels}$$

$$Hausdorff\ distance\ (A,B) = max(h(A,B), h(B,A))$$

where h(A,B) is called the directed Hausdorff distance and is given by

$$h(A,B) = max_{a \epsilon A} min_{b \epsilon B}\ ||a - b||$$

All metrics were calculated by the usage of EvaluateSegmentation tool (25).

A linear regression analysis was performed to examine the differences in the volumes between the manually and the predicted segmentations of PSD using R software version 4.3.1.

To assess the goodness of the developed tool and its performances, both visual inspection and quantitative analysis - based on the DICE coefficient and regression analysis - were conducted by comparing the segmentation of PSD obtained using our developed tool with the only one publicly available (13). As both the proposed and the Hett method were applied on the acquired 3D T2-FLAIR and 3D-T2w spaces, a registration operation is required to compare their results. In particular, we computed a rigid registration from the 3D T2-FLAIR to the 3D-T2w images and applied it to move the 3D T2-FLAIR PSD mask to the 3D-T2w space using a nearest-neighbourhood interpolation.

Results

The results for the DICE score, volumetric similarity coefficient, and Hausdorff distance for both the validation and test sets are presented in Table 1. The performance indices are similar between validation and test sets, suggesting that the training procedure reached a good generalization

level, with the exception of the Hausdorff distance. We further investigated this discrepancy. The manual inspection of the predicted PSD masks in the test set, highlighted the presence of few voxels belonging to the frontal subcutaneous area in a single subject (subject #3) (Figure 8-4). This macroscopic error led to a significant increase in the Hausdorff distance value. However, after manual correction, Hausdorff distance greatly reduced (Table 8-1).

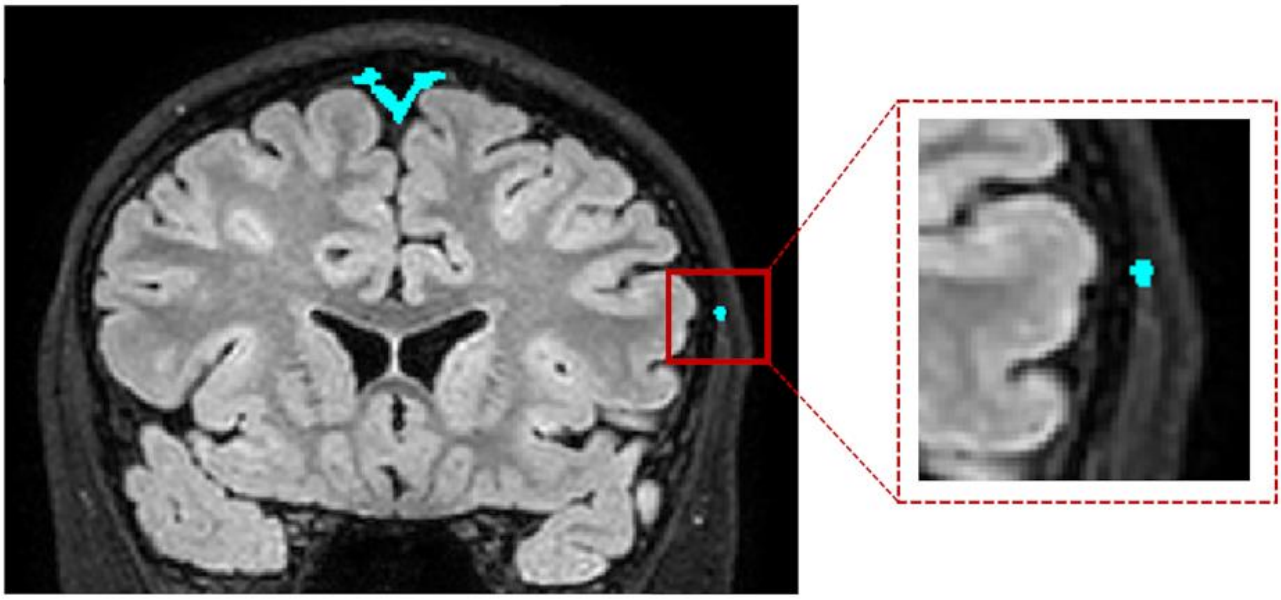

Figure 6-4 Worse case example of automatic PSD segmentation (subject #3) in coronal plane

Table 6-1 DICE coefficient, volumetric similarity and Hausdorff distance for validation and test sets (reported as mean ± standard deviation). After manually correcting of degraded PSD segmentation in subject #3, the mean and standard deviation of the Hausdorff distance in the test set greatly improved and is provided in brackets

Metric	**Validation set**	**Test set**
DICE score coefficient (↑)	0.76 ± 0.03	0.85 ± 0.03
Volumetric similarity (↑)	0.97 ± 0.01	0.97 ± 0.03
Hausdorff distance (↓)	11.12 ± 2.84	22.11 ± 43.77 (8.58 ± 1.80)

Examples of some typical segmentation errors are shown in Figure 8-5. These errors consisted of a few voxels near the PSD area that exhibited similar intensity ranges to the PSD but did not belong to this structure.

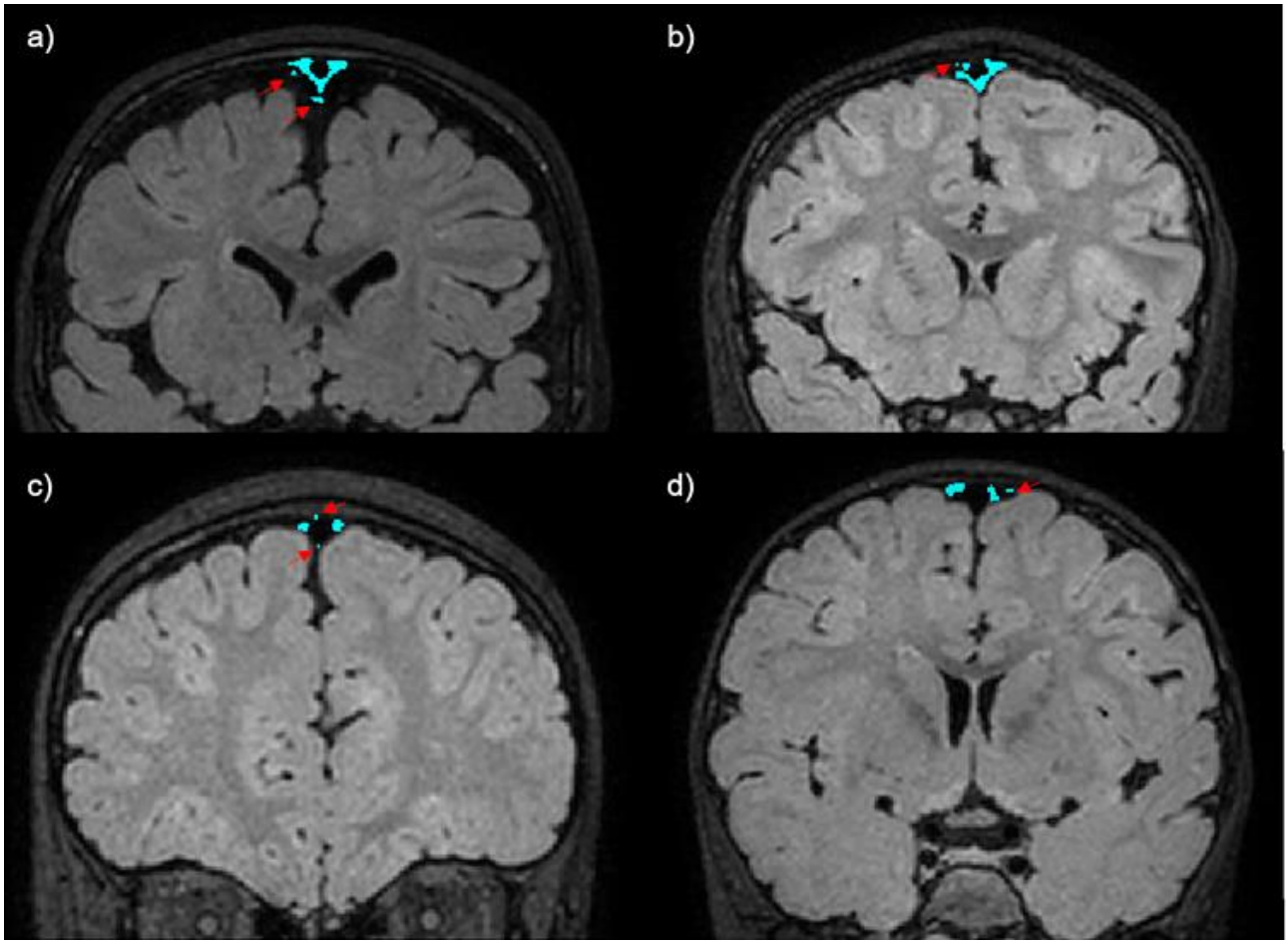

Figure 6-5 Examples of typical errors in predicted PSD segmentations. Panels a), b), c), d) show PSD segmentations (light blue) in the coronal plane for four different subjects. Red arrows indicate the incorrect segmentations

Figure 8-6 shows the results of the linear regression (R^2 = 0.96, F-statistic = 194.6, *p*-value = 6.75e-07) between the PSD volume obtained from the predicted masks and the ground truth masks of the test set. The regression yielded a slope of 0.88 and an intercept of 0.26. Ideally, the parameters of the regression line should match those of the bisector (slope = 1, intercept = 0). It can be observed that the predicted PSD volume is generally lower than the ground truth volume. By computing the 95% confidence intervals for both regression parameters, we found that the interval for the slope includes 1, and the interval for the intercept includes 0, suggesting that the regression line is not significantly different from the bisector (see Table 8-9 S1 in Supplementary Material).

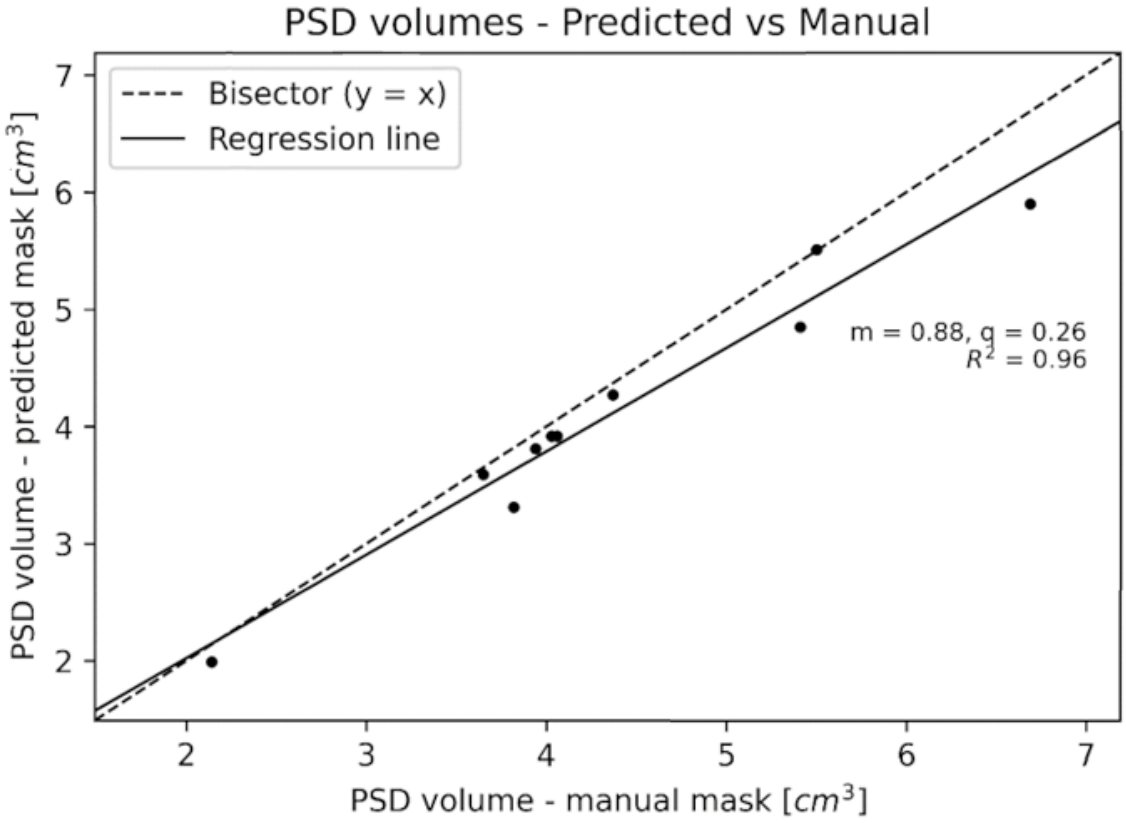

Figure 6-6 Scatter plot of the predicted versus ground truth PSD volumes. The dotted line represents the ideal curve (bisector), while the continuous line represents the linear regression. m = slope, q = intercept

Both qualitative and quantitative analyses were performed to compare the results of PSD segmentation using our tool with the one proposed by Hett and colleagues (13). The qualitative analysis focused on visual inspection of the segmentation results. Figure 8-7 shows an example of the segmentations obtained by the two tools considering one random subject from the test set. Visual examination of 3D-T2w images reveals poor contrast between PSD and the surrounding CSF (which appears bright). However, due to the greater contrast between PSD tissue and the surrounding CSF (which appears dark), 3D T2-FLAIR images offer improved differentiation between the structures of interest, resulting in an easier PSD delineation.

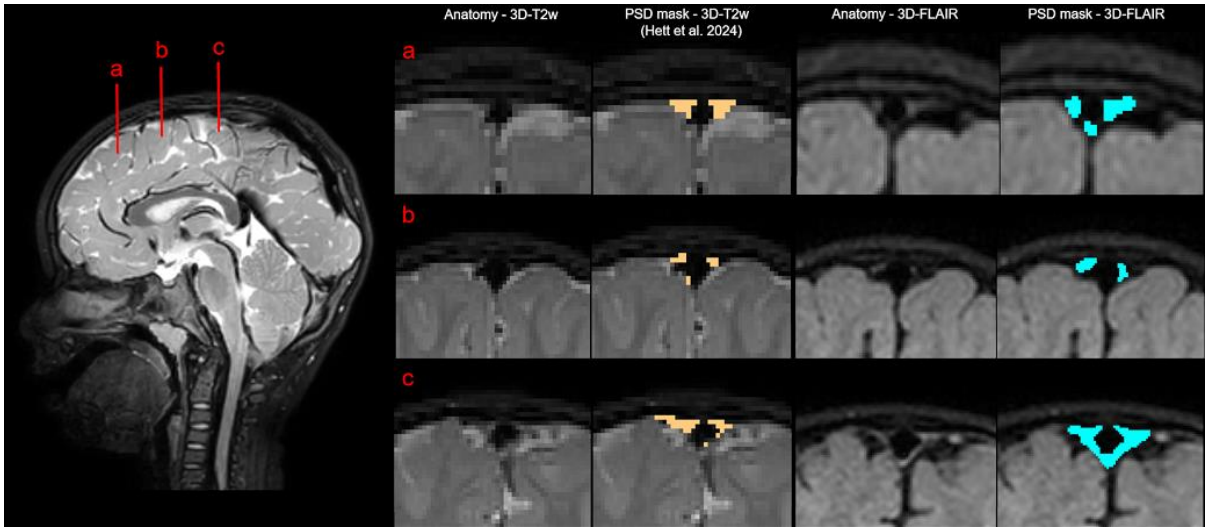

Figure 6-7 PSD segmentations from 3D-T2w and 3D T2-FLAIR. In these figures, PSD is represented in chrome yellow for segmentations derived from 3D-T2w, and in light blue in those obtained from 3D T2-FLAIR. Panels a), b), c) display three coronal slices from a randomly selected subject in the test set.

The quantitative analysis, which involved the calculation of the DICE coefficient between the manual masks (segmented using 3D T2-FLAIR images and registered to 3D-T2w images) and the PSD segmentation predicted by the tool of Hett et al. (13) was calculated for each test subject. This resulted in a DICE score of 0.56 ± 0.04 (mean ± standard deviation). Similarly, the DICE coefficient was computed to compare the PSD segmentations predicted by our developed tool with those predicted by the available tool, yielding a result of 0.57 ± 0.03 (mean ± standard deviation).

In addition, a linear regression analysis between the PSD volumes obtained by the two different tools was performed (Figure 8-8). The regression (R^2 = 0.40, F-statistic = 5.37, *p*-value = 0.04) yielded a slope of 0.43 and an intercept of 1.68. Concerning the 95% confidence intervals for both regression parameters, we found that the interval for the slope doesn't include the 1, and the interval for the intercept includes 0, suggesting that the regression line is significantly different from the bisector (see Table 8-2 S2 in Supplementary Material).

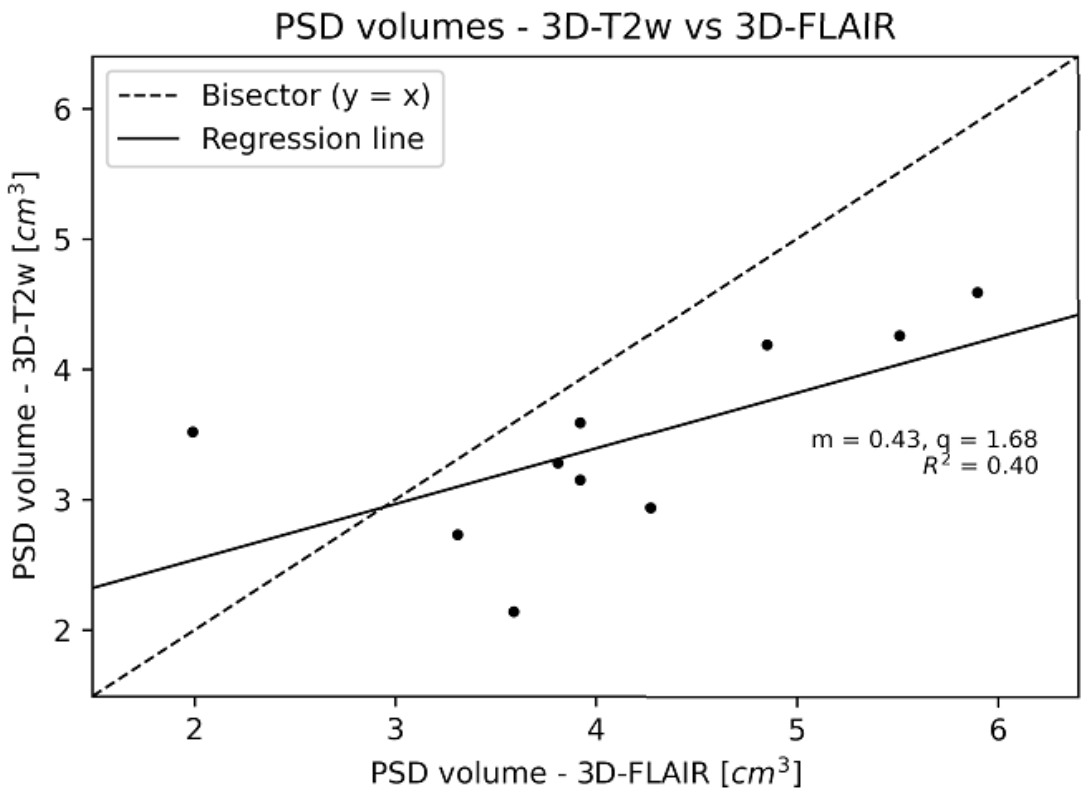

Figure 6-8 Scatter plot of the predicted PSD volumes using the available tool versus the one developed. The dotted line represents the bisector, while the continuous line represents the linear regression. m = slope, q = intercept

Discussion

The objective of this study was to provide clinicians and researchers with a freely available automatic 3D segmentation tool to quantify PSD volume in young children with ASD using readily available 3D T2-FLAIR. To the best of our knowledge, no studies have successfully validated and released a methodology to do so in developing brain. To achieve this aim, we implemented a 3D U-Net-based pipeline to segment PSD on a very young population of children with ASD, using a retrospective database. Segmentation was performed on 3D T2-FLAIR rather than on 3D-T2w images largely due to three reasons. Firstly, 3D T2-FLAIR sequences are commonly acquired in clinical diagnostic protocols making it valuable for translational studies. 3D-T2w images of high resolution are seldom used in a clinic setting defeating the purpose of providing clinicians with an easily applicable method to segment PSD. Secondly, the choice of 3D T2-FLAIR was also motivated by its larger contrast between PSD and adjacent subarachnoid space with respect to clinically acquired 3D-T2w images resulting in an easier identification and manual segmentation of PSD structure. And thirdly, initial studies on PSD that established its role in neuroinflammation and in CSF drainage were performed on 3D T2-FLAIR (1, 2, 15, 26). However, one of the limitations of using 3D T2-FLAIR images is its lack of distinguishing arachnoid granulations (AGs), which are clearly visible on 3D-T2w images. The PSD segmentation resulting from 3D-T2 FLAIR includes AGs

and therefore may overestimate PSD volume. To this effect, it is worthy to note that neonates and children at the age of two years present approximately 0.1 ± 0.3 as the average number of granulations in superior sagittal sinus, while an average of 1.2 ± 2.5 are found in subjects aged 10 years (27). The same authors also report that 75% of the AGs are 4 mm in size in children of 10 years old. Thus, it is highly likely that the overestimation of PSD volume due to AGs is negligible given the limited number and the very small size of AGs in our cohort.

Focusing on the developed algorithm, it achieved good scores across all three metrics on the test set. The observed errors could be automatically and easily corrected by implementing a filter based on the spatial distance between the region of interest around the PSD and the automatic segmentation. Additionally, the tool was applied to a cohort of 3 healthy children (age range: 2-10 years) to qualitatively assess the reliability of the PSD segmentations. Visual inspection of the predicted masks yielded promising results without showing evident errors (see Figure 8-9S1 in Supporting Information). Thus, the proposed tool could be a reliable starting point to automatically segment PSD and to calculate its volume in paediatric population.

In the comparison between our proposed method to segment PSD from 3D T2-FLAIR images with the algorithm available in the literature (13), which considers 3D-T2w images, we observed significant differences in performance metrics. These differences can be attributed in part to the different imaging parameters of the two datasets used. In 3D T2-FLAIR images we observed a higher contrast between the PSD and the adjacent CSF, resulting in an easier and accurate identification of PSD structure by our method. In contrast, in 3D-T2w images this separation is less pronounced, introducing greater difficulty in correctly identifying the PSD (see Figure 8 10 S2a and S2b in Supplementary Material). Image registration represents another factor which influenced our performance metrics. The ground truth segmentations were performed on 3D T2-FLAIR images and then registered to 3D-T2w images to calculate the DICE. This procedure ensures correspondence between the two images, but inevitably introduces differences that may explain the variation in performance between the methods. Furthermore, our model was specifically trained on 3D T2-FLAIR images, giving an advantage in segmentation performance on this type of MR sequence. Nevertheless, the difference in performance does not reflect an inherent superiority of one method over the other, but rather the different configurations of 3D T2-FLAIR and 3D-T2w MR images used. One advantage of the method present in the literature is that it does not limit the segmentation of PSD to its central portion, but it is able to segment the entire structure, including the very frontal and occipital areas. On the other hand, considering our dataset of 3D-T2w images where the PSD is not clearly visible, the method proposed by Hett and colleagues (13) tends to overestimate the volume of PSD by segmenting a structure that is not easy to disentangle in the images.

Limitations

Some limitations of this study should be considered. Firstly, the development of the automatic 3D segmentation tool was limited by the availability of normative data in typically developing children. There are no public datasets containing 3D T2-FLAIR images for typically developing children. Sedation is generally required to scan children at a very young age which further limits the collection of data from an adequate number of healthy children. As a consequence, we included in our dataset ASD children with no major outcome at the MRI examination, with the aim to build a large dataset, improve the algorithm segmentation performance and avoid overfitting.

We are aware that limiting the population of the study to children with ASD has an impact on model robustness in segmenting PSD in patients with different kinds of pathologies: including children with other neurodevelopmental disorders, as well as healthy individuals, would improve the algorithm's reliability. On the other hand, a preliminary visual assessment of the PSD segmentation performance on few healthy children showed promising results. As previously mentioned, our institution's specialized expertise in diagnosing and treating young children with moderate to severe neurodevelopmental disorders provides us with a unique advantage in acquiring clinical MRI scans from a larger cohort of children with ASD. However, developing such a tool specific for children with ASD could be valuable to investigate potential relationships between the PSD volume and other types of data, such as biomarkers directly related with brain neuroinflammation and neurodevelopment, brain morphology and clinical variables within this population. In future work, a larger cohort of developing children will be considered to apply the tool. A third limitation resides in the segmentation itself: the absence or difficulty in distinguishing the prefrontal and occipital components of the PSD from surrounding structures in developing brains led us to focus on the central components of the PSD, as done in a previous work (17). This approach was also adopted to improve the reproducibility of manual segmentation.

Conclusion

In conclusion, the proposed pipeline to train the 3D U-Net based tool allows a reliable segmentation of the PSD in young children with ASD from 3D T2-FLAIR MR images acquired for diagnostic purposes and allows reliable quantification of PSD volume. Segmentation of PSD was obtained by training a simple 3D U-Net on input images with minimal preprocessing and a short inference time on new data. Given the achieved good performances, this algorithm could be used to automatically segment PSD structure as a starting point to further investigate potential relationships between the volume of PSD and other variables, such as brain biomarkers of neuroinflammation and neurodevelopmental processes in children with ASD.

Data Availability Statement

All source data relative to images are available from the corresponding author on reasonable request.

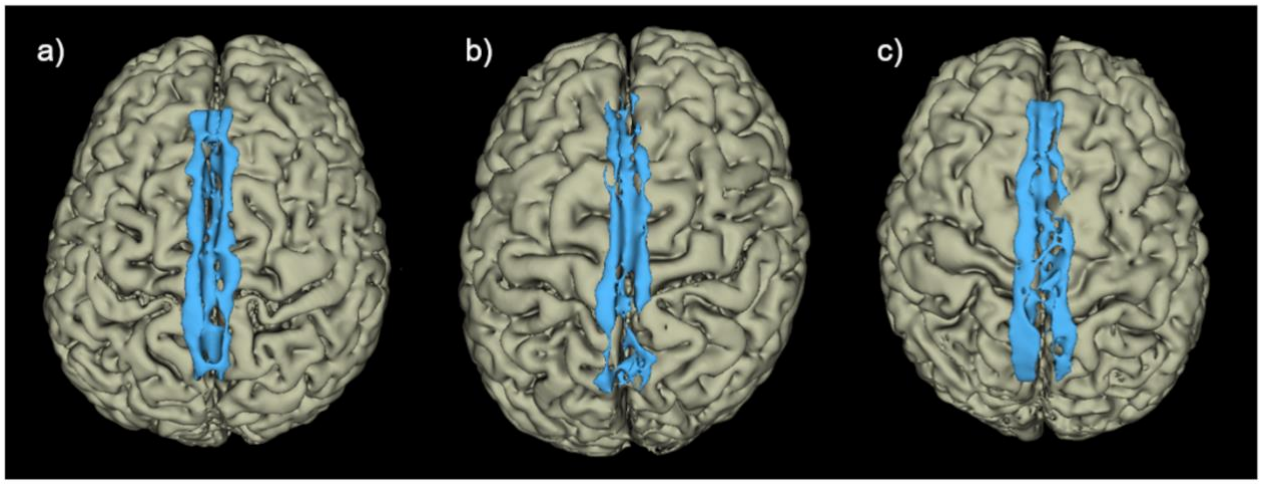
a)
b)
c)

Figure 6-9 S1 Examples of predicted PSD segmentations of three control subjects. a), b), c) 3D rendering of PSD segmentations for each subject.

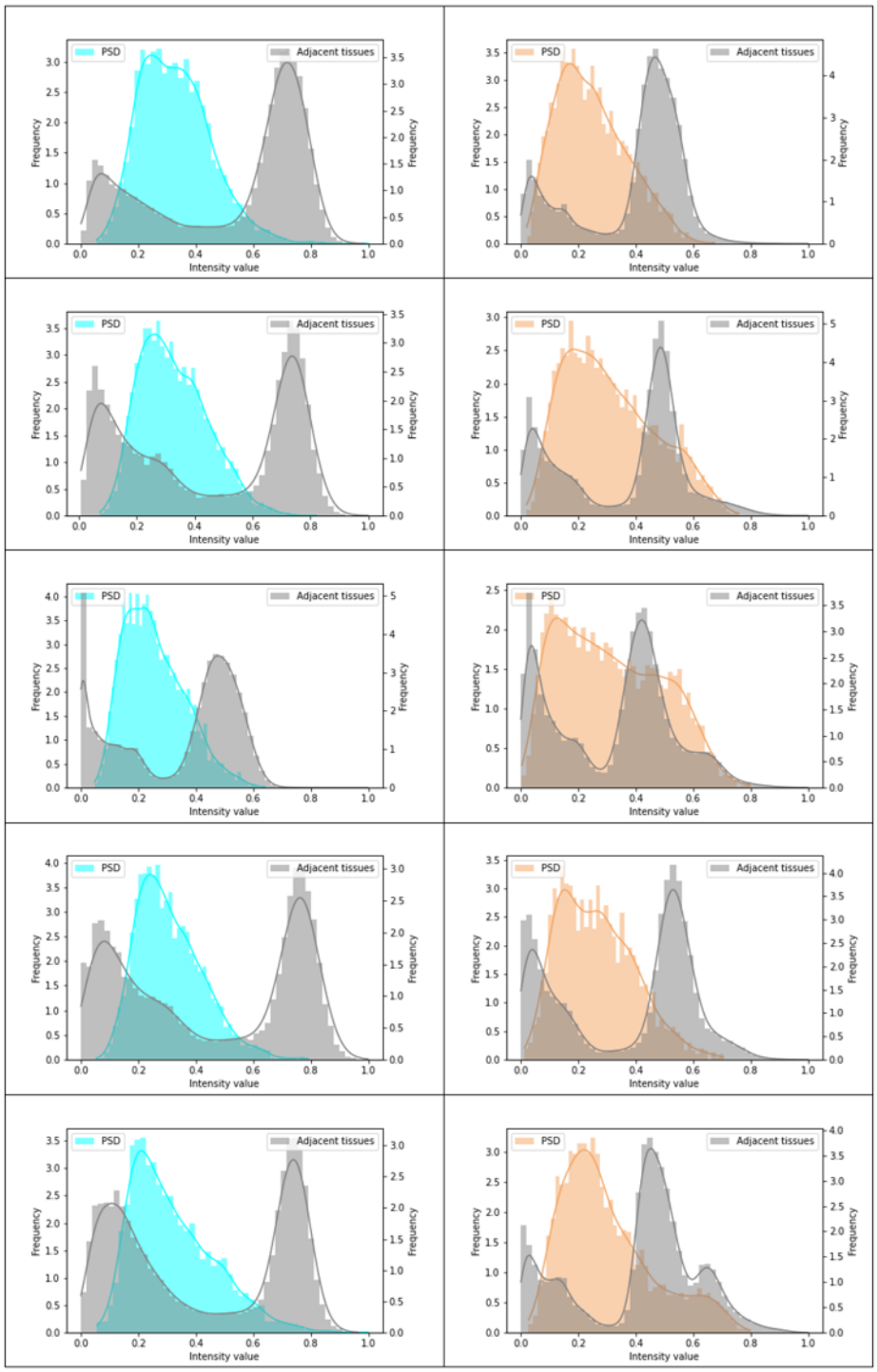

Figure 6-10 S2a Intensity histograms distributions of PSD and surrounded structures. Each row corresponds to a subject (from subject #1 to subject #5) from the test set. Left panel: intensity distributions for 3D T2-FLAIR images, left panel: intensity distributions for 3D-T2w images.

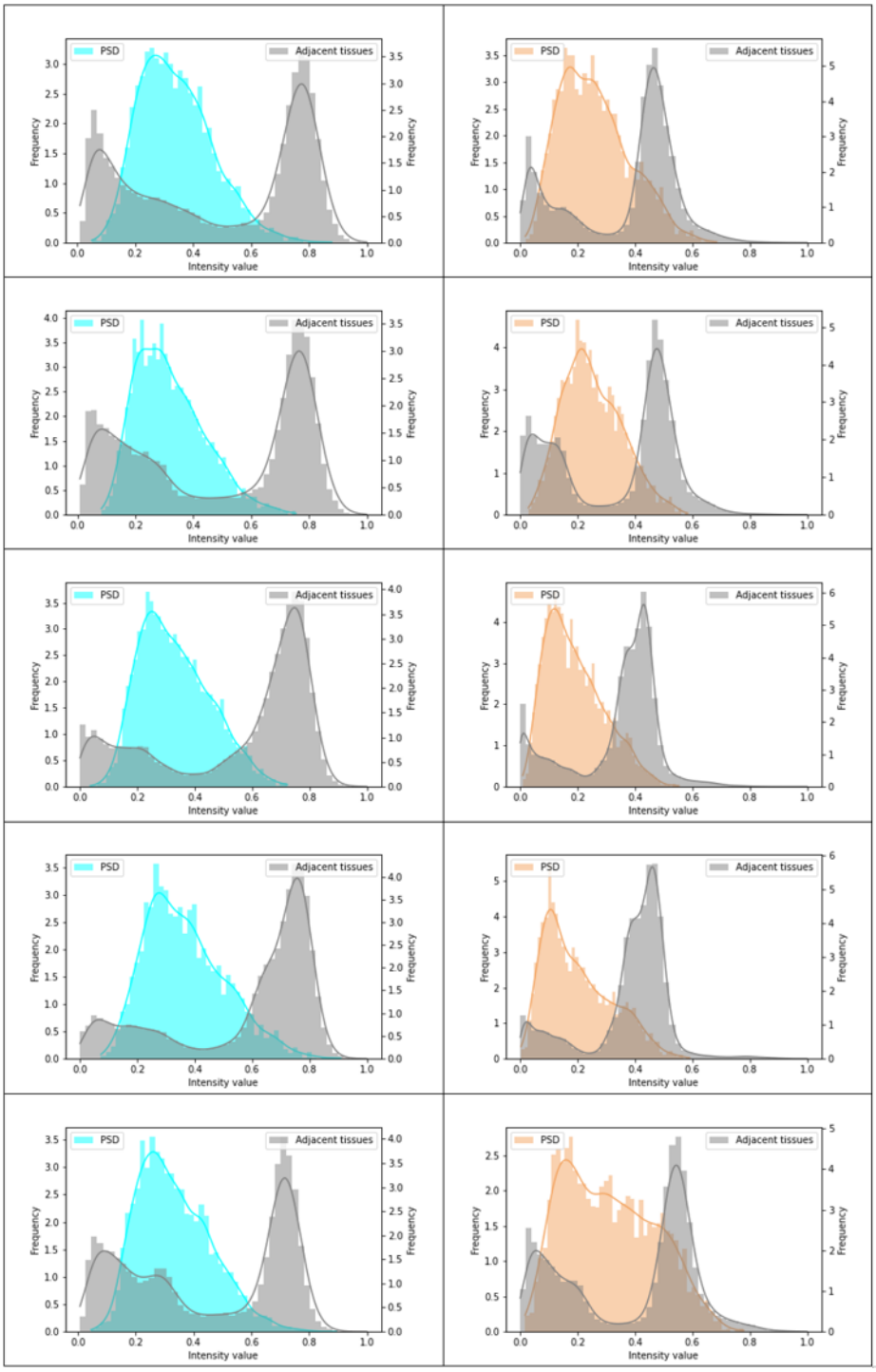

Figure 6-11 S2b Intensity histograms distributions of PSD and surrounded structures. Each row corresponds to a subject (from subject #6 to subject #10) from the test set. Left panel: intensity distributions for 3D T2-FLAIR images, left panel: intensity distributions for 3D-T2w images

Table 6-2 S1 95% confidence interval for the slope and the intercept of the regression line between the PSD volumes predicted by the developed tool and the PSD volumes obtained from the manual segmentation

	2.5%	**97.5%**
Intercept (q)	- 0.40	0.91
Slope (m)	0.73	1.03

Table 6-3 S2 95% confidence interval for the slope and the intercept of the regression line between the PSD volumes obtained using the tool proposed by Hett and colleagues 1 and the PSD volumes obtained by the developed tool

	2.5%	**97.5%**
Intercept (q)	- 0.12	3.49
Slope (m)	0.002	0.85

1. Hett K, McKnight CD, Leguizamon M, et al. Deep learning segmentation of peri-sinus structures from structural magnetic resonance imaging: validation and normative ranges across the adult lifespan. (*Fluids and Barriers of the CNS*. 2024;21(1):15. doi:10.1186/s12987-024-00516-w**)**

Chapter 7 Discussion

This study focuses on identifying structural MRI-based biomarkers of altered fluid dynamics in the developing pediatric brain. PVS and PSD play critical roles in CSF and ISF exchange, solute clearance, and overall fluid drainage in the adult human brain, yet remain underexplored in the developing child brain. Given their established involvement in fluid homeostasis, waste clearance, and immune surveillance in the adult brain, this work aims to quantify PVS and PSD in young children with ASD using semi-automatic, machine learning-based segmentation tools. Given the limited information available in the literature on this topic, a summary of current knowledge regarding the embryological and postnatal development of PVS and PSD in humans is warranted. This would provide a foundation for interpreting the findings and exploring their potential relevance in neurodevelopmental disorders such as ASD.

7.1 Perivascular spaces in the developing brain

7.1.1 Perivascular spaces: role and clinical significance

According to the glymphatic system model proposed by Iliff et al., PVS along penetrating arteries act as conduits for CSF flow from the SAS into the brain parenchyma, while PVS surrounding venules facilitate ISF drainage and the removal of metabolic waste out of the brain. This flow is driven by AQP4 channels located on astrocytic endfeet encasing arterial vessels (421). PVS play a key role in regulating CSF–ISF distribution and maintaining overall brain fluid homeostasis. They also contain specialized perivascular macrophages that transport substances via endocytosis and exocytosis, actively clearing toxic debris and contributing to neuroimmunological defense (422–426). On MRI, PVS have been extensively studied across neurological disorders, with quantification most commonly performed using the gold-standard visual rating scale (427) (Appendix A). Enlarged PVS—characterized by increased number and size—are associated with disease severity and risk factors in hypertensive encephalopathy, cerebral small vessel disease, Alzheimer's disease, and cerebral amyloid angiopathy (231,233,344,428,429). Impaired clearance of fluids and neurotoxic proteins such as amyloid-β and tau leads to their accumulation within the ECS and PVS. Elevated plasma Aβ42/Aβ40 or CSF tau/Aβ42 ratios and PET-detected hypometabolism appear to correlate with enlarged PVS (430,431). Furthermore, PVS quantification in epilepsy and traumatic brain injury has reinforced their potential as imaging biomarkers of disrupted glymphatic function in conditions beyond neurodegenerative diseases (432–434).

Evidence suggests that PVS can be a benign finding, as they are frequently observed in children without significant neurological impairment (298,375) (297). Consequently, their precise clinical significance in pediatric populations has remained uncertain, and no definitive cut-off for number or volume distinguishing healthy from pathological cases has been established. However, while in healthy children, PVS are typically small and incidental; enlarged or prominent PVS have been increasingly reported in various pediatric neurological disorders. Higher PVS frequency has been documented in conditions such as ASD, attention-deficit hyperactivity disorder, epilepsy, periventricular leukoencephalomalacia, and mucopolysaccharidosis (435)(153,338,436,437) (438). The presence and characteristics of PVS in children may be influenced by tightly regulated developmental processes—including neurogenesis, vasculogenesis, gliogenesis, ECM development, synaptogenesis, myelination, and neuronal migration (439). Examples of conditions marked by alterations in such developmental processes are polymicrogyria and craniosynostosis characterized by cortical gray matter maldevelopment in which the surrounding malformed regions exhibit an increased number of PVS (7,435). These studies indicate that, whereas PVS enlargement in adults is primarily linked to cerebrovascular risk factors, aging and external brain injury, in neonates and young children it is more likely driven by underlying neurodevelopmental processes, with their implications for fluid dynamics remaining largely unexplored.

7.1.2 Perivascular spaces in ASD

In recent years, growing attention has been directed toward the role of PVS in ASD. Although research in this area is still emerging, accumulating evidence suggests that alterations in PVS count, size, and spatial distribution may be linked to atypical brain development, cognitive dysfunction, and disrupted fluid homeostasis in ASD (153,353,440). A frequently reported neuroradiological feature in children with ASD is an enlarged SAS compared with non-autistic peers (149,349). Shen et al. observed increased extra-axial CSF (ea-CSF)—defined as CSF within the SAS over the supratentorial cortical surface—in six-month-old infants who later developed ASD, with larger ea-CSF volumes predicting greater symptom severity at 24 months (353). This finding was replicated in a larger longitudinal cohort, showing persistently elevated ea-CSF volumes in high-risk infants (with ≥1 sibling diagnosed with ASD) compared to low-risk infants (only child with ASD in the family) and typically developing controls (369). Subsequent work confirmed that between ages 2–4 years, ea-CSF remained elevated in both high- and low-risk ASD groups relative to controls (370).

More recently, Garic et al. investigated the relationship between PVS enlargement and ea-CSF volume in infants scanned at 12 and 24 months. Infants who developed ASD showed a greater increase in enlarged PVS number over this interval, with enlarged PVS correlating

positively with elevated ea-CSF and sleep disturbances (153). These findings provide evidence for a link between PVS alterations and impaired CSF clearance in ASD. In parallel, Sotgiu et al. reported a non-significant increase in PVS count in ASD children aged 2–7 years compared with controls, but identified significantly greater PVS volume in WM among children under 4 years relative to older children (338). No associations were found with ASD severity; however, a non-significant increase in WM PVS volume was observed in children with sleep abnormalities.

The two studies differ in methodology, leaving our understanding of perivascular spaces (PVS) in children with autism spectrum disorder (ASD) incomplete. The study by Garic et al. focuses on neonates and infants at high or low risk of developing ASD, while Sotgiu et al. study children with ASD aged 2–7 years. Garic et al. employed an in-house PVS scoring system to estimate the number of "enlarged" PVS across the entire brain; however, the term "enlarged" is not clearly defined (153). In contrast, Sotgiu et al. used a visual rating score applied to a single brain slice, though they did not specify the slice's location (338)(Appendix A).

To quantify PVS volume, Sotgiu et al. utilized a semi-automated volumetric method that integrated T1- and T2-weighted images (430). They found a correlation between PVS volume and the scoring-based PVS grade, reporting that both metrics were higher in male children with ASD compared to females. Additionally, PVS volume was significantly greater in children under four years of age than in older children. Although they observed a non-significant increase in PVS number in children with more severe ASD symptoms, the authors concluded that an increased number of PVS may particularly characterize very young male children with ASD who exhibit more severe symptoms.

The works by Shen and Garic indicate a direct correlation between eaCSF, total CSF and children at high risk of developing ASD (151–153). Given that PVS are in direct communication with SAS, these findings collectively support the hypothesis that both increase in PVS number and PVS volume in ASD may reflect delayed CSF clearance, potentially linked to glymphatic system dysfunction.

Our recently published retrospective study focused on quantifying both number and volume of PVS in the whole brain white matter in young children (2-8yr old) hospitalized with confirmed diagnosis of ASD by using an automatic segmentation approach based on a 3D-UNet deep learning algorithm (342). This method, employs a multichannel input consisting of both T1- and T2-weighted 3D MRI sequences (346). The volume and number of PVS were quantified on the whole brain. PVS number and volume were directly and significantly correlated with ea-CSF volume. Both the number and volume of PVS showed a negative correlation with the severity of neurodevelopmental delay, as measured by the Griffiths scale and expressed as developmental quotient (DQ) suggesting that a higher number and volume of PVS was related to a more severe

neurodevelopmental delay. However, no direct positive relationship with disease severity was observed; instead, more severe cases were associated with fewer and smaller PVS. This apparently odd finding might be due to other factors. First, age emerged as a significant factor—younger children exhibited higher PVS number and volume compared with older children with ASD. Given that hospitalization is determined by the presence of more severe symptoms, our cohort consisted of individuals with more severe form of ASD. Milder forms of ASD were not present in our cohort (see Chapter 6). The separate effect of age and severity of disease was not possible to definitively isolate. Second, disease severity may be determined by several other factors including purely neurodevelopmental processes such as malwiring of neurons, poor neuronal migration which have little to do with PVS enlargement. Our study is in agreement with previous studies that PVS parameters are linked to ea-CSF volume in ASD and imply altered CSF drainage in children with ASD. However, what these results mean in terms of the underlying pathophysiological process remains intriguing and may require longitudinal studies (441).

Emerging evidence indicates that neuroinflammation plays a critical role in the pathophysiology and risk of ASD (140,142,143,442). There are several established mechanisms whereby neuroinflammation may result in ASD. Maternal immune activation during pregnancy, infections, and early-life inflammatory events can alter brain development through the release of pro-inflammatory cytokines and microglial activation (443,444). These inflammatory processes may disrupt neural connectivity, synapse formation, and neurotransmitter systems, thereby increasing the likelihood of ASD. Additionally, conditions such as gestational diabetes, maternal infections, and antibiotic use during pregnancy may activate the maternal immune system, allowing immune mediators to cross the placenta and impact the developing fetal brain (142,445). Preterm neonates exhibit a greater number of PVS highlights the ongoing maturational processes of these structures (323). Enlarged PVS have also been linked to sleep-related difficulties in individuals with ASD, reinforcing the hypothesis of a dysregulated glymphatic system in this population.. Sleep issues are common in children with autism, and the enlargement of PVS could indicate underlying issues with the glymphatic system or impaired CSF flow (195,446). Sleep disturbances can exacerbate neuroinflammation by disrupting circadian rhythms (447). Neuroinflammation plays an important role in neurodegenerative diseases in adults by determining reduced capacity to remove toxic metabolites from the brain (448). Since enlargement of PVS in the adults is also attributed to neuroinflammatory process, its role in the developing young brain and enlargement of PVS, necessitates further investigation. Infact, a direct correlation between MRI based PVS quantification parameters and potential neuroinflammatory risk factors has not emerged in the literature and is worth pursuing. The hypothesis that PVS enlargement could be linked to disruptions in the glymphatic system, which is crucial for metabolic waste clearance appears very promising as it carries the potential to serve

as a supplementary marker in diagnostic imaging, potentially helping clinicians in early identification and intervention, particularly in high-risk children with a family history of neurodevelopmental disorders. If PVS are indeed markers of such dysfunctions, interventions targeting sleep and cerebral fluid dynamics may provide beneficial avenues for treatment.

While our study offers valuable insights, there are several limitations that should be considered. The cross-sectional nature and a small cohort limits our ability to establish causal relationships between PVS and neurodevelopmental conditions like ASD. Our study lacks comparison with healthy controls. Since PVS are also present in healthy children, it is crucial to compare findings between ASD and typically developing cohorts. However, access to such control data remains limited due to several challenges. Primarily, obtaining MRI scans of completely healthy young children without sedation is highly unlikely. Consequently, control groups in the 2–5 year age range often include children with mild neurological symptoms rather than entirely asymptomatic individuals. Although MRI without sedation is possible in healthy children, it requires careful preparation—such as scheduling scans during natural sleep times, implementing sleep deprivation protocols, or other strategies—to maximize the likelihood that the child remains still during the procedure. Addressing these logistical challenges is essential for future studies aiming to establish robust pediatric control datasets (419). The effects of sedation on the number and volume of PVS remain unknown; however, it is reasonable to assume that these structural spaces, with the potential to grow or to collapse over time, remain stable during the 30 to 60 minutes of MRI acquisition. Large MRI datasets available online in ASD and healthy children are of limited use as 3D T2w MRI sequences are seldom acquired, sequence that was required to perform PVS segmentation in our study.

7.2 The biological interpretation of the association between PVS count and clinical picture

Increasing evidence suggests that the number and enlargement of PVS visible on MRI may reflect alterations in neurofluid circulation, vascular integrity, or inflammatory activity. Understanding the biological interpretation of this association is particularly important in paediatric populations, where brain development and fluid homeostasis are still evolving.

One proposed mechanism linking increased PVS count or enlargement with clinical manifestations involves altered glymphatic drainage. Under normal conditions, CSF enters the brain along periarterial spaces and exchanges with interstitial fluid before exiting along perivenous pathways. This process facilitates the clearance of metabolic waste products and inflammatory mediators. If this drainage system becomes impaired—due to altered vascular pulsatility, structural changes in perivascular pathways, or dysfunction of astrocytic aquaporin-

4 channels—fluid may accumulate within the perivascular spaces, leading to PVS dilation visible on MRI. Impaired clearance may also contribute to the accumulation of metabolites or inflammatory molecules in brain tissue, potentially influencing neurological function.

A second mechanism relates to vascular factors such as vascular integrity. PVS enlargement may reflect structural changes in small penetrating vessels, including alterations in vascular compliance or endothelial function. In children, developmental changes in the neurovascular unit, including the maturation of the blood–brain barrier and cerebral vasculature, may influence perivascular fluid dynamics. Reduced arterial pulsatility, immature basement membranes or microvascular dysfunction could impair the propulsion of interstitial fluid through perivascular pathways, resulting in increased PVS visibility.

Neuroinflammatory processes may also contribute to the enlargement of PVS. Histologically, the perivascular compartment contains immune cells such as macrophages and plays a role in immune surveillance within the central nervous system. In conditions associated with neuroinflammation, increased cellular infiltration, cytokine activity, or blood–brain barrier permeability may alter perivascular fluid balance and promote dilation of these spaces.

In paediatric populations, the interpretation of PVS enlargement must be approached cautiously. Children exhibit higher baseline brain water content, developing glymphatic pathways, and ongoing vascular and white matter maturation, all of which can influence the appearance of PVS on MRI. In some cases, prominent PVS may represent physiological developmental variation rather than pathology. However, when present in excessive numbers or associated with specific clinical symptoms, enlarged PVS may serve as an imaging biomarker of altered neurofluid circulation, vascular dysfunction, or inflammatory activity.

Enlarged PVS as an effect of underlying neuropathological process (downstream marker)

Microvascular alteration such as thickened or stiffened vessel walls (lipohyalinosis, amyloid angiopathy) may compress or distort PVS, impairing fluid and solute clearance and causing enlargement of PVS and this is typically observed in cerebral small vessel disease and cerebral amyloid angiopathy. Neuroinflammatory processes, deposition of excessive amyloid beta and other toxins, characteristic of Alzheimer's disease and Parkinson's disease may cause obstruction impairing fluid clearance and enlarging perivasccular spaces. Animal models suggest that glymphatic disruption can accelerate amyloid accumulation. Disorders such as normal pressure hydrocephalus or intracranial hypertension may result in alterations of CSF pressure gradients potentially blocking CSF outflow pathways.

Enlarged PVS as a cause of underlying neuropathological process (upstream marker)

Since PVS are filled with basement membranes and contain multiple proteins. Genetic alterations of proteins that alter the walls of these spaces could lead to altered function of PVS thereby being a cause of neurological diseases. In pediatric disorders such as autism spectrum disorder, there is no evidence that enlargement of PVS are a cause of the disease. An abnormal neurovascular development, or immaturity of the several components of the glymphatic system may result in enlargement of PVS.

The obvious question is whether the presence of a high number of PVS in a healthy child represents a risk factor for the development of neurological diseases. However, this appears to be no simple task. In addressing this question, a very rigorous criteria of selection is needed.

Vicious cycle

It is also likely that a vicious cycle is established once the underlying neuropathological process obstructs movement of fluids and removal of solutes. Enlarged PVS can reinforce disease processes:

1. Enlarged PVS → worse glymphatic drainage
2. Poor clearance → more toxic protein buildup
3. Buildup → neuronal stress and vascular injury
4. Vascular injury → further PVS dilation and inflammation

Such a feedback loop could be a central mechanism in damaging white matter, resulting in WM atrophy and further enlargement of PVS. Once enlarged they can become pathogenic themselves, creating a damaging feedback loop. So, they may play a contributory role in maintaining or amplifying underlying pathology — but not as a primary cause. A longitudinal study is necessary to further our understanding.

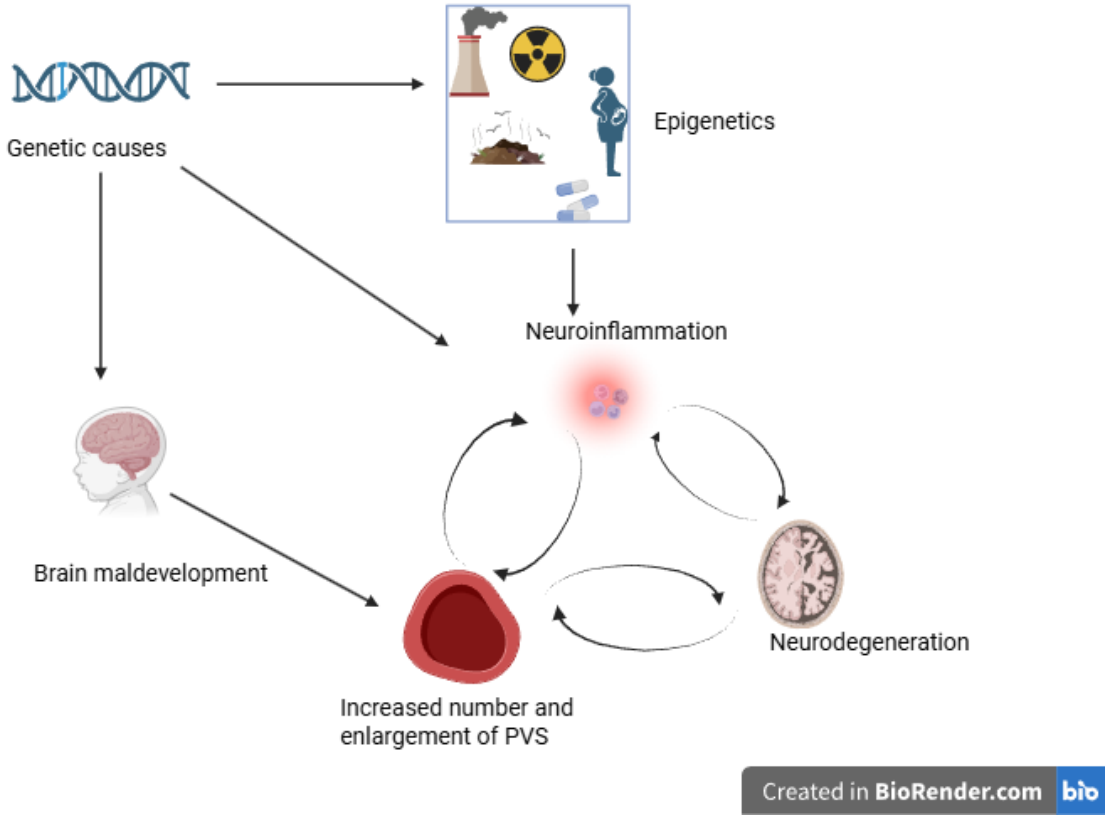

Figure 7-1 Schematic diagram explaining a possible vicious cycle underlying the development of PVS. This figure was made using BioRender.com free version.

7.3 Parasagittal dura in the developing brain

7.3.1 Parasagittal dura: role and clinical significance

Recently, the PSD has been recognized as a key structure within the brain, serving neuroimmunological function and providing a route for clearing ISF and solutes from the brain parenchyma (99,250,383,384). Most of our understanding of this MRI visible structure, derives from animal studies conducted ten years ago in which lymphatic vessels within PSD were identified (65,249). Later, in vivo human MRI studies clearly demonstrated the presence of such vessels within PSD (63). Groundbreaking evidence for solute entry into the PSD from CSF in the SAS came from an in vivo human study in which low–molecular-weight gadolinium was injected into the lumbar intrathecal sac of subjects undergoing evaluation for normal pressure hydrocephalus (389). Peak gadolinium concentration in the PSD was detected 24 hours post-injection (97). In subsequent studies, the same group quantified PSD volume in patients with various neurological disorders and reported that this volume was variable among subjects and type of diseases and reported that intrathecal gadolinium appeared in blood plasma before

reaching the PSD (98). In this study, the authors conclude that PSD is not a major efflux route for CSF and solutes. On the other hand, the role of PSD in neuroimmunosurvellance has been reported (99,383). PSD facilitates interactions between antigen presenting cells in the brain parenchyma and local meningeal immune cells derived from systemic immune system (383). The presence of meningeal lymphatic network within the PSD, drainage of CSF containing soluble brain derived antigens and connections to the deep cervical lymph nodes suggest that PSD may represent a key anatomical hub for neuro immune surveillance. Both blood vessels and meningeal lymphatics within the dura lack tight junctions typically found in the blood brain barrier. This allows for two-way cell trafficking within PSD. Specific T cells recognize brain antigens within the PSD and undergo clonal expansion that has been well-described in experimental models of neuroinflammatory disease such as experimental autoimmune encephalitis but also neurodegenerative diseases such as Parkinson's disease and Alzheimer's disease (385,449,450).

Such novel information led another group of researchers to develop a segmentation tool based on neural networks to quantify PSD volume using high resolution 3D T2-weighted images obtained in MRI (388,451). They found an increase in PSD volume with increasing age and with bulk CSF flow evaluated by using phase contrast MRI, in a large cohort of healthy participants. This tool appeared to be robust in performing segmentation on older adult cohorts but over-estimates PSD volumes in children in the age range of 5-10 years. The same authors also performed a combined PET-MRI based study in patients with varying severity of Alzheimer's disease. PET study was performed using amyloid-β tracer 11C-Pittsburgh Compound B, to quantify amyloid-β in the whole brain. PSD volume was significantly correlated with the degree of burden of amyloid-β in patients with Alzheimer's disease (390). These studies appear to demonstrate that an increase in PSD volume in both aging and Alzheimer's disease is suggestive of possible compensatory hypertrophic response to improve clearance.

With this background, we explored PSD volume in young children with ASD to evaluate its significance with severity of disease and the volume of ea-CSF.

7.3.2 PSD and autism

To date, our published paper presented in Chapter 7 above is the only work in which PSD has been investigated in a pediatric population. Since the only available tool in the literature appears to overestimate PSD volume in children aged 5–10 years (388), I collaborated with biomedical engineers at our institute to develop an in-house segmentation tool based on a convolutional neural network, specifically the U-Net architecture, for quantifying PSD in our cohort of 2–8-year-old children with ASD. These results are presented in Chapter 7. Lacking

access to the high-resolution 3D T2-weighted images used in previous studies by Hett and colleagues, we instead employed high-resolution, clinically feasible 3D-FLAIR sequences, to develop an in house segmentation tool to calculate PSD volume. Similar methodology was used in earlier works by Melin et al. to establish PSD volumes in adult population (98). The network was trained on images from 10 healthy adults (mean age 32.6 ± 12.5 years), which were manually segmented in the coronal plane by myself. We restricted analysis to the central portion of the PSD, excluding frontal and occipital extremities, for four reasons: (1) end-to-end manual segmentation would require delineating over 300 coronal slices per subject (>3,000 slices total), creating excessive visual strain; (2) meningeal tissue and thus PSD are still developing in children, rendering the terminal portions nearly undetectable; (3) the bulk of PSD volume resides in the central brain; and (4) the institute's server memory was insufficient to train the network on larger datasets. As described in the article, we generated a 60° angle on the sagittal image using the anterior and posterior commissures as reference points (Fig. 7-1). Once the 2D U-Net was trained, validation was performed on another two subjects which was manually checked. This network was then tested on 10 children with ASD. Manual corrections were performed. A DICE coefficient of 0.84 was achieved.

In children with ASD, PSD volume showed a significant positive correlation with both total CSF and ea-CSF volume. The positive association between PSD and CSF volumes aligns with existing literature suggesting that the PSD is related to CSF flow dynamics. We also found that PSD volume was negatively correlated with the severity of neurodevelopmental delay—the more severe the delay, the smaller the PSD volume. No correlation was found between PSD volume and clinical severity of ASD. Since, existing literature in aging and Alzheimer's disease suggest that PSD enlargement, likely reflects compensatory hypertrophy, we were expecting PSD volume to be higher in more severe cases of ASD or in cases of severe neurodevelopmental delay. No relationship with ASD severity is likely due to the fact that that our hospitalized children all present with moderate to severe forms of disease, thus an appropriate evaluation with milder forms could not be achieved. However, the reason for reduced PSD volume in children with more severe neurodevelopmental delay requires a different explanation.

Since PSD is composed of meningeal tissue—whose lymphatic structures continue to develop postnatally—and the meninges provide scaffolding essential for neuronal migration and connectivity, it is plausible that PSD in underdeveloped and interferes with neurodevelopmental processes such as neurogenesis and neuronal migration (411). In addition, given that PSD harbors immune cells and participates in immune surveillance, neurodevelopmental delay could partly arise from underdeveloped or dysfunctional meningeal immune tissue, potentially influenced by genetic or environmental (epigenetic) factors. These hypotheses are speculative and warrant further investigation.

Several limitations of our study should be acknowledged. First, the sample size was relatively small, precluding post hoc analyses of potential risk factors such as premature birth, maternal stress, or ASD severity. Second, our U-Net network was trained on healthy adult brains rather than pediatric data. Ideally, training would be performed on healthy child brains; however, given the retrospective design and the impracticality of recruiting healthy children, we trained on adult brains and applied the model to ASD pediatric cases. Chapter 8 addresses this problem whereby we present a UNET which is trained on children. Third, PSD volume measurements were limited to the central portion of the brain. Although this region encompasses roughly two-thirds of the PSD, inclusion of the frontal and occipital extremities would provide a more complete assessment. Despite this constraint, important findings emerged. Fourth, the absence of a typically developing pediatric control group prevented us from establishing normative PSD volume ranges in children—a gap that remains in the literature.

Our ongoing research aims to address these limitations by developing a whole-brain 3D U-Net algorithm to quantify total PSD volume in children aged 2–10 years. In Chapter 8, we developed a 3D U-Net restricted to the central portion of the PSD but trained on children successfully although it may be useful to extract the two ends of the PSD for completeness. We are also in the process of collecting new data on healthy children by recruiting data from other institutes.

7.4 Clinical implications in the developing brain

Despite advances in understanding neurofluid dynamics in the adult brain, clearance pathways in the developing pediatric brain remain poorly understood. In the current work, I have made an attempt to evaluate PVS and PSD parameters based on MRI in children with ASD. Given that PVS and PSD are considered potential MRI biomarkers of altered neurofluid drainage, it is important to explore their significance in the developing brain. Currently, the only other MRI-based biomarker reported in children with ASD is a possible increase in ea- CSF space, which to date has only been qualitatively described. Impaired waste clearance in the developing brain may contribute to early-onset conditions, such as hydrocephalus, periventricular leukomalacia, or neuroinflammation.

Individuals with ASD have a high prevalence of dementia with respect to those without developmental disabilities and ASD (452). While Alzheimer's disease and ASD are two distinct clinical entities there appears to be some potential overlaps specifically related to the production and processing of Amyloid-β precursor protein (APP). APP is a transmembrane protein which stabilizes calcium fluxes across neuronal membranes, facilitates matrix adhesion and inhibits the clotting cascade. It plays a role in neuronal growth and development. Excessive accumulation

of amyloid-β in the brain in autism has been shown and it can cause neuronal dysfunction in idiopathic forms of autism and in duplications of 15q11.2-q13 (352). Subjects with regressive forms of ASD have a high level of secretory APP type alpha (sAPPα) and excessive levels is considered toxic during brain development. In particular it may affect synapse formation, overdifferentiation of stem cells and disrupt the brain immune response (453). The deposition of amyloid is intraneuronal as opposed to extracellular in patients with Alzheimer's disease. Although diseases like Alzheimer's don't present in children, protein handling pathways like IPAD and the glymphatic system may still regulate early dynamics in ASD. Whether alterations in APP processing and secretion of potential toxic amyloid peptides in ASD is related to PSD volume or the number of PVS is an area of potential investigation.

Understanding the maturation of brain fluid clearance pathways in children has important clinical implications. Establishing normative developmental patterns of structures such as PVS and PSD could enable earlier identification of deviations that signal underlying neurodevelopmental disorders, including ASD and other pediatric neurological conditions. Age-specific reference values would improve the diagnostic accuracy of pediatric MRI findings, reducing the risk of overinterpretation of benign age-related features or underrecognition of subtle pathological changes. Moreover, as glymphatic and meningeal lymphatic systems may be more plastic during early development, defining critical windows of maturation could inform the optimal timing of therapeutic interventions to restore or enhance clearance function. If the normal timeline and pattern of glymphatic and lymphatic maturation is known, deviations from this pattern could serve as early imaging biomarkers for neurodevelopmental conditions. Without knowing what "normal" fluid clearance anatomy and function look like at different ages, we risk misinterpreting enlarged PVS, PSD, or extra-axial CSF spaces in children but also in adults. Understanding development could clarify whether these clearance deficits are primary drivers of pathology or secondary consequences of other brain changes. Finally, because these pathways are closely linked to immune surveillance and metabolic homeostasis, a better understanding of their developmental biology may clarify mechanisms by which early-life clearance dysfunction contributes to cognitive impairment, neuroinflammation, and altered brain connectivity.

Studying neurofluid clearance pathways in the developing brain not only advances pediatric neurology but also enriches our understanding of the adult glymphatic system. The maturation of PVS and PSD during childhood establishes the foundational architecture and function from which adult clearance mechanisms evolve. By identifying normative developmental trajectories and points of vulnerability in early life, we can better interpret how age-related changes, disease processes, and compensatory remodeling occur in adults. This is critical for interpreting adult pathologies—e.g., whether enlarged PVS in Alzheimer's disease

represent abnormal persistence of childhood features, a maladaptive remodeling, or an entirely new process. Studying the immature system can highlight core structural requirements for efficient CSF–ISF exchange, such as astrocytic AQP4 polarization or vascular organization. The developmental integrity of IPAD and the glymphatic system may set the stage for long-term brain health, with early impairments potentially predisposing to age-related neurodegenerative diseases. If glymphatic plasticity is high in childhood but declines with age, pediatric studies can help define time windows when interventions to optimize clearance might be most effective—and whether similar reactivation of plasticity is possible in adults.

7.5 Pros and cons of different MRI techniques in assessing neurofluids

Non–contrast-enhanced and contrast-enhanced approaches, each has distinct advantages and limitations. These considerations are particularly important in paediatric imaging, where safety and feasibility must be carefully addressed due to the several anatomical structures still undergoing development. For example, kidney function does not reach adult levels by 1-2 years of age making them vulnerable to gadolinium based toxicity and fluid imbalances.

Non–contrast-enhanced MRI techniques include conventional structural imaging (e.g., T2-weighted and FLAIR sequences), phase-contrast MRI (PC-MRI) for CSF flow quantification, and diffusion-based methods such as DTI, which can provide indirect measures of glymphatic activity. The main advantage of these techniques is their high safety profile, as they do not require the administration of exogenous contrast agents. This makes them particularly suitable for paediatric populations and for longitudinal studies requiring repeated examinations. Additionally, methods such as PC-MRI can provide quantitative measurements of CSF flow velocities. However, non-contrast techniques generally provide indirect assessments of neurofluid circulation, and their sensitivity to subtle abnormalities may be limited. Furthermore, diffusion-based methods are susceptible to motion artefacts, which can be challenging in young children. The use of DTI-ALPS as a measure of glymphatic function is generally not recommended by the broader scientific community, as it assumes perfectly orthogonal fiber orientations, a condition that is seldom present in vivo.

Contrast-enhanced MRI techniques, including dynamic contrast-enhanced MRI (DCE-MRI), contrast-enhanced FLAIR imaging, and delayed post-contrast imaging, allow more direct visualization of fluid pathways and BBB permeability. These methods can provide quantitative parameters related to permeability and tracer clearance, thereby offering valuable insights into glymphatic transport and neurovascular integrity. Nevertheless, the use of gadolinium-based contrast agents (GBCAs) introduces potential risks. Although generally considered safe,

concerns have been raised regarding gadolinium retention in brain tissue following repeated administrations, as well as the rare but serious complication of nephrogenic systemic fibrosis in patients with impaired renal function. The use of GBCAs in paediatric patients presents additional challenges and is discouraged. Children may require sedation or general anesthesia to minimize motion during MRI examinations, increasing procedural complexity. Moreover, the long-term implications of gadolinium deposition in the developing brain remain uncertain, raising ethical considerations for research applications. Intrathecal administration of gadolinium, sometimes used experimentally to study glymphatic circulation, is also off-label and rarely justified in children.

Overall, while contrast-enhanced MRI techniques offer greater sensitivity and more direct assessment of neurofluid dynamics, non–contrast-enhanced methods are generally preferred in paediatric populations due to their superior safety profile and suitability for repeated imaging. Ongoing research is therefore focused on refining advanced non-contrast MRI techniques to improve the characterization of neurofluid circulation without the need for exogenous contrast agents.

7.6 Glymphatic versus IPAD models of clearance in early life

The glymphatic model describes the movement of CSF into the brain along PVS, followed by exchange with ISF within the parenchyma, a process facilitated by AqP-4 channels located on astrocytic endfeet. This fluid mixture is then thought to exit the brain along perivenous spaces, enabling the clearance of metabolic by-products. Evidence supporting the glymphatic model derives primarily from animal studies using tracer imaging and two-photon microscopy, as well as observations linking fluid transport to sleep and to the functional role of aquaporin-4. However, the model has been questioned because much of the experimental evidence comes from anesthetized animals, and the existence of large-scale bulk flow through the dense brain parenchyma remains debated.

An alternative mechanism, the intramural periarterial drainage (IPAD) pathway, proposes that interstitial solutes are cleared along the basement membranes of capillaries and arteries rather than through bulk flow within the parenchyma. In this model, solutes enter the basement membranes surrounding vascular smooth muscle cells and are transported in a direction opposite to blood flow toward leptomeningeal arteries and ultimately to extracranial lymphatic pathways. The driving force for this process is believed to be vasomotion generated by rhythmic contractions of vascular smooth muscle cells. Histological tracer studies and anatomical observations provide support for this mechanism, particularly in the context of impaired amyloid-β clearance in neurodegenerative conditions.

Current evidence suggests that these mechanisms may not be mutually exclusive and that multiple pathways likely contribute to brain fluid and solute clearance. Importantly, developmental factors may significantly influence the efficiency of periarterial drainage in early life. In particular, the vascular smooth muscle cells that generate vasomotion and the structural organization of vascular basement membranes may not fully mature in infancy and early childhood. There is scarsity of cerebral vasculature in the neonates and cerebral blood flow increases gradually to adult levels in the first few years. The immaturity of these components may reduce the efficiency of periarterial clearance pathways, potentially altering interstitial fluid dynamics and metabolite removal during early brain development. Consequently, developmental differences in vascular structure and the development of the interstitial ECM must be carefully considered when interpreting studies of glymphatic or periarterial clearance mechanisms in pediatric populations.

7.7 The limitations of structural MRI as an indirect marker of fluid dynamics

One major limitation is that structural MRI cannot directly measure CSF flow or ISF circulation. The presence of enlarged PVS, ventricular enlargement, or increased extra-axial CSF may suggest alterations in fluid drainage or glymphatic function, but these findings do not reveal the underlying mechanisms responsible for the changes. For example, PVS enlargement may reflect impaired interstitial fluid clearance, vascular remodeling, or inflammatory processes, but structural imaging alone cannot distinguish between these possibilities.

Another limitation relates to the temporal resolution of structural MRI. Neurofluid circulation is a dynamic process influenced by arterial pulsatility, respiration, and sleep–wake cycles. Static images capture only a single time point and therefore cannot characterize dynamic flow patterns or clearance rates within the glymphatic system.

Structural MRI is also limited by spatial resolution and partial-volume effects, particularly when evaluating small structures such as perivascular spaces. Small PVS may fall below the resolution threshold of clinical MRI scanners, while larger spaces may be difficult to differentiate from small cystic lesions or lacunar infarcts without additional imaging sequences.

These limitations become even more significant in paediatric populations, where rapid developmental changes influence the MRI appearance of brain tissues and fluid compartments. During infancy and early childhood, the brain undergoes substantial changes in water content, myelination, and tissue composition. Neonatal brains contain a higher proportion of water

compared with adult brains, which leads to different signal characteristics on T1- and T2-weighted images. As myelination progresses, the signal intensity of white matter gradually changes, altering the contrast between CSF, grey matter, and white matter.

These developmental processes can complicate the interpretation of neurofluid-related imaging findings. For instance, higher brain water content and immature myelination may increase the visibility of fluid-filled spaces on T2-weighted images, potentially leading to overestimation of PVS burden or other fluid compartments. Similarly, evolving tissue contrast during early development may make it difficult to accurately distinguish between physiological developmental features and pathological alterations in neurofluid circulation.

Furthermore, developmental changes in brain volume and ventricular size occur naturally during childhood, making it challenging to establish reliable normative references for neurofluid markers across different ages. As a result, the interpretation of structural MRI findings must take into account age-specific developmental trajectories.

In summary, while structural MRI provides valuable anatomical information and can identify imaging markers associated with neurofluid pathways, it remains an indirect and static representation of fluid dynamics. The interpretation of such markers is further complicated in paediatric populations by rapid developmental changes in brain water content and myelination, which can influence both the appearance and the quantification of neurofluid-related structures. Consequently, structural MRI findings should ideally be complemented with advanced imaging techniques or longitudinal data to better understand the functional dynamics of neurofluid circulation.

7.8 Associations between PVS burden and extra-axial CSF volume and observed frontal predominance of PVS.

Associations between PVS burden and extra-axial CSF volume should be interpreted primarily as correlative findings, potentially reflecting shared alterations in neurofluid circulation, developmental variability, or vascular characteristics. A correlation between PVS burden and extra-axial CSF volume indicates that the two variables vary together across individuals, but it does not establish that one directly causes the other. Structural MRI alone cannot determine causal relationships between these compartments.

The frontal predominance of PVS may arise from a combination of developmental maturation patterns, vascular anatomy of medullary arteries, regional glymphatic drainage pathways, and imaging-related factors. The frontal white matter is supplied by long medullary arteries branching

from cortical vessels. The perivascular pathways surrounding these vessels extend deep into the white matter and may be particularly prominent or susceptible to dilation when fluid clearance mechanisms are altered. Differences in arterial pulsatility and vascular compliance in these vessels could also influence perivascular fluid movement. Further longitudinal and functional imaging studies are needed to clarify the biological mechanisms underlying these observations.

7.9 PSD volume as a marker of altered drainage capacity rather than structural or inflammatory variation

The interpretation of PSD volume as a marker of altered drainage capacity requires careful consideration of both biological and methodological factors. One hypothesis is that increased PSD volume may reflect altered or reduced efficiency of CSF and ISF drainage. The dural venous sinuses and surrounding meningeal compartments are thought to play a role in CSF resorption and glymphatic outflow, including interactions with meningeal lymphatic vessels. In this context, expansion of PSD compartments could represent fluid accumulation secondary to impaired clearance, analogous to the dilation of perivascular spaces observed when interstitial drainage is disrupted. Nevertheless, interpreting PSD enlargement purely as a marker of impaired drainage may be overly simplistic. Changes in PSD volume could also arise from structural or inflammatory variations within the meninges and surrounding tissues. For example, variations in dural thickness, connective tissue composition, or venous sinus anatomy normally influence the apparent size of these spaces on MRI. Inflammatory processes affecting the meninges could also alter local fluid balance or tissue permeability, potentially contributing to increased PSD volume independent of drainage capacity.

Developmental Considerations: In paediatric populations, additional caution is warranted because the meningeal and venous systems continue to mature during childhood. Developmental differences in dural structure, venous sinus morphology, and CSF circulation may influence the appearance and size of PSD compartments on imaging. Consequently, increased PSD volume in children may reflect normal developmental variability rather than pathological alterations in drainage function.

Segmentation Bias and Anatomical Complexity: Accurate quantification of PSD volume is technically challenging due to the complex anatomy of the dural venous sinuses, including the superior sagittal sinus, transverse sinuses, and associated venous lacunae. These regions contain a heterogeneous mixture of structures—such as venous blood, arachnoid granulations, connective tissue septa, and small CSF-filled spaces—which can produce similar signal intensities on conventional MRI sequences. Automated or semi-automated segmentation

algorithms may therefore struggle to reliably distinguish PSD compartments from adjacent structures. For instance, arachnoid granulations, which protrude into venous sinuses and participate in CSF absorption, may be misclassified as fluid spaces during segmentation. Similarly, partial-volume effects at the interface between CSF, venous blood, and dura can introduce measurement errors, particularly when imaging resolution is limited.

These challenges may lead to systematic overestimation or underestimation of PSD volume, especially in regions where the sinus walls are irregular or where multiple tissue types coexist within a small spatial area. Such segmentation biases are particularly relevant in studies that rely on automated volumetric measurements.

7.10 Generalisability of the 3D U-Net segmentation model across scanners

3D U-Net–based deep learning models have become increasingly common for automated segmentation of neuroanatomical structures in MRI. These models offer high efficiency and reproducibility compared with manual or semi-automated approaches. However, when applying a trained model across different scanners, field strengths, and datasets, several factors must be considered to ensure the generalisability and reliability of the segmentation results. The performance of a 3D U-Net model is strongly influenced by the characteristics of the training dataset, including scanner manufacturer, acquisition protocols, and magnetic field strength (e.g., 1.5T vs 3T). MRI images acquired from different scanners may vary in signal-to-noise ratio, spatial resolution, contrast properties, and intensity distributions. These variations can affect the model's ability to accurately recognize anatomical features if they differ substantially from the training data.

Deep learning models trained on data from a single scanner or a single acquisition protocol may therefore exhibit reduced performance when applied to external datasets. To improve generalisability, models are ideally trained using heterogeneous datasets that include images from multiple scanners, field strengths, and institutions. Additional strategies such as intensity normalization, data augmentation, and domain adaptation techniques can also help mitigate scanner-related variability. When properly validated on external datasets, 3D U-Net models can demonstrate good cross-scanner performance, but external validation is essential before applying the model to new populations or imaging protocols.

Another important consideration is distinguishing true biological change from methodological variability when analysing longitudinal volumetric measurements derived from automated segmentation.

Threshold for biologically meaningful change: to interpret longitudinal volumetric changes reliably, studies often define a minimum detectable change or test–retest variability threshold. This threshold represents the magnitude of change required to exceed expected measurement variability. In many MRI volumetric studies, test–retest variability for automated segmentation methods is typically in the range of 3–10%, depending on the structure being measured, image resolution, and model performance. Consequently, longitudinal changes smaller than this range may reflect methodological noise rather than true biological change. For this reason, volumetric changes exceeding approximately 5–10% are often considered more likely to represent biologically meaningful alterations, although the exact threshold depends on the specific structure and imaging protocol. Establishing dataset-specific reproducibility metrics through test–retest experiments is therefore important for accurate interpretation.

Implications for Neurofluid Imaging Studies: In studies examining structures related to neurofluid dynamics, such as PVS, extra-axial CSF compartments and PSD, careful attention must be paid to these methodological factors. Because these structures can be small and sensitive to imaging resolution, segmentation models may be particularly susceptible to scanner variability or partial-volume effects. Therefore, robust interpretation of longitudinal changes requires: external validation of the segmentation model; Consistent imaging protocols across time points; Quantification of test–retest reliability; Consideration of the minimum detectable change threshold

7.11 The comparative potential of PVS and PSD as biomarkers of altered neurofluid dynamics, and the design of an ideal longitudinal or multimodal study

PVS and PSD may be complementary biomarkers. PVS reflects upstream perivascular fluid dynamics, PSD reflects downstream drainage capacity. Neither alone provides definitive functional information, but together they can offer a more holistic picture of neurofluid alterations in ASD.

An ideal study design would be longitudinal, multimodal, high-resolution MRI with flow-sensitive and diffusion-based sequences, combined with standardized neurodevelopmental assessments, can help distinguish developmental variability from altered drainage, and

potentially link early neurofluid changes to later ASD phenotypes. In addition, the role of sedation on PVS and PSD is unknown and must be taken into consideration in future studies.

7.12 Challenges in pediatric MRI

Pediatric MRI comes with a unique set of challenges that differ from adult imaging because of developmental, technical, and patient-management factors. Researchers must additionally be mindful that a pediatric MRI requires careful communication with both the child and their caregivers to reduce anxiety, often involving the use of age-appropriate explanations, mock scanners, and other child-friendly strategies to create a more tolerable imaging experience.

7.12.1 Myelination

In neonatal MRI, the evaluation of myelination presents distinct challenges due to the immature state of the newborn brain. At birth, much of the white matter is unmyelinated or only partially myelinated, resulting in markedly different signal characteristics from those seen in the mature brain, including an inversion of gray- white matter contrast on conventional T1- and T2-weighted images (Fig 4-1). Myelination progresses rapidly in the first months of life but at region-specific rates, requiring careful age-matched interpretation to avoid misclassifying normal maturation as pathology or overlooking subtle abnormalities. Furthermore, delayed or atypical myelination can mimic various white matter disorders, necessitating integration of imaging findings with gestational age, clinical history, and, in some cases, follow-up studies. Technical considerations, such as optimizing sequence parameters and minimizing motion artifacts in unsedated infants, are essential to reliably assess myelination patterns in this population.

7.12.2 Developmental timeline of brain structures

Several MRI based atlases have been developed to assist clinicians and researchers to interpret images in relationship with the age of the developing brain (454,455). However, these atlases are based on sequences acquired with parameters used in clinical practice and what is normal on research sequences may be different and difficult to interpret. In addition to myelination growth trajectories, the baby brain is constantly changing in terms of cortical folding, lobar growth and tissue composition with changes in vascular density, intra- and extracellular water concentrations. These age-dependent variations alter signal intensities and gray–white matter contrast, making adult imaging standards inapplicable and necessitating age-specific normative data for accurate assessment. Additionally, certain findings, such as prominent PVS, benign cystic structures, may be normal variants in children but could be misinterpreted as pathological in the absence of developmental context.

Neonatal and infant head and body are smaller in size. Imaging protocols must therefore be adapted from adult standards, with adjustments to sequence parameters, coil selection, and field-of-view to account for differences in relaxation times and tissue properties in pediatric patients. Safety considerations are also heightened, as children's smaller body mass and ongoing development necessitate stricter adherence to limits on specific absorption rate, gradient switching and high magnetic field strengths (456).

7.12.3 Motion artifacts and possible effect of sedation

One of the most significant issues is patient cooperation, as children, particularly infants and toddlers, often struggle to remain still for the extended periods required for high-quality imaging. This predisposes to motion artifacts, which can substantially degrade image quality and limit diagnostic accuracy. This is particularly true in research settings where high resolution sequences and novel sequences may be time consuming. In many cases, sedation or general anesthesia becomes necessary to minimize movement, but these interventions introduce additional concerns, including the risks associated with pharmacologic agents, the need for specialized monitoring, and potential effects on neurodevelopment when repeated imaging is required. Recent evidence however does suggest that adverse effects due to sedation in MRI are negligible (457). Also, sedation will interfere with normal brain physiology by affecting cardiovascular parameters. Examining brain perfusion, neurovascular coupling and CSF dynamics is therefore difficult.

7.12.4 Feed and swaddle technique

To reduce sedation in neonates, the "feed-and-swaddle" technique is a widely used, non-pharmacological approach to minimize motion during MRI in neonates and young infants, reducing or eliminating the need for sedation. This method leverages the natural sleep cycle of the infant to achieve stillness during image acquisition. Prior to the scan, the infant is fed—ideally immediately before positioning in the scanner—to induce a postprandial sleep state. Once the infant is drowsy or asleep, they are gently swaddled in a warm blanket to provide physical comfort, restrict limb movement, and maintain body temperature in the cool MRI environment. Ear protection is applied to reduce exposure to scanner noise, which can otherwise disturb sleep and induce movement. The technique requires careful environmental preparation, including dim lighting, minimal handling, and a quiet scanning room, to maximize the likelihood of sustained sleep. When executed effectively, the feed-and-swaddle method allows for acquisition of high-quality images in this age group without the risks associated with sedation or anesthesia. However, its success is age-dependent, generally being most effective in infants under three to

four months of age, before voluntary movement becomes more frequent and prolonged sleep more difficult to maintain in the scanner.

In neurofluid research, sleep represents a critical variable influencing fluid dynamics and must be accounted for when interpreting findings.

7.12.5 Lack of data on healthy infants and ethical considerations

Most of the reasons illustrated above, form the basis for the lack of high-quality healthy control data set in pediatric MRI research. MRI can be stressful for children. Exposing healthy children to sedation purely for research purposes raises ethical concerns and will fail to meet institutional review board approval criteria. Also, parents are more reluctant to enroll healthy children in studies involving long scan times, loud noises, or confined spaces, especially without direct clinical benefit. Scheduling can be difficult, as participation often conflicts with school or family obligations. The need for specialized preparation, mock scanner training, or child-life support can limit study feasibility. The reporting of incidental findings presents complex legal and ethical challenges. Because pediatric brain structure and MRI contrast change rapidly with age, large datasets are required to cover all developmental stages. This increases the recruitment burden and cost compared to adult studies. Obtaining high-quality pediatric MRI data often requires child-friendly infrastructure, such as mock scanners, dedicated pediatric coils, and trained personnel. Longitudinal healthy-control data is especially scarce because retaining participants over years is logistically difficult and costly.

7.13 Future directions

Despite the numerous challenges inherent to pediatric MRI, it remains essential to develop strategies that enable the acquisition of high-quality data on brain development and physiology in the growing brain. Advancing this knowledge is critical for elucidating the pathophysiological basis of neurological disorders, thereby informing targeted treatment approaches and guiding investment in effective preventive strategies.

7.13.1 Large dataset of healthy subjects

The establishment of a large, high-quality MRI dataset of the pediatric brain would represent a transformative resource for neuroscience and clinical medicine. Such a dataset would enable the mapping of normative developmental trajectories for brain structure, myelination, connectivity, and functional organization across infancy, childhood, and adolescence, providing robust age-specific reference standards that are currently lacking. This

normative framework would significantly improve the accuracy of detecting deviations associated with developmental, genetic, and acquired neurological disorders, allowing for earlier and more precise diagnosis. Large-scale pediatric MRI data would also serve as a critical foundation for machine learning and artificial intelligence models tailored to pediatric neuroimaging.

7.13.2 Longitudinal studies

Longitudinal studies to track PVS number and volume over time in both healthy and those at risk for neurodevelopmental disorders could be worthwhile, given the promising results in identifying enlarged PVS as a potential biomarker. Similarly, the development of PSD during the first few years of life would strengthen our knowledge of the normal appearing PSD tissue. Such research would facilitate our understanding into how early-life brain changes influence later cognitive, behavioral, and clinical outcomes, advancing our understanding of the pathophysiological basis of a wide range of neurological conditions including fluid dynamics.

7.13.3 Omics-imaging

The integration of omics technologies with neuroimaging—often referred to as “omics imaging”— may offer a powerful approach for advancing the understanding of ASD and the relevance of PVS and PSD structural markers. Omics methodologies, encompassing genomics, transcriptomics, proteomics, metabolomics, and other molecular profiling techniques, provide detailed insights into the biological pathways implicated in ASD (458–460). When these molecular data are combined with structural and functional brain imaging, it becomes possible to directly link cellular and biochemical alterations to specific neuroanatomical regions, networks, and developmental trajectories. This multimodal approach has the potential to identify biologically meaningful ASD subtypes, thereby addressing the disorder’s well-recognized heterogeneity. Furthermore, correlating molecular signatures with imaging phenotypes may elucidate the mechanisms through which disruptions in processes such as synaptic regulation, immune function, and neuroinflammation manifest as measurable changes in cortical thickness, white matter integrity, and functional connectivity. Such integrated datasets also provide a fertile ground for developing robust biomarkers for early diagnosis, prognosis, and monitoring of treatment response. Ultimately, omics imaging could enable precision medicine strategies in ASD by guiding targeted interventions that are tailored to an individual’s unique molecular and neurodevelopmental profile, while also informing the timing of these interventions to maximize developmental benefit.

In my ongoing IRB-approved research, biofluid samples—including tears, nasal secretions, and blood—are being collected and stored for proteomic analysis aimed at identifying signatures of ASD. These molecular profiles are examined in relation to MRI-derived biomarkers, such as PVS and PSD. Establishing such correlations would provide clinical context and significance for the MRI-based structural markers that form the focus of this thesis.

7.14 Conclusions

In our cohort, PVS and PSD metrics in children with ASD demonstrated significant associations with CSF volume and neurodevelopmental measures, underscoring their potential as MRI-based biomarkers of altered neurofluid drainage in early life. These findings extend prior work on extra-axial CSF enlargement in ASD by suggesting that perivascular and parasagittal structures may also reflect underlying disturbances in fluid clearance pathways. Understanding the maturation of these systems in the developing brain has important clinical implications. Establishing normative developmental trajectories for PVS and PSD could enable earlier identification of deviations indicative of neurodevelopmental disorders, including ASD, epilepsy, and pediatric cerebrovascular disease. Understanding how clearance pathways form, refine, and stabilize in early life may reveal vulnerable points where age-related decline begins, offering a mechanistic link between pediatric and adult disease processes.

Appendix A PVS visual rating scale

Grade 0: No PVS are visible.

Grade 1: 1 to 10 PVS.

Grade 2: 11 to 20 PVS.

Grade 3: 21 to 40 PVS.

Grade 4: More than 40 PVS.

For reference see (164,427).

Appendix B Diagnostic Criteria for Autism Spectrum Disorder (ASD) Based on *Diagnostic and Statistical Manual of Mental Disorders, 5th Edition*, Text Revision[a]

- To meet diagnostic criteria for ASD according to DSM-5, a child must have persistent deficits in each of 3 areas of social communication and interaction (see A.1. through A.3. below) plus at least 2 of 4 types of restricted, repetitive behaviors (see B.1. through B.4. below).

A. Persistent deficits in social communication and social interaction across multiple contexts, as manifested by the following, currently or by history (examples are illustrative, not exhaustive; see below):

1. Deficits in social-emotional reciprocity, ranging, for example, from abnormal social approach and failure of normal back-and-forth conversation; to reduced sharing of interests, emotions, or affect; to failure to initiate or respond to social interactions.

2. Deficits in nonverbal communicative behaviors used for social interaction, ranging, for example, from poorly integrated verbal and nonverbal communication; to abnormalities in eye contact and body language or deficits in understanding and use of gestures; to a total lack of facial expressions and nonverbal communication.

3. Deficits in developing, maintaining, and understanding relationships, ranging, for example, from difficulties adjusting behavior to suit various social contexts; to difficulties in sharing imaginative play or in making friends; to absence of interest in peers.

- *Specify* current severity: Severity is based on social communication impairments and restricted repetitive patterns of behavior. (See below.)

A. Restricted, repetitive patterns of behavior, interests, or activities, as manifested by at least two of the following, currently or by history (examples are illustrative, not exhaustive; see text):

1. Stereotyped or repetitive motor movements, use of objects, or speech (eg, simple motor stereotypies, lining up toys or flipping objects, echolalia, idiosyncratic phrases).

2. Insistence on sameness, inflexible adherence to routines, or ritualized patterns or verbal nonverbal behavior (eg, extreme distress at small changes, difficulties with transitions, rigid thinking patterns, greeting rituals, need to take same route or eat food every day).

3. Highly restricted, fixated interests that are abnormal in intensity or focus (eg, strong attachment to or preoccupation with unusual objects, excessively circumscribed or perseverative interest).

4. Hyper- or hyporeactivity to sensory input or unusual interests in sensory aspects of the environment (eg, apparent indifference to pain/temperature, adverse response to specific sounds or textures, excessive smelling or touching of objects, visual fascination with lights or movement).

- *Specify* current severity: Severity is based on social communication impairments and restricted, repetitive patterns of behavior. (See below.)

A. Symptoms must be present in the early developmental period (but may not become fully manifest until social demands exceed limited capacities or may be masked by learned strategies in later life).

B. Symptoms cause clinically significant impairment in social, occupational, or other important areas of current functioning.

C. These disturbances are not better explained by intellectual disability (intellectual developmental disorder) or global developmental delay. Intellectual disability and autism spectrum disorder frequently co-occur; to make comorbid diagnoses of autism spectrum disorder and intellectual disability, social communication should be below that expected for general developmental level.

- Note: Individuals with a well-established *DSM-IV* diagnosis of autistic disorder, Asperger disorder, or pervasive developmental disorder not otherwise specified should be given the diagnosis of ASD. Individuals who have marked deficits in social communication, but whose symptoms do not otherwise meet criteria for ASD, should be evaluated for social (pragmatic) communication disorder.

- *Specify* if:

- With or without accompanying intellectual impairment

- With or without accompanying language impairment (Coding note: use additional code to identify the associated medical or genetic condition.)

- Associated with another neurodevelopmental, mental, or behavioral disorder (Coding note: use additional code[s] to identify the associated neurodevelopmental, mental, or behavioral disorder[s].)

- With catatonia

- Associated with a known medical or genetic condition or environmental factor

Chapter 8 References

1. Agarwal N. Neurofluid interactive dynamics: a holistic approach to the physiology and clinical implications for neurological diseases.

2. Agarwal N, Lewis LD, Hirschler L, Rivera LR, Naganawa S, Levendovszky SR, et al. Current Understanding of the Anatomy, Physiology, and Magnetic Resonance Imaging of Neurofluids: Update From the 2022 “ISMRM Imaging Neurofluids Study group” Workshop in Rome. J Magn Reson Imaging. 2024;59(2):431–49.

3. Benveniste H, Lee H, Volkow ND. The Glymphatic Pathway: Waste Removal from the CNS via Cerebrospinal Fluid Transport. Neurosci [Internet]. 2016 Dec 30;23(5):454–65. Available from: http://journals.sagepub.com/doi/10.1177/1073858417691030

4. Gato A, Alonso MI, Martín C, Carnicero E, Moro JA, De la Mano A, et al. Embryonic cerebrospinal fluid in brain development: Neural progenitor control. Croat Med J. 2014;55(4):299–305.

5. Lau LW, Cua R, Keough MB, Haylock-Jacobs S, Yong VW. Pathophysiology of the brain extracellular matrix: a new target for remyelination. Nat Rev Neurosci [Internet]. 2013 Oct 29;14(10):722–9. Available from: https://www.nature.com/articles/nrn3550

6. Ma L, Chang Q, Pei F, Liu M, Zhang W, Hong YK, et al. Skull progenitor cell-driven meningeal lymphatic restoration improves neurocognitive functions in craniosynostosis. Cell Stem Cell [Internet]. 2023 Nov;30(11):1472-1485.e7. Available from: https://linkinghub.elsevier.com/retrieve/pii/S1934590923003594

7. Zibitt M, Makhoul V, Yu JC, Nguyen K, Williams JK. Glymphatics, Cranium, and the Brain Homeostasis. FACE [Internet]. 2023 Jun 28;4(2):218–27. Available from: http://journals.sagepub.com/doi/10.1177/27325016231160291

8. Saunders NR, Liddelow SA, Dziegielewska KM. Barrier mechanisms in the developing brain. Front Pharmacol. 2012;3 MAR(March):1–18.

9. Stolp HB, Liddelow SA, Sá-Pereira I, Dziegielewska KM, Saunders NR. Immune responses at brain barriers and implications for brain development and neurological function in later life. Front Integr Neurosci. 2013;7(AUG):1–14.

10. Gato A, Moro JA, Alonso MI, Pastor JF, Represa JJ, Barbosa E. Chondroitin sulphate proteoglycan and embryonic brain enlargement in the chick. Anat Embryol (Berl) [Internet]. 1993 Jul;188(1). Available from: http://link.springer.com/10.1007/BF00191455

11. Alonso MI, Gato A, Moro JA, Martin P, Barbosa E. Involvement of Sulfated Proteoglycans in Embryonic Brain Expansion at Earliest Stages of Development in Rat Embryos. Cells Tissues Organs [Internet]. 1999;165(1):1–9. Available from: https://karger.com/CTO/article/doi/10.1159/000016667

12. Lowery LA, Sive H. Totally tubular: The mystery behind function and origin of the brain ventricular system. BioEssays. 2009;31(4):446–58.

13. Schoenwolf GC, Desmond ME. Neural tube occlusion precedes rapid brain enlargement. J Exp Zool [Internet]. 1984 Jun;230(3):405–7. Available from: https://onlinelibrary.wiley.com/doi/10.1002/jez.1402300309

14. García-Lecea M, Kondrychyn I, Fong SH, Ye ZR, Korzh V. In vivo Analysis of Choroid Plexus Morphogenesis in Zebrafish. Lopez-Schier H, editor. PLoS One [Internet]. 2008 Sep 1;3(9):e3090. Available from: https://dx.plos.org/10.1371/journal.pone.0003090

15. Gómez DG, DiBenedetto AT, Pavese AM, Firpo A, Hershan DB, Potts DG. Development of Arachnoid Villi and Granulations in Man. Cells Tissues Organs [Internet]. 1981;111(3):247–58. Available from: https://karger.com/AAN/article/doi/10.1159/000145473

16. Dziegielewska KM, Ek J, Habgood MD, Saunders NR. Development of the choroid plexus. Microsc Res Tech. 2001;52(1):5–20.

17. Kompaníková P, Bryja V. Regulation of choroid plexus development and its functions. Cell Mol Life Sci [Internet]. 2022;79(6):1–15. Available from: https://doi.org/10.1007/s00018-022-04314-1

18. Lun MP, Monuki ES, Lehtinen MK. Development and functions of the choroid plexus–cerebrospinal fluid system. Nat Rev Neurosci [Internet]. 2015 Aug 15;16(8):445–57. Available from: https://www.nature.com/articles/nrn3921

19. Arnaud K, Di Nardo AA. Choroid plexus trophic factors in the developing and adult brain. Front Biol (Beijing). 2016;11(3):214–21.

20. Johanson CE. Choroid Plexus-Cerebrospinal Fluid Transport Dynamics: Support of Brain Health and a Role in Neurotherapeutics [Internet]. Conn's Translational Neuroscience. Elsevier Inc.; 2017. 233–261 p. Available from: http://dx.doi.org/10.1016/B978-0-12-802381-5.00020-8

21. Ghersi-Egea JF, Strazielle N, Catala M, Silva-Vargas V, Doetsch F, Engelhardt B. Molecular anatomy and functions of the choroidal blood-cerebrospinal fluid barrier in health and disease. Acta Neuropathol [Internet]. 2018;135(3):337–61. Available from:

https://doi.org/10.1007/s00401-018-1807-1

22. Parada C, Gato Á, Bueno D. Mammalian Embryonic Cerebrospinal Fluid Proteome Has Greater Apolipoprotein and Enzyme Pattern Complexity than the Avian Proteome. J Proteome Res [Internet]. 2005 Dec 1;4(6):2420–8. Available from: https://pubs.acs.org/doi/10.1021/pr050213t

23. Zappaterra MD, Lisgo SN, Lindsay S, Gygi SP, Walsh CA, Ballif BA. A Comparative Proteomic Analysis of Human and Rat Embryonic Cerebrospinal Fluid. J Proteome Res [Internet]. 2007 Sep 1;6(9):3537–48. Available from: https://pubs.acs.org/doi/10.1021/pr070247w

24. Parada C, Gato A, Aparicio M, Bueno D. Proteome analysis of chick embryonic cerebrospinal fluid. Proteomics [Internet]. 2006 Jan 9;6(1):312–20. Available from: https://analyticalsciencejournals.onlinelibrary.wiley.com/doi/10.1002/pmic.200500085

25. Hébert JM, Mishina Y, McConnell SK. BMP Signaling Is Required Locally to Pattern the Dorsal Telencephalic Midline. Neuron [Internet]. 2002 Sep;35(6):1029–41. Available from: https://linkinghub.elsevier.com/retrieve/pii/S0896627302009005

26. Bueno D, Parvas M, Garcia-Fernàndez J. The embryonic blood-cerebrospinal fluid barrier function before the formation of the fetal choroid plexus: role in cerebrospinal fluid formation and homeostasis. Croat Med J [Internet]. 2014 Aug;55(4):306–16. Available from: https://www.ncbi.nlm.nih.gov/pmc/articles/PMC4157384/

27. Yamasaki M, Nonaka M, Bamba Y, Teramoto C, Ban C, Pooh RK. Diagnosis, treatment, and long-term outcomes of fetal hydrocephalus. Semin Fetal Neonatal Med [Internet]. 2012 Dec;17(6):330–5. Available from: https://linkinghub.elsevier.com/retrieve/pii/S1744165X12000868

28. Antila S, Karaman S, Nurmi H, Airavaara M, Voutilainen MH, Mathivet T, et al. Development and plasticity of meningeal lymphatic vessels. J Exp Med [Internet]. 2017 Dec 4;214(12):3645–67. Available from: https://rupress.org/jem/article/214/12/3645/42289/Development-and-plasticity-of-meningeal-lymphatic

29. Papaiconomou C, Bozanovic-Sosic R, Zakharov A, Johnston M. Does neonatal cerebrospinal fluid absorption occur via arachnoid projections or extracranial lymphatics? Am J Physiol Integr Comp Physiol [Internet]. 2002 Oct 1;283(4):R869–76. Available from: https://www.physiology.org/doi/10.1152/ajpregu.00173.2002

30. Mollanji R, Papaiconomou C, Boulton M, Midha R, Johnston M. Comparison of cerebrospinal fluid transport in fetal and adult sheep. Am J Physiol - Regul Integr Comp Physiol. 2001;281(4 50-4):1215–23.

31. Mehta NH, Sherbansky J, Kamer AR, Carare RO, Butler T, Rusinek H, et al. The Brain-Nose Interface: A Potential Cerebrospinal Fluid Clearance Site in Humans. Front Physiol. 2022;12(January).

32. Bálint L, Ocskay Z, Deák BA, Aradi P, Jakus Z. Lymph Flow Induces the Postnatal Formation of Mature and Functional Meningeal Lymphatic Vessels. Front Immunol. 2020;10(January):1–19.

33. Fox RJ, Walji AH, Mielke B, Petruk KC, Aronyk KE. Anatomic details of intradural channels in the parasagittal dura: A possible pathway for flow of cerebrospinal fluid. Neurosurgery. 1996;39(1):84–91.

34. Fame RM, Lehtinen MK. Emergence and Developmental Roles of the Cerebrospinal Fluid System. Dev Cell [Internet]. 2020;52(3):261–75. Available from: https://doi.org/10.1016/j.devcel.2020.01.027

35. Kahle KT, Kulkarni A V, Limbrick DD, Warf BC. Hydrocephalus in children. Lancet [Internet]. 2016 Feb;387(10020):788–99. Available from: https://linkinghub.elsevier.com/retrieve/pii/S0140673615606948

36. Vinchon M, Rekate H, Kulkarni A V. Pediatric hydrocephalus outcomes: a review. Fluids Barriers CNS [Internet]. 2012 Dec 27;9(1):18. Available from: https://fluidsbarrierscns.biomedcentral.com/articles/10.1186/2045-8118-9-18

37. Radoš M, Živko M, Periša A, Orešković D, Klarica M. No Arachnoid Granulations—No Problems: Number, Size, and Distribution of Arachnoid Granulations From Birth to 80 Years of Age. Front Aging Neurosci [Internet]. 2021 Jul 1;13. Available from: https://www.frontiersin.org/articles/10.3389/fnagi.2021.698865/full

38. Lopes MBS. Meninges: Embryology. Meningiomas. 2009;25–9.

39. Nicholas DS, Weller RO. The fine anatomy of the human spinal meninges. J Neurosurg [Internet]. 1988 Aug;69(2):276–82. Available from: https://thejns.org/view/journals/j-neurosurg/69/2/article-p276.xml

40. Mack J, Squier W, Eastman JT. Anatomy and development of the meninges: implications for subdural collections and CSF circulation. Pediatr Radiol [Internet]. 2009 Mar 23;39(3):200–10. Available from: http://link.springer.com/10.1007/s00247-008-1084-6

41. Adeeb N, Deep A, Griessenauer CJ, Mortazavi MM, Watanabe K, Loukas M, et al. The intracranial arachnoid mater: A comprehensive review of its history, anatomy, imaging, and pathology. Child's Nerv Syst. 2013;29(1):17–33.

42. Agarwal N, Carare RO. Cerebral Vessels: An Overview of Anatomy, Physiology, and Role in the Drainage of Fluids and Solutes. Front Neurol [Internet]. 2020;11:611485. Available from: http://www.ncbi.nlm.nih.gov/pubmed/33519691

43. O'Rahilly RMF. The Meninges in Human Development. J Neuropathol Exp Neurol. 1986;45(5):588–608.

44. Decimo I, Dolci S, Panuccio G, Riva M, Fumagalli G, Bifari F. Meninges: A Widespread Niche of Neural Progenitors for the Brain. Neurosci [Internet]. 2021 Oct 16;27(5):506–28. Available from: https://journals.sagepub.com/doi/10.1177/1073858420954826

45. Halfter W, Dong S, Yip YP, Willem M, Mayer U. A Critical Function of the Pial Basement Membrane in Cortical Histogenesis. J Neurosci [Internet]. 2002 Jul 15;22(14):6029–40. Available from: https://www.jneurosci.org/lookup/doi/10.1523/JNEUROSCI.22-14-06029.2002

46. Borrell V, Marín O. Meninges control tangential migration of hem-derived Cajal-Retzius cells via CXCL12/CXCR4 signaling. Nat Neurosci [Internet]. 2006 Oct 10;9(10):1284–93. Available from: https://www.nature.com/articles/nn1764

47. Mercier F, Hatton GI. Connexin 26 and basic fibroblast growth factor are expressed primarily in the subpial and subependymal layers in adult brain parenchyma: Roles in stem cell proliferation and morphological plasticity? J Comp Neurol [Internet]. 2001 Feb 26;431(1):88–104. Available from: https://onlinelibrary.wiley.com/doi/10.1002/1096-9861(20010226)431:1%3C88::AID-CNE1057%3E3.0.CO;2-D

48. Stylianopoulou F, Herbert J, Soares MB, Efstratiadis A. Expression of the insulin-like growth factor II gene in the choroid plexus and the leptomeninges of the adult rat central nervous system. Proc Natl Acad Sci [Internet]. 1988 Jan;85(1):141–5. Available from: https://pnas.org/doi/full/10.1073/pnas.85.1.141

49. Siegenthaler JA, Ashique AM, Zarbalis K, Patterson KP, Hecht JH, Kane MA, et al. Retinoic Acid from the Meninges Regulates Cortical Neuron Generation. Cell [Internet]. 2009 Oct;139(3):597–609. Available from: https://linkinghub.elsevier.com/retrieve/pii/S0092867409012525

50. Choe Y, Siegenthaler JA, Pleasure SJ. A Cascade of Morphogenic Signaling Initiated by the

Meninges Controls Corpus Callosum Formation. Neuron. 2012;73(4):698–712.

51. Como CN, Kim S, Siegenthaler J. Stuck on you: Meninges cellular crosstalk in development. Curr Opin Neurobiol. 2023;79:1–18.

52. Dasgupta K, Jeong J. Developmental biology of the meninges. 2019;(December 2018):1–12.

53. Radakovits R, Barros CS, Belvindrah R, Patton B, Muller U. Regulation of Radial Glial Survival by Signals from the Meninges. J Neurosci [Internet]. 2009 Jun 17;29(24):7694–705. Available from: https://www.jneurosci.org/lookup/doi/10.1523/JNEUROSCI.5537-08.2009

54. Shah T, Leurgans SE, Mehta RI, Yang J, Galloway CA, Bentley KLDM. Arachnoid granulations are lymphatic conduits that communicate with bone marrow and dura-arachnoid stroma. 2023;220(2).

55. Lewis HW. THE PATHWAYS OF ESCAPE FROM THE SUBARACHNOID SPACES WITH PARTICULAR REFERENCE TO THE ARACH- NOID VILLI. . J Med Res [Internet]. 1914 Jan 1;XXXI:50–96. Available from: https://www.ncbi.nlm.nih.gov/pmc/articles/PMC2094443/pdf/jmedres00049-0059.pdf

56. O'CONNELL JEA. SOME OBSERVATIONS ON THE CEREBRAL VEINS. Brain [Internet]. 1934;57(4):484–503. Available from: https://academic.oup.com/brain/article-lookup/doi/10.1093/brain/57.4.484

57. Suy R, Thomis S, Fourneau I. The discovery of lymphatic system in the seventeenth century. Part I: The early history. Acta Chir Belg. 2016;116(4):260–6.

58. Breslin JW, Yang Y, Scallan JP, Sweat RS, Adderley SP, Murfee WL. Lymphatic vessel network structure and physiology. Compr Physiol. 2019;9(1):207–99.

59. Wiig H, Swartz MA. Interstitial fluid and lymph formation and transport: physiological regulation and roles in inflammation and cancer. Physiol Rev. 2012 Jul;92(3):1005–60.

60. Natale G, Bocci G, Ribatti D. Scholars and scientists in the history of the lymphatic system. J Anat. 2017;231(3):417–29.

61. Mascagni P. Vasorum lymphaticorum corporis humani historia et ichnographia. 1777;

62. Bucchieri F, Farina F, Zummo G, Cappello F. Lymphatic vessels of the dura mater: A new discovery? J Anat. 2015;227(5):702–3.

63. Absinta M, Ha SK, Nair G, Sati P, Luciano NJ, Palisoc M, et al. Human and nonhuman primate meninges harbor lymphatic vessels that can be visualized noninvasively by MRI. Elife [Internet]. 2017 Oct 3;6:780. Available from: http://elifesciences.org/lookup/doi/10.7554/eLife.29738

64. Louveau A, Plog BA, Antila S, Alitalo K, Nedergaard M, Kipnis J. Understanding the functions and relationships of the glymphatic system and meningeal lymphatics. J Clin Invest [Internet]. 2017 Sep 1;127(9):3210–9. Available from: https://www.jci.org/articles/view/90603

65. Aspelund A, Antila S, Proulx ST, Karlsen TV, Karaman S, Detmar M, et al. A dural lymphatic vascular system that drains brain interstitial fluid and macromolecules. J Exp Med. 2015;212(7):991–9.

66. Clancy B, Darlington RB, Finlay BL. TRANSLATING DEVELOPMENTAL TIME ACROSS MAMMALIAN SPECIES. 2001;105(1):7–17.

67. Kuban KC, Gilles FH. Human telencephalic angiogenis. Ann Neurol [Internet]. 1985 Jun 7;17(6):539–48. Available from: https://onlinelibrary.wiley.com/doi/10.1002/ana.410170603

68. Marin-Padilla M. Early vascularization of the embryonic cerebral cortex: Golgi and electron microscopic studies. J Comp Neurol [Internet]. 1985 Nov 8;241(2):237–49. Available from: https://onlinelibrary.wiley.com/doi/10.1002/cne.902410210

69. Marín-Padilla M. The human brain intracerebral microvascular system: development and structure. 2012 Sep 8;1–14. Available from: message:%3C09BCC7435F7EA34AB7DFD1920980CC43015034C15C@wcssmbxmail1p%3E

70. Nelson MD, Gonzalez-Gomez I, Gilles FH. The search for human telencephalic ventriculofugal arteries. Am J Neuroradiol. 1991;12(2):215–22.

71. Román GC. On the history of lacunes, Etat criblé, and the white matter lesions of vascular dementia. Cerebrovasc Dis. 2002;13(SUPPL. 2):1–6.

72. Virchow R. XII. Ueber die Erweiterung kleinerer Gefiifse. Arch Pathol Anat und Physiol und Klin Med. 1851;3:427–62.

73. Robin C. Recherches sur quelques particularites de la structure des capillaires de l'encephale. J Physiol Homme Anim. 1859;2:537–48.

74. Carare RO, Bernardes-Silva M, Newman TA, Page AM, Nicoll JAR, Perry VH, et al. Solutes, but not cells, drain from the brain parenchyma along basement membranes of capillaries and arteries: significance for cerebral amyloid angiopathy and neuroimmunology. Neuropathol Appl Neurobiol [Internet]. 2008 Apr 1;34(2):131–44. Available from: http://doi.wiley.com/10.1111/j.1365-2990.2007.00926.x

75. Zhang ET, Inman CBE, Weller RO. Interrelationships of the pia mater and the perivascular (Virchow-Robin) spaces in the human cerebrum. J Anat [Internet]. 1990 Jan 1;170:111–23. Available from: https://www.ncbi.nlm.nih.gov/pmc/articles/PMC1257067/pdf/janat00040-0112.pdf

76. Vargová L, Syková E. Extracellular space diffusion and extrasynaptic transmission. Physiol Res. 2008;57(SUPPL. 3).

77. Syková E, Svoboda J, Polák J, Chvátal A. Extracellular volume fraction and diffusion characteristics during progressive ischemia and terminal anoxia in the spinal cord of the rat. J Cereb Blood Flow Metab. 1994;14(2):301–11.

78. Nakamura K, Brown RA, Araujo D, Narayanan S, Arnold DL. Correlation between brain volume change and T2 relaxation time induced by dehydration and rehydration: Implications for monitoring atrophy in clinical studies. NeuroImage Clin. 2014;6:166–70.

79. Lei Y, Han H, Yuan F, Javeed A, Zhao Y. The brain interstitial system: Anatomy, modeling, in vivo measurement, and applications. Prog Neurobiol [Internet]. 2017 Oct 1;157:230–46. Available from: http://dx.doi.org/10.1016/j.pneurobio.2015.12.007

80. Ferrer-Ferrer M, Dityatev A. Shaping Synapses by the Neural Extracellular Matrix. Front Neuroanat [Internet]. 2018 May 15;12. Available from: http://journal.frontiersin.org/article/10.3389/fnana.2018.00040/full

81. Ashok K. S, Gabriele Z. The Interstitial System of the Brain in Health and Disease. Aging Dis. 2020;11(1):200.

82. Fawcett JW, Oohashi T, Pizzorusso T. The roles of perineuronal nets and the perinodal extracellular matrix in neuronal function. Nat Rev Neurosci [Internet]. 2019;20(8):451–65. Available from: http://dx.doi.org/10.1038/s41583-019-0196-3

83. Hensch TK. Critical period regulation. Annu Rev Neurosci. 2004;27:549–79.

84. Bandtlow CE, Zimmermann DR. Proteoglycans in the Developing Brain: New Conceptual Insights for Old Proteins. Physiol Rev [Internet]. 2000 Jan 10;80(4):1267–90. Available from: https://www.physiology.org/doi/10.1152/physrev.2000.80.4.1267

85. Kerrisk ME, Cingolani LA, Koleske AJ. ECM receptors in neuronal structure, synaptic plasticity, and behavior [Internet]. 1st ed. Vol. 214, Progress in Brain Research. Elsevier B.V.; 2014. 101–131 p. Available from: http://dx.doi.org/10.1016/B978-0-444-63486-3.00005-0

86. Araya C, Carmona-Fontaine C, Clarke JDW. Extracellular matrix couples the convergence movements of mesoderm and neural plate during the early stages of neurulation. Dev Dyn. 2016;245(5):580–9.

87. Abdallah MW, Michel TM. Matrix metalloproteinases in autism spectrum disorders. J Mol Psychiatry. 2013;1(1):16.

88. Ioannidis V, Pandey R, Bauer HF, Schön M, Bockmann J, Boeckers TM, et al. Disrupted extracellular matrix and cell cycle genes in autism-associated Shank3 deficiency are targeted by lithium. Mol Psychiatry [Internet]. 2024;29(3):704–17. Available from: http://dx.doi.org/10.1038/s41380-023-02362-y

89. Eidahl JML, Rognum TO, Stray-Pedersen A, Opdal SH. Brain water content in sudden unexpected infant death. Forensic Sci Med Pathol [Internet]. 2023 Feb 3;19(4):507–16. Available from: https://link.springer.com/10.1007/s12024-023-00584-8

90. Young A, Brown LK, Ennis S, Beattie RM, Johnson MJ. Total body water in full-term and preterm newborns: systematic review and meta-analysis. Arch Dis Child - Fetal Neonatal Ed [Internet]. 2021 Sep;106(5):542–8. Available from: https://fn.bmj.com/lookup/doi/10.1136/archdischild-2020-321112

91. Gottschalk A, Scafidi S, Toung TJK. Brain water as a function of age and weight in normal rats. PLoS One [Internet]. 2021;16(9 September):1–6. Available from: http://dx.doi.org/10.1371/journal.pone.0249384

92. Dobbing J, Sands J. Quantitative growth and development of human brain. Arch Dis Child. 1973;48(10):757–67.

93. Iliff JJ, Wang M, Liao Y, Plogg BA, Peng W, Gundersen GA, et al. A paravascular pathway facilitates CSF flow through the brain parenchyma and the clearance of interstitial solutes, including amyloid β. Sci Transl Med [Internet]. 2012 Aug 15;4(147):147ra111-147ra111. Available from: http://stm.sciencemag.org/cgi/doi/10.1126/scitranslmed.3003748

94. Eide PK, Ringstad G. MRI with intrathecal MRI gadolinium contrast medium administration: a possible method to assess glymphatic function in human brain. Acta Radiol Short Reports [Internet]. 2015 Nov 4;4(11):205846011560963–5. Available from:

http://journals.sagepub.com/doi/10.1177/2058460115609635

95. Ringstad G, Eide PK, Naganawa S, Agarwal N. Gadolinium-Based Imaging and the Study of Neurofluid Dynamics. Neuroimaging Clin N Am [Internet]. 2025;(Lc). Available from: https://doi.org/10.1016/j.nic.2024.12.008

96. Eide PK, Lashkarivand A, Hagen-Kersten ÅA, Gjertsen Ø, Nedregaard B, Sletteberg R, et al. Intrathecal Contrast-Enhanced Magnetic Resonance Imaging of Cerebrospinal Fluid Dynamics and Glymphatic Enhancement in Idiopathic Normal Pressure Hydrocephalus. Front Neurol. 2022;13(April):1–21.

97. Ringstad G, Eide PK. Cerebrospinal fluid tracer efflux to parasagittal dura in humans. Nat Commun [Internet]. 2020 Jan 11;11(1):1–9. Available from: http://dx.doi.org/10.1038/s41467-019-14195-x

98. Melin E, Ringstad G, Valnes LM, Eide PK. Human parasagittal dura is a potential neuroimmune interface. Commun Biol [Internet]. 2023 Mar 11;6(1):260. Available from: http://dx.doi.org/10.1038/nri3621

99. Mundt S, Keller A, Greter M. The dural sinus hub: more than just a brain drain. Cell [Internet]. 2021;184(4):858–60. Available from: https://doi.org/10.1016/j.cell.2021.01.040

100. Kress BT, Iliff JJ, Xia M, Wang M, Wei HS, Zeppenfeld D, et al. Impairment of paravascular clearance pathways in the aging brain. Ann Neurol [Internet]. 2014 Dec 26;76(6):845–61. Available from: https://onlinelibrary.wiley.com/doi/10.1002/ana.24271

101. Holst CB, Brøchner CB, Vitting-Seerup K, Møllgård K. Astrogliogenesis in human fetal brain: complex spatiotemporal immunoreactivity patterns of patterns of GFAP, S100, AQP4 and YKL-40. J Anat [Internet]. 2019 Sep 22;235(3):590–615. Available from: https://onlinelibrary.wiley.com/doi/10.1111/joa.12948

102. Castañeyra-Ruiz L, González-Marrero I, Hernández-Abad LG, Carmona-Calero EM, Pardo MR, Baz-Davila R, et al. AQP4 labels a subpopulation of white matter-dependent glial radial cells affected by pediatric hydrocephalus, and its expression increased in glial microvesicles released to the cerebrospinal fluid in obstructive hydrocephalus. Acta Neuropathol Commun [Internet]. 2022 Mar 28;10(1):41. Available from: https://actaneurocomms.biomedcentral.com/articles/10.1186/s40478-022-01345-4

103. Mayo F, González-Vinceiro L, Hiraldo-González L, Calle-Castillejo C, Morales-Alvarez S, Ramírez-Lorca R, et al. Aquaporin-4 Expression Switches from White to Gray Matter Regions during Postnatal Development of the Central Nervous System. Int J Mol Sci

[Internet]. 2023 Feb 3;24(3):3048. Available from: https://www.mdpi.com/1422-0067/24/3/3048

104. Lunde LK, Camassa LMA, Hoddevik EH, Khan FH, Ottersen OP, Boldt HB, et al. Postnatal development of the molecular complex underlying astrocyte polarization. Brain Struct Funct [Internet]. 2015;220(4):2087–101. Available from: http://dx.doi.org/10.1007/s00429-014-0775-z

105. Song J, Li Z, Xue X, Meng J, Zhu W, Hu S, et al. Neonatal stress disrupts the glymphatic system development and increases the susceptibility to Parkinson's disease in later life. CNS Neurosci Ther [Internet]. 2024 Feb 8;30(2). Available from: https://onlinelibrary.wiley.com/doi/10.1111/cns.14587

106. Wei F, Song J, Zhang C, Lin J, Xue R, Shan LD, et al. Chronic stress impairs the aquaporin-4-mediated glymphatic transport through glucocorticoid signaling. Psychopharmacology (Berl) [Internet]. 2019 Apr 3;236(4):1367–84. Available from: http://link.springer.com/10.1007/s00213-018-5147-6

107. Di Palma C, Goulay R, Chagnot S, Martinez De Lizarrondo S, Anfray A, Salaun J, et al. Cerebrospinal fluid flow increases from newborn to adult stages. Dev Neurobiol [Internet]. 2018 Sep 2;78(9):851–8. Available from: https://onlinelibrary.wiley.com/doi/10.1002/dneu.22622

108. Brinker T, Stopa E, Morrison J, Klinge P. A new look at cerebrospinal fluid circulation. Fluids Barriers CNS [Internet]. 2014 Jan 1;11(1):10. Available from: http://fluidsbarrierscns.biomedcentral.com/articles/10.1186/2045-8118-11-10

109. Ma Q, Ineichen B V., Detmar M, Proulx ST. Outflow of cerebrospinal fluid is predominantly through lymphatic vessels and is reduced in aged mice. Nat Commun. 2017;8(1).

110. Bradbury BYMWB, Cole DF. The role of the lymphatic system in drainage of cerebrospinal fluid and aqueous humor. 1980;299:353–65.

111. Agarwal N, Carare RO. Cerebral Vessels: An Overview of Anatomy, Physiology, and Role in the Drainage of Fluids and Solutes. Front Neurol [Internet]. 2021 Jan 13 [cited 2021 Jan 13];11. Available from: chrome-extension://dagcmkpagjlhakfdhnbomgmjdpkdklff/enhanced-reader.html?openApp&pdf=https%3A%2F%2Ffjfsdata01prod.blob.core.windows.net%2Farticles%2Ffiles%2F611485%2Fpubmed-zip%2F.versions%2F1%2F.package-entries%2Ffneur-11-611485%2Ffneur-11-611485.pdf%3Fs

112. Carare RO, Aldea R, Bulters D, Alzetani A, Birch AA, Richardson G, et al. Vasomotion Drives Periarterial Drainage of Aβ from the Brain. Neuron [Internet]. 2020 Feb 1;105(3):400–1. Available from: https://linkinghub.elsevier.com/retrieve/pii/S0896627320300118

113. Aldea R, Weller RO, Wilcock DM, Carare RO, Richardson G. Cerebrovascular Smooth Muscle Cells as the Drivers of Intramural Periarterial Drainage of the Brain. Front Aging Neurosci [Internet]. 2019 Jan 23;11:217–53. Available from: https://www.frontiersin.org/article/10.3389/fnagi.2019.00001/full

114. van Veluw SJ, Hou SS, Calvo-Rodriguez M, Arbel-Ornath M, Snyder AC, Frosch MP, et al. Vasomotion as a Driving Force for Paravascular Clearance in the Awake Mouse Brain. Neuron [Internet]. 2020 Feb 1;105(3):549-561.e5. Available from: https://linkinghub.elsevier.com/retrieve/pii/S0896627319309286

115. Carare RO, Aldea R, Agarwal N, Bacskai BJ, Bechman I, Boche D, et al. Clearance of interstitial fluid (ISF) and CSF (CLIC) group—part of Vascular Professional Interest Area (PIA): Cerebrovascular disease and the failure of elimination of Amyloid-β from the brain and retina with age and Alzheimer's disease-Opportunities for . Alzheimer's Dement Diagnosis, Assess Dis Monit. 2020;12(1):1–7.

116. Hawkes CA, Sullivan PM, Hands S, Weller RO, Nicoll JAR, Carare RO. Disruption of arterial perivascular drainage of amyloid-β from the brains of mice expressing the human APOE ε4 allele. PLoS One. 2012;7(7):1–11.

117. Keable A, Fenna K, Yuen HM, Johnston DA, Smyth NR, Smith C, et al. Deposition of amyloid β in the walls of human leptomeningeal arteries in relation to perivascular drainage pathways in cerebral amyloid angiopathy. Biochim Biophys Acta - Mol Basis Dis. 2016;

118. Thomsen MS, Routhe LJ, Moos T. The vascular basement membrane in the healthy and pathological brain. J Cereb Blood Flow Metab. 2017;37(10):3300–17.

119. Thomsen MS, Birkelund S, Burkhart A, Stensballe A, Moos T. Synthesis and deposition of basement membrane proteins by primary brain capillary endothelial cells in a murine model of the blood–brain barrier. J Neurochem [Internet]. 2017 Mar 8;140(5):741–54. Available from: https://onlinelibrary.wiley.com/doi/10.1111/jnc.13789

120. Zhou M, Schools GP, Kimelberg HK. Development of GLAST(+) Astrocytes and NG2(+) Glia in Rat Hippocampus CA1: Mature Astrocytes Are Electrophysiologically Passive. J Neurophysiol [Internet]. 2006 Jan;95(1):134–43. Available from: http://www.physiology.org/doi/10.1152/jn.00570.2005

121. Barber AJ, Lieth E. Agrin accumulates in the brain microvascular basal lamina during development of the blood-brain barrier. Dev Dyn an Off Publ Am Assoc Anat. 1997 Jan;208(1):62–74.

122. Coelho-Santos V, Shih AY. Postnatal development of cerebrovascular structure and the neurogliovascular unit. Wiley Interdiscip Rev Dev Biol. 2020;9(2):1–20.

123. Daneman R, Zhou L, Kebede AA, Barres BA. Pericytes are required for blood brain barrier integrity during embryogenesis. Nature. 2010;468(7323):562–6.

124. Janzer RC, Raff MC. Astrocytes induce blood-brain barrier properties in endothelial cells. Vol. 325, Nature. 1987. p. 253–7.

125. Pearce WJ. Fetal Cerebrovascular Maturation: Effects of Hypoxia. Semin Pediatr Neurol [Internet]. 2018 Dec;28:17–28. Available from: https://linkinghub.elsevier.com/retrieve/pii/S1071909118300329

126. HARNARINE-SINGH D, HYDE JB. Post-natal Growth of the Arterial Net in the Human Cerebral Pia Mater. Nature [Internet]. 1970 Jan;225(5227):86–7. Available from: https://www.nature.com/articles/225086a0

127. Xu L, Nirwane A, Yao Y. Basement membrane and blood-brain barrier. Stroke Vasc Neurol. 2019;4(2):78–82.

128. Semple BD, Blomgren K, Gimlin K, Ferriero DM, Noble-Haeusslein LJ. Brain development in rodents and humans: Identifying benchmarks of maturation and vulnerability to injury across species. Prog Neurobiol [Internet]. 2013 Jul;106–107:1–16. Available from: https://linkinghub.elsevier.com/retrieve/pii/S0301008213000300

129. Hirota T, King BH. Autism Spectrum Disorder. JAMA [Internet]. 2023 Jan 10;329(2):157. Available from: https://jamanetwork.com/journals/jama/fullarticle/2800182

130. Evans B. How autism became autism. Hist Human Sci [Internet]. 2013 Jul 8;26(3):3–31. Available from: https://journals.sagepub.com/doi/10.1177/0952695113484320

131. Oztenekecioglu B, Mavis M, Osum M, Kalkan R. Genetic and Epigenetic Alterations in Autism Spectrum Disorder. Glob Med Genet [Internet]. 2021 Dec 15;08(04):144–8. Available from: http://www.thieme-connect.de/DOI/DOI?10.1055/s-0041-1735540

132. Boulanger-Bertolus J, Pancaro C, Mashour GA. Increasing Role of Maternal Immune Activation in Neurodevelopmental Disorders. Front Behav Neurosci [Internet]. 2018 Oct 5;12. Available from: https://www.frontiersin.org/article/10.3389/fnbeh.2018.00230/full

133. Careaga M, Van de Water J, Ashwood P. Immune Dysfunction in Autism: A Pathway to Treatment. Neurotherapeutics [Internet]. 2010 Jul;7(3):283–92. Available from: https://linkinghub.elsevier.com/retrieve/pii/S1878747923002209

134. Ashwood P, Wills S, Van de Water J. The immune response in autism: a new frontier for autism research. J Leukoc Biol [Internet]. 2006 May 12;80(1):1–15. Available from: https://academic.oup.com/jleukbio/article/80/1/1/6922516

135. Inui T, Kumagaya S, Myowa-Yamakoshi M. Neurodevelopmental Hypothesis about the Etiology of Autism Spectrum Disorders. Front Hum Neurosci [Internet]. 2017 Jul 11;11. Available from: http://journal.frontiersin.org/article/10.3389/fnhum.2017.00354/full

136. Sanders SJ, He X, Willsey AJ, Ercan-Sencicek AG, Samocha KE, Cicek AE, et al. Insights into Autism Spectrum Disorder Genomic Architecture and Biology from 71 Risk Loci. Neuron [Internet]. 2015 Sep;87(6):1215–33. Available from: https://linkinghub.elsevier.com/retrieve/pii/S0896627315007734

137. Dichter GS. Functional magnetic resonance imaging of autism spectrum disorders. Dialogues Clin Neurosci [Internet]. 2012 Sep 30;14(3):319–51. Available from: https://www.tandfonline.com/doi/full/10.31887/DCNS.2012.14.3/gdichter

138. Ismail MMT, Keynton RS, Mostapha MMMO, ElTanboly AH, Casanova MF, Gimel'farb GL, et al. Studying Autism Spectrum Disorder with Structural and Diffusion Magnetic Resonance Imaging: A Survey. Front Hum Neurosci [Internet]. 2016 May 11;10. Available from: http://journal.frontiersin.org/Article/10.3389/fnhum.2016.00211/abstract

139. Robinson-Agramonte M de los A, Noris García E, Fraga Guerra J, Vega Hurtado Y, Antonucci N, Semprún-Hernández N, et al. Immune Dysregulation in Autism Spectrum Disorder: What Do We Know about It? Int J Mol Sci [Internet]. 2022 Mar 11;23(6):3033. Available from: https://www.mdpi.com/1422-0067/23/6/3033

140. Hughes HK, Moreno RJ, Ashwood P. Brain Behavior and Immunity Innate immune dysfunction and neuroinflammation in autism spectrum disorder (ASD). Brain Behav Immun [Internet]. 2023;108(December 2022):245–54. Available from: https://doi.org/10.1016/j.bbi.2022.12.001

141. Li X, Chauhan A, Sheikh AM, Patil S, Chauhan V, Li XM, et al. Elevated immune response in the brain of autistic patients. J Neuroimmunol [Internet]. 2009 Feb;207(1–2):111–6. Available from: https://linkinghub.elsevier.com/retrieve/pii/S0165572808004906

142. Pardo CA, Vargas DL, Zimmerman AW. Immunity, neuroglia and neuroinflammation in

autism. Int Rev Psychiatry [Internet]. 2005 Jan 11;17(6):485–95. Available from: http://www.tandfonline.com/doi/full/10.1080/02646830500381930

143. Bjørklund G, Saad K, Chirumbolo S, Kern JK, Geier DA, Geier MR, et al. Immune dysfunction and neuroinflammation in autism spectrum disorder. 2016;257–68.

144. Goines PE, Ashwood P. Cytokine dysregulation in autism spectrum disorders (ASD): Possible role of the environment. Neurotoxicol Teratol [Internet]. 2013;36:67–81. Available from: http://dx.doi.org/10.1016/j.ntt.2012.07.006

145. Goines P, Van de Water J. The immune system's role in the biology of autism. Curr Opin Neurol [Internet]. 2010 Apr;23(2):111–7. Available from: https://journals.lww.com/00019052-201004000-00005

146. Love C, Sominsky L, O'Hely M, Berk M, Vuillermin P, Dawson SL. Prenatal environmental risk factors for autism spectrum disorder and their potential mechanisms. BMC Med [Internet]. 2024;22(1). Available from: https://doi.org/10.1186/s12916-024-03617-3

147. Román P, Ruiz-González C, Rueda-Ruzafa L, Cardona D, Requena M, Alarcón R. Exposure to Environmental Pesticides and the Risk of Autism Spectrum Disorders: A Population-Based Case-Control Study. Medicina (B Aires) [Internet]. 2024 Mar 14;60(3):479. Available from: https://www.mdpi.com/1648-9144/60/3/479

148. Patel S, Dale RC, Rose D, Heath B, Nordahl CW, Rogers S, et al. Maternal immune conditions are increased in males with autism spectrum disorders and are associated with behavioural and emotional but not cognitive co-morbidity. Transl Psychiatry [Internet]. 2020;10(1). Available from: http://dx.doi.org/10.1038/s41398-020-00976-2

149. Ambrosino S, Elbendary H, Lequin M, Rijkelijkhuizen D, Banaschewski T, Baron-Cohen S, et al. In-depth characterization of neuroradiological findings in a large sample of individuals with autism spectrum disorder and controls. NeuroImage Clin. 2022;35(July).

150. Boddaert N, Zilbovicius M, Philipe A, Robel L, Bourgeois M, Barthélemy C, et al. MRI findings in 77 children with non-syndromic autistic disorder. PLoS One. 2009;4(2).

151. Shen MD. Cerebrospinal fluid and the early brain development of autism. J Neurodev Disord. 2018;10(1):1–10.

152. Shen MD, Kim SH, McKinstry RC, Gu H, Hazlett HC, Nordahl CW, et al. Increased Extra-axial Cerebrospinal Fluid in High-Risk Infants Who Later Develop Autism. Biol Psychiatry [Internet]. 2017 Aug;82(3):186–93. Available from: https://linkinghub.elsevier.com/retrieve/pii/S0006322317312179

153. Garic D, McKinstry RC, Rutsohn J, Slomowitz R, Wolff J, Macintyre LC, et al. Enlarged Perivascular Spaces in Infancy and Autism Diagnosis, Cerebrospinal Fluid Volume, and Later Sleep Problems. JAMA Netw Open. 2023;6(12):E2348341.

154. Iadecola C, Nedergaard M. Glial regulation of the cerebral microvasculature. Nat Neurosci [Internet]. 2007 Oct 26;10(11):1369–76. Available from: http://www.nature.com/articles/nn2003

155. Agarwal N, Contarino C, Toro EF. Neurofluids: A holistic approach to their physiology, interactive dynamics and clinical implications for neurological diseases. Veins Lymphat [Internet]. 2019 Sep 10;8(3):49–58. Available from: https://www.pagepressjournals.org/index.php/vl/article/view/8470

156. Beggs CB. Cerebral venous outflow and cerebrospinal fluid dynamics. Veins Lymphat [Internet]. 2014 Dec 23;3(3):1–8. Available from: http://www.pagepressjournals.org/index.php/vl/article/view/vl.2014.1867

157. Louveau A, Smirnov I, Keyes TJ, Eccles JD, Rouhani SJ, Peske JD, et al. Structural and functional features of central nervous system lymphatic vessels. Nature [Internet]. 2015 Jun 1;523(7560):337–41. Available from: http://www.nature.com/doifinder/10.1038/nature14432

158. Agarwal N, Port JD. Neuroimaging: Anatomy meets function. Neuroimaging: Anatomy Meets Function. 2017.

159. Hill MA, Nourian Z, Ho IL, Clifford PS, Martinez-Lemus L, Meininger GA. Small Artery Elastin Distribution and Architecture—Focus on Three Dimensional Organization. Microcirculation. 2016;23(8):614–20.

160. Blinder P, Tsai PS, Kaufhold JP, Knutsen PM, Suhl H, Kleinfeld D. The cortical angiome: An interconnected vascular network with noncolumnar patterns of blood flow. Nat Neurosci. 2013;

161. Tsai PS, Kaufhold JP, Blinder P, Friedman B, Drew PJ, Karten HJ, et al. Correlations of neuronal and microvascular densities in murine cortex revealed by direct counting and colocalization of nuclei and vessels. J Neurosci. 2009;

162. MacGregor Sharp M, Bulters D, Brandner S, Holton J, Verma A, Werring DJ, et al. The fine anatomy of the perivascular compartment in the human brain: relevance to dilated perivascular spaces in cerebral amyloid angiopathy. Neuropathol Appl Neurobiol [Internet]. 2018 Feb 27;1–9. Available from: http://doi.wiley.com/10.1111/nan.12480

163. Hutchings M, Weller RO. Anatomical relationships of the pia mater to cerebral blood vessels in man. J Neurosurg [Internet]. 1986 Sep 1;65(3):316–25. Available from: https://pubmed.ncbi.nlm.nih.gov/3734882

164. Wardlaw JM, Smith EE, Biessels GJ, Cordonnier C, Fazekas F, Frayne R, et al. Neuroimaging standards for research into small vessel disease and its contribution to ageing and neurodegeneration. Lancet Neurol [Internet]. 2013 Aug 1;12(8):822–38. Available from: https://linkinghub.elsevier.com/retrieve/pii/S1474442213701248

165. Hase Y, Polvikoski TM, Firbank MJ, Craggs LJL, Hawthorne E, Platten C, et al. Small vessel disease pathological changes in neurodegenerative and vascular dementias concomitant with autonomic dysfunction. Brain Pathol. 2020;

166. Horsburgh K, Wardlaw JM, van Agtmael T, Allan SM, Ashford MLJ, Bath PM, et al. Small vessels, dementia and chronic diseases - molecular mechanisms and pathophysiology. Clin Sci. 2018;

167. Hamel E. Perivascular nerves and the regulation of cerebrovascular tone. J Appl Physiol [Internet]. 2006 Mar 1;100(3):1059–64. Available from: http://www.physiology.org/doi/10.1152/japplphysiol.00954.2005

168. Fantini S, Sassaroli A, Tgavalekos KT, Kornbluth J. Cerebral blood flow and autoregulation: current measurement techniques and prospects for noninvasive optical methods. Neurophotonics [Internet]. 2016 Jun 21;3(3):031411. Available from: http://neurophotonics.spiedigitallibrary.org/article.aspx?doi=10.1117/1.NPh.3.3.031411

169. Toussay X, Basu K, Lacoste B, Hamel E. Locus coeruleus stimulation recruits a broad cortical neuronal network and increases cortical perfusion. J Neurosci. 2013;33(8):3390–401.

170. Rayshubskiy A, Wojtasiewicz TJ, Mikell CB, Bouchard MB, Timerman D, Youngerman BE, et al. Direct, intraoperative observation of ~0.1Hz hemodynamic oscillations in awake human cortex: Implications for fMRI. Neuroimage [Internet]. 2014 Feb 15;87(C):323–31. Available from: http://dx.doi.org/10.1016/j.neuroimage.2013.10.044

171. Zanatta P, Toffolo GM, Sartori E, Bet A, Baldanzi F, Agarwal N, et al. The human brain pacemaker: Synchronized infra-slow neurovascular coupling in patients undergoing non-pulsatile cardiopulmonary bypass. Neuroimage. 2013;72.

172. Gould IG, Tsai P, Kleinfeld D, Linninger A. The capillary bed offers the largest hemodynamic resistance to the cortical blood supply. J Cereb Blood Flow Metab [Internet]. 2016 Nov

13;37(1):52–68. Available from: http://journals.sagepub.com/doi/10.1177/0271678X16671146

173. Di Russo J, Hannocks MJ, Luik AL, Song J, Zhang X, Yousif L, et al. Vascular laminins in physiology and pathology. Matrix Biology. 2017.

174. Yousif LF, Di Russo J, Sorokin L. Laminin isoforms in endothelial and perivascular basement membranes. Cell Adhesion and Migration. 2013.

175. Abbott NJ, Rönnbäck L, Hansson E. Astrocyte-endothelial interactions at the blood-brain barrier. Nature Reviews Neuroscience. 2006.

176. Searson PC. The blood-brain barrier: an engineering perspective [Internet]. 2013. p. 1–22. Available from: https://www.ncbi.nlm.nih.gov/pmc/articles/PMC3757302/pdf/fneng-06-00007.pdf

177. Hannocks MJ, Pizzo ME, Huppert J, Deshpande T, Abbott NJ, Thorne RG, et al. Molecular characterization of perivascular drainage pathways in the murine brain. J Cereb Blood Flow Metab. 2018;

178. Bell RD, Sagare AP, Friedman AE, Bedi GS, Holtzman DM, Deane R, et al. Transport pathways for clearance of human Alzheimer's amyloid β-peptide and apolipoproteins E and J in the mouse central nervous system. J Cereb Blood Flow Metab. 2007;

179. Taoka T, Fukusumi A, Miyasaka T, Kawai H, Nakane T, Kichikawa K, et al. Structure of the Medullary Veins of the Cerebral Hemisphere and Related Disorders. Radiographics [Internet]. 2017 Jan 1;37(1):281–97. Available from: http://pubs.rsna.org/doi/10.1148/rg.2017160061

180. Schmidek HH, Auer LM, Kapp JP. The cerebral venous system. Neurosurgery [Internet]. 1985 Oct 1;17(4):663–78. Available from: http://eutils.ncbi.nlm.nih.gov/entrez/eutils/elink.fcgi?dbfrom=pubmed&id=3903542&retmode=ref&cmd=prlinks

181. Batson O V. THE FUNCTION OF THE VERTEBRAL VEINS AND THEIR ROLE IN THE SPREAD OF METASTASES. Ann Surg [Internet]. 1940 Jul 1;112(1):138–49. Available from: http://content.wkhealth.com/linkback/openurl?sid=WKPTLP:landingpage&an=00000658-194007000-00016

182. Pearce JMS. The Craniospinal Venous System. Eur Neurol [Internet]. 2006 Oct 1;56(2):136–8. Available from: http://www.karger.com/?doi=10.1159/000095706

183. Tobinick E, Vega CP. The cerebrospinal venous system: anatomy, physiology, and clinical implications. MedGenMed [Internet]. 2006 Feb 22;8(1):53. Available from: http://eutils.ncbi.nlm.nih.gov/entrez/eutils/elink.fcgi?dbfrom=pubmed&id=16915183&retmode=ref&cmd=prlinks

184. Ayanzen RH, Bird CR, Keller PJ, McCully FJ, Theobald MR, Heiserman JE. Cerebral MR venography: normal anatomy and potential diagnostic pitfalls. AJNR Am J Neuroradiol [Internet]. 2000 Jan 1;21(1):74–8. Available from: http://eutils.ncbi.nlm.nih.gov/entrez/eutils/elink.fcgi?dbfrom=pubmed&id=10669228&retmode=ref&cmd=prlinks

185. Kiliç T, Akakin A. Anatomy of cerebral veins and sinuses. Front Neurol Neurosci [Internet]. 2008 Jan 1;23:4–15. Available from: https://www.karger.com/Article/FullText/111256

186. MacGregor Sharp M, Criswell TP, Dobson H, Finucane C, Verma A, Carare RO. Solving an Old Dogma: Is it an Arteriole or a Venule? Front Aging Neurosci. 2019;11(October).

187. Földi M, Gellért A, Kozma M, Poberai M, Zoltán OT, Csanda E. New contributions to the anatomical connections of the brain and the lymphatic system. Acta Anat (Basel). 1966;64(4):498–505.

188. Weller RO, Sharp MM, Christodoulides M, Carare RO, Møllgård K. The meninges as barriers and facilitators for the movement of fluid, cells and pathogens related to the rodent and human CNS. Acta Neuropathol [Internet]. 2018 Jan 24;135(3):363–85. Available from: https://doi.org/10.1007/s00401-018-1809-z

189. Orešković D, Radoš M, Klarica M. New Concepts of Cerebrospinal Fluid Physiology and Development of Hydrocephalus. Pediatr Neurosurg [Internet]. 2016 Dec 21;(0):1–9. Available from: https://www.karger.com/?doi=10.1159/000452169

190. Ahn JH, Cho H, Kim JH, Kim SH, Ham JS, Park I, et al. Meningeal lymphatic vessels at the skull base drain cerebrospinal fluid. Nature [Internet]. 2019 Jul 20;572(7767):1–29. Available from: http://dx.doi.org/10.1038/s41586-019-1419-5

191. Abbott NJ. Evidence for bulk flow of brain interstitial fluid: significance for physiology and pathology. Neurochem Int [Internet]. 2004 Sep 1;45(4):545–52. Available from: http://linkinghub.elsevier.com/retrieve/pii/S0197018603002675

192. Syková E, Nicholson C. Diffusion in brain extracellular space. Physiol Rev [Internet]. 2008 Oct 1;88(4):1277–340. Available from: http://www.physiology.org/doi/10.1152/physrev.00027.2007

193. Hablitz LM, Vinitsky HS, Sun Q, Stæger FF, Sigurdsson B, Mortensen KN, et al. Increased glymphatic influx is correlated with high EEG delta power and low heart rate in mice under anesthesia. Sci Adv. 2019;5(2).

194. Hauglund NL, Pavan C, Nedergaard M. Cleaning the sleeping brain – the potential restorative function of the glymphatic system. Vol. 15, Current Opinion in Physiology. 2020. p. 1–6.

195. Xie L, Kang H, Xu Q, Chen MJ, Liao Y, Thiyagarajan M, et al. Sleep drives metabolite clearance from the adult brain. Science (80-) [Internet]. 2013 Oct 18;342(6156):373–7. Available from: http://www.sciencemag.org/cgi/doi/10.1126/science.1241224

196. Cserr HF. Role of secretion and bulk flow of brain interstitial fluid in brain volume regulation. Ann N Y Acad Sci [Internet]. 1988 Jan 1;529:9–20. Available from: http://eutils.ncbi.nlm.nih.gov/entrez/eutils/elink.fcgi?dbfrom=pubmed&id=3395070&retmode=ref&cmd=prlinks

197. Hladky SB, Barrand MA. Elimination of substances from the brain parenchyma: efflux via perivascular pathways and via the blood–brain barrier. Fluids Barriers CNS [Internet]. 2018 Oct 16;15(1):1–73. Available from: https://doi.org/10.1186/s12987-018-0113-6

198. Tarasoff-Conway JM, Carare RO, Osorio RS, Glodzik L, Butler T, Fieremans E, et al. Clearance systems in the brain—implications for Alzheimer disease. Nat Rev Neurol [Internet]. 2015 Jul 21;11(8):457–70. Available from: http://www.nature.com/articles/nrneurol.2015.119

199. Iliff JJ, Wang M, Zeppenfeld DM, Venkataraman A, Plog BA, Liao Y, et al. Cerebral Arterial Pulsation Drives Paravascular CSF-Interstitial Fluid Exchange in the Murine Brain. J Neurosci [Internet]. 2013 Nov 13;33(46):18190–9. Available from: http://www.jneurosci.org/cgi/doi/10.1523/JNEUROSCI.1592-13.2013

200. Asgari M, de Zélicourt D, Kurtcuoglu V. Glymphatic solute transport does not require bulk flow. Nat Publ Gr [Internet]. 2016 Nov 26;1–11. Available from: http://dx.doi.org/10.1038/srep38635

201. Ray LA, Heys JJ. Fluid Flow and Mass Transport in Brain Tissue. Fluids [Internet]. 2019 Dec 1;4(4):133–96. Available from: https://www.mdpi.com/2311-5521/4/4/196

202. Martinac AD, Bilston LE. Computational modelling of fluid and solute transport in the brain. Biomech Model Mechanobiol [Internet]. 2020;19(3):781–800. Available from: https://doi.org/10.1007/s10237-019-01253-y

203. Faghih MM, Sharp MK. Is bulk flow plausible in perivascular, paravascular and paravenous channels? Fluids Barriers CNS [Internet]. 2018 May 21;15(1):1–10. Available from: https://doi.org/10.1186/s12987-018-0103-8

204. Jin BJ, Smith AJ, Verkman AS. Spatial model of convective solute transport in brain extracellular space does not support a “glymphatic” mechanism. J Gen Physiol. 2016;

205. Attems J, Jellinger K, Thal DR, Van Nostrand W. Review: Sporadic cerebral amyloid angiopathy. Neuropathol Appl Neurobiol. 2011;

206. Carare RO, Hawkes CA, Jeffrey M, Kalaria RN, Weller RO. Review: Cerebral amyloid angiopathy, prion angiopathy, CADASIL and the spectrum of protein elimination failure angiopathies (PEFA) in neurodegenerative disease with a focus on therapy. Neuropathol Appl Neurobiol. 2013;39(6):593–611.

207. Casley Smith JR, Foldi Borcsok E, Foldi M. The prelymphatic pathways of the brain as revealed by cervical lymphatic obstruction and the passage of particles. Br J Exp Pathol. 1976;57(2):179–88.

208. Weller RO, Kida S, Zhang ET. Pathways of fluid drainage from the brain--morphological aspects and immunological significance in rat and man. Brain Pathol [Internet]. 1992 Oct 1;2(4):277–84. Available from: http://eutils.ncbi.nlm.nih.gov/entrez/eutils/elink.fcgi?dbfrom=pubmed&id=1341963&retmode=ref&cmd=prlinks

209. Diem AK, Tan M, Bressloff NW, Hawkes C, Morris AWJ, Weller RO, et al. A Simulation Model of Periarterial Clearance of Amyloid-β from the Brain. Front Aging Neurosci [Internet]. 2016 Feb 12;8:511–45. Available from: http://journal.frontiersin.org/Article/10.3389/fnagi.2016.00018/abstract

210. Sharp MK, Diem AK, Weller RO, Carare RO. Peristalsis with Oscillating Flow Resistance: A Mechanism for Periarterial Clearance of Amyloid Beta from the Brain. Ann Biomed Eng [Internet]. 2015 Sep 19;44(5):1–13. Available from: papers3://publication/doi/10.1007/s10439-015-1457-6

211. Fultz NE, Bonmassar G, Setsompop K, Stickgold RA, Rosen BR, Polimeni JR, et al. Coupled electrophysiological, hemodynamic, and cerebrospinal fluid oscillations in human sleep. Science (80-). 2019;366(6465):628–31.

212. Kellie G 1829. An account of the appearances observed in the dissection of two of three individuals presumed to have perished in the storm of the 3d, and whose bodies were

discovered in the vicinity of Leith on the morning of the 4th, November 1821 : with some reflectio. 2015 Nov 28;1–92. Available from: https://ia801309.us.archive.org/7/items/b22384315/b22384315.pdf

213. Mokri B. The Monro-Kellie hypothesis: applications in CSF volume depletion. Neurology [Internet]. 2001 Jun 26;56(12):1746–8. Available from: http://www.neurology.org/cgi/doi/10.1212/WNL.56.12.1746

214. Wilson MH. Monro-Kellie 2.0: The dynamic vascular and venous pathophysiological components of intracranial pressure. J Cereb Blood Flow Metab [Internet]. 2016 May 11;36(8):1338–50. Available from: http://journals.sagepub.com/doi/10.1177/0271678X16648711

215. Linninger AA, Tangen K, Hsu CY, Frim D. Cerebrospinal Fluid Mechanics and Its Coupling to Cerebrovascular Dynamics. Annu Rev Fluid Mech [Internet]. 2016 Jan 3;48(1):219–57. Available from: http://www.annualreviews.org/doi/10.1146/annurev-fluid-122414-034321

216. Greitz D, Wirestam R, Franck A, Nordell B, Thomsen C, Ståhlberg F. Pulsatile brain movement and associated hydrodynamics studied by magnetic resonance phase imaging. The Monro-Kellie doctrine revisited. Neuroradiology [Internet]. 1992 Jan 1;34(5):370–80. Available from: http://eutils.ncbi.nlm.nih.gov/entrez/eutils/elink.fcgi?dbfrom=pubmed&id=1407513&retmode=ref&cmd=prlinks

217. Lee SJ, King MA, Sun J, Xie HK, Subhash G, Sarntinoranont M. Measurement of viscoelastic properties in multiple anatomical regions of acute rat brain tissue slices. J Mech Behav Biomed Mater [Internet]. 2014 Jan 1;29(c):213–24. Available from: http://dx.doi.org/10.1016/j.jmbbm.2013.08.026

218. Budday S, Nay R, de Rooij R, Steinmann P, Wyrobek T, Ovaert TC, et al. Mechanical properties of gray and white matter brain tissue by indentation. J Mech Behav Biomed Mater [Internet]. 2015 Jun;46:318–30. Available from: https://linkinghub.elsevier.com/retrieve/pii/S1751616115000673

219. Kruse SA, Rose GH, Glaser KJ, Manduca A, Felmlee JP, Jack CR, et al. Magnetic resonance elastography of the brain. Neuroimage. 2008;

220. Hatt A, Cheng S, Tan K, Sinkus R, Bilston LE. MR Elastography Can Be Used to Measure Brain Stiffness Changes as a Result of Altered Cranial Venous Drainage During Jugular Compression. AJNR Am J Neuroradiol [Internet]. 2015 Oct 8;36(10):1971–7. Available from:

http://www.ajnr.org/lookup/doi/10.3174/ajnr.A4361

221. Sweeney MD, Kisler K, Montagne A, Toga AW, Zlokovic B V. The role of brain vasculature in neurodegenerative disorders. Nat Neurosci [Internet]. 2018 Oct 24;21(10):1318–31. Available from: http://www.nature.com/articles/s41593-018-0234-x

222. Kalaria RN, Pax AB. Increased collagen content of cerebral microvessels in Alzheimer's disease. Brain Res. 1995;

223. Vanherle L, Matuskova H, Don-Doncow N, Uhl FE, Meissner A. Improving Cerebrovascular Function to Increase Neuronal Recovery in Neurodegeneration Associated to Cardiovascular Disease. Front Cell Dev Biol. 2020;8(February):1–8.

224. Wolters FJ, Zonneveld HI, Hofman A, Van Der Lugt A, Koudstaal PJ, Vernooij MW, et al. Cerebral perfusion and the risk of dementia: A population-based study. Circulation. 2017;136(8):719–28.

225. Montagne A, Barnes SR, Sweeney MD, Halliday MR, Sagare AP, Zhao Z, et al. Blood-Brain barrier breakdown in the aging human hippocampus. Neuron. 2015;

226. Dumont M, Roy M, Jodoin PM, Morency FC, Houde JC, Xie Z, et al. Free Water in White Matter Differentiates MCI and AD From Control Subjects. Front Aging Neurosci. 2019;

227. MacGregor Sharp M, Saito S, Keable A, Gatherer M, Aldea R, Agarwal N, et al. Demonstrating a reduced capacity for removal of fluid from cerebral white matter and hypoxia in areas of white matter hyperintensity associated with age and dementia. Acta Neuropathol Commun [Internet]. 2020 Dec 8;8(1):131. Available from: https://actaneurocomms.biomedcentral.com/articles/10.1186/s40478-020-01009-1

228. Weller RO, Wisniewski H, Shulman K, Terry RD. Experimental hydrocephalus in young dogs: Histological and ultrastructural study of the brain tissue damage. J Neuropathol Exp Neurol. 1971;

229. Moody DM, Brown WR, Challa VR, Anderson RL. Periventricular venous collagenosis: association with leukoaraiosis. Radiology [Internet]. 1995 Feb 1;194(2):469–76. Available from: http://pubs.rsna.org/doi/10.1148/radiology.194.2.7824728

230. Nan D, Cheng Y, Feng L, Zhao M, Ma D, Feng J. Potential Mechanism of Venous System for Leukoaraiosis: From post-mortem to in vivo Research. Neurodegener Dis. 2020;130021(71):101–8.

231. Banerjee G, Kim HJ, Fox Z, Jäger HR, Wilson D, Charidimou A, et al. MRI-visible perivascular

space location is associated with Alzheimer's disease independently of amyloid burden. Brain [Internet]. 2017 Feb 17;140(4):1107–16. Available from: https://academic.oup.com/brain/article/140/4/1107/3003279

232. Hurford R, Charidimou A, Fox Z, Cipolotti L, Jager R, Werring DJ. MRI-visible perivascular spaces: relationship to cognition and small vessel disease MRI markers in ischaemic stroke and TIA. J Neurol Neurosurg Psychiatry [Internet]. 2014 Apr 10;85(5):522–5. Available from: http://jnnp.bmj.com/cgi/doi/10.1136/jnnp-2013-305815

233. Brown R, Benveniste H, Black SE, Charpak S, Dichgans M, Joutel A, et al. Understanding the role of the perivascular space in cerebral small vessel disease. Cardiovasc Res [Internet]. 2018 May 2;114(11):1462–73. Available from: https://academic.oup.com/cardiovascres/article/114/11/1462/4991897

234. Francis F, Ballerini L, Wardlaw JM. Perivascular spaces and their associations with risk factors, clinical disorders and neuroimaging features: A systematic review and meta-analysis. Int J Stroke [Internet]. 2019 Feb 14;27:174749301983032–13. Available from: http://journals.sagepub.com/doi/10.1177/1747493019830321

235. Agarwal N, Klein W, Tuura ROG. MR Imaging of Neurofluids in the Developing Brain. Neuroimaging Clin NA [Internet]. 2025; Available from: Magnetic resonance imaging of neurofluids in the developing brain

236. Iliff JJ, Lee H, Yu M, Feng T, Logan J, Nedergaard M, et al. Brain-wide pathway for waste clearance captured by contrast-enhanced MRI. J Clin Invest [Internet]. 2013 Mar 1;123(3):1299–309. Available from: http://www.jci.org/articles/view/67677

237. Dekaban AS, Sadowsky D. Changes in brain weights during the span of human life: Relation of brain weights to body heights and body weights. Ann Neurol [Internet]. 1978 Oct 7;4(4):345–56. Available from: https://onlinelibrary.wiley.com/doi/10.1002/ana.410040410

238. Yong Y, Cai Y, Lin J, Ma L, Han H, Li F. Advancement in modulation of brain extracellular space and unlocking its potential for intervention of neurological diseases [Internet]. Vol. 2, Med-X. Springer Nature Singapore; 2024. Available from: https://doi.org/10.1007/s44258-024-00021-7

239. Long KR, Huttner WB. How the extracellular matrix shapes neural development. Open Biol [Internet]. 2019 Jan 9;9(1). Available from: https://royalsocietypublishing.org/doi/10.1098/rsob.180216

240. McComb JG. Cerebrospinal fluid physiology of the developing fetus. Am J Neuroradiol. 1992;13(2):595–9.

241. Armstrong DL. Measurement of the subarachnoid space by ultrasound in preterm infants. Arch Dis Child - Fetal Neonatal Ed [Internet]. 2002 Mar 1;86(2):124F – 126. Available from: https://fn.bmj.com/lookup/doi/10.1136/fn.86.2.F124

242. Wandel A, Weissbach T, Katorza E, Ziv-Baran T. Subarachnoid Space Measurements in Apparently Healthy Fetuses Using MR Imaging. Am J Neuroradiol. 2023;44(6):716–21.

243. Sari E, Sari S, Akgün V, Özcan E, Ìnce S, Babacan O, et al. Measures of ventricles and evans' index: From neonate to adolescent. Pediatr Neurosurg. 2015;50(1):12–7.

244. Gómez DG, DiBenedetto AT, Pavese AM, Firpo A, Hershan DB, Potts DG. Development of Arachnoid Villi and Granulations in Man. Cells Tissues Organs [Internet]. 1981;111(3):247–58. Available from: https://www.karger.com/Article/FullText/145473

245. de Angelis LC, Witte MH, Bellini T, Bernas M, Boccardo F, Ramenghi LA, et al. Brain lymphatic drainage system in fetus and newborn: Birth of a new era of exploration. Lymphology. 2018;51(4):140–7.

246. Fame RM, MacDonald JL, Macklis JD. Development, specification, and diversity of callosal projection neurons. Trends Neurosci [Internet]. 2011 Jan 1;34(1):41–50. Available from: http://dx.doi.org/10.1016/j.tins.2010.10.002

247. Jain A, Ang PS, Matrongolo MJ, Tischfield MA. Understanding the development, pathogenesis, and injury response of meningeal lymphatic networks through the use of animal models. Cell Mol Life Sci [Internet]. 2023;80(11):1–12. Available from: https://doi.org/10.1007/s00018-023-04984-5

248. Shang T, Liang J, Kapron CM, Liu J. Pathophysiology of aged lymphatic vessels. Aging (Albany NY) [Internet]. 2019 Aug 28;11(16):6602–13. Available from: https://www.aging-us.com/lookup/doi/10.18632/aging.102213

249. Louveau A, Smirnov I, Keyes TJ, Eccles JD, Rouhani SJ, Peske JD, et al. Structural and functional features of central nervous system lymphatic vessels. Nature [Internet]. 2015 Jul 16;523(7560):337–41. Available from: http://www.nature.com/articles/nature14432

250. Tavares GA, Louveau A. Meningeal lymphatics: An immune gateway for the central nervous system. Cells. 2021;10(12):1–11.

251. Alves de Lima K, Rustenhoven J, Kipnis J. Meningeal Immunity and Its Function in

Maintenance of the Central Nervous System in Health and Disease. Annu Rev Immunol [Internet]. 2020 Apr 26;38(1):597–620. Available from: https://www.annualreviews.org/doi/10.1146/annurev-immunol-102319-103410

252. Albayram MS, Smith G, Tufan F, Tuna IS, Bostancıklıoğlu M, Zile M, et al. Non-invasive MR imaging of human brain lymphatic networks with connections to cervical lymph nodes. Nat Commun. 2022;13(1):1–14.

253. Eide PK, Pripp AH, Ringstad G. Magnetic resonance imaging biomarkers of cerebrospinal fluid tracer dynamics in idiopathic normal pressure hydrocephalus. Brain Commun [Internet]. 2020 Jul 1;2(2). Available from: https://academic.oup.com/braincomms/article/doi/10.1093/braincomms/fcaa187/5958116

254. Naganawa S, Ito R, Taoka T, Yoshida T, Sone M. The Space between the Pial Sheath and the Cortical Venous Wall May Connect to the Meningeal Lymphatics. Magn Reson Med Sci [Internet]. 2020;19(1):1–4. Available from: https://www.jstage.jst.go.jp/article/mrms/19/1/19_bc.2019-0099/_article

255. Yağmurlu K, Sokolowski JD, Çırak M, Urgun K, Soldozy S, Mut M, et al. Anatomical Features of the Deep Cervical Lymphatic System and Intrajugular Lymphatic Vessels in Humans. Brain Sci [Internet]. 2020 Dec 9;10(12):953. Available from: https://www.mdpi.com/2076-3425/10/12/953

256. Terrie E Inder and Petra S. Huppi. IN VIVO STUDIES OF BRAIN DEVELOPMENT BYM AGNETIC RESONANCE TECHNIQUES. Ment Retard Dev Disabil Rev. 2001;344(16):1215–21.

257. Youn SW, Lee J. From 2D to 4D Phase-Contrast MRI in the Neurovascular System: Will It Be a Quantum Jump or a Fancy Decoration? J Magn Reson Imaging. 2022;55(2):347–72.

258. Rivera-Rivera LA, Vikner T, Eisenmenger L, Johnson SC, Johnson KM. Four-dimensional flow MRI for quantitative assessment of cerebrospinal fluid dynamics: Status and opportunities. NMR Biomed. 2024;37(7):1–23.

259. Moser KW, Georgiadis JG, Buckius RO. On the accuracy of EPI-based phase contrast velocimetry. Magn Reson Imaging. 2000;18(9):1115–23.

260. Dreha-Kulaczewski S, Joseph AA, Merboldt KD, Ludwig HC, Gartner J, Frahm J. Inspiration Is the Major Regulator of Human CSF Flow. J Neurosci [Internet]. 2015 Feb 11;35(6):2485–91. Available from: https://www.jneurosci.org/lookup/doi/10.1523/JNEUROSCI.3246-

14.2015

261. Markl M, Schnell S, Wu C, Bollache E, Jarvis K, Barker AJ, et al. Advanced flow MRI: emerging techniques and applications. Clin Radiol [Internet]. 2016 Aug;71(8):779–95. Available from: https://linkinghub.elsevier.com/retrieve/pii/S0009926016000325

262. Liu P, Owashi K, Monnier H, Metanbou S, Capel C, Balédent O. Validating the accuracy of real-time phase-contrast MRI and quantifying the effects of free breathing on cerebrospinal fluid dynamics. Fluids Barriers CNS. 2024;21(1):1–14.

263. Takizawa K, Matsumae M, Sunohara S, Yatsushiro S, Kuroda K. Characterization of cardiac- and respiratory-driven cerebrospinal fluid motion based on asynchronous phase-contrast magnetic resonance imaging in volunteers. Fluids Barriers CNS [Internet]. 2017 Dec 27;14(1):25. Available from: http://fluidsbarrierscns.biomedcentral.com/articles/10.1186/s12987-017-0074-1

264. Sahoo P, Kollmeier JM, Wenkel N, Badura S, Gärtner J, Frahm J, et al. CSF and venous blood flow from childhood to adulthood studied by real-time phase-contrast MRI. Child's Nerv Syst [Internet]. 2024 May 11;40(5):1377–88. Available from: https://link.springer.com/10.1007/s00381-024-06275-1

265. Williams SD, Setzer B, Fultz NE, Valdiviezo Z, Tacugue N, Diamandis Z, et al. Neural activity induced by sensory stimulation can drive large-scale cerebrospinal fluid flow during wakefulness in humans. Nedergaard M, editor. PLOS Biol [Internet]. 2023 Mar 30;21(3):e3002035. Available from: https://dx.plos.org/10.1371/journal.pbio.3002035

266. Ringstad G, Vatnehol SAS, Eide PK. Glymphatic MRI in idiopathic normal pressure hydrocephalus. Brain [Internet]. 2017 Oct 1;140(10):2691–705. Available from: https://academic.oup.com/brain/article/140/10/2691/4085293

267. Naganawa S, Nakane T, Kawai H, Taoka T. Differences in Signal Intensity and Enhancement on MR Images of the Perivascular Spaces in the Basal Ganglia versus Those in White Matter. Magn Reson Med Sci [Internet]. 2018 Jan 1;17(4):301–7. Available from: https://www.jstage.jst.go.jp/article/mrms/17/4/17_mp.2017-0137/_article

268. Naganawa S, Taoka T, Ito R, Kawamura M. The Glymphatic System in Humans: Investigations With Magnetic Resonance Imaging. Invest Radiol. 2024;59(1):1–12.

269. Osch MJP Van, Wåhlin A, Scheyhing P, Mossige I, Hirschler L, Mogensen K, et al. Human brain clearance imaging : Pathways taken by magnetic resonance imaging contrast agents after administration in cerebrospinal fluid and blood. 2024;(October 2023):1–22.

270. Heye AK, Culling RD, Valdés Hernández MDC, Thrippleton MJ, Wardlaw JM. Assessment of blood-brain barrier disruption using dynamic contrast-enhanced MRI. A systematic review. NeuroImage Clin [Internet]. 2014;6:262–74. Available from: http://dx.doi.org/10.1016/j.nicl.2014.09.002

271. Rochetams BB, Marechal B, Cottier JP, Gaillot K, Sembely-Taveau C, Sirinelli D, et al. T1-weighted dynamic contrast-enhanced brain magnetic resonance imaging: A preliminary study with low infusion rate in pediatric patients. Neuroradiol J. 2017;30(5):429–36.

272. Taoka T, Masutani Y, Kawai H, Nakane T, Matsuoka K, Yasuno F, et al. Evaluation of glymphatic system activity with the diffusion MR technique: diffusion tensor image analysis along the perivascular space (DTI-ALPS) in Alzheimer's disease cases. Jpn J Radiol [Internet]. 2017 Feb 11;35(4):172–8. Available from: papers3://publication/doi/10.1007/s11604-017-0617-z

273. Yin Y, Peng Y, Nie L, Li X, Xiao Y, Jiang H, et al. Impaired glymphatic system revealed by DTI-ALPS in cerebral palsy due to periventricular leukomalacia: relation with brain lesion burden and hand dysfunction. Neuroradiology [Internet]. 2024 Feb 22;66(2):261–9. Available from: https://link.springer.com/10.1007/s00234-023-03269-9

274. Pu W, Wei S, Qiu M, Chen X, Zou W, Ge Y, et al. Dysfunction of the glymphatic system in childhood absence epilepsy. Front Neurosci [Internet]. 2023 Dec 8;17. Available from: https://www.frontiersin.org/articles/10.3389/fnins.2023.1312676/full

275. Lee DA, Park BS, Ko J, Park S hyung, Park J, Kim IH, et al. Glymphatic system function in patients with newly diagnosed focal epilepsy. Brain Behav. 2022;(January):1–8.

276. Kim J, Lee DA, Lee H, Park KM. Glymphatic system dysfunction in patients with occipital lobe epilepsy. J Neuroimaging [Internet]. 2023 May 10;33(3):455–61. Available from: https://onlinelibrary.wiley.com/doi/10.1111/jon.13083

277. Lin L ping, Su S, Hou W, Huang L, Zhou Q, Zou M, et al. Glymphatic system dysfunction in pediatric acute lymphoblastic leukemia without clinically diagnosed central nervous system infiltration: a novel DTI-ALPS method. Eur Radiol [Internet]. 2023 Mar 8;33(5):3726–34. Available from: https://link.springer.com/10.1007/s00330-023-09473-8

278. Margoni M, Pagani E, Meani A, Preziosa P, Mistri D, Gueye M, et al. Cognitive Impairment Is Related to Glymphatic System Dysfunction in Pediatric Multiple Sclerosis. Ann Neurol [Internet]. 2024 Jun 13;95(6):1080–92. Available from: https://onlinelibrary.wiley.com/doi/10.1002/ana.26911

279. Zhao C, OuYang Y, Zhang G, Zang D, Xia J, Liang G, et al. Association of Glymphatic and White Matter Impairment With the Postoperative Outcome of Pediatric Hydrocephalus. Neurosurgery [Internet]. 2024 Jun 24; Available from: https://journals.lww.com/10.1227/neu.0000000000003050

280. Chen Y, Wang M, Su S, Dai Y, Zou M, Lin L, et al. Assessment of the glymphatic function in children with attention-deficit/hyperactivity disorder. Eur Radiol [Internet]. 2024;34(3):1444–52. Available from: https://doi.org/10.1007/s00330-023-10220-2

281. Taoka T, Ito R, Nakamichi R, Nakane T, Kawai H, Naganawa S. Diffusion Tensor Image Analysis ALong the Perivascular Space (DTI-ALPS): Revisiting the Meaning and Significance of the Method. Magn Reson Med Sci. 2024;23(3):268–90.

282. Zhang W, Zhou Y, Wang J, Gong X, Chen Z, Zhang X, et al. Glymphatic clearance function in patients with cerebral small vessel disease. Neuroimage [Internet]. 2021;238(May):118257. Available from: https://doi.org/10.1016/j.neuroimage.2021.118257

283. Le Bihan D, Breton E, Lallemand D, Grenier P, Cabanis E, Laval-Jeantet M. MR imaging of intravoxel incoherent motions: application to diffusion and perfusion in neurologic disorders. Radiology [Internet]. 1986 Nov 1;161(2):401–7. Available from: http://pubs.rsna.org/doi/abs/10.1148/radiology.161.2.3763909

284. Wong SM, Backes WH, Drenthen GS, Zhang CE, Voorter PHM, Staals J, et al. Spectral Diffusion Analysis of Intravoxel Incoherent Motion MRI in Cerebral Small Vessel Disease. J Magn Reson Imaging [Internet]. 2020 Apr;51(4):1170–80. Available from: http://www.ncbi.nlm.nih.gov/pubmed/31486211

285. Jakab A, Tuura R, Kottke R, Kellenberger CJ, Scheer I. Intra-voxel incoherent motion MRI of the living human foetus: technique and test–retest repeatability. Eur Radiol Exp [Internet]. 2017 Dec 22;1(1):26. Available from: https://eurradiolexp.springeropen.com/articles/10.1186/s41747-017-0031-4

286. Jakab A, Tuura RL, Kottke R, Ochsenbein-Kölble N, Natalucci G, Nguyen TD, et al. Microvascular perfusion of the placenta, developing fetal liver, and lungs assessed with intravoxel incoherent motion imaging. J Magn Reson Imaging [Internet]. 2018 Jul 27;48(1):214–25. Available from: https://onlinelibrary.wiley.com/doi/10.1002/jmri.25933

287. Detre JA, Alsop DC. Perfusion magnetic resonance imaging with continuous arterial spin labeling: methods and clinical applications in the central nervous system. Eur J Radiol [Internet]. 1999 May 1;30(2):115–24. Available from:

http://eutils.ncbi.nlm.nih.gov/entrez/eutils/elink.fcgi?dbfrom=pubmed&id=10401592&retmode=ref&cmd=prlinks

288. Alsop DC, Detre JA, Golay X, Günther M, Hendrikse J, Hernandez-Garcia L, et al. Recommended implementation of arterial spin-labeled perfusion MRI for clinical applications: A consensus of the ISMRM perfusion study group and the European consortium for ASL in dementia. Magn Reson Med [Internet]. 2015 Jan 8;73(1):102–16. Available from: https://onlinelibrary.wiley.com/doi/10.1002/mrm.25197

289. Dickie BR, Parker GJM, Parkes LM. Measuring water exchange across the blood-brain barrier using MRI. Prog Nucl Magn Reson Spectrosc [Internet]. 2020;116:19–39. Available from: https://doi.org/10.1016/j.pnmrs.2019.09.002

290. Wang J, Fernández-Seara MA, Wang S, St Lawrence KS. When perfusion meets diffusion: In vivo measurement of water permeability in human brain. J Cereb Blood Flow Metab. 2007;27(4):839–49.

291. Lindner T, Bolar DS, Achten E, Barkhof F, Bastos-Leite AJ, Detre JA, et al. Current state and guidance on arterial spin labeling perfusion MRI in clinical neuroimaging. Magn Reson Med. 2023;89(5):2024–47.

292. Proisy M, Bruneau B, Rozel C, Tréguier C, Chouklati K, Riffaud L, et al. Arterial spin labeling in clinical pediatric imaging. Diagn Interv Imaging [Internet]. 2016 Feb 1;97(2):151–8. Available from: http://linkinghub.elsevier.com/retrieve/pii/S2211568415002971

293. Wintermark M, Lepori D, Cotting J, Roulet E, Van Melle G, Meuli R, et al. Brain perfusion in children: Evolution with age assessed by quantitative perfusion computed tomography. Pediatrics. 2004;113(6 I):1642–52.

294. C Chiron, C Raynaud, B Mazière, M Zilbovicius, L Laflamme, M C Masure, O Dulac, M Bourguignon AS. Changes in regional cerebral blood flow during brain maturation in children and adolescents. J Nucl Med. 1992;33(5):696–703.

295. Satterthwaite TD, Shinohara RT, Wolf DH, Hopson RD, Elliott MA, Vandekar SN, et al. Impact of puberty on the evolution of cerebral perfusion during adolescence. Proc Natl Acad Sci [Internet]. 2014 Jun 10;111(23):8643–8. Available from: https://pnas.org/doi/full/10.1073/pnas.1400178111

296. Virchow R. Ueber die Erweiterung kleinerer Gefäfse. Arch für Pathol Anat und Physiol und für Klin Med [Internet]. 1851 Oct;3(3):427–62. Available from: http://link.springer.com/10.1007/BF01960918

297. Lynch KM, Sepehrband F, Toga AW, Choupan J. Brain perivascular space imaging across the human lifespan. Neuroimage [Internet]. 2023;271(March):120009. Available from: https://doi.org/10.1016/j.neuroimage.2023.120009

298. Piantino J, Boespflug EL, Schwartz DL, Luther M, Morales AM, Lin A, et al. Characterization of MR imaging-visible perivascular spaces in the white matter of healthy adolescents at 3T. Am J Neuroradiol. 2020;41(11):2139–45.

299. Bouvy WH, Zwanenburg JJM, Reinink R, Wisse LEM, Luijten PR, Kappelle LJ, et al. Perivascular spaces on 7 Tesla brain MRI are related to markers of small vessel disease but not to age or cardiovascular risk factors. J Cereb Blood Flow Metab. 2016;36(10):1708–17.

300. Wang DJ, Hua J, Cao D, Ho ML. Neurofluids and the glymphatic system: anatomy, physiology, and imaging. Br J Radiol. 2023;96(1151).

301. Groeschel S, Brockmann K, Hanefeld F. Virchow-Robin spaces on magnetic resonance images of children with adrenoleukodystrophy. Eur J Paediatr Neurol. 2007;11(3):142–5.

302. Potter GM, Chappell FM, Morris Z, Wardlaw JM. Cerebral perivascular spaces visible on magnetic resonance imaging: Development of a qualitative rating scale and its observer reliability. Cerebrovasc Dis. 2015;39(3–4):224–31.

303. Moses J, Sinclair B, Law M, O'Brien TJ, Vivash L. Automated Methods for Detecting and Quantitation of Enlarged Perivascular spaces on MRI. J Magn Reson Imaging. 2023;57(1):11–24.

304. Waymont JMJ, Valdés Hernández M del C, Bernal J, Duarte Coello R, Brown R, Chappell FM, et al. Systematic review and meta-analysis of automated methods for quantifying enlarged perivascular spaces in the brain. Neuroimage. 2024;297(May).

305. Erin A. Yamamoto, Seiji Koike, Caitlyn Wong, Laura E. Dennis, Madison N. Luther, Avery Scatena, Seva Khambadkone, Jeffrey J. Iliff, Miranda M. Lim, Swati R. Levendovszky, Jonathan E. Elliott, Giuseppe Barisano, Eva M. Müller-Oehring, Angelica M. Morales, JP. Biological sex and BMI influence the longitudinal evolution of adolescent and young adult MRI- visible perivascular spaces. 2024;1–25.

306. Barisano G, Sheikh-Bahaei N, Law M, Toga AW, Sepehrband F. Body mass index, time of day and genetics affect perivascular spaces in the white matter. J Cereb Blood Flow Metab. 2021;41(7):1563–78.

307. Liu C, Habib T, Salimeen M, Pradhan A, Singh M, Wang M, et al. Quantification of visible

Virchow–Robin spaces for detecting the functional status of the glymphatic system in children with newly diagnosed idiopathic generalized epilepsy. Seizure [Internet]. 2020 May;78:12–7. Available from: https://linkinghub.elsevier.com/retrieve/pii/S105913112030056X

308. Biedroń A, Steczkowska M, Kubik A, Kaciński M. Dilatation of Virchow-Robin spaces in children hospitalized at pediatric neurology department. Neurol Neurochir Pol. 2014;48(1):39–44.

309. Nancy Rollins, K, Carol Deline M, Morriss C. Prevalence and clinical significance of dilated Virchow-Robin spaces in childhood. Radiology. 1993;189:53–7.

310. Millichap JG. Significance of MRI Perivascular Spaces in MS. Pediatr Neurol Briefs [Internet]. 2008 Oct 1;22(10):79. Available from: http://www.pediatricneurologybriefs.com/article/10.15844/pedneurbriefs-22-10-9/

311. Plamper M, Born M, Gohlke B, Schreiner F, Schulte S, Splittstößer V, et al. Cerebral MRI and Clinical Findings in Children with PTEN Hamartoma Tumor Syndrome: Can Cerebral MRI Scan Help to Establish an Earlier Diagnosis of PHTS in Children? Cells. 2020;9(7).

312. Sisman J, Chalak L, Heyne R, Pritchard M, Weakley D, Brown LS, et al. Lenticulostriate vasculopathy in preterm infants: a new classification, clinical associations and neurodevelopmental outcome. J Perinatol [Internet]. 2018;38(10):1370–8. Available from: http://dx.doi.org/10.1038/s41372-018-0206-8

313. Romero R, Espinoza J, Gonçalves L, Kusanovic J, Friel L, Hassan S. The Role of Inflammation and Infection in Preterm Birth. Semin Reprod Med [Internet]. 2007 Jan;25(1):021–39. Available from: http://www.thieme-connect.de/DOI/DOI?10.1055/s-2006-956773

314. Aribisala BS, Wiseman S, Morris Z, Valdés-Hernández MC, Royle NA, Maniega SM, et al. Circulating inflammatory markers are associated with magnetic resonance imaging-visible perivascular spaces but not directly with white matter hyperintensities. Stroke. 2014;45(2):605–7.

315. Wuerfel J, Haertle M, Waiczies H, Tysiak E, Bechmann I, Wernecke KD, et al. Perivascular spaces - MRI marker of inflammatory activity in the brain? Brain. 2008;131(9):2332–40.

316. Bouyssi-Kobar M, Murnick J, Brossard-Racine M, Chang T, Mahdi E, Jacobs M, et al. Altered Cerebral Perfusion in Infants Born Preterm Compared with Infants Born Full Term. J Pediatr [Internet]. 2018;193:54-61.e2. Available from:

https://doi.org/10.1016/j.jpeds.2017.09.083

317. Ortinau C, Neil J. The neuroanatomy of prematurity: Normal brain development and the impact of preterm birth. Clin Anat [Internet]. 2015 Mar 15;28(2):168–83. Available from: https://onlinelibrary.wiley.com/doi/10.1002/ca.22430

318. Freeman MR. Specification and Morphogenesis of Astrocytes. Science (80-) [Internet]. 2010 Nov 5;330(6005):774–8. Available from: https://www.science.org/doi/10.1126/science.1190928

319. Miranda MJ, Olofsson K, Sidaros K. Noninvasive measurements of regional cerebral perfusion in preterm and term neonates by magnetic resonance arterial spin labeling. Pediatr Res. 2006;60(3):359–63.

320. Tortora D, Mattei PA, Navarra R, Panara V, Salomone R, Rossi A, et al. Prematurity and brain perfusion: Arterial spin labeling MRI. NeuroImage Clin [Internet]. 2017;15(August 2016):401–7. Available from: http://dx.doi.org/10.1016/j.nicl.2017.05.023

321. Kehrer M, Krägeloh-Mann I, Goelz R, Schöning M. The Development of Cerebral Perfusion in Healthy Preterm and Term Neonates. Neuropediatrics. 2003;34(6):281–6.

322. De Vis JB, Petersen ET, De Vries LS, Groenendaal F, Kersbergen KJ, Alderliesten T, et al. Regional changes in brain perfusion during brain maturation measured non-invasively with Arterial Spin Labeling MRI in neonates. Eur J Radiol [Internet]. 2013;82(3):538–43. Available from: http://dx.doi.org/10.1016/j.ejrad.2012.10.013

323. Kim JY, Nam Y, Kim S, Shin NY, Kim HG. MRI-visible Perivascular Spaces in the Neonatal Brain. Radiology. 2023;307(2).

324. Li X, Lin Z, Liu C, Bai R, Wu D, Yang J. Glymphatic Imaging in Pediatrics. J Magn Reson Imaging. 2023;1523–41.

325. Benjamin J, O'Leary C, Hur S, Gurevich A, Klein WM, Itkin M. Imaging and Interventions for Lymphatic and Lymphatic-related Disorders. Radiology. 2023;307(3).

326. Mäkinen T, Boon LM, Vikkula M, Alitalo K. Lymphatic Malformations: Genetics, Mechanisms and Therapeutic Strategies. Circ Res [Internet]. 2021 Jun 25;129(1):136–54. Available from: https://www.ahajournals.org/doi/10.1161/CIRCRESAHA.121.318142

327. Sleutjes J, Kleimeier L, Leenders E, Klein W, Draaisma J. Lymphatic Abnormalities in Noonan Syndrome Spectrum Disorders: A Systematic Review. Mol Syndromol. 2022;13(1):1–11.

328. Lee VK, Reynolds WT, Wallace J, Beluk N, Badaly D, Lo CW, et al. Quantitative Magnetic Resonance Cerebral Spinal Fluid Flow Properties and Executive Function Cognitive Outcomes in Congenital Heart Disease. medRxiv : the preprint server for health sciences. United States; 2024.

329. Bagge CN, Henderson VW, Laursen HB, Adelborg K, Olsen M, Madsen NL. Risk of Dementia in Adults With Congenital Heart Disease. Circulation [Internet]. 2018 May;137(18):1912–20. Available from: https://www.ahajournals.org/doi/10.1161/CIRCULATIONAHA.117.029686

330. Hildebrandt M, Amann K, Schröder R, Pieper T, Kolodziejczyk D, Holthausen H, et al. White matter angiopathy is common in pediatric patients with intractable focal epilepsies. Epilepsia. 2008;49(5):804–15.

331. Karmazyn B, Dagan O, Vidne BA, Horev G, Kornreich L. Neuroimaging findings in neonates and infants from superior vena cava obstruction after cardiac operation. Pediatr Radiol. 2002;32(11):806–10.

332. McLaughlin JF, Loeser JD, Roberts TS. Acquired hydrocephalus associated with superior vena cava syndrome in infants. Child's Nerv Syst [Internet]. 1997 Mar 14;13(2):59–63. Available from: http://link.springer.com/10.1007/s003810050042

333. Barlow CF. CSF dynamics in hydrocephalus—With special attention to external hydrocephalus. Brain Dev [Internet]. 1984;6(2):119–27. Available from: http://dx.doi.org/10.1016/S0387-7604(84)80060-1

334. Murphy VA, Shen MD, Kim SH, Cornea E, Styner M, Gilmore JH. Extra-axial Cerebrospinal Fluid Relationships to Infant Brain Structure, Cognitive Development, and Risk for Schizophrenia. Biol Psychiatry Cogn Neurosci Neuroimaging [Internet]. 2020 Jul;5(7):651–9. Available from: https://linkinghub.elsevier.com/retrieve/pii/S245190222030077X

335. Runge K, van Elst LT, Maier S, Nickel K, Denzel D, Matysik M, et al. Cerebrospinal fluid findings of 36 adult patients with autism spectrum disorder. Brain Sci. 2020;10(6):1–18.

336. Xie L, Kang H, Xu Q, Chen MJ, Liao Y, Thiyagarajan M, et al. Sleep Drives Metabolite Clearance from the Adult Brain. Science (80-) [Internet]. 2013 Oct 18;342(6156):373–7. Available from: https://www.science.org/doi/10.1126/science.1241224

337. Krishnamurthy S, Li J, Shen Y, Duncan TM, Jenrow KA, Haacke EM. Normal macromolecular clearance out of the ventricles is delayed in hydrocephalus. Brain Res [Internet]. 2018 Jan 1;1678:337–55. Available from:

https://doi.org/10.1016/j.brainres.2017.10.013

338. Sotgiu MA, Lo Jacono A, Barisano G, Saderi L, Cavassa V, Montella A, et al. Brain perivascular spaces and autism: clinical and pathogenic implications from an innovative volumetric MRI study. Front Neurosci. 2023;17(June):1–10.

339. Agarwal N, Frigerio G, Rizzato G, Ciceri T, Mani E, Lanteri F, et al. Parasagittal dural volume correlates with cerebrospinal fluid volume and developmental delay in children with autism spectrum disorder. Commun Med [Internet]. 2024;4(1):191. Available from: https://doi.org/10.1038/s43856-024-00622-8

340. Aspelund A, Alitalo K. Yoda1 opens the lymphatic path for craniosynostosis therapy. J Clin Invest. 2024;134(4):10–3.

341. Matrongolo MJ, Ang PS, Wu J, Jain A, Thackray JK, Reddy A, et al. Piezo1 agonist restores meningeal lymphatic vessels, drainage, and brain-CSF perfusion in craniosynostosis and aged mice. J Clin Invest [Internet]. 2024 Feb 15;134(4). Available from: https://www.jci.org/articles/view/171468

342. Frigerio G, Rizzato G, Peruzzo D, Ciceri T, Mani E, Lanteri F, et al. Perivascular Space Burden in Children With Autism Spectrum Disorder Correlates With Neurodevelopmental Severity. J Magn Reson Imaging [Internet]. 2025 Jun 29;1–11. Available from: https://onlinelibrary.wiley.com/doi/10.1002/jmri.70023

343. Gouveia-Freitas K, Bastos-Leite AJ. Perivascular spaces and brain waste clearance systems: relevance for neurodegenerative and cerebrovascular pathology. Neuroradiology [Internet]. 2021;63(10):1581–97. Available from: https://doi.org/10.1007/s00234-021-02718-7

344. Wardlaw JM, Benveniste H, Nedergaard M, Zlokovic B V., Mestre H, Lee H, et al. Perivascular spaces in the brain: anatomy, physiology and pathology. Nature Reviews Neurology. 2020.

345. Boutinaud P, Tsuchida A, Laurent A, Adonias F, Hanifehlou Z, Nozais V, et al. 3D Segmentation of Perivascular Spaces on T1-Weighted 3 Tesla MR Images With a Convolutional Autoencoder and a U-Shaped Neural Network. Front Neuroinform. 2021;15(June):1–21.

346. Lan H, Lynch KM, Custer R, Shih N, Sherlock P, Toga AW, et al. Weakly supervised perivascular spaces segmentation with salient guidance of Frangi filter. Magn Reson Med [Internet]. 2023 Jun 24;89(6):2419–31. Available from:

https://onlinelibrary.wiley.com/doi/10.1002/mrm.29593

347. Lynch M, Pham W, Sinclair B, O'Brien TJ, Law M, Vivash L. Perivascular spaces as a potential biomarker of Alzheimer's disease. Front Neurosci [Internet]. 2022 Oct 18;16. Available from: https://www.frontiersin.org/articles/10.3389/fnins.2022.1021131/full

348. Wang L, Wang B, Wu C, Wang J, Sun M. Autism Spectrum Disorder: Neurodevelopmental Risk Factors, Biological Mechanism, and Precision Therapy. Int J Mol Sci [Internet]. 2023 Jan 17;24(3):1819. Available from: https://www.mdpi.com/1422-0067/24/3/1819

349. Pizzolorusso F, Paparella MT, Pizzolorusso I, Masino F, Guglielmi G. Magnetic resonance imaging in autism spectrum disorders: clinical and neuroradiological phenotypes. Acta Biomed. 2023;94(2).

350. Taber KH, Shaw JB, Loveland KA, Pearson DA, Lane DM, Hayman LA. Accentuated Virchow-Robin Spaces in the Centrum Semiovale in Children with Autistic Disorder. J Comput Assist Tomogr. 2004;28(2):263–8.

351. Ecker C. Brain Anatomy and Its Relationship to Behavior in Adults With Autism Spectrum Disorder. Arch Gen Psychiatry [Internet]. 2012 Feb 1;69(2):195. Available from: http://archpsyc.jamanetwork.com/article.aspx?doi=10.1001/archgenpsychiatry.2011.1251

352. Wegiel J, Frackowiak J, Mazur-Kolecka B, Schanen NC, Cook EH, Sigman M, et al. Abnormal Intracellular Accumulation and Extracellular Aβ Deposition in Idiopathic and Dup15q11.2-q13 Autism Spectrum Disorders. Borchelt DR, editor. PLoS One [Internet]. 2012 May 2;7(5):e35414. Available from: https://dx.plos.org/10.1371/journal.pone.0035414

353. Shen MD, Nordahl CW, Young GS, Wootton-Gorges SL, Lee A, Liston SE, et al. Early brain enlargement and elevated extra-axial fluid in infants who develop autism spectrum disorder. Brain. 2013;136(9):2825–35.

354. Ramirez J, Berezuk C, McNeely AA, Gao F, McLaurin J, Black SE. Imaging the Perivascular Space as a Potential Biomarker of Neurovascular and Neurodegenerative Diseases. Cell Mol Neurobiol [Internet]. 2016 Mar 17;36(2):1–11. Available from: papers3://publication/doi/10.1007/s10571-016-0343-6

355. Glasser MF, Sotiropoulos SN, Wilson JA, Coalson TS, Fischl B, Andersson JL, et al. The minimal preprocessing pipelines for the Human Connectome Project. Neuroimage [Internet]. 2013 Oct;80:105–24. Available from:

https://linkinghub.elsevier.com/retrieve/pii/S1053811913005053

356. Association AP. Diagnostic and Statistical Manual of Mental Disorders. Fifth. Washington DC: American Psychiatric Association; 2013.

357. Rutter, M., Le Couteur, A., and Lord C. Autism diagnostic interview-revised. Los Angeles (CA): Western Psychological Services; 2003.

358. Lord, C., Rutter, M., DiLavore, P.C., Risi, S., Gotham K. Autism Diagnostic Observation Schedule, 2nd edition (ADOS-2). Los Angeles (CA): Western Psychological Services; 2012.

359. Gotham K, Pickles A, Lord C. Standardizing ADOS Scores for a Measure of Severity in Autism Spectrum Disorders. J Autism Dev Disord [Internet]. 2009 May 12;39(5):693–705. Available from: http://link.springer.com/10.1007/s10803-008-0674-3

360. Esler AN, Bal VH, Guthrie W, Wetherby A, Weismer SE, Lord C. The Autism Diagnostic Observation Schedule, Toddler Module: Standardized Severity Scores. J Autism Dev Disord [Internet]. 2015 Sep 2;45(9):2704–20. Available from: http://link.springer.com/10.1007/s10803-015-2432-7

361. Luiz DM, Foxcroft CD, Povey JL. The Griffiths Scales of Mental Development: A Factorial Validity Study. South African J Psychol [Internet]. 2006 Mar 2;36(1):192–214. Available from: http://journals.sagepub.com/doi/10.1177/008124630603600111

362. Iglesias JE, Cheng-Yi Liu, Thompson PM, Zhuowen Tu. Robust Brain Extraction Across Datasets and Comparison With Publicly Available Methods. IEEE Trans Med Imaging [Internet]. 2011 Sep;30(9):1617–34. Available from: http://ieeexplore.ieee.org/document/5742706/

363. AVANTS B, EPSTEIN C, GROSSMAN M, GEE J. Symmetric diffeomorphic image registration with cross-correlation: Evaluating automated labeling of elderly and neurodegenerative brain. Med Image Anal [Internet]. 2008 Feb;12(1):26–41. Available from: https://linkinghub.elsevier.com/retrieve/pii/S1361841507000606

364. Jenkinson, M. Mickael Pechaud SS. BET2: MR-based estimation of brain, skull and scalp surfaces. In: Eleventh Annual Meeting of the Organization for Human Brain Mapping. 2005.

365. Tustison NJ, Avants BB, Cook PA, Yuanjie Zheng, Egan A, Yushkevich PA, et al. N4ITK: Improved N3 Bias Correction. IEEE Trans Med Imaging [Internet]. 2010 Jun;29(6):1310–20. Available from: http://ieeexplore.ieee.org/document/5445030/

366. Avants BB, Tustison NJ, Wu J, Cook PA, Gee JC. An Open Source Multivariate Framework

for n-Tissue Segmentation with Evaluation on Public Data. Neuroinformatics [Internet]. 2011 Dec 5;9(4):381–400. Available from: http://link.springer.com/10.1007/s12021-011-9109-y

367. Fortin JP, Cullen N, Sheline YI, Taylor WD, Aselcioglu I, Cook PA, et al. Harmonization of cortical thickness measurements across scanners and sites. Neuroimage [Internet]. 2018 Feb;167:104–20. Available from: https://linkinghub.elsevier.com/retrieve/pii/S105381191730931X

368. Akaike H. Information theory and an extension of the maximum likelihood principle. editors. Proceedings of the Second International Symposium on Information Theory. B. N Petrovand S Caski, editor. Budapest, Hungary; 1973. 267–281 p.

369. Shen MD, Kim SH, McKinstry RC, Gu H, Hazlett HC, Nordahl CW, et al. Increased Extra-axial Cerebrospinal Fluid in High-Risk Infants Who Later Develop Autism. Biol Psychiatry [Internet]. 2017;82(3):186–93. Available from: http://dx.doi.org/10.1016/j.biopsych.2017.02.1095

370. Shen MD, Nordahl CW, Li DD, Lee A, Angkustsiri K, Emerson RW, et al. Extra-axial cerebrospinal fluid in high-risk and normal-risk children with autism aged 2–4 years: a case-control study. The Lancet Psychiatry. 2018;5(11):895–904.

371. Peterson M, Prigge MBD, Bigler ED, Zielinski B, King JB, Lange N, et al. Evidence for normal extra-axial cerebrospinal fluid volume in autistic males from middle childhood to adulthood. 2021;

372. Gilmore JH, Knickmeyer RC, Gao W. Imaging structural and functional brain development in early childhood. Nat Rev Neurosci [Internet]. 2018 Mar 16;19(3):123–37. Available from: https://www.nature.com/articles/nrn.2018.1

373. Antila S, Karaman S, Nurmi H, Airavaara M, Voutilainen MH, Mathivet T, et al. Development and plasticity of meningeal lymphatic vessels. J Exp Med. 2017;214(12):3645–67.

374. Yamamoto EA, Bagley JH, Geltzeiler M, Sanusi OR, Dogan A, Liu JJ, et al. The perivascular space is a conduit for cerebrospinal fluid flow in humans: A proof-of-principle report. Proc Natl Acad Sci [Internet]. 2024 Oct 15;121(42). Available from: https://pnas.org/doi/10.1073/pnas.2407246121

375. Kim HG, Shin NY, Nam Y, Yun E, Yoon U, Lee HS, et al. MRI-visible Dilated Perivascular Space in the Brain by Age: The Human Connectome Project. Radiology. 2023;306(3).

376. Lun MP, Monuki ES, Lehtinen MK. Development and functions of the choroid plexus-

cerebrospinal fluid system. Nat Rev Neurosci. 2015;16(8):445–57.

377. Agarwal N, Frigerio G, Rizzato G, Ciceri T, Mani E, Lanteri F, et al. Parasagittal dural volume correlates with cerebrospinal fluid volume and developmental delay in children with autism spectrum disorder. Commun Med. 2024;4(1):191.

378. Duperron MG, Knol MJ, Le Grand Q, Evans TE, Mishra A, Tsuchida A, et al. Genomics of perivascular space burden unravels early mechanisms of cerebral small vessel disease. Nat Med [Internet]. 2023 Apr 17;29(4):950–62. Available from: https://www.nature.com/articles/s41591-023-02268-w

379. Wegiel J, Kuchna I, Nowicki K, Imaki H, Wegiel J, Marchi E, et al. The neuropathology of autism: Defects of neurogenesis and neuronal migration, and dysplastic changes. Acta Neuropathol. 2010;119(6):755–70.

380. Courchesne E, Pierce K, Schumann CM, Redcay E, Buckwalter JA, Kennedy DP, et al. Mapping early brain development in autism. Neuron. 2007;56(2):399–413.

381. Kim DE, Park JH, Schellingerhout D, Ryu WS, Lee SK, Jang MU, et al. Mapping the Supratentorial Cerebral Arterial Territories Using 1160 Large Artery Infarcts. JAMA Neurol. 2019;76(1):72–80.

382. Dong SZ, Zhu M, Bulas D. Techniques for minimizing sedation in pediatric MRI. J Magn Reson Imaging. 2019;50(4):1047–54.

383. Rustenhoven J, Drieu A, Mamuladze T, de Lima KA, Dykstra T, Wall M, et al. Functional characterization of the dural sinuses as a neuroimmune interface. Cell [Internet]. 2021;184(4):1000-1016.e27. Available from: https://doi.org/10.1016/j.cell.2020.12.040

384. Raper D, Louveau A, Kipnis J. How Do Meningeal Lymphatic Vessels Drain the CNS? Trends Neurosci [Internet]. 2016 Sep 1;39(9):581–6. Available from: https://linkinghub.elsevier.com/retrieve/pii/S0166223616300716

385. Louveau A, Herz J, Alme MN, Salvador AF, Dong MQ, Viar KE, et al. CNS lymphatic drainage and neuroinflammation are regulated by meningeal lymphatic vasculature. Nat Neurosci [Internet]. 2018;21(10):1380–91. Available from: http://dx.doi.org/10.1038/s41593-018-0227-9

386. Rustenhoven J, Kipnis J. Brain borders at the central stage of neuroimmunology. Nature [Internet]. 2022 Dec 15;612(7940):417–29. Available from: https://www.nature.com/articles/s41586-022-05474-7

387. Park M, Kim JW, Ahn SJ, Cha YJ, Suh SH. Aging is positively associated with peri-sinus lymphatic space volume: Assessment using 3t black-blood mri. J Clin Med. 2020;9(10):1–10.

388. Hett K, McKnight CD, Eisma JJ, Elenberger J, Lindsey JS, Considine CM, et al. Parasagittal dural space and cerebrospinal fluid (CSF) flow across the lifespan in healthy adults. Fluids Barriers CNS [Internet]. 2022;19(1):1–14. Available from: https://doi.org/10.1186/s12987-022-00320-4

389. Melin E, Eide PK, Ringstad G. In vivo assessment of cerebrospinal fluid efflux to nasal mucosa in humans. Sci Rep [Internet]. 2020 Dec 11;10(1):14974. Available from: https://www.nature.com/articles/s41598-020-72031-5

390. Song AK, Hett K, Eisma JJ, McKnight CD, Elenberger J, Stark AJ, et al. Parasagittal dural space hypertrophy and amyloid-β deposition in Alzheimer's disease. Brain Commun [Internet]. 2023;5(3):1–12. Available from: https://doi.org/10.1093/braincomms/fcad128

391. Muhle RA, Reed HE, Stratigos KA, Veenstra-VanderWeele J. The Emerging Clinical Neuroscience of Autism Spectrum Disorder. JAMA Psychiatry [Internet]. 2018 May 1;75(5):514. Available from: http://archpsyc.jamanetwork.com/article.aspx?doi=10.1001/jamapsychiatry.2017.4685

392. Walensky RP, Bunnell R, Kent CK, Gottardy AJ, Leahy MA, Martinroe JC, et al. Morbidity and Mortality Weekly Report Prevalence and Characteristics of Autism Spectrum Disorder Among Children Aged 8 Years-Autism and Developmental Disabilities Monitoring Network, 11 Sites, United States, 2020 Surveillance Summaries Centers for Disease. MMWR Surveill Summ. 2023;Summer(2).

393. Yin J, Schaaf CP. Autism genetics – an overview. Prenat Diagn [Internet]. 2017 Jan 10;37(1):14–30. Available from: https://obgyn.onlinelibrary.wiley.com/doi/10.1002/pd.4942

394. Rylaarsdam L, Guemez-Gamboa A. Genetic Causes and Modifiers of Autism Spectrum Disorder. Front Cell Neurosci [Internet]. 2019 Aug 20;13. Available from: https://www.frontiersin.org/article/10.3389/fncel.2019.00385/full

395. Toscano CVA, Barros L, Lima AB, Nunes T, Carvalho HM, Gaspar JM. Neuroscience and Biobehavioral Reviews Neuroinflammation in autism spectrum disorders : Exercise as a " pharmacological " tool. Neurosci Biobehav Rev [Internet]. 2021;129(March):63–74. Available from: https://doi.org/10.1016/j.neubiorev.2021.07.023

396. Wechsler D. Wechsler Intelligence Scale for Children – Fourth UK Edition (WISC-IV UK) [Internet]. Marshall LA, Coyne I, editors. British Psychological Society; 2004. Available from: https://explore.bps.org.uk/lookup/doi/10.53841/bpstest.2004.wisc4

397. Siddique N, Paheding S, Elkin CP, Devabhaktuni V. U-Net and Its Variants for Medical Image Segmentation: A Review of Theory and Applications. IEEE Access [Internet]. 2021;9:82031–57. Available from: https://ieeexplore.ieee.org/document/9446143/

398. Ronneberger O, Fischer P, Brox T. U-Net: Convolutional Networks for Biomedical Image Segmentation. In 2015. p. 234–41. Available from: http://link.springer.com/10.1007/978-3-319-24574-4_28

399. Ciceri T, Squarcina L, Giubergia A, Bertoldo A, Brambilla P, Peruzzo D. Review on deep learning fetal brain segmentation from Magnetic Resonance images. Artif Intell Med [Internet]. 2023 Sep;143:102608. Available from: https://linkinghub.elsevier.com/retrieve/pii/S0933365723001227

400. Ringstad G, Eide PK. Molecular trans-dural efflux to skull bone marrow in humans with CSF disorders. Brain [Internet]. 2022 May 24;145(4):1464–72. Available from: https://academic.oup.com/brain/article/145/4/1464/6440036

401. Shah T, Leurgans SE, Mehta RI, Yang J, Galloway CA, de Mesy Bentley KL, et al. Arachnoid granulations are lymphatic conduits that communicate with bone marrow and dura-arachnoid stroma. J Exp Med. 2023;220(2).

402. Klarica M, Radoš M, Orešković D. The Movement of Cerebrospinal Fluid and Its Relationship with Substances Behavior in Cerebrospinal and Interstitial Fluid. Neuroscience [Internet]. 2019 Aug;414:28–48. Available from: https://linkinghub.elsevier.com/retrieve/pii/S030645221930449X

403. Coupé P, Catheline G, Lanuza E, Manjón JV. Towards a unified analysis of brain maturation and aging across the entire lifespan: A MRI analysis. Hum Brain Mapp [Internet]. 2017 Nov 24;38(11):5501–18. Available from: https://onlinelibrary.wiley.com/doi/10.1002/hbm.23743

404. Tanaka C, Matsui M, Uematsu A, Noguchi K, Miyawaki T. Developmental trajectories of the fronto-temporal lobes from infancy to early adulthood in healthy individuals. Dev Neurosci. 2013;34(6):477–87.

405. Lee JK, Andrews DS, Ozonoff S, Solomon M, Rogers S, Amaral DG, et al. Archival Report Longitudinal Evaluation of Cerebral Growth Across Childhood in Boys and Girls With

Autism Spectrum Disorder. Biol Psychiatry [Internet]. 2021;90(5):286–94. Available from: https://doi.org/10.1016/j.biopsych.2020.10.014

406. Fame RM, Lehtinen MK. Review Emergence and Developmental Roles of the Cerebrospinal Fluid System. Dev Cell [Internet]. 2020;52(3):261–75. Available from: https://doi.org/10.1016/j.devcel.2020.01.027

407. Peterson M, Whetten C, Clark AM, Nielsen JA. No difference in extra-axial cerebrospinal fluid volumes across neurodevelopmental and psychiatric conditions in later childhood and adolescence. J Neurodev Disord [Internet]. 2023;15(1):1–13. Available from: https://doi.org/10.1186/s11689-023-09477-x

408. Gogtay N, Giedd JN, Lusk L, Hayashi KM, Greenstein D, Vaituzis AC, et al. Dynamic mapping of human cortical development during childhood through early adulthood. Proc Natl Acad Sci U S A. 2004;101(21):8174–9.

409. Frassanito P, Bianchi F, Pennisi G, Massimi L, Tamburrini G, Caldarelli M. The growth of the neurocranium: literature review and implications in cranial repair. Child's Nerv Syst [Internet]. 2019 Sep 14;35(9):1459–65. Available from: http://link.springer.com/10.1007/s00381-019-04193-1

410. Yanev P, Poinsatte K, Hominick D, Khurana N, Zuurbier KR, Berndt M, et al. Impaired meningeal lymphatic vessel development worsens stroke outcome. J Cereb Blood Flow Metab [Internet]. 2019 Jan 1;79:271678X18822921. Available from: http://journals.sagepub.com/doi/10.1177/0271678X18822921

411. Decimo I, Dolci S, Panuccio G, Riva M, Fumagalli G, Bifari F. Meninges: A Widespread Niche of Neural Progenitors for the Brain. Neuroscientist. 2021;27(5):506–28.

412. Bifari F, Berton V, Pino A, Kusalo M, Malpeli G, Di Chio M, et al. Meninges harbor cells expressing neural precursor markers during development and adulthood. Front Cell Neurosci. 2015;9:383.

413. Azmitia EC, Saccomano ZT, Alzoobaee MF, Boldrini M, Whitaker-Azmitia PM. Persistent Angiogenesis in the Autism Brain: An Immunocytochemical Study of Postmortem Cortex, Brainstem and Cerebellum. J Autism Dev Disord. 2016 Apr;46(4):1307–18.

414. Vasudevan A, Long JE, Crandall JE, Rubenstein JLR, Bhide PG. Compartment-specific transcription factors orchestrate angiogenesis gradients in the embryonic brain. Nat Neurosci [Internet]. 2008 Apr 16;11(4):429–39. Available from: https://www.nature.com/articles/nn2074

415. Wardlaw JM, Benveniste H, Nedergaard M, Zlokovic B V., Charpak S, Smith KJ, et al. Reply to: Rethink the classical view of cerebrospinal fluid production. Nat Rev Neurol. 2021;17(9):590–1.

416. Benveniste H, Heerdt PM, Fontes M, Rothman DL, Volkow ND. Glymphatic System Function in Relation to Anesthesia and Sleep States. Anesth Analg. 2019;128(4):747–58.

417. Zhao G, Han H, Wang W, Jia K. Propofol rather than isoflurane accelerates the interstitial fluid drainage in the deep rat brain. Int J Med Sci. 2021;18(3):652–9.

418. Eide PK, Ringstad G. Cerebrospinal fluid egress to human parasagittal dura and the impact of sleep deprivation. Brain Res [Internet]. 2021;1772(July):147669. Available from: https://doi.org/10.1016/j.brainres.2021.147669

419. Dean DC 3rd, Dirks H, O'Muircheartaigh J, Walker L, Jerskey BA, Lehman K, et al. Pediatric neuroimaging using magnetic resonance imaging during non-sedated sleep. Pediatr Radiol. 2014 Jan;44(1):64–72.

420. Nivedita Agarwal, Giulia Frigerio, letizia losa, Tommaso Ciceri, Elisa Mani, Fabiola Lanteri, Massimo Molteni, Roxana Octavia Carare DP. Figshare. 2024. Parasagittal dural space is linked to cerebrospinal fluid in young children with autism spectrum disorder. Available from: https://doi.org/10.6084/m9.figshare.24582369.v4

421. Rasmussen MK, Mestre H, Nedergaard M. The glymphatic pathway in neurological disorders. Lancet Neurol [Internet]. 2018;17(11):1016–24. Available from: http://dx.doi.org/10.1016/S1474-4422(18)30318-1

422. Wen W, Cheng J, Tang Y. Brain perivascular macrophages: current understanding and future prospects. Brain [Internet]. 2024;147(1):39–55. Available from: https://doi.org/10.1093/brain/awad304

423. Gu X, Song Q, Zhang Q, Huang M, Zheng M, Chen J, et al. Clearance of two organic nanoparticles from the brain via the paravascular pathway. J Control Release [Internet]. 2020 Jun;322:31–41. Available from: https://linkinghub.elsevier.com/retrieve/pii/S0168365920301589

424. Owens T, Bechmann I, Engelhardt B. Perivascular spaces and the two steps to neuroinflammation. J Neuropathol Exp Neurol. 2008;67(12):1113–21.

425. Carare RO, Hawkes CA, Weller RO. Afferent and efferent immunological pathways of the brain. Anatomy, Function and Failure. Brain Behav Immun [Internet]. 2014 Feb 1;36(C):9–14. Available from: http://dx.doi.org/10.1016/j.bbi.2013.10.012

426. Ineichen B V., Okar S V., Proulx ST, Engelhardt B, Lassmann H, Reich DS. Perivascular spaces and their role in neuroinflammation. Neuron [Internet]. 2022;110(21):3566–81. Available from: https://doi.org/10.1016/j.neuron.2022.10.024

427. MacLullich AMJ, Wardlaw JM, Ferguson KJ, Starr JM, Seckl JR, Deary IJ. Enlarged perivascular spaces are associated with cognitive function in healthy elderly men. J Neurol Neurosurg Psychiatry [Internet]. 2004 Nov 1;75(11):1519–23. Available from: http://jnnp.bmj.com/cgi/doi/10.1136/jnnp.2003.030858

428. Charidimou A, Meegahage R, Fox Z, Peeters A, Vandermeeren Y, Laloux P, et al. Enlarged perivascular spaces as a marker of underlying arteriopathy in intracerebral haemorrhage: a multicentre MRI cohort study. J Neurol Neurosurg Psychiatry [Internet]. 2013 May 7;84(6):624–9. Available from: http://jnnp.bmj.com/cgi/doi/10.1136/jnnp-2012-304434

429. Charidimou A, Boulouis G, Frosch MP, Baron JC, Pasi M, Albucher JF, et al. The Boston criteria version 2.0 for cerebral amyloid angiopathy: a multicentre, retrospective, MRI–neuropathology diagnostic accuracy study. Lancet Neurol. 2022;21(8):714–25.

430. Kapoor A, Gaubert A, Yew B, Jang JY, Dutt S, Li Y, et al. Enlarged perivascular spaces and plasma Aβ42/Aβ40 ratio in older adults without dementia. Neurobiol Aging [Internet]. 2023 Aug;128:43–8. Available from: https://linkinghub.elsevier.com/retrieve/pii/S0197458023000726

431. Shi X, Zhou N, Sun B, Wu Y, Hu Y, Ning Y. Perivascular Space Predicts Brain Hypometabolism of Individuals with Underlying Amyloid Pathology. J Alzheimer's Dis [Internet]. 2022 Nov 22;90(3):1329–37. Available from: https://journals.sagepub.com/doi/full/10.3233/JAD-220426

432. Hlauschek G, Nicolo J, Sinclair B, Law M, Yasuda CL, Cendes F, et al. Role of the glymphatic system and perivascular spaces as a potential biomarker for post-stroke epilepsy. Epilepsia Open [Internet]. 2024 Feb 14;9(1):60–76. Available from: https://onlinelibrary.wiley.com/doi/10.1002/epi4.12877

433. Hicks AJ, Sinclair B, Shultz SR, Pham W, Silbert LC, Schwartz DL, et al. Associations of Enlarged Perivascular Spaces With Brain Lesions, Brain Age, and Clinical Outcomes in Chronic Traumatic Brain Injury. Neurology [Internet]. 2023 Jul 4;101(1). Available from: https://www.neurology.org/doi/10.1212/WNL.0000000000207370

434. Walter AE, Savalia K, Yoon J, Morrison J, Schneider ALC, Diaz-Arrastia R, et al. Change in Enlarged Perivascular Spaces over Time and Associations with Outcomes After Traumatic Brain Injury. Neurotrauma Reports [Internet]. 2024 May 1;5(1):738–48. Available from:

https://www.liebertpub.com/doi/10.1089/neur.2024.0026

435. Rauch M, Lachner K, Frickel L, Lauer M, Adenauer SJ, Neuhaus E, et al. Focally Enlarged Perivascular Spaces in Pediatric and Adolescent Patients with Polymicrogyria—an MRI Study. Clin Neuroradiol. 2025;35(1):87–93.

436. Boddaert N, Zilbovicius M, Philipe A, Robel L, Bourgeois M, Barthélemy C, et al. MRI Findings in 77 Children with Non-Syndromic Autistic Disorder. Baune B, editor. PLoS One [Internet]. 2009 Feb 10;4(2):e4415. Available from: https://dx.plos.org/10.1371/journal.pone.0004415

437. Choi A, Bak D, Cho AR, Asma-ull H, Nam Y, Kim HG. Neonatal brain perivascular space volume as a predictor of neurodevelopmental outcomes at 24 months [Internet]. 2025. Available from: http://medrxiv.org/lookup/doi/10.1101/2025.05.26.25328343

438. Calleja Gero ML, González Gutiérrez-Solana L, López Marín L, López Pino MA, Fournier Del Castillo C, Duat Rodríguez A. Hallazgos neurorradiológicos en una serie de pacientes con mucopolisacaridosis. Neurología [Internet]. 2012 Sep;27(7):407–13. Available from: https://linkinghub.elsevier.com/retrieve/pii/S0213485311004166

439. Huisman TAGM. Unraveling the Mystery of the Perivascular Spaces and Glymphatic System of the Neonatal Central Nervous System. Radiology. 2023;307(2):2022–3.

440. Sotgiu S, Barisano G, Cavassa V, Puci MV, Sotgiu MA, Nuvoli A, et al. Cognitive Brain Networks and Enlarged Perivascular Spaces: Implications for Symptom Severity and Support Needs in Children with Autism. J Clin Med 2025, Vol 14, Page 3029 [Internet]. 2025;14(9):3029. Available from: https://www.mdpi.com/2077-0383/14/9/3029/htm%0Ahttps://www.mdpi.com/2077-0383/14/9/3029

441. Bernal J, Menze I. Editorial for “Perivascular Space Burden in Children With Autism Spectrum Disorder Correlates With Neurodevelopmental Severity.” J Magn Reson Imaging. 2025;1–2.

442. Matta SM, Hill-yardin EL, Crack PJ. Brain , Behavior , and Immunity The influence of neuroinflammation in Autism Spectrum Disorder. Brain Behav Immun [Internet]. 2019;79(October 2018):75–90. Available from: https://doi.org/10.1016/j.bbi.2019.04.037

443. Fiorentino M, Sapone A, Senger S, Camhi SS, Kadzielski SM, Buie TM, et al. Blood–brain barrier and intestinal epithelial barrier alterations in autism spectrum disorders. Mol Autism [Internet]. 2016 Dec 29;7(1):49. Available from: http://molecularautism.biomedcentral.com/articles/10.1186/s13229-016-0110-z

444. Suzuki K, Matsuzaki H, Iwata K, Kameno Y, Shimmura C, Kawai S, et al. Plasma Cytokine Profiles in Subjects with High-Functioning Autism Spectrum Disorders. Yoshikawa T, editor. PLoS One [Internet]. 2011 May 27;6(5):e20470. Available from: https://dx.plos.org/10.1371/journal.pone.0020470

445. Bilbo SD, Block CL, Bolton JL, Hanamsagar R, Tran PK. Beyond infection - Maternal immune activation by environmental factors, microglial development, and relevance for autism spectrum disorders. Exp Neurol [Internet]. 2018 Jan;299:241–51. Available from: https://linkinghub.elsevier.com/retrieve/pii/S0014488617301760

446. Garic D. The Important Link Between Sleep and Brain Health in Autism. Biol Psychiatry Cogn Neurosci Neuroimaging. 2023;8(1):3–5.

447. Zielinski MR, Gibbons AJ. Neuroinflammation, Sleep, and Circadian Rhythms. Front Cell Infect Microbiol [Internet]. 2022 Mar 22;12. Available from: https://www.frontiersin.org/articles/10.3389/fcimb.2022.853096/full

448. Sun Y rui, Lv QK, Liu JY, Wang F, Liu CF. New perspectives on the glymphatic system and the relationship between glymphatic system and neurodegenerative diseases. Neurobiol Dis [Internet]. 2025;205(January):106791. Available from: https://doi.org/10.1016/j.nbd.2025.106791

449. Alves De Lima K, Rustenhoven J, Kipnis J. Meningeal Immunity and Its Function in Maintenance of the Central Nervous System in Health and Disease. Annu Rev Immunol. 2020;38:597–620.

450. Da Mesquita S, Louveau A, Vaccari A, Smirnov I, Cornelison RC, Kingsmore KM, et al. Functional aspects of meningeal lymphatics in ageing and Alzheimer's disease. Nature [Internet]. 2018 Jul 25;560(7717):185–91. Available from: http://www.nature.com/articles/s41586-018-0368-8

451. Eisma JJ, McKnight CD, Hett K, Elenberger J, Han CJ, Song AK, et al. Deep learning segmentation of the choroid plexus from structural magnetic resonance imaging (MRI): validation and normative ranges across the adult lifespan. Fluids Barriers CNS [Internet]. 2024 Feb 29;21(1):21. Available from: https://fluidsbarrierscns.biomedcentral.com/articles/10.1186/s12987-024-00525-9

452. Vivanti G, Lee WL, Ventimiglia J, Tao S, Lyall K, Shea LL. Prevalence of Dementia Among US Adults With Autism Spectrum Disorder. JAMA Netw Open [Internet]. 2025 Jan 2;8(1):e2453691. Available from: https://jamanetwork.com/journals/jamanetworkopen/fullarticle/2828643

453. Bailey AR, Hou H, Song M, Obregon DF, Portis S, Barger S, et al. GFAP expression and social deficits in transgenic mice overexpressing human sAPPα. Glia [Internet]. 2013 Sep 10;61(9):1556–69. Available from: https://onlinelibrary.wiley.com/doi/10.1002/glia.22544

454. Jelacic S, de Regt D, Weinberger E. Interactive Digital MR Atlas of the Pediatric Brain. RadioGraphics [Internet]. 2006 Mar;26(2):497–501. Available from: http://pubs.rsna.org/doi/10.1148/rg.262055009

455. Ciceri T, Casartelli L, Montano F, Conte S, Squarcina L, Bertoldo A, et al. Fetal brain MRI atlases and datasets: A review. Neuroimage [Internet]. 2024;292(April):120603. Available from: https://doi.org/10.1016/j.neuroimage.2024.120603

456. Malik SJ, Hand JW, Carmichael DW, Hajnal J V. Evaluation of specific absorption rate and heating in children exposed to a <scp>7T MRI</scp> head coil. Magn Reson Med [Internet]. 2022 Sep 6;88(3):1434–49. Available from: https://onlinelibrary.wiley.com/doi/10.1002/mrm.29283

457. Mallory MD, Travers C, Cravero JP, Kamat PP, Tsze D, Hertzog JH. Pediatric Sedation/Anesthesia for <scp>MRI</scp> : Results From the Pediatric Sedation Research Consortium. J Magn Reson Imaging [Internet]. 2023 Apr 12;57(4):1106–13. Available from: https://onlinelibrary.wiley.com/doi/10.1002/jmri.28392

458. Al-Ayadhi L, Halepoto DM. Role of proteomics in the discovery of autism biomarkers. J Coll Physicians Surg Pakistan. 2013;23(2):137–43.

459. Ponzini E, Ami D, Duse A, Santambrogio C, De Palma A, Di Silvestre D, et al. Single-tear proteomics: A feasible approach to precision medicine. Int J Mol Sci. 2021;22(19):1–16.

460. Ponzini E, Santambrogio C, De Palma A, Mauri P, Tavazzi S, Grandori R. Mass spectrometry-based tear proteomics for noninvasive biomarker discovery. Mass Spectrom Rev. 2022;41(5):842–60.